DISTRIBUTED PHASED ARRAY ANTENNAS IN WIDE AREA RFID

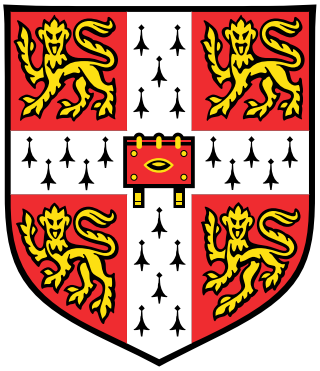

Ajeck Mbanwie Ndifon

Wolfson College

University of Cambridge

A thesis submitted for the degree of

Doctor of Philosophy

September 2019

Declaration

I hereby declare that except where specific reference is made to the work of others, the contents of this dissertation are original and have not been submitted in whole or in part for consideration for any other degree or qualification in this, or any other university. This dissertation is my own work and contains nothing which is the outcome of work done in collaboration with others, except as specified in the text and Acknowledgements. This dissertation contains fewer than 65,000 words including appendices, bibliography, footnotes, tables and equations and has fewer than 150 figures.

Ajeck M. Ndifon
September 2019

Abstract

DISTRIBUTED PHASED ARRAY ANTENNAS IN WIDE AREA RFID

Ultra High Frequency (UHF) Radio Frequency Identification (RFID) has gained importance over the past two decades in many applications such as stock management, asset tracking and access control. For wide area applications, Distributed Antenna Systems (DAS) have been used to obtain good coverage with few antennas by making use of multiple spatially distributed antennas and phase dithering. This implements a far-field beamforming that maximises the instantaneous power at a tag. Separately, phased array antennas have also been used to increase the read range by increasing the effective field of view of an antenna and overcoming multipath fading through beam steering. This dissertation explores a combination of both approaches to improve RFID read ranges in wide interrogation zones.

Distributed antenna arrays are explored in the context of delivering high tag detection probabilities in a multi-cell RFID system, while maximising inter-antenna separations. A Distributed Antenna Array System (DAAS) is designed and shown to be capable of providing comparable performance to a fixed DAS system with fewer antennas. The properties of the system are further studied and its upper performance limit is explored by modelling a hypothetical perfectly steerable antenna array. The concept of using perfectly steerable arrays is further explored to propose a cell-less RFID system, in which cell allocation in wide area RFID is replaced with a tag location-based interrogation requiring the global reader antenna population to be used for interrogation of all tags, leading to significant potential increases in inter-antenna separation, and consequently good coverage with fewer antennas. It is also argued that this system leads to the avoidance of complex reader anti-collision policies, since only a single central reader is now required. Finally, the design of a wide-scan-angle antenna array is presented as a compromise solution for perfectly steerable antennas, whist still keeping the desired property of being flat panel. A 3D RFID multi-antenna model is presented and used for simulating and analysing the various described systems and for system planning.

Ajeck M. Ndifon

Acknowledgements

I wish to express my utmost gratitude to my supervisor, Prof. Ian White, for his guidance throughout the course of my PhD, with special mention of the invaluable advice and support during the early stages. I also wish to thank my advisor, Prof. Richard Penty, for many useful comments during group meetings. I am also immensely appreciative of the extensive technical advice and discussions I had with Dr Michael Crisp in many aspects of my work, especially in relation to performing experiments and various aspects relating to RF an antenna propagation.

Much gratitude also to all the members of the CPS group including Dr Adrian Wonfor, without whom, many aspects of research would have been a lot less smooth, Shuai Yang (now Dr), who introduced me to the lab, as well as Zhe, Nic and Rui, with whom I had many useful discussions.

I wish also to express gratitude to many friends at Wolfson, especially Andy and Christine for support during my time at the College.

I am forever grateful to my parents for unconditional support in all aspects of life.

And finally, I thank God for the gift of Life.

Contents

1 Introduction and Motivation **1**

1.1 Introduction to the RFID Distributed Antenna System 3

1.2 The need for Phased array antennas in Wide Area RFID 5

1.3 Outline and Contributions 7

2 Background and Literature **10**

2.1 Background on RFID 10

2.1.1 A Brief History of RFID 10

2.1.2 RFID Operating Principles 12

2.1.3 Recent Developments in RFID 16

2.1.4 Standards and Protocols 16

2.2 Problems in Wide Area RFID and proposed solutions 19

2.2.1 RFID Network Planning 19

2.2.2 Fading 26

2.3 Antenna Arrays in RFID 28

2.3.1 A History of Antenna Arrays 29

2.3.2 Components of a phased array antenna 30

2.3.3 Antenna Array Classification 33

2.3.4 Phased Array Applications in RFID 36

2.4 Summary 38

3 A Novel 3D model for multi-antenna Wide Area RFID Simulation **39**

3.1 Review of RFID Propagation Models 40

3.2 Theoretical Background on Antenna Radiation 42

3.3 Model Description 44

3.3.1 Field Interpolation . . . 46
3.3.2 Coordinate Transformations . . . 47
3.3.3 Tag receive power . . . 47
3.3.4 Verification with simple test case . . . 49
3.3.5 Multipath . . . 51
3.3.6 Model Validation . . . 56
3.4 Performance Evaluation . . . 59
3.5 Case Study: Diversity Schemes in a Multi-antenna RFID System . . . 61
3.5.1 Time Division Multiplexing (TDM) . . . 63
3.5.2 Frequency hopping . . . 65
3.5.3 Phase hopping . . . 67
3.6 Summary . . . 68

4 An Investigation into Multicasting approaches with Phased Array Antennas in RFID Systems 69

4.1 Antenna Design and Measurement . . . 70
4.1.1 Antenna Requirements . . . 70
4.1.2 Background theory on phased array antennas . . . 71
4.1.3 Design of Antenna Array . . . 73
4.1.4 Pattern measurements . . . 78
4.2 Comparison of Multiplexing approaches in an RFID Array System . . . 80
4.2.1 Simulation . . . 80
4.2.2 Experimental Demonstration . . . 84
4.2.3 What about increasing the number of arrays? . . . 89
4.3 Summary . . . 92

5 An RFID Distributed Antenna Array System 93

5.1 A Primer study on a single Phased Array Antenna . . . 95
5.1.1 Beamforming . . . 96
5.1.2 Simulation Results . . . 97
5.1.3 Experimental Demonstration . . . 98
5.2 Simulations on Distributed Fixed and Antenna Array Systems . . . 103
5.2.1 Distributed Fixed Antenna Systems . . . 103

5.2.2 Distributed Antenna Array System . . . 105
5.2.3 Analysis and Discussion . . . 109
5.3 Experimental Demonstration . . . 110
5.3.1 Experimental Setup . . . 110
5.3.2 Discussion . . . 111
5.3.3 Adaptive Steering Transmit Power Control . . . 113
5.4 Use of a Single Port reader . . . 119
5.4.1 Experimental Demonstration . . . 120
5.5 Summary . . . 122

6 Perfectly Steerable DAAS and towards a Non-Cellular DAAS 124
6.1 Perfectly Steerable DAAS . . . 125
6.1.1 Raster scan study on different cell areas . . . 129
6.1.2 Removing Multipath . . . 132
6.1.3 Limited Elevation scan angle . . . 134
6.2 Non-cellular Perfectly Steerable DAAS . . . 139
6.2.1 An Infinitely Large Non-Cellular DAAS System . . . 143
6.3 System Resilience to antenna Failure . . . 149
6.3.1 Cellular System . . . 149
6.3.2 Non-cellular system . . . 151
6.4 Summary . . . 154

7 Conclusion and Future work 155
7.1 Conclusion . . . 155
7.1.1 Wide Area RFID Antenna Modelling . . . 156
7.1.2 The Distributed Antenna Array System . . . 156
7.1.3 Perfectly Steerable DAAS and Cell-less RFID . . . 157
7.2 Future Work . . . 159
7.2.1 Practical Implementation of Non Cellular DAAS . . . 159
7.2.2 Massive MIMO for RFID . . . 160
7.2.3 RFID DAAS over Ethernet cable . . . 161
7.2.4 A wide-angle scan metasurface antenna . . . 163

List of Figures

1.1 General Identification examples for different objects 1

1.2 A passive RFID interrogation showing a reader interrogating a tagged object 2

1.3 A typical four-antenna cell wide area RFID cellular system with nine readers ($R1 - R9$) assigned to nine cells. It is seen that the power distribution within the cell (insert) contains peaks and troughs due to the interference resulting from the four antennas. These can be resolved by TDM or phase diversity as shown. 5

1.4 Envisioned distributed antenna array system, with antennas capable of scanning all surrounding cells, as a single antenna array can steer its beam pattern electronically, leading to reduced system complexity. 6

2.1 Working Principle of UHF RFID 13

2.2 Block diagram of a monostatic RFID reader 14

2.3 Components of a UHF RFID tag 15

2.4 Protocol description. 17

2.5 Example of an RFID query with reader query, tag RN16 , and reader acknowledgement of RN16. 18

2.6 Reader Collision avoidance. Source: citeDobkinweb 20

2.7 A wide area RFID interrogation volume divided into multiple four-antenna rectangular cells. Antennas are shown only for one cell 24

2.8 Limiting RFID range to avoid multipath fading. Peaks and troughs are caused by reflections and avoided by limiting the operating range. 26

2.9 A phased array architecture, showing each antenna element fed by a phase-shifted version of the input signal 28

2.10 2D phased array feed network examples 31

2.11 Architecture of a three-bit delay-line switched digital phase shifter with a range of 180^0. 32
2.12 General Architecture for passive (a) and active (b) arrays 34
2.13 A 4×4 butler matrix with four switchable beams. Feeding ports 1-4 activates beams 1-4 respectively. Multiple beams are produced by exciting multiple corresponding ports 35

3.1 Tags with different orientations z, x and y polarisations 45
3.2 Field interpolation 2D illustration. The simulated values are done at 5^0 intervals shown by the red plot. The electric field is required in a direction corresponding to the blue dot, and is obtained by a bilinear interpolation . 46
3.3 Experiment to test model in a simple case with a single antenna pointing downward and tags forming a grid on XY plane. 49
3.4 Model test example for down-pointing antenna at 3m height and 3D grid of tags, showing cuts at the planes $X = 0, Y = 0$ and $Z = 1m$ 50
3.5 Model Test with antenna pointing vertically downwards for tags on the plane $Z = 1m$ 51
3.6 RFID model showing ground reflection modelling using virtual antenna images and Fresnel coefficients 52
3.7 Model test example for down-pointing antenna at 3m height and 3D grid of tags with dielectric ground, showing cuts at the planes $X = 0, Y = 0$ and $Z = 1m$ 54
3.8 Model Test with antenna pointing vertically downwards for tags on the plane $Z = 1m$ with dielectric ground 56
3.9 Setup for model validation. A single antenna pointing at a defined angle to the vertical, and the power received by each tag, making a 2D grid on a defined height in the xy plane. 57
3.10 Model comparison with FEKO for antenna tilted 45^0 in free space 58
3.11 Model comparison with FEKO for antenna tilted 90^0 with perfect ground . 58
3.12 Model comparison with FEKO for antenna tilted 45^0 with a concrete ground 59
3.13 Tag read histogram for power distributions in Fig 3.7b 60
3.14 Tag read cdf for power distributions in Fig 3.8 60

3.15 Setup for case study investigating multi-antenna multiplexing schemes in a four-antenna RFID cell system 61
3.16 Power distribution of a four-antenna system as seen by tags on plane Z=1m, showing intra-cell multi-antenna mutual interference in an $8m \times 8m$ zone, leading to blind spots 62
3.17 Tag cdf of multi-antenna system with mutual interference 62
3.18 Power distribution of a four-antenna system as seen by tags on plane Z=1m for TDM system 63
3.19 Tag cdf for TDM system 63
3.20 Tag power variation at different horizontal separations from antenna 65
3.21 A four-antenna system with frequency hopping for 865.6-867.4 MHz (ETSI narrow band) shows little reduction of nulls 66
3.22 A four-antenna system with frequency hopping for 860-960 MHz (RFID global band) shows significant null resolution 66
3.23 Power distribution of a four-antenna system as seen by tags on plane Z=1m for a phase hopping system 67
3.24 Comparing different multiplexing schemes in a four-antenna RFID system . 67

4.1 Common methods for obtaining circular polarisation in patch antennas . . 74
4.2 Single antenna element beam pattern 75
4.3 Sequential Rotation Technique showing rotated antenna elements, polarisation and phases of the signal feeds. The arrows show the polarisation of the electric field for each antenna element 76
4.4 Simulated antenna 3D pattern simulations at different (ϕ, θ) scan directions 77
4.5 Manufactured antenna samples 78
4.6 Antenna beam pattern pointing to broadside direction showing cut at $\phi = 0°$ 78
4.7 Antenna beam pattern steered to $(45°, 45°)$ showing cut at $\phi = 45°$ 79
4.8 Setup for array multicast experiment 80
4.9 Beam states for array multicasting experiment, at an elevation angle of 30°. The broadside (maximum at $\phi = 0°, \theta = 0°$) beam is not shown 81
4.10 Simulation results showing cdf for three different array multicasting schemes 81

4.11 Simulation results for three different array multi-casting schemes: Beam steering + Time Division Multiplexing, Beam steering (No phase dithering) and Beam steering + beam steering for z, y and x tag polarisations for tags at Z=1m plane. 82
4.12 Multiport Reader structure 84
4.13 Multicast RFID System Architecture 85
4.14 Diagrammatic representation of experimental setup showing transmit arrays, receive antennas and RFID tags. The number of crosses indicate the relative concentrations of tags at different locations (total = 100) 86
4.15 Experimental comparison of different multicasting schemes (complemetary) cumulative tag reads and (left) and power differences for commonly detected tags (right) 87
4.16 Experimental comparison of different multicasting schemes a reduced power 88
4.17 Rectangular and Hexagonal antenna arrangement 89
4.18 Simulation results for three different array multicasting schemes in a four-array system. The rows represent (from left to right) the z, y and x tag orientations respectively. The first column represents the TDM scheme. The second column represents beam steering without phase diversity. The third column is the system with beam steering and phase diversity 90
4.19 Simulation results for three different array multicasting schemes in a four-array system for four and six-array system. 91

5.1 A typical four-antenna RFID cell 94
5.2 Phased array antenna case study 96
5.3 Power distribution on plane X=2.5m for a single antenna array 97
5.4 Power distribution on plane X=2.5m for a fixed antenna 98
5.5 cdf for tags on plane X=2.5m for single antenna array 98
5.6 Control circuit for array showing system diagram (top) and manufactured PCB (bottom). The circuit takes in a single modulated carrier and performs beam steering. Beam steering is controlled via an onboard MCU. . . 99
5.7 Phase shifting characterisation of beam control PCB 101
5.8 Antenna front (left) and back (right) showing PCB mounted on antenna, together with the four power amplifiers 101

5.9 Experiment comparing read success rate of tag arrays for scanning antenna array and a fixed antenna 102
5.10 Experiment comparing single fixed antenna and single antenna array . . . 102
5.11 Experimental setup for comparison of fixed and array distributed antenna system. This model represents a single cell in a multi-cell wide area RFID system. The antenna are placed at the cell vertices. 103
5.12 Fixed antenna RFID system 104
5.13 Power Distribution for fixed four-antenna Distributed Antenna System for antenna tilt angle of 70^{0} 104
5.14 cdf plot of fixed antenna system for different antenna tilt angles 105
5.15 Switched antenna array RFID system with a Butler matrix-fed array at each cell vertex. Each array can switch between four different beams and scan each surrounding cell. 106
5.16 A Butler-type matrix for a 2×2 array showing input ports and the corresponding beam. e.g. feeding Port A generates Beam A 107
5.17 Power distribution for switched array antenna system of four arrays located at vertex of cell 108
5.18 Power distribution for steerable array antenna system of four arrays located at vertex of cell 108
5.19 Cumulative distribution of tag received power for a distributed system of fixed and array antenna 109
5.20 Laboratory experiment setup 111
5.21 Cumulative tags read against RSSI for four-antenna system of fixed antennas (blue) and antenna arrays (red) 112
5.22 Cumulative tags read against time for four-antenna system of fixed antennas (blue) and antenna arrays (red) 113
5.23 Power gain introduced by power scaling compared to no-scaling case. The dB difference in power distributions is plotted. 114
5.24 cumulative distribution of tag received power for a distributed system of fixed and array antennas 114

5.25 Maximum array gain with progressive excitation phases (θ) and ϕ showing gain degradation at the edges. Because of the directional nature of patch antennas, and the limitations of a 2×2 array, the actual scan angle is significantly lower. 116
5.26 Cumulative tag read success rate with RSSI for fixed antenna system achieving 95% (297 tags) after 10 minutes (blue) and antenna array system achieving 97% (302 tags) and antenna array system with added power achieving 100% (312 tags) 117
5.27 Simulation of s2 inventory session. The first value of received power above tag threshold (-15dBm) is used instead of cumulative maximum. 118
5.28 RFID Distributed Antenna Array System with multi-port reader using separate RF and control cables to each antenna (a) and single port reader using single coaxial cable in daisy-chain arrangement for both RF and control signals (b) 119
5.29 Single port DAAS system implementation using a diplexer for the reader end (left) and a directional coupler, amplifier and bias-T for the antenna end (right) 120
5.30 PCB implementing diplexing and RF tapping functionality for single reader port RFID Distributed Antenna Array System 121
5.31 Single port RFID DAAS experiment compared with a four-port system . . 122

6.1 Raster scan system with perfectly steerable antennas. All antennas are steered to a particular location, and phase dithering is applied to maximise power there. The raster scanning procedure is followed to cover the entire cell. 126
6.2 Geometrical rotation of a standard antenna as a model for a perfectly steerable antenna. Rotating the d antenna by upto $\theta_{max} = \pm 90^0$ in elevation and $\phi_{max} = 360^0$ in azimuth is used to represent perfect 2D beam steering. 127
6.3 System of four antennas at vertices of a $12m \times 12m$ cell pointing to different target locations (X). Antennas are on the $Z = 3m$ plane and indicated by circles. Only Y-polarised tags are used on the $Z = 1m$ plane. 128
6.4 Simulation of power distribution produced by a fixed antenna system, with all four antennas pointing to the centre of a $8m \times 8m$ room 129

6.5 Power distributions for system of four perfectly steerable antennas using raster scanning in cells of different cell sizes: $8m \times 8m, 12m \times 12m, 14m \times 14m, 16m \times 16m$ and $20m \times 20m$. 130
6.6 cdf for perfectly steerable DAAS system for different cell sizes $8m \times 8m, 12m \times 12m, 14m \times 14m, 16m \times 16m$ and $20m \times 20m$. Comparison is made with a standard fixed DAS in a $8m \times 8m$ cell. 131
6.7 Power distributions of distributed system of four 10dB-perfectly steerable antenna for a cell of antenna separations 16m and 20m. Only a single quadrant is shown. 132
6.8 cdf for different room sizes with multipath, without multipath, and with a 20 dB antenna 133
6.9 Power distribution for $12m \times 12m$ room for antenna limited to maximum elevation steering angles $45^0, 60^0, 75^0$ and 90^0. The power distribution is seen to improve with increased maximum scan angle as expected. 135
6.10 cdf plot for antennas with different maximum elevation angles in a 12m × 12m room 136
6.11 cdf plot for antennas with different maximum elevation angles in a 12mx12m room 138
6.12 cdf plot for antennas with different maximum elevation angles in a 12mx12m room and antenna-tag plane separation of 5m, showing that an antenna capable of 60 degrees can perform similarly to a perfectly steerable antenna. . 138
6.13 Cellular raster scan system (left, a) and non-cellular system (right, b). The red crosses (X) in the cellular system indicate idle antennas, which are absent in the non-cellular system, thereby better performance is expected. 140
6.14 Power distribution produced by a multi-cell system of perfectly steerable antennas. Only the central cell has been scanned. Furthermore, only the bottom left quadrant of this cell has been scanned to exploit the symmetry of the system. Antenna separation is 20m 141
6.15 Power distribution produced by a multi-cell system of perfectly steerable antennas showing scanned quadrant of central cell. 141
6.16 cdf for cellular and non-cellular DAAS for various antenna separations. Comparison is made with a fixed DAS system (blue) 142

6.17 Interpreting a regular grid of equally separated antennas as concentric rings of antennas. The rectangular rings are approximated as equi-areal circular rings of an equal number of antennas to estimate the contribution of each ring to the received power in the central cell. Crosses of different colours represent antennas on different concentric rings. 143
6.18 Power distributions due to antenna on Ring 2 and on Ring 3 in a system of $8m \times 8m$ antenna separation. Only the central area (within border) has been scanned 145
6.19 cdf for Ring 2 and Ring 3 in a system of $8m \times 8m$ antenna separation, showing close agreement in their delivered power. This verifies the assertion of equal power delivery by each ring. 145
6.20 Power distribution of rings 1 and 2 vs Ring 2 only for scanning a $24m \times 24m$ area. 147
6.21 cdf of rings 1 and 2 vs Ring 2 only for scanning a $24m \times 24m$ area. It is seen that without the central ring, minimum tag power degrades by 1.5dB and 4.5 dB for vertical and horizontal tags respectively. 148
6.22 Effect of antenna failure on perfectly steerable cellular system power distribution in $8m \times 8m$ cell 150
6.23 cdf for different scenarios of antenna failure in cellular perfectly steerable array system with $8m \times 8m$ antenna separation 151
6.24 Effect of antenna failure on fixed antenna system power distribution in $8m \times 8m$ cell 152
6.25 cdf for different scenarios of antenna failure in non-cellular perfectly steerable array system with $8m \times 8m$ antenna separation 153

7.1 From periodic DAAS to Ring DAAS system 159
7.2 RFID MIMO tag pattern switching for a 1×4 tag array showing different beams 161
7.3 RFID over ethernet block diagram 162
7.4 Proposed daisy chain RFID DAAS 162

7.5 Design simulated as a 3x3 array antenna, where each element is a 2x2 sequentially rotated sub-array. A quadrifilar splitter provides sequential phase shifts of 0, 90, 180 and 270 degrees at each of four output ports for sequentially rotated sub-arrays. 164
7.6 Simulated 6x6 metasurface antenna showing gain patterns and axial ratio for different steering angles in elevation plane at azimuth angle of 45^0. . Plot is cut at $\phi = 45^0$ 164

Nomenclature

Abbreviations

RFID	Radio Frequency Identification
DAS	Distributed Antenna System
TDM	Time Division Multiplexing
FDM	Frequency Division Multiplexing
ETSI	European Telecommunications Standards Institute
FCC	Federal Communications Commission
DAAS	Distributed Antenna Array System
EFIE	Electric Field Integral Equation
UHF	Ultra High Frequency
CP	Circular polarisation
LP	Linear polarisation
dBiC	antenna gain w.r.t CP isotropic antenna
pdf	probability density function
cdf	cumulative distribution function
EIRP	Equivalent Isotropic Radiated Power
TE	Transverse Electric
TM	Transverse Magnetic
ASIC	Application Specific Integrated Circuit

TDMA	Time Division Multiple Access
FDMA	Frequency Division Multiple Access
STDMA	Space Time Division Multiple Access
Tx	Transmitter
Rx	Receiver

Symbols

$\boldsymbol{E}$	Electric field
$\boldsymbol{H}$	Magnetic field
$\boldsymbol{J}$	Electric current density
$\boldsymbol{A}$	Magnetic vector potential
$\boldsymbol{F}$	Radiation vector
f	frequency
$\hat{\boldsymbol{r}}$	radial direction vector
d	distance
G	Antenna gain
P	Power
λ	wavelength
ε_r	dielectric constant
τ	Reflection coefficient
θ	elevation angle
ϕ	azimuth angle

Chapter 1

Introduction and Motivation

The general problem of identifying objects can be reduced to assigning unique IDs to the objects alongside extra associated information such as a name, colour, count, type and location. There exist several different identification methods for different objects used in daily life. These include number plates for cars, student ID cards and bar codes for general retail as shown in Fig 1.1.

Figure 1.1: General Identification examples for different objects

When the means of identification is radio waves, the technology has come to be called

Radio Frequency Identification (RFID).

RFID is a wireless technology used for automatic identification and data capture. It allows any object tagged with a transponder to be identified from a distance, and even provide environmental information such as temperature or pressure if the transponder or tag is equipped with an appropriate integrated sensor. The technology has found applications in numerous areas such as retail stock management, warehouse stock management, portal systems and real-time asset tracking. It is gradually replacing the incumbent barcode technology in these applications principally due to the fact that RFID can query a large number of objects simultaneously from a long distance without requiring line-of-sight. On the other hand, barcode identification requires line of sight, close proximity, and queries objects sequentially. This has led to RFID being adopted by many retailers especially for high value products, as barcode technology is still economically more competitive.

An RFID communication system consists of an RFID reader or interrogator and a tag or transponder [1] . The reader sends queries to the tag via a connected antenna, and receives a response from the tag. The tag, which is attached to the item to be identified, normally consists of an integrated circuit (IC) and a small antenna. The IC handles communication protocols, while the antenna enables data transfer through free space with the reader. The commands from the reader are backscattered by the tag with its ID and other information, a process known as backscatter communication. The RFID communication process is illustrated in Fig 1.2. More detail on the operation of RFID is given in chapter 2.

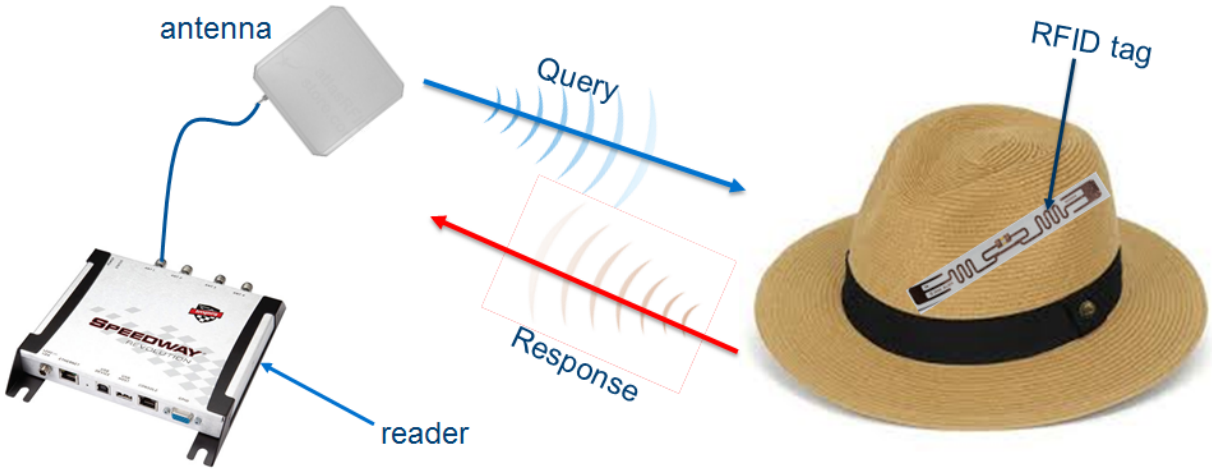

Figure 1.2: A passive RFID interrogation showing a reader interrogating a tagged object

RFID can be divided into passive, semi-passive and active RFID. The latter two both use external batteries at the tag, while passive RFID tags lack a power source and rectify the interrogating RF signal to power up its IC. As a result, passive RFID tags need relatively high activation power levels or sensitivity. The reader, on the other hand, is capable of detecting signals with relatively low powers. Consequently, the problem of getting power to the tag is much more challenging than that of getting power from the tag back to the reader for detection. A tag is therefore highly probably read if it receives sufficient activation power from the reader. A critical problem therefore in passive RFID is to optimise the downlink path. i.e deliver maximum power to the tags, with minimal reader and antenna resources. This dissertation seeks to address this problem using phased array antennas.

1.1 Introduction to the RFID Distributed Antenna System

The above setup involving a single RFID reader and antenna is sufficient for multiple tag detection in small physical areas, depending on the scattering properties of the environment. However, many retail and warehouse applications require the provision of coverage to tagged items over wide areas (wide area RFID), spanning hundreds or thousands of square meters. As a result, multiple readers and antennas are required for the provision of full coverage to the whole area of interest. A cellular approach is usually employed to divide the interrogation zone into cells, each covered by a unique reader. A significant problem in RFID is optimising and scheduling RFID reader transmissions in order to enable inter-operation of the readers to provide full coverage with minimal resources. This is the global RFID planning problem.

A related problem is that of maximising the size of each cell, while maintaining full cell coverage, called cellular planning. Each reader may be attached to numerous antennas in order to extend the interrogation area of the reader and maximise the size of the cell, while decreasing the number of readers required to provide full coverage. Cellular planning is therefore required to optimise the antenna radiation properties, positioning and orientations so as to maximise the power delivered to the tags, while maximising the size of the cell.

However, the use of multiple antennas leads to interference when more than one antenna transmits simultaneously. This causes blind spots in the cell. i.e. points of destructive interference, where tags cannot be sufficiently powered so as to be detected, leading to degradation of system performance, as the probability of detecting a tag is severely diminished. The deep blue areas in Fig 1.3 are points of destructive interference and potential blind spots.

The traditional solution to this problem is the use of an intracellular time division multiplexing (TDM) scheme, in which all antennas for the cell in question are assigned separate time slots in which to transmit [2]. In this way, the blind spots due to antenna-antenna interference are avoided since only one antenna transmits at any instant.

More recently, the concept of an RFID Distributed Antenna System (DAS) with phase diversity was introduced [3]. Here, the same signal is multicast to all transmit antennas, with each having a randomly varying phase shift. The effect of this is a changing interference pattern in the resultant field distribution, as the phases of the interacting fields are changing with time. This implies that positions of constructive interference and destructive interference (potential blind spots) are being moved with time. Because a tag read is dependent solely on the instantaneous power delivered, it is necessary only that each position (or tag) momentarily experiences constructive interference. As a result, the time cumulative power distribution pattern as seen by the tags in this system is far superior to that of a traditional TDM system, as all antennas are made use of, leading to much higher read accuracies being reported.

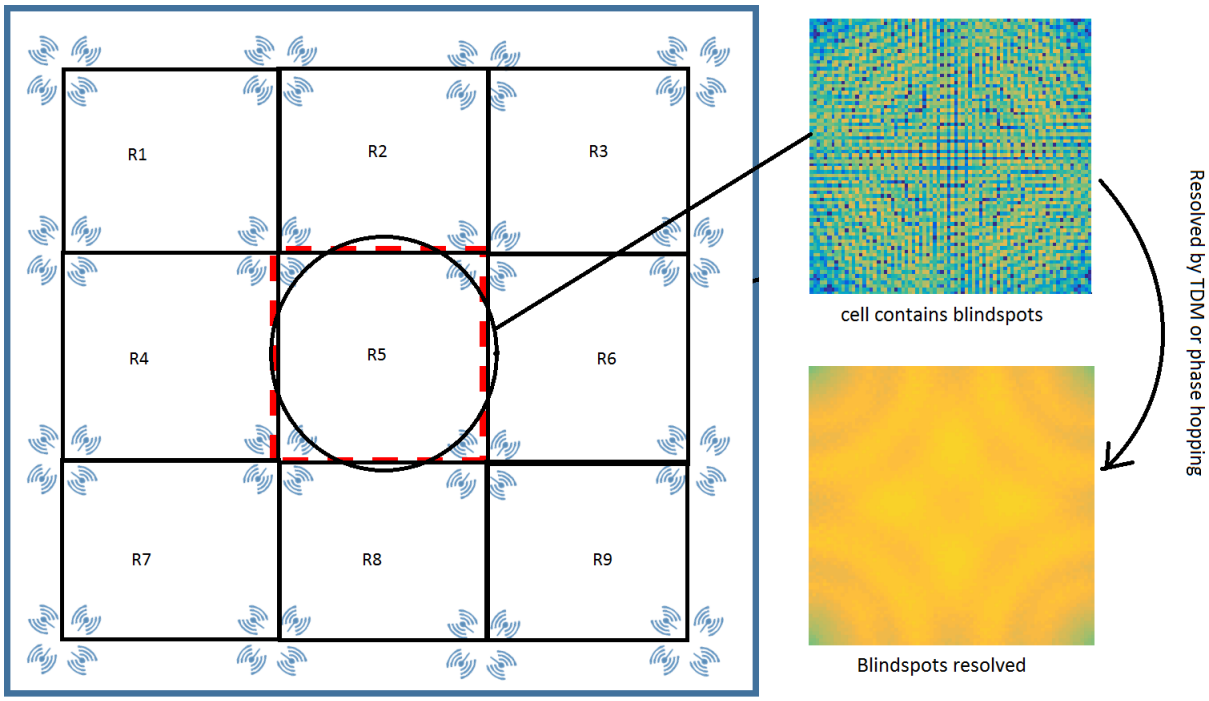

Figure 1.3: A typical four-antenna cell wide area RFID cellular system with nine readers ($R1 - R9$) assigned to nine cells. It is seen that the power distribution within the cell (insert) contains peaks and troughs due to the interference resulting from the four antennas. These can be resolved by TDM or phase diversity as shown.

1.2 The need for Phased array antennas in Wide Area RFID

A phased array antenna or antenna array is a network of collocated, inter-connected antennas, which work together in order to boost the radiation pattern of the whole over a single-element antenna in terms of gain and beam diversity. i.e., increased gain due to multiple antenna elements and beam steering from phasing. The array of antennas, each being excited by the same or a different signal amplitude and phase act as a single antenna with a modifiable far-field pattern. The beam can be steered electronically to transmit or receive maximally in a particular direction, while rejecting signals from some other directions.

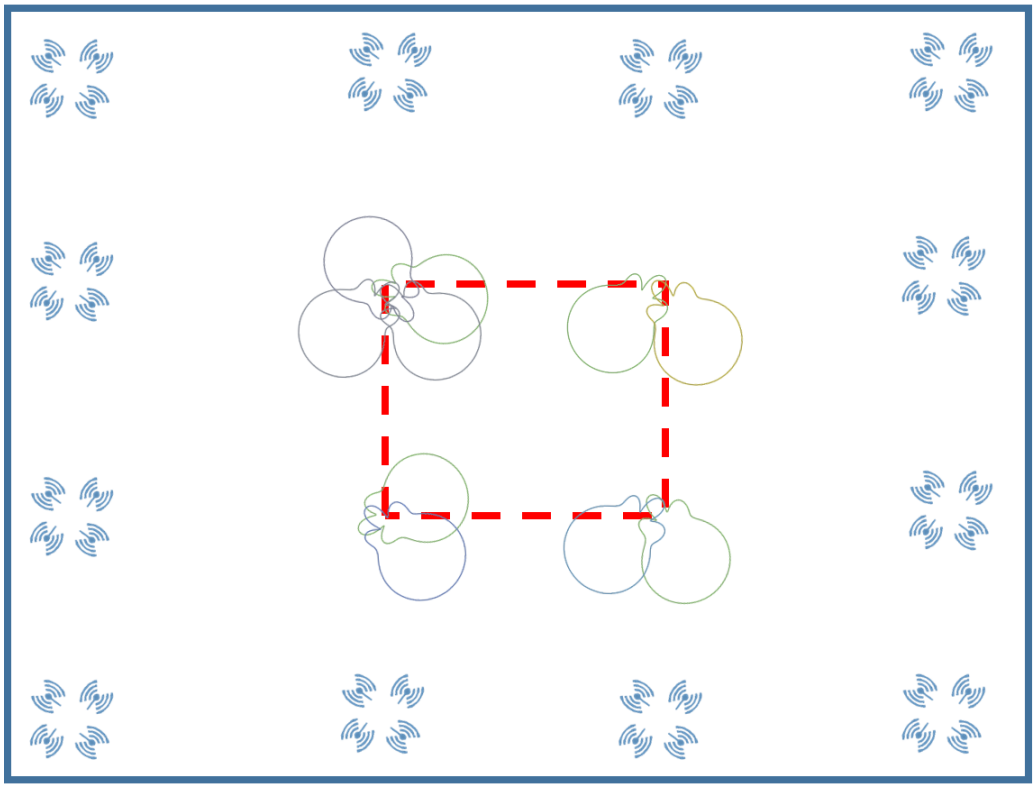

Figure 1.4: Envisioned distributed antenna array system, with antennas capable of scanning all surrounding cells, as a single antenna array can steer its beam pattern electronically, leading to reduced system complexity.

Several studies have been done on the use of phased array antennas for improving the read capability of RFID by using phased array antennas in isolation [4, 5, 6], as well as commercial systems such as the Mojix Starflex [7]. However, little has been done to apply phased array antennas to Distributed Antenna Systems in the context of wide area RFID. The aim of this dissertation is to extend the application of phased array antennas to the RFID Distributed Antenna System described above in order to obtain a more efficient wide area RFID system. As can be inferred from Fig 1.3, coverage of a large area divided into multiple cells will require a large number of antennas. The example presented is a rectangular arrangement and requires four antennas per cell, in a pattern repeated across the coverage area [8]. Due to the fact that antenna arrays can be used to perform beam steering, a single antenna could be used to address multiple cells, as seen in Fig 1.4. As a result, a single phased array antenna could replace several fixed antennas, thereby reducing the overall system complexity. Such a solution could provide a more efficient implementation of the RFID DAS system. This dissertation explores the use of

such distributed arrays to maximise the power delivered to the tag in a wide area setting. Furthermore, due to beam steering, different multipath channels are available, which will provide a higher signal integrity compared to a fixed antenna system.

Finally, because steerable antennas can be made to maximise transmission in an arbitrary direction, the fixed, cellular approach to wide area RFID is made redundant. This instead opens up the possibility of designing wide area RFID systems which use tag location-targeted inventories, rather than inventories based on cells allocated to particular reader and antennas. The cellular system uses a fixed reader allocation scheme as shown in Fig 1.3, in which a fixed number of antennas is assigned to a particular cell. The steerable beam pattern of antenna arrays allows for a system in which all the antennas are made to cooperatively maximise the power delivered to the tags at a particular location. This opens the way to massive reductions in antenna count as each location is queried by all antennas, rather than a fixed reader-assigned number.

An additional implication for such a system is a simplified space division multiplexing solution to the reader collision avoidance problems in RFID. Because the antennas are centrally controlled, which all contribute to tag detection in the entire interrogation zone, complex reader frequency and time allocation algorithms for reader interference mitigation could be avoided. For these reasons, the application of antenna arrays in wide area RFID is worth studying.

1.3 Outline and Contributions

This dissertation is structured as follows:

Chapter 2 contains relevant background information about RFID and phased array antennas, and the literature associated with the problems of wide area RFID.

In Chapter 3, a new RFID propagation model is presented, which is capable of simulating multi-antenna RFID systems in multipath environments. The model makes use of electric field interactions between antennas to obtain the power received by one antenna due to radiation from one or more other antennas. The use of realistic antenna radiation patterns for both the tag and the reader antennas using full wave simulation models or measured antenna patterns means that, unlike previous models, several real-world parameters such as polarisation and antenna orientations are intrinsically modelled. The model

is validated against Method of Moments Simulations from commercial package-FEKO. Several test cases are also presented from popular application examples, and important observations are presented. Using multiple antennas, a time division multiplexing scheme, phase hopping, frequency hopping are investigated. The best and worst tag locations are identified based on their orientations, and effective system planning is therefore possible. The model provides a useful tool for studies in the following chapters on multiple phased array antenna systems by allowing rapid evaluation of the performance of antennas with different properties.

Chapter 4 describes the design of a phased array antenna for use in experiments in the rest of the dissertation. Based on discussed requirements and constraints, a 2×2, 10 dBiC, circularly polarised antenna array is designed with steer-ability up to 360° in azimuth and 45° in elevation, and characterised as well. The second part of the chapter uses two phased array antennas to investigate different antenna multi-casting methods for interrogating RFID tags using phased array antennas. Three different methods are compared experimentally: Beam steering with (1) Time Division Multiplexing, (2) simultaneous transmission and no phase dithering and (3) simultaneous transmission and phase dithering. It is shown that a theoretical 2dB of additional tag received power can be obtained using simultaneous transmission with phase dithering over the TDM scheme, and 1.2 dB over the case without phase dithering. This will lead to potential increased interrogation areas with the same tag detection rate and number of antennas. Experiments conducted showed an 8% increase in tag detection over the case without phase hopping, and a 20 % over the TDM scheme. Simulations with more antennas show that increasing the number of antennas increases the advantage of simultaneous transmit systems over the TDM system, but the phase dithering advantage does not increase.

In chapter 5, a distributed system of phased array antennas, called Distributed Antenna Array System (DAAS), is designed and demonstrated. First of all, a primer experiment comparing a standard fixed antenna and a phased array antenna interrogating a given tag population is performed, and the array is shown to detect up to four times as many tags as the fixed antenna. Further to this, a single cell of four distributed antennas is demonstrated: A fixed DAS and an array DAS (DAAS), of four antennas each, are compared. It is shown that with the array system, the required number of antennas could be decreased by a factor of four, with a slight increase in antenna separation, thereby greatly reducing

the complexity of wide area RFID DAS systems. A method of boosting the power delivered to the tag during scanning is presented. This is achieved by compensating for the decrease in antenna gain due to beam steering by increasing the conducted power into the antenna. and in this way the overall power delivered to the tag is increased. Further to this, a single port distributed antenna array system is also presented, whereby the RFID signal and control signal for the antenna array are carried along a single coaxial line, thereby greatly reducing the complexity of the system. This makes it possible to obtain a DAS system with a standard single port RFID reader, which previously required specialised multi-port readers.

Chapter 6 explores the limits of distributed antenna array systems for RFID by considering a cooperative raster scan of several antennas. We consider the ideal case of a perfect antenna array, unrestricted by limited scanning angles of designed antennas, and evaluate the theoretical limits of the separation that can be achieved between antennas, and maintain a performance equal to that of a fixed system. It is shown that, depending on the tag orientation, a system of individually perfectly steerable antennas could lead to an increase of up to 2.5 times in antenna separation over a fixed system ie $> 6\times$ the area, while allowing a four-fold antenna count reduction for large cells. The system is also characterised in terms of decreasing steering angles to determine design criteria for practical antennas. It is found that with a steering angle of 75^0, a similar performance is achievable to a perfectly steerable system under certain conditions. Finally, the concept of a cell-less or non-cellular wide area RFID system is introduced, in which, rather than assigning antennas to particular cells, all available antennas are used to scan a desired tag location and boost tag received power. It is shown that antenna separations of up to six times that of the fixed cell systems is achievable, while allowing a four-fold antenna count reduction.

Chapter 7 is the closing chapter, in which conclusions are made and recommendations are suggested for future work in the field.

Chapter 2

Background and Literature

This chapter presents the background material and literature review on concepts covered in this dissertation. The first section gives background information on RFID. The second section presents problems and attempted solutions to the problems of wide area RFID. The third section covers phased array antennas, and up-to-date applications in RFID.

2.1 Background on RFID

2.1.1 A Brief History of RFID

The early history of RFID is closely related to radar, as both involve communication by backscattering of electromagnetic waves from a target. Although originally suggested by Maxwell, it was Hertz (and later on Marconi), who first showed that metals reflected radio waves [9]. This concept was used by Christian Hulsmeyer in 1904 for avoiding collisions by detecting reflections from nearby ships [10]. RFID, however, or backscatter communication, really took effect during the second world war, when reflected waves were used to identify enemy aircraft by the allied powers (the so-called Identify, Friend or Foe or IFF), and during which period, much of the developmental work in radar was done [11, 12]. The applications were nonetheless mainly for military purposes, until the 1960s, when fundamental research into what would become RFID was conducted by several different labs, noteworthy amongst which are R.F Harrington's loaded scatterers [13] and J. H. Vogelman's Radar echoes [11]. From the 1970s, much developmental work into RFID was performed mainly for the purposes of animal and vehicle tracking, as well as automation. Also, the explosion in CMOS technology led to the shrinking size and large scale man-

ufacture of tags, which hitherto, were made of discrete components [11]. This led to a wide adoption of the technology, as it became more cost-effective. The 1980s saw the application of RFID to practical problems such as animal tracking, industrial control and toll collection. The 1990s saw large scale implementation of RFID, and the involvement of many commercial players in the market for a plurality of applications, which led to various attempts at industrial standardisation, and standards such as the ISO 18000 and EPC Global RFID standards were born [14]. A concise history of RFID development in the 20th century has been documented by Landt [11].

The 21st century has seen the adoption of RFID into everyday life, as significant investment by Walmart and other retail giants to replace their barcode identification technology with RFID gave the technology, which was then in the early adoption stage, a significant vote of confidence [14]. As RFID systems began to be more widely deployed in the early 2000s, the deployment of multiple readers for wide area coverage and the associated problems were extensively studied. This led to an increase in research effort to solve the problems associated with multiple reader interrogations, thereby leading to various anti-collision algorithms being developed. The late 2000s and the 2010s have also seen some significant developments in RFID, such as sensor-integrated RFID tags, the development of passive compute platforms on RFID tags, chip-less RFID tags and smart RFID systems. The technology has today formed a multi-billion dollar industry, and in 2018 alone, more than 15 billion UHF RFID tags were sold [15]

The reasons for the rapid adoption of RFID can be understood from its numerous advantages over the barcode. First of all, RFID does not require line of sight in order to communicate, as it uses RF technology rather than optics of barcode technology. It also enables identification over a longer distance, with up to 10 m of range being possible, as compared to close proximity of a few inches for bar code identification. Coupled with other advantages such as increased counterfeit immunity, faster identification rates, higher tag memory, many simultaneous reads and low human oversight, the continuing reduction of the cost of mass manufacture of integrated chips has accelerated the wide adoption of RFID technology [16]. This has been complemented by the emergence of the Internet of Things (IoT), of which RFID is a major component, as readers are connected to the network, enabling the global identification and tracking of objects in real time [17].

2.1.2 RFID Operating Principles

Three categories of RFID can be identified based on their power requirement- passive, semi-passive and active. Active RFID tags are powered by batteries, are usually more expensive, and so are used on high-value items. They are capable of self-broadcasting their IDs and of long distance communication, up to hundreds of meters.

Semi-passive tags contain a battery source, but do not initiate communication. The battery is used only when a communication session has been launched. Solar tags could also be included in this category.

Passive tags are battery-less and powered entirely by the interrogating signal from the reader. These are of particular interest as their low cost enable them to be the most economically competitive. Depending on the application, passive RFID is divided into several frequency bands of operation, as summarised in Table 2.1. Electromagnetic waves

Band	**RFID Frequency**
The Low Frequency (LF) band	134 kHz
The High Frequency (HF) band	13.56 MHz
The Ultra High Frequency (UHF) band	860 - 960 MHz
The Microwave band	2.4 GHz

Table 2.1: Main RFID Frequency bands

of these different bands vary in properties, which dictate the applications of the corresponding RFID technologies. The LF and HF bands work on the principle of inductive coupling, and are short range as a result. LF signals are capable of penetrating water, salt, tissue and even metal, achieving better performance in these than in air. As a consequence, they are used for animal tagging. They are also used for access control in buildings, as the short range ensures some security. HF tags are also short-ranged, but are capable of higher rates (tens of kbps). They are used in contactless payment and access control.

UHF and microwave tags on the other hand operate by radiative transfer, and provide long read ranges of up to 10 m. They also provide comparatively high data rates (hundreds of kbps). UHF tags operate in the $860 - 960$ MHz range (the exact band depends on geographical region), which is tightly regulated, as it may interfere with other com-

munication services. However, it offers longer ranges than microwave tags which operate in the $2.4 - 2.45$ GHz unregulated band.

The focus of this work is on passive UHF RFID, and all subsequent discussion is based on this, unless stated otherwise.

Passive UHF RFID Operating Principles

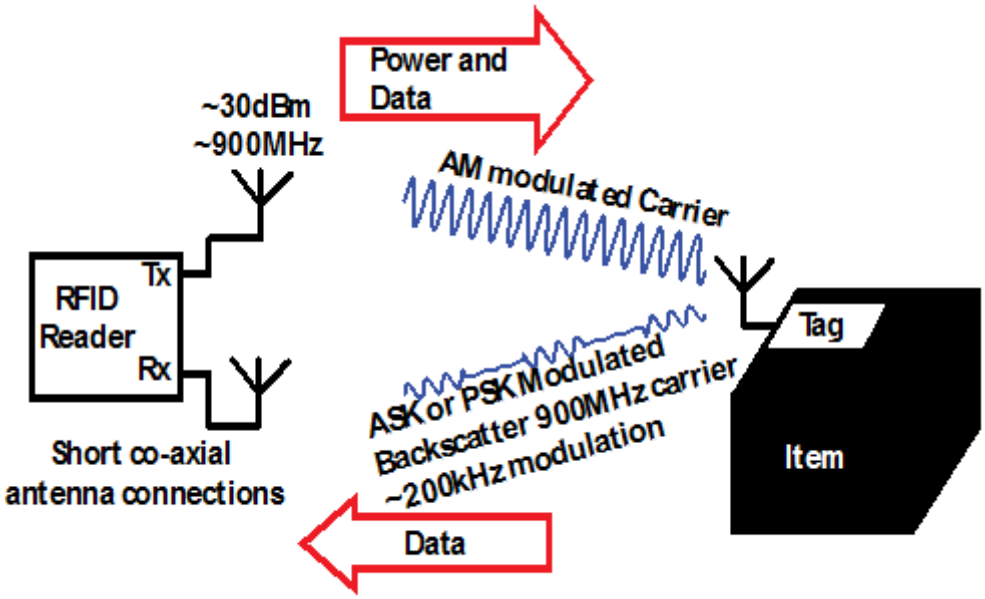

Figure 2.1: Working Principle of UHF RFID

A passive UHF RFID system consists of a reader (interrogator) and a tag (transponder). The tag is attached to the object which needs to be identified or tracked. The reader is connected to an antenna, through which queries from the reader are transmitted to the tag via radiation. In the reverse link, the antenna also transduces the received backscatter signal from the tag to the reader for processing. The tag responds with its uniquely assigned ID, as well as other associated information. The response from the tag is based on load modulation, whereby the tag's antenna-to-chip impedance is modulated with the response, which in turn modulates the backscattered signal. Fig 2.1 illustrates the operating principle of an RFID system. The system can be arranged in either a monostatic or bistatic mode. The monostatic configuration uses a single antenna for both transmission and reception, and an isolator (directional coupler or circulator) to isolate the two paths. The bistatic configuration uses two separate antennas for transmission and reception.

For a tag to be read, two conditions must be satisfied. It must (i) receive from the reader

sufficient power to activate its internal circuitry (threshold power) and (ii) backscatter sufficient power to the reader above the reader's sensitivity. Most commercial tags have threshold power of ~ -15 to -20 dBm, and readers typically have sensitivities of ~ -82dBm (monostatic) to ~ -90dBm (bistatic).

Consider the example of trying to detect an RFID tag with using a reader transmit power, say 27 dBm. Using a reader antenna of gain $G_t = 8$ dB, and a tag of gain $G_r = 2$ dB, the range for the down link using the Friis free space equation is $d = \sqrt{\frac{P_t G_t G_r}{P_s}\left(\frac{\lambda}{4\pi}\right)^2} \approx 16m$ for a tag sensitivity of $P_s = -20$ dBm (assuming free space propagation only and a frequency of 866 MHz). The reverse link range for a reader with sensitivity of -82 dBm will be $\sim 88m$. This shows that the UHF RFID channel is downlink limited. i.e the problem of getting sufficient power to the tag is much harder than getting the tag response to the reader. It can safely be assumed therefore that a tag will almost certainly be read if it receives above-threshold power. Getting sufficient power to the tag is therefore of paramount importance, and this dissertation is focussed on downlink tag power delivery.

UHF RFID Readers RFID readers or interrogators are responsible for synthesising the RFID signal and all processing of received tag responses. A typical reader architecture is shown in Fig 2.2.

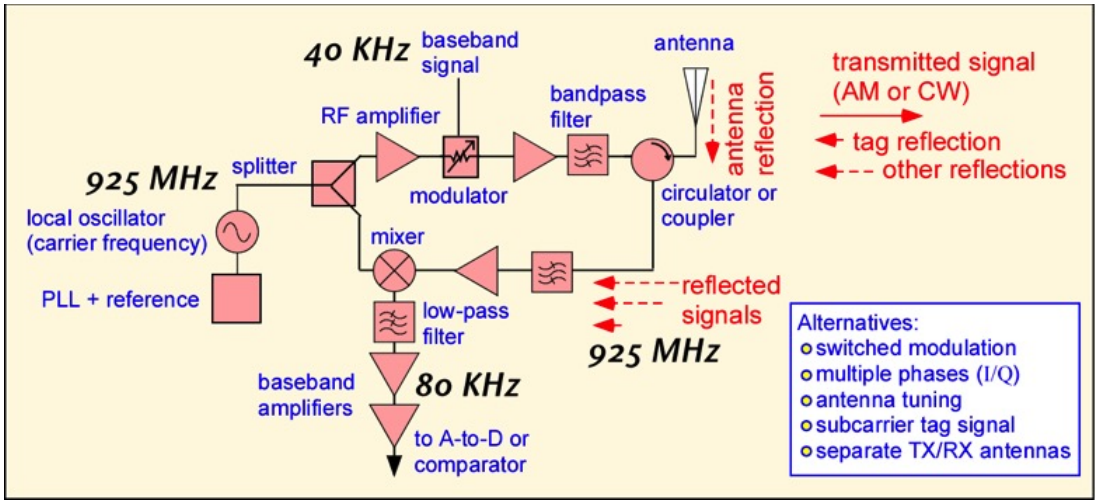

Figure 2.2: Block diagram of a monostatic RFID reader [1]

The reader generates the RF carrier signal and modulates it with the base band signal ($\sim kHz$) for transmission to the tag. In the reverse direction, it also receives the modulated backscatter signal from the tag to extract the tag's information. Important design objectives for RFID readers include quick read rates and high sensitivity.

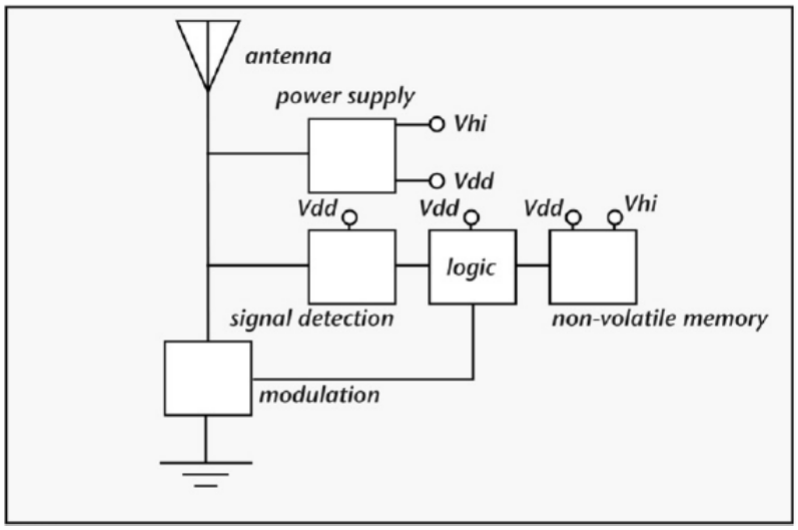

Figure 2.3: Components of a UHF RFID tag [1]

UHF RFID tags UHF RFID tags are battery-less and operate by backscatter modulation. i.e the incident signal from the reader is modulated with the tag's response and scattered back to the reader. The tag comprises two main components: an Application Specific Integrated Circuit (ASIC) and tag antenna. A block diagram of a typical tag ASIC is shown in Fig 2.3. The main components of the tag IC include a power-harvesting circuit, which converts incident RF signal into DC power. The IC typically needs about 1-3 V and a few microamps to tens of microamps of current [1]. The voltage requirement is satisfied by employing a voltage multiplier circuit, typically composed of a number of diodes in series. The second component is a communications circuit for modulating, demodulating and implementing the required protocol . Finally, there is a load modulation circuit to allow backscatter modulation of the received signal [18]. Backscatter communication is done by the tag presenting a modulated antenna-to-chip impedance to the incident signal. The modulation format could be ASK (in which the real impedance is modulated) or PSK (in which the reactance is modulated). Modulating the amplitude implies no power is absorbed in one of the states, and as a result, PSK modulation delivers more power to the tag. For the tag antenna, a compromise between size and gain is made. The length of a half-wave dipole at 900 MHz is 16cm, which is too long for most applications. Compromise designs such as meandered dipoles are used to shorten the antennas, albeit with reduced gain as well.

2.1.3 Recent Developments in RFID

The 21st century has seen several advancements in the development of RFID technology. As the technology has become ever more widely deployed, research has been carried out to improve its performance. The maturity of the microelectronics industry has permitted the development of tag ASICs in compact forms, cheaply manufactured. Developments in other fields such as Micro-electro-mechanical sensors (MEMS) and low power solid-state sensors has permitted the integration of these sensors unto RFID tags, thereby enabling the sensing of several environmental factors in addition to item identification. i.e. sensor-integrated tags. The most common have been temperature [19], gas [20], humidity [21], bacteria in food [22], strain [23] and spectral fingerprints [24].

Another significant development in the past decade has been the development of passive microcontroller-integrated tags, allowing simple computations to be performed in real time. An example is the Wireless Identification and Sensing Platform (WISP), a general purpose 16-bit microcontroller, which follows the RFID Gen2 protocol [25]. This has led to some compute-intensive applications being done on RFID tags, including motion sensing [26], self-localising UHF RFID cameras [27], cryptography [28], passive data logging [29], as well as indoor acoustic localisation [30]. The main problems with these are their low duty cycles due to the high power requirements, and the inflexible and bulky structure.

In a drive to further reduce the cost of RFID, chip-less tags have been developed, as the IC costs greatest in an RFID tag [31]. Chip-less tags depend on the physical structure of the tag to produce a unique electromagnetic signature, and therefore require no IC. They can be divided into time domain and frequency domain tags. Time domain chip-less RFID is based on the delay signature of the pulse reflected from the tag [32, 33], while frequency domain chip-less RFID is based on the spectral signature of a multi-resonant structure [34, 35].

2.1.4 Standards and Protocols

The explosion in adoption of RFID necessitated, as in all communication interfaces, the establishment of standards and protocols in order to enable interoperability among different manufacturers. The latest RFID global standard is the EPC UHF Gen 2v2 or ISO / IEC 18000-63 [36], and regulates implementations of UHF RFID. The communication protocol is outlined in Fig 2.4. Reader functions include singulation, inventory, reading

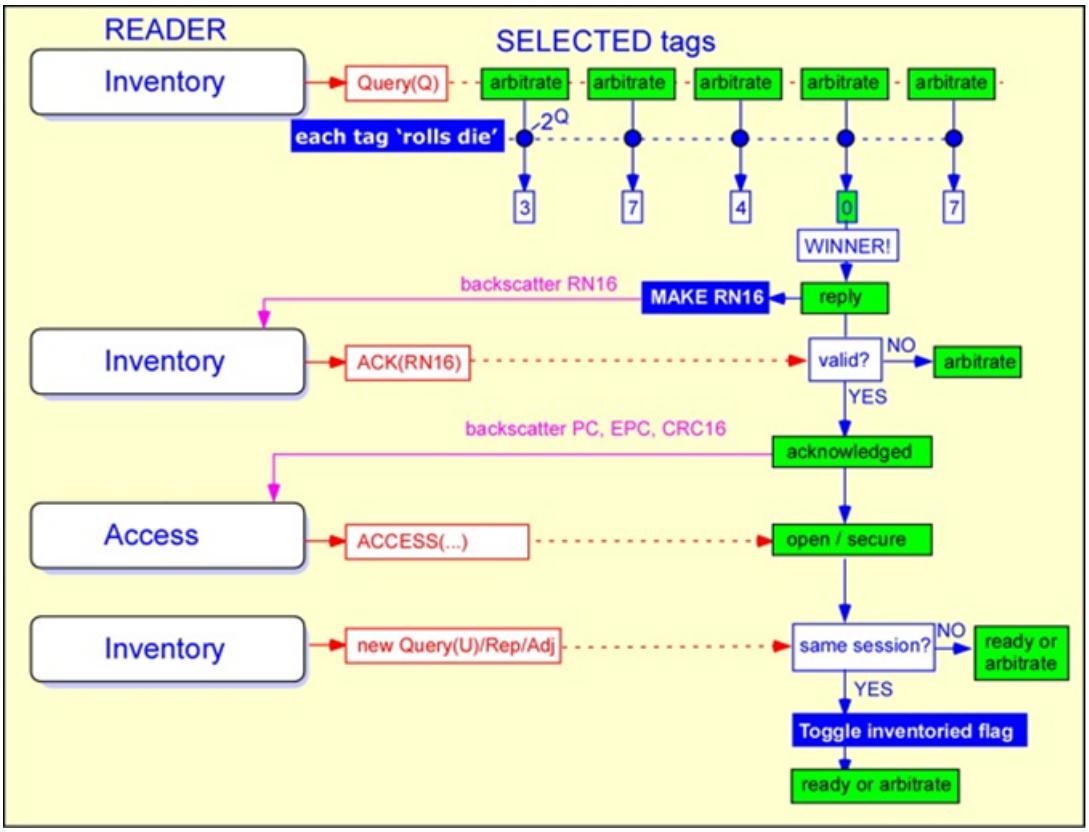

Figure 2.4: Protocol description [18]

and writing. The different actions follow a similar series of steps to access a tag summarised in figure 2.4. First, the reader sends a query with a random integer, Q. Each tag that receives this query responds with a random number between 0 and $2^Q - 1$ (RN16). The tag that picks a zero replies first, and after every cycle, each tag random number is decremented by one, until all tags have replied. The replying tag receives an acknowledgement from the reader. If the acknowledgement is valid, the tag replies with its Electronic Product Code (EPC), alongside a CRC number. Fig 2.5 shows an example of an RFID query session.

Two modulation formats are specified by the protocol standard- FM0 and Miller Modulation Subcarrier (MMS) as shown in Fig 2.5. FM0 represents a 0 by a high to low transition, and a 1 by keeping the voltage constant. MMS is achieved by multiplying the FM0 signal by 2,4 or 8 square waves for each symbol. This reduces the data rate by the corresponding amount, but shifts the energy spectrum of the signal away from the carrier, thus enabling better detection in the presence of phase noise [18].

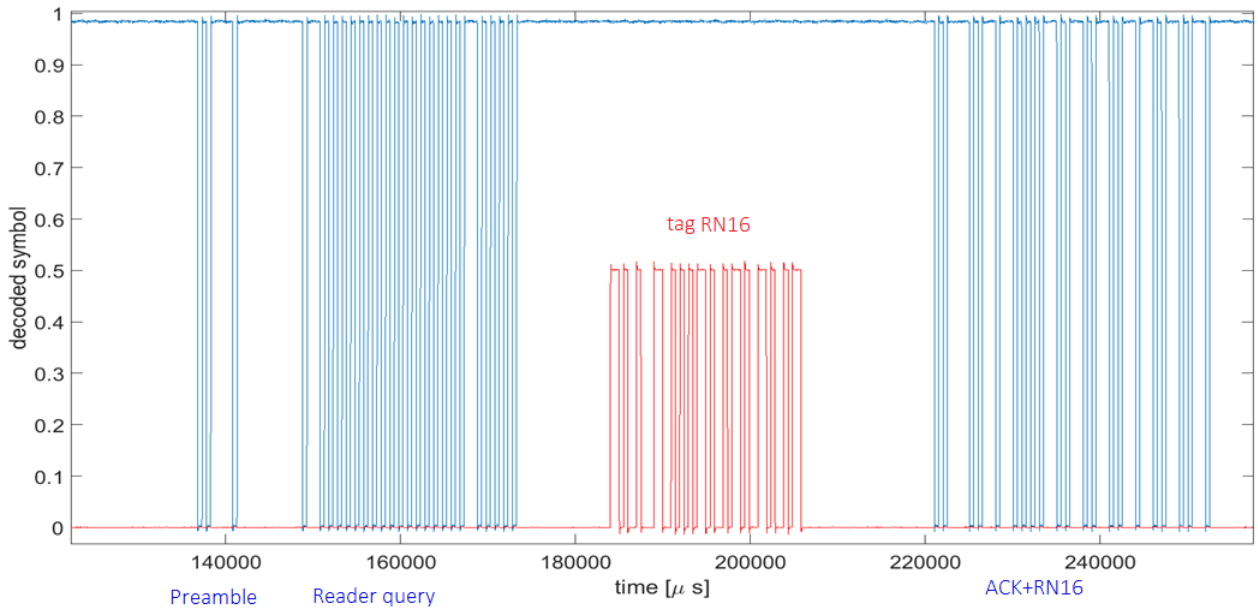

Figure 2.5: Example of an RFID query with reader query, tag RN16 , and reader acknowledgement of RN16.

RFID regulations vary worldwide, but for the purposes of this work, the European regulations [36] have been followed, unless otherwise specified. The standard specifies two frequency bands. The original $865 - 868$ MHz band specifies a maximum Equivalent Isotropically Radiated Power (EIRP) of 2W, and has been used throughout this work. The more recent frequency band $915 - 921$ MHz was added during the research stage of this work, and specifies a maximum EIRP of 4W. The principles used throughout this dissertation also apply nonetheless.

2.2 Problems in Wide Area RFID and proposed solutions

Initial RFID applications were all based on hand-held readers and portal systems, in which the relative motion between the reader and tags could be relied upon to allow detection of tags in areas with unfavourable geometry or to overcome problems of multipath. This is a result of a human agent moving and scanning the tags on a shelf for example. For large area applications (e.g in warehouses), the labour cost becomes excessive, and automated solutions are necessary, thus the emergence of ceiling mounted antennas and readers. This new development comes with a number of challenges.

First, ceiling mounted antennas are fixed, and as a result, the separation between the antennas and tags is fixed. Therefore, their relative motion can no longer be relied upon to overcome multipath. This leads to the problem of fading in fixed RFID systems.

Second, wide areas make use of multiple readers and antennas, which increase the overall cost and complexity of installation and maintenance. Therefore, reducing the reader and antenna density while maintaining good read accuracy is a necessity. This requires careful optimisation, and leads to the problem of network planning in wide area RFID.

This section covers both problems: network planning and fading problems in wide area RFID

2.2.1 RFID Network Planning

As has been stated above, wide areas require multiple readers to provide full coverage. The interrogation zone is usually divided into cells, with each cell allocated to a specific reader as in Fig 2.6. Effective network planning is therefore required to obtain an efficient implementation for cell allocation so as to ensure smooth running of the system. Two principal RFID network optimisation problems can be distinguished: Global planning and Cell planning.

Global planning

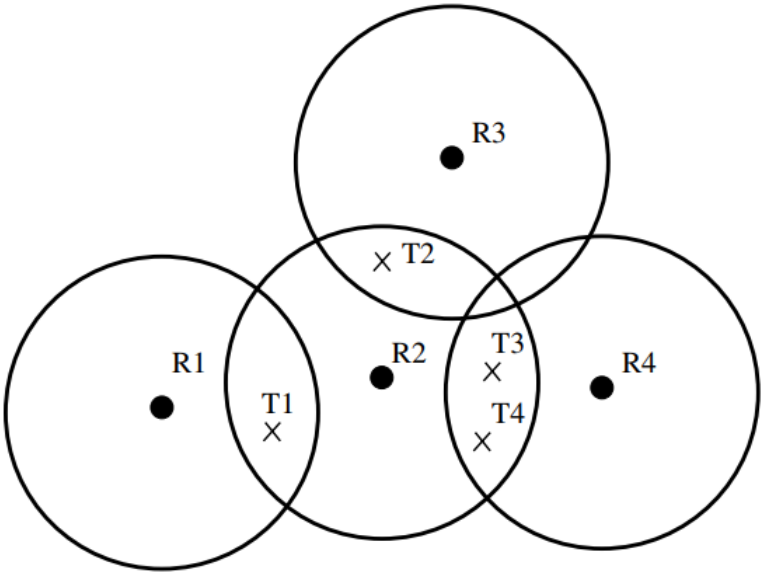

Figure 2.6: Reader Collision avoidance. Source: citeDobkinweb

Global planning is involved with the global RFID network deployment and aims to *Optimise network performance with the minimum set of readers.*
Network performance is defined in terms of different factors.

(i) Global tag coverage

The most important performance criterion for an RFID system is the coverage. i.e every tag in the interrogation zone must be able to receive enough power to activate its internal circuitry, and backscatter a response which can be detected by the reader. For a tag to be covered it must be able to receive power above its threshold power from at least one reader, and also be able to backscatter enough power to the same reader, which is above the reader's sensitivity. The threshold power of a tag is the minimum amount of power required by the tag in order to activate its internal circuitry and trigger a response. For most passive tags, this value is ~ -15 to -20 dBm, depending on the operation being carried out on the tag. The sensitivity of a reader is the minimum amount of power backscattered from an RFID tag that must be received by the reader for a tag to be detected. As has been demonstrated in the previous section above, due to the asymmetry of the RFID channel, it is necessary only that the tag receives above-threshold power to

be considered detected.

In a multi-cell or multi-reader network, the coverage of a reader is the subset of the tag space for which the reader in question delivers above threshold power. Tag coverage planning ensures that each tag is covered by at lest one reader. i.e. for each tag, there exists at least one reader which can deliver enough power to activate it.

Satisfying this condition alone does not result in an efficient system implementation, as it could so happen that a single tag is covered by multiple readers, thereby rendering some of the readers redundant. This leads to the problem of optimal coverage, whose aim is to minimise the number of readers required to provide full coverage for the interrogation area. For example, only Reader $R2$ in Fig 2.6 is required to provide full coverage, rendering all other readers ($R1, R3,$ and $R4$) redundant. This leads to an inefficient system, as more readers than required are used, reader anti-collision policies are needed, and redundant tag reads are reported.

In the context of providing optimal coverage, the problem of redundant reader elimination has been extensively studied in mobile ad-hoc wireless RFID networks, where the minimum set of readers are required to be operating at any given time. Attempted solutions to the problem have included centralised solutions, which use a central server with global knowledge of the system [37]. Less efficient decentralised solutions to the problem are usually stochastic, and $\sim 70\%$ as efficient as the centralised solutions [38, 39, 40, 41, 42]. This dissertation is focussed primarily on fixed multi-cell RFID systems, and these are generally not applicable.

(ii) Interference and Collision Problems

Another important consideration for planning RFID systems is collision. The problem of collisions has been extensively studied in the context of wide area RFID, and could be classified into tag and reader collisions. Tag collisions are discussed in the next section in the context of cell planning.

Reader Collisions Reader collisions occur between multiple simultaneously transmitting readers, and can be divided into two main categories: Multiple reader-to-tag and reader-to-reader collisions.

multiple reader-to-tag collisions occur when a tag is in the interrogation zone of multiple readers, and is interrogated by more than one reader simultaneously. As a result,

the tag receives a distorted signal resulting from the interference of signals from the interrogating readers. This occurs because the interrogation zones of RFID readers in a wide area system are usually not disjoint, e.g., readers $R2$ and $R3$ in Fig 2.6. Therefore, tags could be found in the intersection of the coverage zones of more than one reader, leading to a severely degraded probability of detection of the tag by any of the readers.

The difficulty in solving this kind of collision lies in the fact that the tag is of limited functionality, and cannot differentiate between frequencies, but rather responds to all interrogation signals without discrimination.

The second class of reader collision is **reader-to-reader or inter-cell or inter-reader interference**, which occurs when a reader's transmission interferes directly with the communication of another reader, thereby degrading its tag read probability. If two readers R_1 and R_2, separated by a distance of $D(R_1, R_2)$ have a radial range of d_1 and d_2 respectively, then an inter-reader collision will occur if $D(R_1, R_2) < d_1 + d_2$. This could occur even when tags are not in the interrogation zone of multiple readers. Several solutions are employed to resolve reader collision problems. The solutions could be divided into two main categories: scheduling and control-based methods.

Scheduling methods involve the allocation of resources, mainly time (Time Division Multiple Access, TDMA) [43, 44] and frequency (Frequency Division Multiple Access, FDMA) [45] to readers, so as to enable collision-free communication. However, in a dense network of readers, the efficiency of a TDMA solution is degraded, as the average read time for each reader is limited. Similarly, few channels generally available for RFID render FDMA an ineffective solution to the problem. Combined FDMA/TDMA has been used to solve the problem [46]. This is akin to the well-studied Radio Allocation Optimisation Problem, and has been solved by several optimisation algorithms [47].

Spatial separation of readers in order to minimise the overlap of their coverage zones is another solution to reader collisions. This has been applied in Space Time Division Multiple Access (STDMA), in which knowledge of the spatial distribution of readers is used to enhance the efficiency of time and frequency allocation [46]. e.g if it is known that $R1$ and $R3$ are separated enough to avoid interference, they can be assigned the same frequency and time slots.

Control-based methods use dynamic control of the reader transmit power to dynamically adjust the coverage zones of readers, thereby allowing potentially interfering readers

to detect tags [48]. The requirement for reader synchronisation makes this impractical for large networks.

In addition to the above specific solutions to the collision and interference problems in RFID networks, RFID network planning has been approached from a more general standpoint of trying to optimise the different parameters, taking into account the coverage, collisions, optimal tag allocation, as well as other factors such as load balancing (even tag distribution among readers) and energy efficiency requirements. A global cost function is defined as a weighted sum of the mentioned parameters and optimised. Several stochastic algorithms have been used to address the problem of RFID network planning and cell allocation in this way, such as particle swarm optimisation, genetic algorithms, bee foraging algorithms, plant growth simulation algorithms [49, 50, 51, 52, 53]. Sicheng et al. presented a deterministic optimisation procedure based on multi-cell systems for the signal to interference ratio as cost function [54].

Cell planning

Whereas global planning is concerned with the global tag population, cell planning is concerned with optimisation within a cell. This is done at the level of the antennas and involves the design of the antenna patterns, the placement of the antenna with respect to the tags, their relative orientations, as well as considerations for tag polarisations.

Furthermore, modern RFID readers provide multiple RF ports for multi-antenna support in order to maximise the coverage zone of an individual reader, leading to a Distributed Antenna System (DAS). Planning and optimisation is required in order to obtain the best relative positions and orientations as well as suitable multiplexing schemes to avoid interference. Accurate models are therefore necessary for predicting the performance and planning for RFID systems. These are reviewed in Chapter 3.

Two major types of collisions can be identified in an RFID system at the level of cell planning.

(i) Tag collisions

Tag collisions occur when multiple tags attempt to respond the broadcast signal of a single reader simultaneously, leading to interference among the different tag signals, and

difficulties in resolution at the reader. This occurs when multiple tags are activated simultaneously by a single reader. Attempted solutions involve ALOHA and slotted ALOHA algorithms [55], recursive tree-based traversal of tag binary IDs (Tree Walking Algorithm) [56] and binary tree splitting schemes [57]. Some RFID network planning optimisers have been presented which take into account the gain pattern of the antennas and tags, and seek for example to maximise coverage in a given interrogation zone [58]

(ii) Antenna-antenna interference

Intra-cell collisions or antenna-antenna interference or collisions occur in a single multi-antenna cell of a multi-reader RFID system (see Fig 2.7) when multiple antennas are transmitting simultaneously. Because the reader operates at a single frequency, all connected antennas also transmit at the same frequency, and therefore interference occurs between them. This leads to peaks and troughs in the power distribution of the interrogation area, caused by constructive and destructive interference. When the destructive interference is below the threshold power of the tag, the region is said to be a blind spot, where a tag cannot be read.

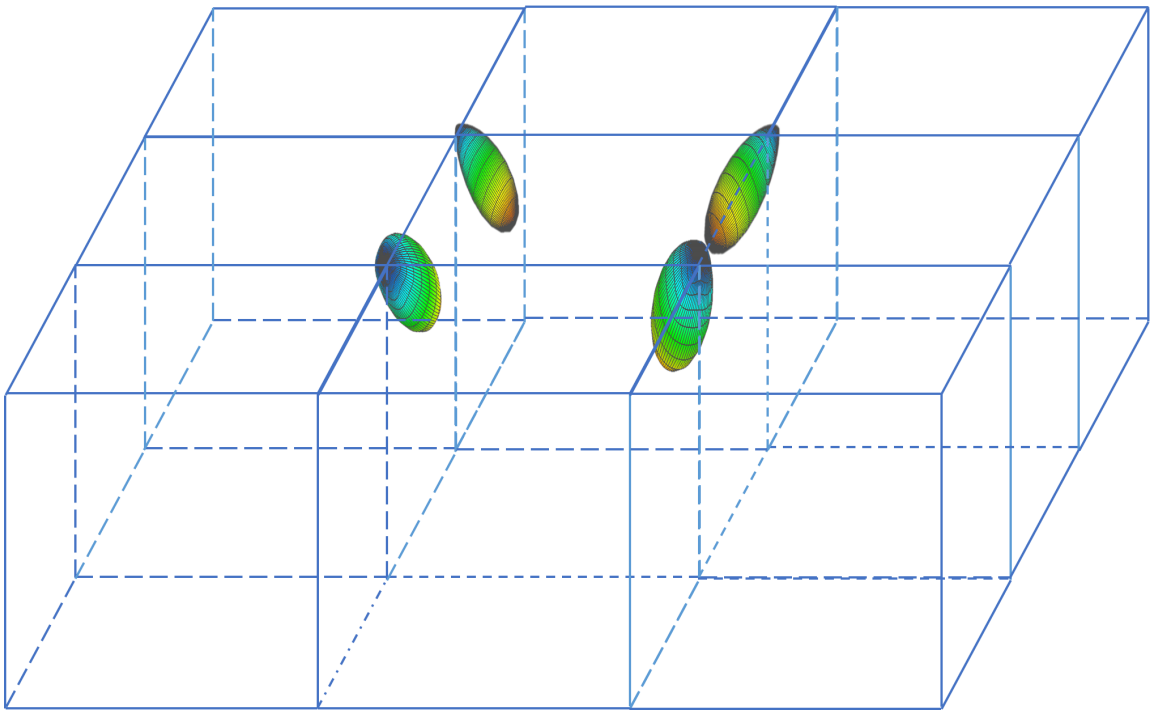

Figure 2.7: A wide area RFID interrogation volume divided into multiple four-antenna rectangular cells. Antennas are shown only for one cell

Several multiplexing schemes have been implemented with distributed antennas in order to resolve interference. Most common amongst them is the Time Division Multiplexing (TDM) scheme in which antennas are allocated disjoint time slots during which to transmit. This prevents simultaneous antenna transmissions, and therefore interference is eliminated between antennas. TDM is a selective combination diversity scheme, and has the effect of selecting the the antenna that maximises the power for each tag. The downside with this is that maximum use is not made of the available antennas, as only one antenna is required to power up a tag.

The Distributed Antenna System (DAS) with phase diversity has been used to overcome this problem [3]. Phase diversity is a diversity combining technique, as the fields from all the antennas are summed at each tag, and therefore significant improvements are possible. Here, all antennas are set to simultaneously transmit with a random time-varying phase shift applied to each. This leads to a temporal variation in the power distribution pattern in the interrogation area. As a result, the dead spots described previously (points in the room which receive less than the tag threshold) are moved around as the phase is dithered. Similarly, points of constructive interference are also moved around. The result is that each tag momentarily experiences constructive interference. Improvements of up to 40% over the conventional TDM system have been reported [3]

Since all the antennas in a cell are connected to a single reader, frequency diversity is not applicable, as all antennas transmit at the same frequency.

Because the Distributed Antenna Systems use the same signal multicast over several antennas to provide coverage for a single cell, a multi-cell system will still face the inter-reader collision problems described above. As a result, frequency and time anti-collision schemes as described still need to be implemented at a global level. A comparison of these different schemes will be performed in the next chapter using simulations of a multiple antenna arrangement.

Another benefit of multiple antennas is that it allows diversely oriented tags to be more easily read, since the relative reader antenna-tag orientation varies from antenna to antenna [59].

2.2.2 Fading

Another major problem in wide area fixed RFID systems is fading. Fading in wireless communication refers to the deviation in the signal strength from that expected from free space propagation equations (Friis equation), caused by several factors such as multipath, shadows and precipitation. In RFID, of principal concern is multipath fading, as indoor applications are most common, and multiple reflections cause the received signals to be faded. Fading in RFID has been widely studied using probabilistic models [60]. Methods to overcome fading include:

Range Limitation in portal systems

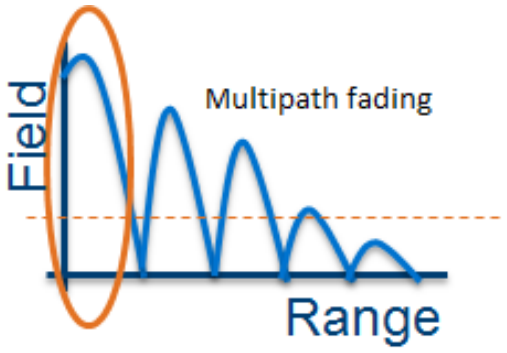

Figure 2.8: Limiting RFID range to avoid multipath fading. Peaks and troughs are caused by reflections and avoided by limiting the operating range.

In portal application systems such as airport security, the conventional solution is to limit the range of the RFID system to the region without fading. Fading causes deviations in received power from the predictions given by free space models. Limiting the operating range of the system to the region with no significant effects from multipath resolves the problem as shown in Fig 2.8. In this way, the effects of multipath are avoided. The disadvantage of this is evidently the limited range of the system, as well as the fact that it cannot be effectively applied to multi-antenna systems in wide area RFID.

Use of Multi-antenna tags

Another method for combatting fading is the use of multi-antenna tags, and it has been shown that an RFID tag with multiple uncorrelated antennas (for example, using cross

polarised antennas) can overcome small scale fading, as was demonstrated with a two antenna tag [61].

Reader Antenna Diversity

The next method for overcoming fading is the use of multiple antennas to provide spatial diversity to the system. Due to the fact that different antennas experience different channel paths, a diversity scheme which appropriately selects or combines the different channel paths for different antennas will produce better results than for a single antenna. Phased array antennas are also used to overcome fading, and can be thought of as a local DAS system, being made up of several antennas in the near field of one another and using specified phase and amplitude relationships to synthesise beams in particular directions. Using beamforming techniques, the multipath can be varied as the beam is steered, thereby fading is overcome. They also provide greater immunity to adverse environments e.g. in the presence of metals, since beam steering can minimise multipath effects [62]. Also the use of many element antenna arrays will produce narrow beams, thereby further minimising reflections. Antenna arrays have already been applied in RFID research, mainly for beam diversity and localisation.

Frequency Diversity

Another diversity technique commonly employed in wireless systems to overcome fading is frequency diversity [63, 64]. Since multipath fading results from interference due to direct and scattered signals, the effect is frequency (wavelength) dependent. As a result, some frequencies are less faded for any given scattering environment, which means that frequency diversity increases resilience to multipath fading, leading to a better overall performance. However, the low bandwidth of RFID, especially in the European Union and the United Kingdom limits the applicability of frequency diversity [36]. It has been shown to provide only minor benefits [3]. However, when applied over the global RFID frequency band, significant improvements were reported [65], although this is not allowed by the regulations [36].

2.3 Antenna Arrays in RFID

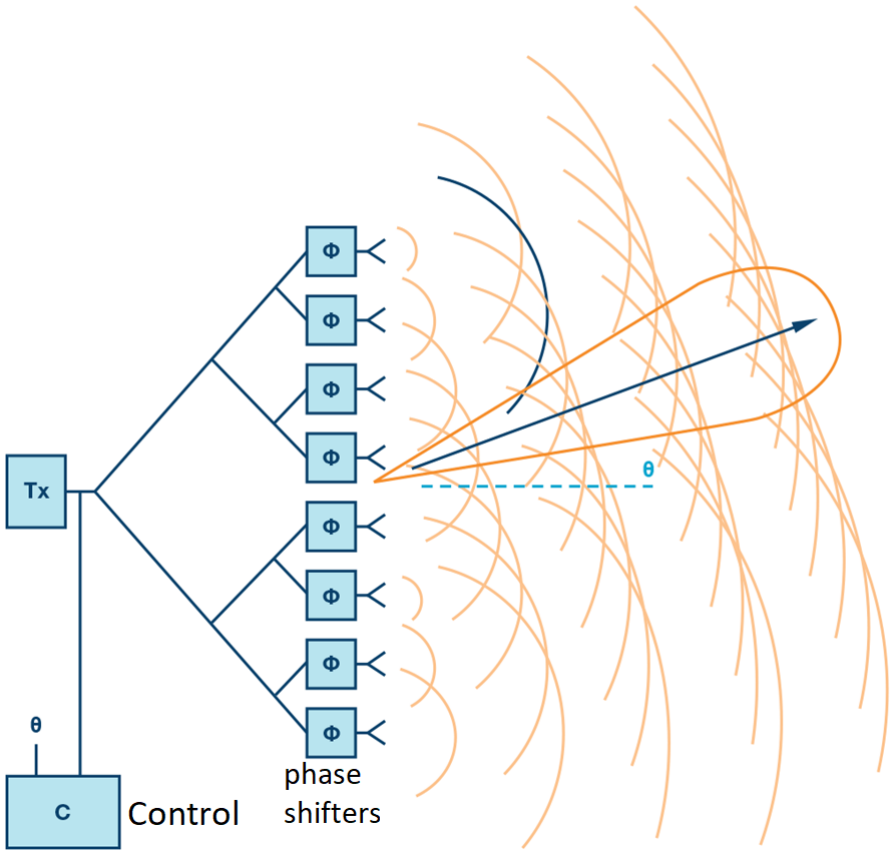

Figure 2.9: A phased array architecture, showing each antenna element fed by a phase-shifted version of the input signal [66]

An antenna array is a group of collocated, interconnected antenna elements acting as a single transmit or receive antenna, as their individual patterns interfere with each other's to produce an enhanced pattern in the far-field. An example of an 8-element array is shown in Fig 2.9. When the different elements in the array are fed with appropriately phased signals, the beam can be steered to a pre-determined direction, and is called a phased array antenna (for simplicity, the terms antenna array, array antenna and phased array antenna will be used interchangeably throughout this dissertation, unless specified). This provides an alternative to mechanically steered antennas in many applications such as in satellite and deep space communications, where the use of gimbals and servo-motors limit the lifetime of such antennas [9]. In addition, mechanical rotation systems are invariably slow. Phased array antennas, on the other hand, provide a means for rapid beam steering, as well as adaptive and multiple beam forming.

2.3.1 A History of Antenna Arrays

The origins of antenna arrays can be traced to early attempts in the late 19th and early 20th century by several researchers such as Marconi, J.A Fleming and Sidney Brown to obtain enhanced gain for long range communication by using multiple antennas [9, 67]. However, Ferdinand Braun has been credited with the development of the first phased array antenna, as he demonstrated a three-antenna steered beam with vertical monopoles in a triangular pattern, and produced beams offset by 60^0 and 120^0 from the main beam direction in 1905 [68]. Research on antenna arrays continued during the 1910s and 1920s, but was accelerated by the second world war, as several nations raced to develop technology that would detect enemy aircraft at long range. In this sense, phased arrays and RFID share a common history. The Chain Home system in Britain, the Mammut 1 in Germany and the Microwave Early Warning System in the United States are notable examples [9]. Also, the cavity magnetron, which had earlier been developed in the 1920s, was vastly improved in the 1940s to produce 3GHz pulses at much higher powers than previously possible. This was hugely significant in the development of array technology, as much larger phased array radars with higher detection resolutions could be developed. The post-war period saw advances in computing power, leading to quick array processing capability, and methods of beamforming such as the Dolph-Tchebyshev, Taylor, Hobbels-Applebaum and Least Mean Square methods were developed. There was also the advancement in phased array development for use in Radio astronomy such as the Interplanetary Scintillation Array (IPS), which led to the first detection of a pulsar, for which a Nobel Prize was awarded [69]. The emergence in the 1960s of solid state phase shifters brought about the ability to rapidly control the phases of individual antenna elements in the array, hence the development of Passive Electronically Scanned Arrays (PESAs). A PESA is a phased array antenna in which a single transceiver module is split into multiple chains, and each is electronically phased and fed into each element of the array. These enable electronic beam steering of a single beam, as well as multiple fixed beams at a single frequency. They were a huge improvement over mechanically steered arrays, as much faster scanning times were now possible. The 1970s saw the development of practical methods to produce patch antennas, which led to the cheap manufacture of large arrays, together with the ability to conform them to non-planar surfaces [70]. Further developments in solid state electronics in the 1980s saw the size of both receivers

and transmitters shrink to the point where each antenna could be equipped with its own transceiver unit, leading to Active Electronically Scanned Arrays (AESAs). AESAs were more advanced than PESAs in that they allow the formation of multiple simultaneous beams at multiple frequencies, as each antenna has its own transmit/receive module.

The applications of phased arrays today vary widely from increasing capacity in mobile communications in 4G and 5G to deep space exploration such as the Square Kilometre Array [71]. Radio broadcast stations use phased array antennas to increase the range of their broadcast by increasing the gain. The most widely used application is in phased array radars, in which the rapid scan capability of electronically scanned arrays enable the scanning of large areas for the detection of ships, spacecraft and missiles.

2.3.2 Components of a phased array antenna

In order to design a phased array antenna, the required components include a power distribution network, phase shifters, and amplifiers.

(*i*) Power distribution network The array power distribution or divider network enables the appropriate distribution of the signal to each element of the antenna array by making use of several RF splitters/couplers. The splitters/couplers are used to divide the source signal into components which feed the antenna elements for transmission. In the receive direction, they also combine the RF components from all antenna elements to the receiver. They are passive reciprocal networks. In some array feed architectures, e.g. serial feed networks, directional couplers could be used in which the signal is being tapped as it travels along as in Fig 2.10. Examples of array feed networks for 2D arrays are shown in Fig 2.10.

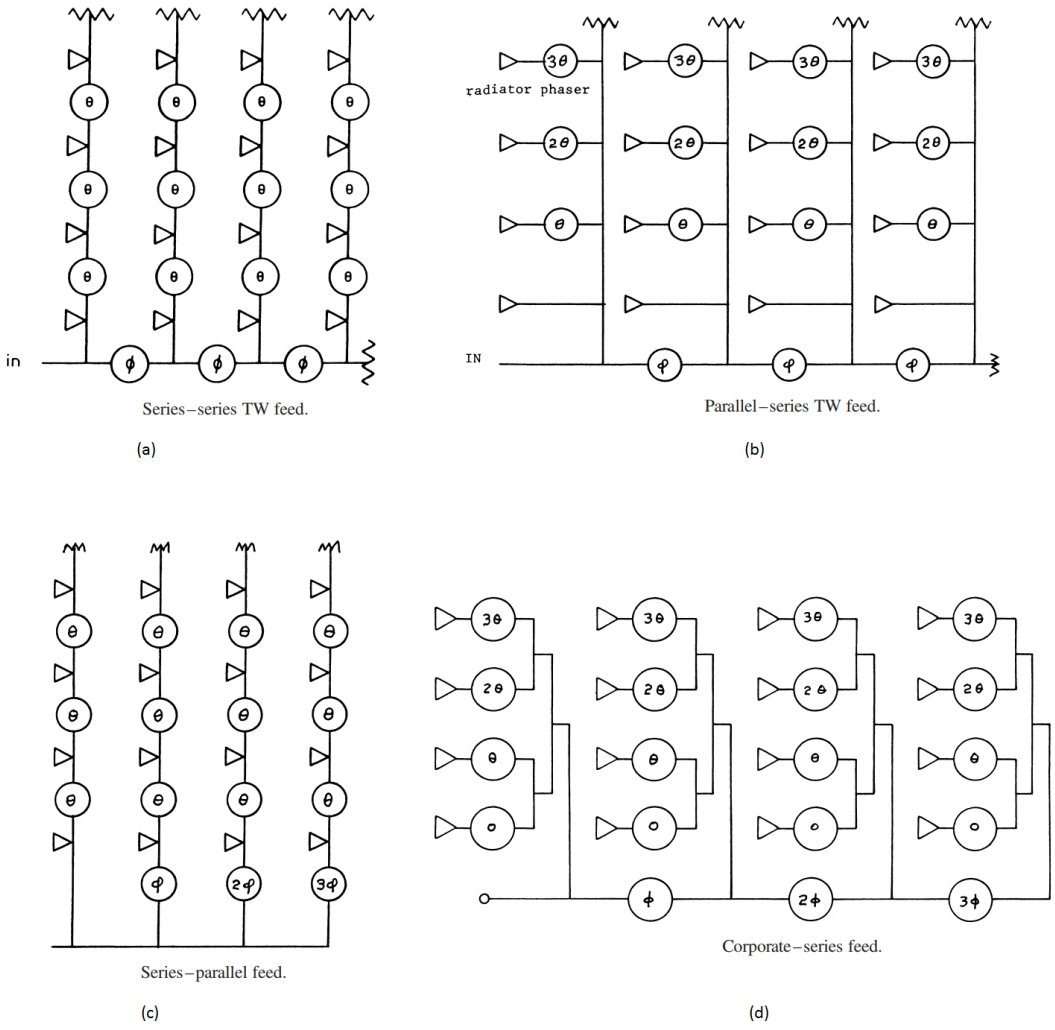

Figure 2.10: 2D phased array feed network examples [72]

(*ii*) Phase Shifters

Phase shifters are used to apply a phase or time delay to the signal into each antenna element in order to produce steered beams. Depending on the application, the phase shifters used could be fixed or variable. For fixed beam systems, a fixed delay line is used such as a length of microstrip in PCB or of coaxial cable. The required length, d, of waveguide material required for a specified phase shift $\Delta\Theta$ is calculated from $\Delta\Theta = \frac{2\pi f d\sqrt{\varepsilon}}{c}$, where f is the frequency of the signal, c is the speed of light in air and ε is the relative permittivity of the waveguiding structure (such as the PCB or coaxial cable). However, they suffer from low bandwidth since they are specified at a single frequency. They find applications in switched beam feed networks such as Butler matrices. Mechanical variation of the length, and therefore phase delay of waveguiding structures has also been

used to obtain beam steering [73].

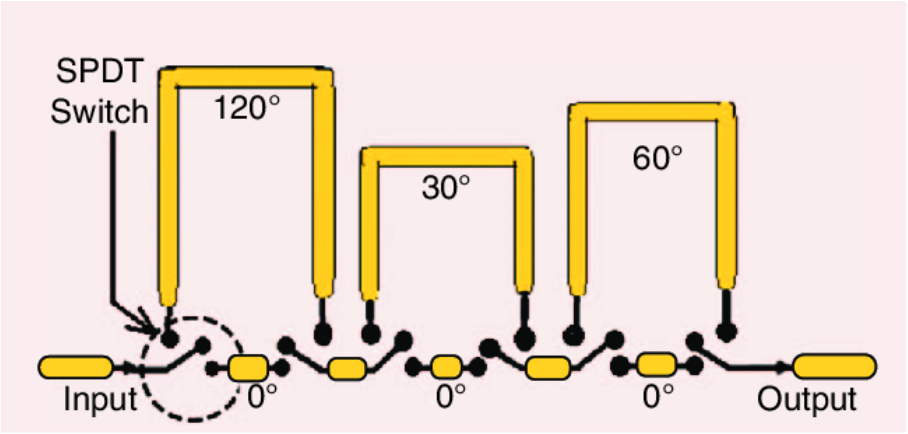

Figure 2.11: Architecture of a three-bit delay-line switched digital phase shifter with a range of 180^0. [74].

Variable phase shifters enable electronic variation of the signal phase, and therefore are applicable in obtaining arbitrary beam patterns with rapid scan times. They could be analogue (voltage-controlled) or digital.

Analogue phase shifters provide continuously variable phase shifts over the range by applying an electric voltage. Examples include ferroelectric waveguides, which obtain phase shifts by the voltage-variable dielectric constant [75]. Another popular kind of phase shifter is the reflection phase shifter, which uses a quadrature hybrid coupler and a voltage-variable capacitors (varactors) to implement phase shift. Analogue phase shifters are normally more susceptible to noise present on the voltage control line [75].

Digital phase shifters provide phase shift in switchable blocks or bits, as the example in Fig 2.11. Multiple RF paths are available, and are selected using switches based on the desired phase shift. Phases are available in quanta, and hence they suffer from quantisation errors, but are less susceptible to noise. Methods of designing phase shift blocks include delay lines, high pass /low pass filters and loaded lines [75].

Photonic delay lines are also employed in phased array antennas using optical fibre or free space at the sub-array level [72].

(*iii*) Amplifiers

Amplifiers are used to control the total radiated output power form an antenna. This is important in many regulated communication systems like RFID, where a maximum EIRP

is specified. In the receive link, a Low Noise Amplifier (LNA) is used. In phased array applications, non-uniform array feeds are useful for certain beam synthesis algorithms such as the binomial and Dolph-Tchebyshev beamformers, as well as in adaptive beamformers. Variable attenuators are usually employed before the phase shifters in order to obtain these power ratios for the elements, whereas power amplifiers are employed after the phase shifters to drive the antennas at high power. Switches are used to switch between the uplink and downlink.

Other components which are important to the design of phased array antennas include hybrid couplers and Rf crossovers. These are used mainly in fixed feed networks such as Butler matrices, in which they provide passive phasing of signals to obtain switched beam arrays.

2.3.3 Antenna Array Classification

Antenna arrays can be classified into active and passive depending on the amplification structure of the array, and into switched and dynamic arrays depending on the method of beamforming.

Passive and Active Arrays

Passive arrays use a single large central Transmit/Receive Module (TRM) before the power distribution network. This leads to generally less power available at the antenna elements due to losses in the feed network and phase shifters. Because they contain a single TRM, passive arrays can only steer a single beam at a single frequency at any given time. Active arrays, on the other hand contain multiple TRMs, and can therefore steer multiple beams at multiple frequencies simultaneously. Active arrays also enable digital beamforming. A passive and active array architecture are shown in Fig 2.12.

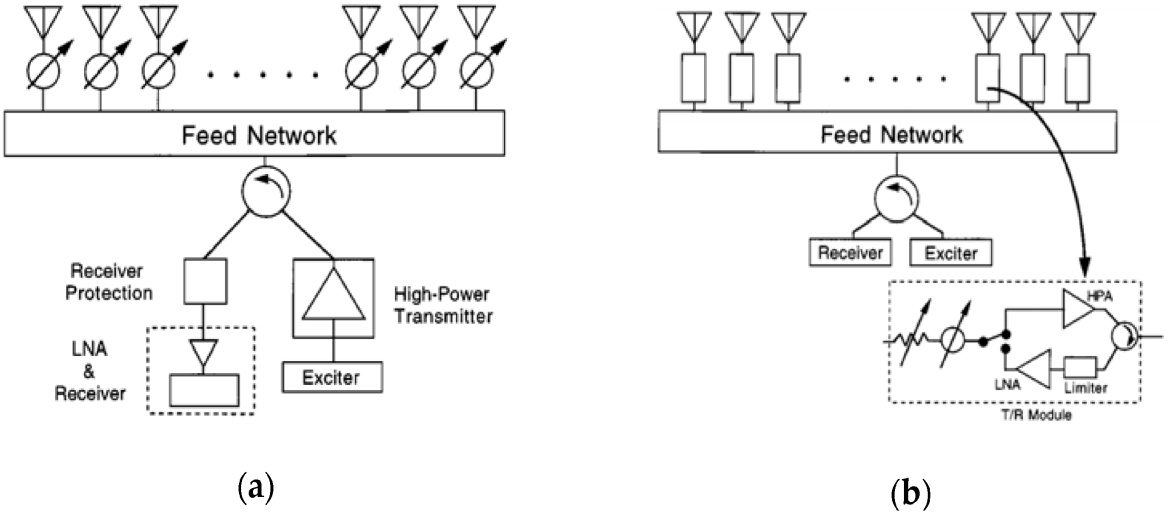

Figure 2.12: General Architecture for passive (a) and active (b) arrays

Switched and Dynamic Arrays

Another classification of phased array antennas, based on the method of beamforming is into switched and dynamic/adaptive arrays.

Switched beam arrays

Switched beam arrays have several available fixed beam patterns, which are selected depending on the desired scan direction. They have the advantage of being simple, as they make use of passive RF components which can be designed in microstrip, such as fixed phase shifters, cross overs, hybrid couplers and splitters/combiners. They provide diversity by producing multiple beams or switched beams, selected based on desired transmit/receive direction. Examples include the Butler matrix and the Blass matrix. A 4×4 Butler matrix is shown in Fig 2.13.

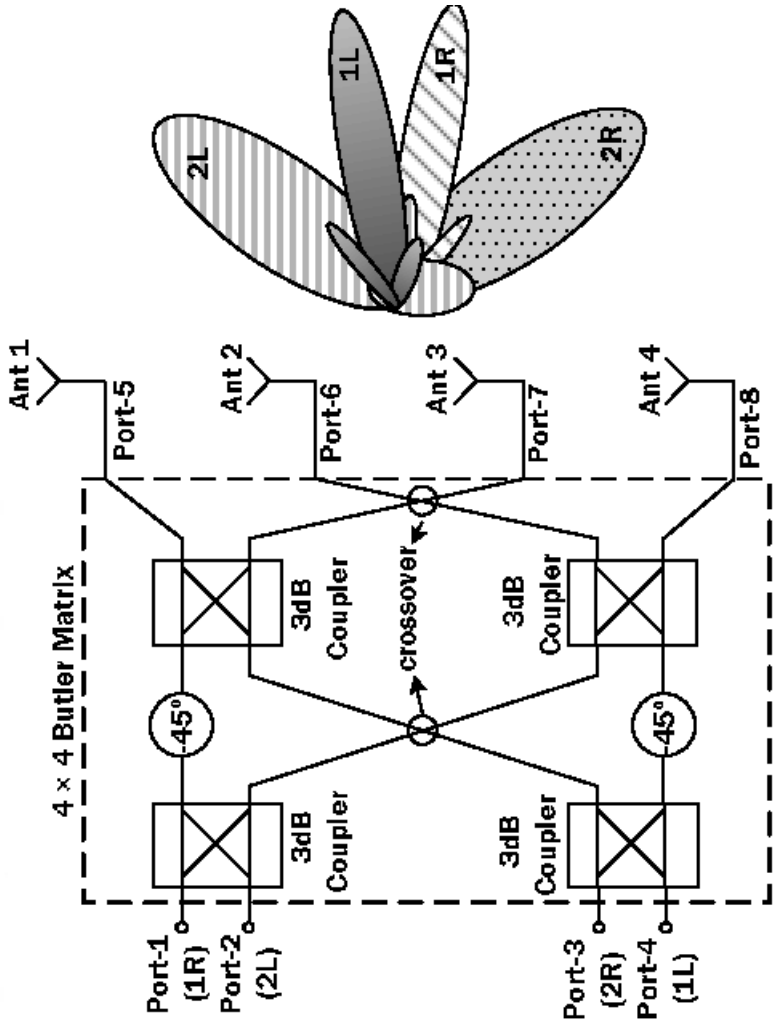

Figure 2.13: A 4×4 butler matrix with four switchable beams[76]. Feeding ports 1-4 activates beams 1-4 respectively. Multiple beams are produced by exciting multiple corresponding ports

First proposed in 1961 [77] as an improvement to the Blass Matrix [78], the Butler matrix is a widely used fixed beamforming network consisting of fixed phase shifters and hybrid couplers only, with an $n \times n$ input-output structure, where n is a power of two. It feeds the elements with a progressive phase difference without any change to the amplitude, thereby producing a uniform linear array. It switches between n possible orthogonal beams, by switching on the input signal to the corresponding port. Multiple beams can be formed simultaneously due to the orthogonality of the matrix [77]. Butler matrices have also been used to provide side lobe cancellation in antenna arrays [79].

Dynamic Arrays

The limitations of fixed arrays lie in the inflexibility of the system, as the beam directions have to be designed with a priori knowledge of the desired beam patterns, and with limited scope for modification. Also, the discrete nature of the beams in a switched system, as illustrated in Fig 2.13 makes it unlikely that the an available beam can maximise transmission or reception in all directions. Furthermore, although Butler matrices have been applied in interference rejection [80], simultaneous, dynamic maximum signal reception and interference rejection is impossible. Dynamic arrays on the other hand, make use of programmable phase shifters and attenuators/amplifiers to allow the formation of beams which can be steered temporally to an infinite number of directions. They allow the maximum versatility in terms of the beams that can be formed, and are used for designing smart antenna systems, as they allow adaptive beam formation. i.e. beam-forming dependent on some system feedback, which are not possible with the fixed beamformers. The degree of flexibility depends on the resolution of the phase shifters or attenuators.

2.3.4 Phased Array Applications in RFID

The relatively low global operating frequencies for UHF RFID ($\sim 860 - 960MHz$) make antenna arrays unattractive for RFID due to the corresponding large antenna footprints. As a result, limited application has been made of RFID phased array antennas. Several applications have however been reported in both academia and industry, albeit with low element-count arrays.

One of the main motivations for using antenna arrays in RFID is beam diversity, which enhances read rates. Lee et al. reported a 1×4 array using a 4×4 Butler matrix, producing six beams in the upper hemisphere of the antenna at angles $\pm 12^0, \pm 39^0$ and $\pm 68^0$ [5]. This gives an effective wider 3dB beam width to the antenna, and therefore more tags can be covered compared to a fixed antenna. However, scanning is only possible in a single plane. Weisteger et al. produced a 2×2 array using a modified Butler matrix, capable of producing four beams steerable in azimuth to $45^0, 135^0, 225^0$ and 315^0 at an elevation angle of 30^0 [81]. A comparison was made with a standard fixed antenna in interrogating a box of tags, and a 50% improvement was reported. Similar designs have been reported with similar tag read improvements [6, 82, 62]. A 3×3 antenna array has also been reported by Li et al. [83] using a 4×4 Butler matrix. Only three of the four

Butler matrix ports were used as the array was divided into three sub-arrays of three antennas each. Scanning angles of up to 50^0 in elevation were reported. The antenna was shown to detect 100% of tags placed in a metal cavity, which is an extreme multipath environment. This is due to the spatial diversity provided as the beams are switched. A fixed antenna was reported to read 30% less tags in a similar experiment [83]. 2D scanning arrays provide extra diversity, and so provide much more improvement in tag reads. The mentioned applications have all been switched beam arrays which select from a finite number of available beams as discussed earlier, thereby limiting the amount of spatial diversity added to the system.

Applications employing dynamic phased arrays have also been reported. Hassan et al. presented a 1×4 array with antenna element amplitude and phase control in the baseband using a vector modulator [84]. An improvement over a fixed antenna of up to 15 dB in the power received by a tag was recorded at points of extreme fading. Karmakar et al. reported a 2×3 array using four-bit phase shifters [85]. These are capable of $2^4 = 16$ electronically controllable phase states per antenna, and therefore a much larger possible number of beams compared to the Butler matrix reported above. A comparison with a fixed antenna was not performed in this paper. The same author presented a similar array design using an FPGA to do beam control [86]. Liao et al. also presented a 1x4 array using a microcontroller-controlled four-bit phase shifter, making possible a large number of beams.

There has also been some commercial applications of phased arrays in RFID, for example the xArray antenna-integrated reader from Impinj utilises switched beam patterns with dual-linear polarised antennas, and is capable of producing 52 beams [87]. Similarly, the Starflex Turbo antenna system from Mojix uses phased array antennas [7].

The limitations of size, stemming from the low frequency band ($860 - 960$ MHz) used globally for RFID is resolvable at higher frequencies, in which larger RFID arrays are more practical, and have been demonstrated especially at 2.4 GHz and 5.8 GHz [88, 89]. Apart from enhanced power delivery and tag detection, which are the focus of this dissertation, antenna arrays have found applications in other areas of RFID.

One crucial and well-researched application of phased arrays in RFID is tag localisation. Direction finding algorithms are normally based on phased array antennas. The relative phase of the received signal between the various elements in an array are used to de-

termine the direction of the incoming signal, and the relative direction of the tag as a result. The most widely applied direction finding algorithms are the various variants of the MUSIC [90] and ESPRIT algorithms [91]. The location of the tag is then found using multilateration from several arrays [92, 93] or combined with RSS information to estimate the range[94].

The use of different beam states for sectorisation RFID tags has also been used for localising tags [95, 96]. This allows a tag to be classified to a particular sector of a room based on the array's beam. Narrower beams lead to more localisation precision.

Antenna arrays have been used with blind source separation techniques to separate overlapping tag signals, thereby reducing tag collisions [97].

2.4 Summary

This chapter has presented some RFID background and relevant literature on wide area RFID, inter-cell RFID network planning, and fading in wide area RFID. The application of phased array antennas to RFID reported were mainly in isolation, without consideration for multiple arrays cooperatively providing coverage while beam steering or a multi-cell wide area RFID system employing phased arrays. This dissertation researches these problems. The methods in which multiple phased array antennas could be used together to interrogate a particular zone are investigated. Multiple phased array antennas acting cooperatively in a wide area with multiple cells are also investigated suing multiple phased array antennas. For the design of such systems, a model is required to provide fast simulations of multiple interacting antennas, which is done in the following chapter. The next chapter introduces a useful model for rapid electromagnetic simulations in wide area RFID systems.

Chapter 3

A Novel 3D model for multi-antenna Wide Area RFID Simulation

It has been established in the preceding chapter that the growing need for automated (hands-free) and wide area RFID applications requires careful planning in order to maximise coverage with minimal resources. This requires sufficient power to be delivered to the tags in order to activate them. The second requirement is to combat the problem of interference. Both conditions need to be satisfied at both the global level (global tag coverage and inter-cell or inter-reader collision avoidance) and the the local level (cell coverage and intra-cell collision avoidance). The latter tries to resolve problems of interference in the context of a single cell. Since a reader addressing a single cell could feed multiple antennas, some planning and optimisation is required within the cell at the level of the antennas. This involves the relative locations of antennas, their orientations, radiation patterns, as well as the multicasting/multiplexing method. The goal of such planning is to maximise cellular coverage with minimal resources, usually antenna count. As a result, accurate models are required to understand the distribution of power by a given set of antennas, as received by the tag population for system planning to be effective. This chapter presents a new model capable of modelling antenna interactions in a complex wide area RFID environment, which is useful for cellular coverage planing.

3.1 Review of RFID Propagation Models

Radio propagation models provide a mathematical representation of wireless communication channels, and allow predictions to be made about communicating over the channel. Many attempts have been made with different levels of complexity in using propagation models to model RFID environments in order to aid system planning. The read range is generally considered to be the single most important performance indicator in an RFID system. For wide area deployments, this translates into the area each antenna can cover, and consequently the separation between neighbouring antennas becomes the key factor. It is therefore necessary to maximise antenna separation while maintaining optimal coverage. A good propagation model, capable of modelling multi-antenna interactions, is necessary for this.

The simplest and most common models for estimating the range in RFID systems are based on the Friis equation, which takes into account the free space path loss, and determines the range based on the antenna gains and transmit power [98, 99, 100, 101, 102]. The received power at a tag antenna, P_r, of gain, G_r, for a reader transmit power of P_t and gain, G_t, at a carrier wavelength of λ, and with a reader-tag separation distance of d, is given by

$$P_r = P_t G_t G_r \left(\frac{\lambda}{4\pi d}\right)^2 \tag{3.1}$$

If P_r is greater than the threshold power, then the tag is assumed to be detectable (neglecting the uplink, due to the RFID channel asymmetry established in Chapter 2). The Friis equation is a useful tool for simple performance estimation, but cannot account for several factors such as multipath, radiation patterns (and therefore, propagation in directions other than the maximum gain) and relative tag-reader antenna orientation, which require the inclusion of further complexity into the simple Friis model.

A modified path loss model, which can take into account a single ground reflection has also been applied to obtain a more realistic picture of the system [49, 98, 103]. The received power in this case is [98]:

$$P_r = P_t G_t G_r \left(\frac{\lambda}{4\pi d}\right)^2 \left|1 + \Gamma(\theta)\frac{d_f}{d} e^{-j\frac{2\pi(d_f - d}{\lambda}}\right|^2 \tag{3.2}$$

where $\Gamma(\theta)$ is the reflection coefficient due to ground reflections at incidence angle of θ, and d_f is the length of the indirect path to the tag from the transmit antenna. This enables the effect of multipath due to ground reflections to be modelled.

Furthermore, some publications have used empirical models for antenna radiation patterns in order to model the effect of the reader antenna patterns on the overall system, thereby allowing the study of angular gain variation on the system [54, 104, 58]. This is especially important as most RFID reader antennas are directional, and cannot be accurately modelled using an omnidirectional model. Sicheng et al. used an analytical approximation to an antenna radiation pattern defined in terms of desired antenna gain and beamwidth, which approximates to an ellipsoidal beam pattern [54]. Dimitriou et al. also defined an equivalent read region in the vicinity of an antenna, having taken into account first order reflections, which justifies experimentally the use of an ellipsoidal approximation to the antenna gain pattern [104]. However, this breaks down in a situation where more than one antenna is transmitting simultaneously in a coherent manner, due to the fact that, the interactions amongst the antennas cannot be modelled using an ellipsoid.

Ray-tracing models have been used for site-specific modelling solutions, making use of full wave simulations for the antenna reader gain patterns, thereby enabling the modelling of antenna interactions [105]. However, isotropic tag patterns were used, which makes it impossible to study the effect of different tag orientations on the performance of the system. This is crucial because a majority of tags are dipole antennas, and their performance depends highly on orientation. Furthermore, the use of a full ray tracing model is not well suited to wide area RFID simulations due to the time complexity involved.

Reports have also been made on studies of fading effects in the context of non-specific statistical models. Different fading models have been used to characterise RFID links, most notably Rayleigh fading [106, 107] and Rician fading [107, 108]. Statistical models treat the channel as a Finite Impulse Response (FIR) filter with transfer function $h(t)$, such that the received signal is a sum of all multiple paths the signal can take to the tag, and is given by the convolution (in the time domain) of the impulse response, $h(t)$, and the transmitted signal, $x(t)$:

$$y(t) = \sum_{n} h(t)x(t - \tau_n) \tag{3.3}$$

where τ_n is the delay of the nth path. The channel response function $h(t)$ needs to be chosen for the specific application, and is crucial to the model accuracy.

In this chapter, a propagation model is presented based on realistic antenna patterns from either full wave simulations or measured antenna beam patterns for both the reader

and tag antennas. The model is based on the electric field interaction between antennas and tags using the antenna effective length formulation. As a result, factors such as reader or tag antenna orientation effects, polarisation, gain, power levels, side or back lobes and matching are implicitly modelled. The model also lends itself well to multi-antenna systems simulations, as the phase information is preserved in the electric field. It will be used to investigate several case studies at the end of the chapter.

In the next section, a general description of the antenna radiation problem, and how this integrates into the model used throughout this work is presented. In this light, beginning with Maxwell's equations, the Electric Field Integral Equation (EFIE) is derived, from which the model presented in this dissertation proceeds. The propagation and antenna interactions are then presented.

3.2 Theoretical Background on Antenna Radiation

Antenna radiation problems, in general, involve obtaining solutions to the Maxwell Equations for a given set of electromagnetic sources and boundary conditions. For respective source charge and current densities ρ and $\boldsymbol{J}$, the Maxwell equations (in harmonic form) read [109]:

$$\nabla \cdot \mathbf{D} = \rho \tag{3.4}$$

$$\nabla \cdot \mathbf{B} = 0 \tag{3.5}$$

$$\nabla \times \mathbf{E} = -j\omega\mathbf{B} \tag{3.6}$$

$$\nabla \times \mathbf{H} = \mathbf{J} + j\omega\mathbf{D} \tag{3.7}$$

where $\boldsymbol{E}$ is the electric field, $\boldsymbol{H}$, the magnetic field, $\boldsymbol{D}$, the electric flux density and $\boldsymbol{B}$, the magnetic flux density. Our interest lies in integrating these equations to obtain solutions for the electric and magnetic fields $\boldsymbol{E}, \boldsymbol{H}$. The last two equations are of particular interest in antenna problems. Two methods - direct and indirect- exist for solving these [110]. Direct methods involve direct integration of the source currents, $\boldsymbol{J}$, to obtain the radiated fields $\boldsymbol{E}, \boldsymbol{H}$. A simpler problem, usually employed in antenna simulators, is by introducing the vector and scalar potentials $\boldsymbol{A}$ and ϕ, and then differentiating to obtain the radiated fields $\boldsymbol{E}, \boldsymbol{H}$.

The indirect solution is constructed using potential functions resulting from the 2nd and

3rd equations. Because $\boldsymbol{B}$ is solenoidal (zero divergence), a magnetic vector potential, $\boldsymbol{A}$, can be introduced, enabling $\boldsymbol{B}$ to be written as $\boldsymbol{B} = \boldsymbol{\nabla} \times \boldsymbol{A}$. Substituting this into the 3rd equation results in

$$\nabla \times \mathbf{E} = -j\omega \nabla \times \boldsymbol{A} \tag{3.8}$$

$$\implies \nabla \times (\mathbf{E} + j\omega \mathbf{A}) = 0 \tag{3.9}$$

the quantity $\boldsymbol{E} + j\omega \boldsymbol{A}$ having a curl of $\mathbf{0}$, which allows it to be represented as a scalar gradient potential. Hence, the two new equations

$$\mathbf{B} = \nabla \times \mathbf{A} \tag{3.10}$$

$$\mathbf{E} = -\nabla\phi - j\omega \mathbf{A} \tag{3.11}$$

which, together with the Lorenz guage condition [111]

$$\nabla \cdot \mathbf{A} + j\omega\mu\epsilon\phi = 0 \tag{3.12}$$

results in the Helmholtz equation for the magnetic vector potential

$$\nabla^2 \mathbf{A} + k^2 \mathbf{A} = -\mathbf{J} \tag{3.13}$$

The solution for $\boldsymbol{A}$ is obtained using the Green function solution: Radiation from an antenna is excited by the current density $\boldsymbol{J}$, which generates the magnetic vector potential, $\boldsymbol{A}$, given by

$$\mathbf{A}(\mathbf{r}) = \iiint_V \mathbf{J}(\mathbf{r} - \mathbf{r_0}) \mathbf{G}(\mathbf{r} - \mathbf{r_0}) d^3 r \tag{3.14}$$

where $\boldsymbol{G}$ is the Green function solution to the Helmholtz equation with dirac-delta source

$$\nabla^{\mathbf{2}} \mathbf{G} + k^2 \mathbf{G} = -\delta^3(r) \tag{3.15}$$

where

$$\mathbf{G}(\mathbf{r}) = \frac{e^{-jk|\mathbf{r}-\mathbf{r_0}|}}{4\pi|\mathbf{r} - \mathbf{r_0}|} \tag{3.16}$$

$\boldsymbol{A}$ can then be used to obtain the electric field (by substituting Eqn 3.12 into Eqn 3.11)

$$\mathbf{E}(\mathbf{r}) = -\nabla\phi - j\omega \mathbf{A} \tag{3.17}$$

$$= -j\omega\mu \mathbf{A} + \frac{1}{j\omega\epsilon} \nabla(\nabla . \mathbf{A}) \tag{3.18}$$

$$\tag{3.19}$$

This is the Electric Field Integral Equation (EFIE), and forms the basis for solving antenna radiation problems. It allows the computation of the electric field given a current distribution $\boldsymbol{J}$ from several sources. The solution is usually obtained by numerical methods. e.g the Method of Moments (MoM) and the Fast Multipole Method (FMM). Because UHF RFID is a long range technology, only long range antenna interactions are of interest, and therefore, the far-field approximation is sufficient. Using the arguments of Balanis [110], the far-field magnetic vector potential, $\boldsymbol{A}$, can be approximated by

$$\mathbf{A}(r \to \infty) = \frac{\mu}{4\pi}\frac{e^{-jkr}}{r}\iiint_V \mathbf{J}(\mathbf{r}')e^{j\mathbf{k}.\mathbf{r}'}d^3r' \tag{3.20}$$

where

$$\mathbf{F} \equiv \iiint_V \mathbf{J}(r')e^{j\mathbf{k}.\mathbf{r}'}d^3r' \tag{3.21}$$

is called the radiation vector of the antenna.
It can then be shown that that, in the far field [111]:

$$\mathbf{E}(r \to \infty, \theta, \phi) = -jk\eta\frac{1}{4\pi}\frac{1}{r}e^{-jkr}\mathbf{F}_\perp(\theta, \phi) \tag{3.22}$$

which is solely dependent on the angular bases (θ, ϕ). $\mathbf{F}_\perp(\theta, \phi)$ is the component of the radiation vector orthogonal to the propagation direction. This gives us the electric far field of an antenna with a given source, and will form the starting point of the model used in this dissetation. All antenna simulations performed in this work result from the commercial full wave software- FEKO, unless otherwise stated.

3.3 Model Description

The model is based on propagating the electric field corresponding to the RFID signal from the reader antennas and interacting them with the tag antennas in a 3D environment. The field propagated, described by Eqn 3.22, is generated by the reader antenna. This quantity has units of voltage and propagates with a $1/r$ decay to give an electric field at some point in space away from the origin. This point must be in the far field of the antenna for the equations to be valid. ie $r >> \frac{2l^2}{\lambda}$, where l is the longest dimension of the radiating structure, and λ is the wavelength. This works out to be about $0.9m$ for a UHF RFID antenna of about 0.4m. As stated earlier, the FEKO MoM solver was used to generate antenna radiation patterns, and the far field electric field pattern is used,

which corresponds to Eqn 3.22 [112]. Therefore, an antenna can be modelled with a specific output power, and its 3D field components extracted for use in these simulations (alternatively the port input power could be set arbitrarily and the electric field pattern scaled accordingly in the model). The electric field in this format can be (with slight modification) obtained from most commercial EM simulation packages, or indeed from direct antenna measurements (e.g. by the StarLab system [113]). The field patterns are imported into MATLAB, in which the rest of the model is implemented. As is usually the case in practice, the antennas used at the reader side are circularly polarised patch antennas, while at the tag end, dipole antennas are used as shown in Figs 3.1.

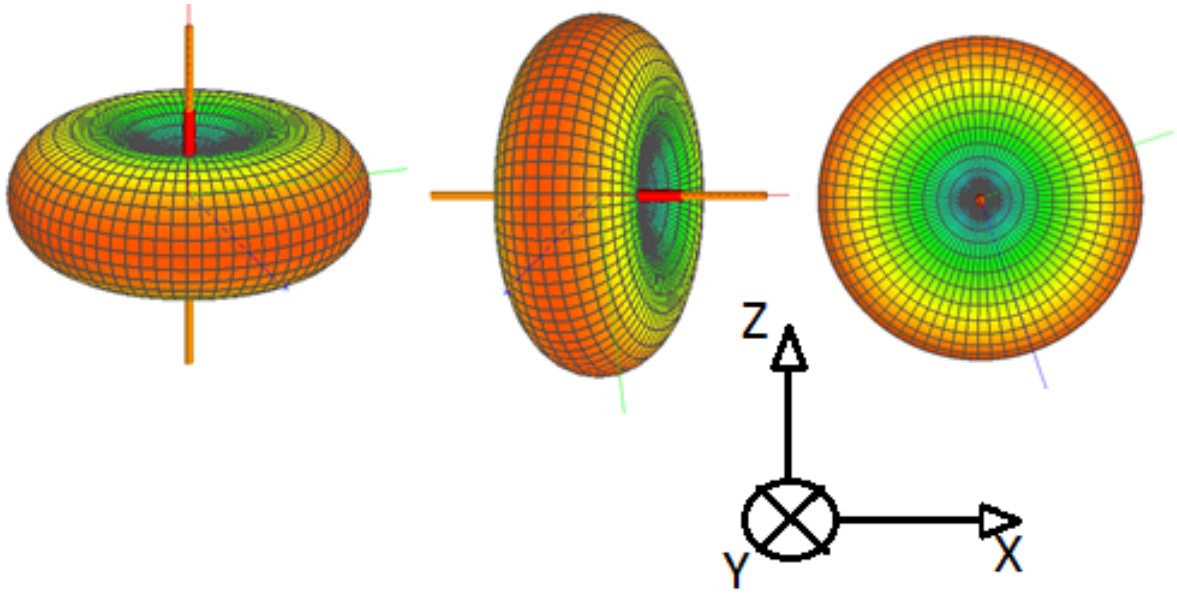

Figure 3.1: Tags with different orientations z, x and y polarisations

Before the propagation equations are implemented, it is necessary to interpolate the antenna electric field, as well as perform necessary transformations on the fields. This is described below.

3.3.1 Field Interpolation

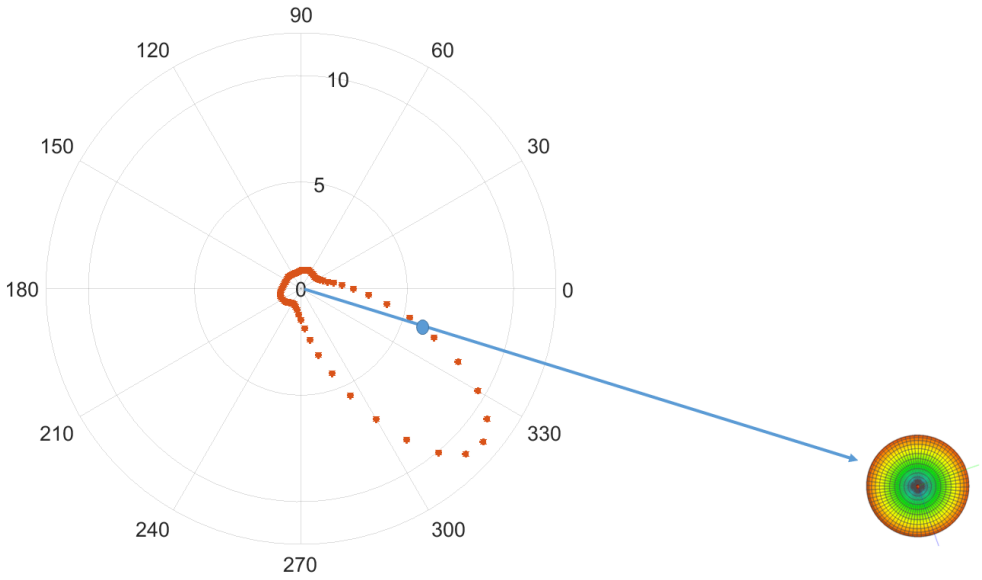

Figure 3.2: Field interpolation 2D illustration. The simulated values are done at 5^0 intervals shown by the red plot. The electric field is required in a direction corresponding to the blue dot, and is obtained by a bilinear interpolation

To evaluate the electric field incident on a tag due to a particular antenna, the field is computed at the tag based on the directional relation between them. However, full wave simulations and antenna measurement software evaluate the fields at discrete angular steps, and therefore not all required points on the Cartesian plane map directly to the antenna field pattern as shown in Fig. 3.2. An interpolation is therefore required to be performed on the field pattern to fill the gaps, and provide a good approximation of the field for any desired angle, and therefore any tag in space. The unit vector from the antenna to the location of interest is computed, and the angular direction (θ, ϕ) corresponding to this position is determined. An interpolated value for the electric field is then obtained for this direction using a bilinear interpolation. Given that the fields are known at the points $(\theta_1, \phi_1), (\theta_1, \phi_2), (\theta_2, \phi_1)$ and (θ_2, ϕ_2), it is required to estimate the field at angular direction (θ, ϕ). The field estimate is given by [114]

$$\mathbf{E}(\theta,\phi) = \frac{1}{(\theta_2-\theta_1)(\phi_2-\phi_1)} \begin{bmatrix} \theta_2-\theta & \theta-\theta_1 \end{bmatrix} \begin{bmatrix} \mathbf{E}(\theta_1,\phi_1) & \mathbf{E}(\theta_1,\phi_2) \\ \mathbf{E}(\theta_2,\phi_1) & \mathbf{E}(\theta_2,\phi_2) \end{bmatrix} \begin{bmatrix} \phi_2-\phi \\ \phi-\phi_1 \end{bmatrix} \tag{3.23}$$

Bilinear interpolations are amongst MATLAB's in-built GPU-accelerated functions, and therefore can be implemented without modification if running on a graphics card. The same procedure applies for interpolating the tag radiation pattern.

3.3.2 Coordinate Transformations

The field pattern above is in the local spherical coordinate system of the antenna. However, in order to perform interactions with tags, a global Cartesian system is defined in which all antennas and tags lie, and in which all geometrical transformations of tags and antennas are performed.

A transformation, $\mathbf{T}$, on a vector field, $\mathbf{E}(\mathbf{r})$, is performed by first transforming the basis vectors, $\mathbf{r}$, by $\mathbf{T}$ to a new reference frame with basis vectors, $\mathbf{r'}$, to obtain a field, $\mathbf{E}(\mathbf{r'})$, in the new coordinate system. An inverse transformation is then applied to the new field to obtain the transformed field in the original coordinate system. i.e.

$$\mathbf{r'} = \mathbf{T}\mathbf{r} \tag{3.24}$$

gives a transformed coordinate frame. The transformation is then applied to the new field to obtain the transformed field in the original coordinate system. i.e.

$$\mathbf{E'}(\mathbf{r}) = \mathbf{T^{-1}}\mathbf{E}(\mathbf{r'}) = \mathbf{T^{-1}}\mathbf{E}(\mathbf{T}(\mathbf{r})) \tag{3.25}$$

The transformation of interest here is rotation (for antenna and tag orientation), given by the composite rotation matrix $R = R_x(\theta_x)R_y(\theta_y)R_z(\theta_z)$, where $R_i(\theta_i)$ represents rotation about the i axis by angle θ_i, where

$$R_x(\theta_x) = \begin{pmatrix} 1 & 0 & 0 \\ 0 & \cos\theta_x & -\sin\theta_x \\ 0 & \sin\theta_x & \cos\theta_x \end{pmatrix}, R_y(\theta_y) = \begin{pmatrix} \cos\theta_y & 0 & \sin\theta_y \\ 0 & 1 & 0 \\ -\sin\theta_y & 0 & \cos\theta_y \end{pmatrix}, R_z(\theta_z) = \begin{pmatrix} \cos\theta_z & -\sin\theta_z & 0 \\ \sin\theta_z & \cos\theta_z & 0 \\ 0 & 0 & 1 \end{pmatrix} \tag{3.26}$$

The implementation is performed by first calculating the unit vector, $\hat{r}$, from the antenna to the test (x, y, z) location of interest, and then applying Eqn 3.25 to the unit vector.

3.3.3 Tag receive power

The downlink describes the path from the reader antenna to the tag antenna. The reader antenna field from Eqn 3.22, after the above interpolation and transformation process, is

propagated through free space to the tag according to

$$\mathbf{E} = \mathbf{E_0}\frac{e^{j\mathbf{k}.\mathbf{r}}}{r} \tag{3.27}$$

Where $\boldsymbol{r}$ is the displacement from the reader antenna, $\boldsymbol{k} = \frac{2\pi}{\lambda}\hat{\boldsymbol{r}}$ is the wavevector and $\boldsymbol{E(r)}$ is the electric field strength at $\boldsymbol{r}$. The field received at the tag interacts with the tag's antenna to provide power to the tag. The field incident on the tag is

$$\mathbf{E_{in}} = \mathbf{E_0}\frac{e^{j\mathbf{k}.\mathbf{d}}}{d} \tag{3.28}$$

where $\boldsymbol{d}$ is the direction vector from the antenna to the tag, $d = |\boldsymbol{d}|$ is the distance from the antenna to the tag. Using the vector effective length, $\boldsymbol{L}$, of the tag , the open circuit voltage across the terminals of the tag's antenna can be obtained: [111].

$$V_{OC} = \mathbf{E_{in}} \cdot \mathbf{L} \tag{3.29}$$

The effective length of an antenna is a vector quantity which gives the voltage produced by 1V/m of electric field across its open terminal [115, 111]. It is defined as the ratio of the orthogonal component of the radiation vector to the exciting current i_{in}, for the tag antenna [115]

$$\mathbf{L} = \frac{-\mathbf{F}_\perp}{i_{in}} \tag{3.30}$$

where $\mathbf{F}_\perp$ is the perpendicular component of the radiation vector, as defined in Eqn 3.22, and i_{in} is the antenna exciting current.

Therefore, the effective length vector can be calculated using results from antenna simulations or measurements, thereby allowing the tag open circuit voltage to be calculated, from which the power is obtained. If perfect matching between the tag antenna and load is assumed, the received power at the tag can be obtained from [109].

$$P_r = \frac{V_{oc}^2}{8R_L} \tag{3.31}$$

R_L is the real part of the tag impedance, although, the effects of antenna mismatch could be included.

The hybrid modelling approach using method of moments to calculate the electric field pattern along with a geometric optics approach allows for rapid simulation of wide areas with modest computing resources.

3.3.4 Verification with simple test case

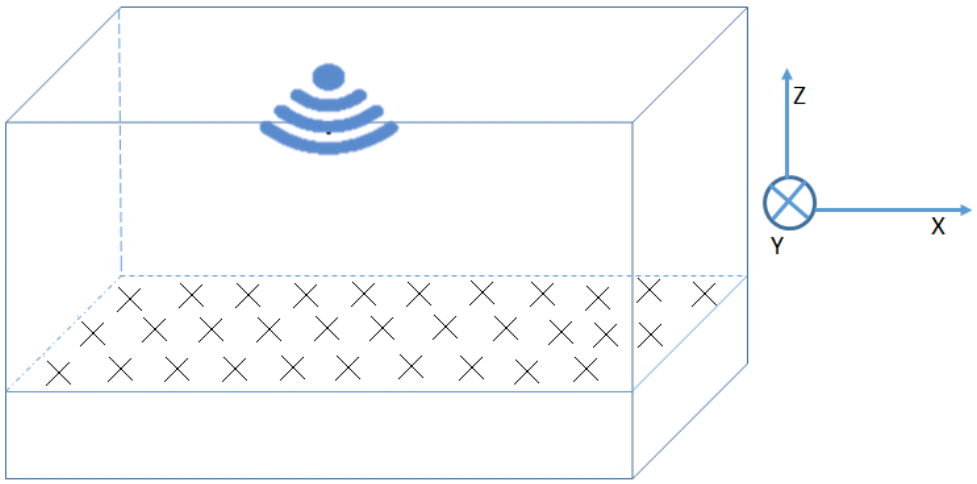

Figure 3.3: Experiment to test model in a simple case with a single antenna pointing downward and tags forming a grid on XY plane.

In this section, an example to demonstrate the predicted field patterns generated by the model is presented. The test experiment used here is illustrated in Fig 3.3. A circularly polarised antenna at a height of 3m from ground level is pointing vertically downwards. The entire 3D volume of $8m \times 8m \times 3m$ is filled with tags (dipole antennas). In this demonstration, the tags are oriented in different directions (x, y, z) to consider the effect of polarisation on the received power distribution. The value at each point in space gives the power received by the tag located at that point (Eqn 3.31). The power distributions for this simulation are presented in Fig 3.4 with X, Y and Z plane cuts for z and y oriented tags. The Z plane cut is shown in Fig 3.5 for all three tag polarisations. The reader has an antenna gain of 8 dB and transmit power of 27 dBm, while the gain of the tags is 2dB.

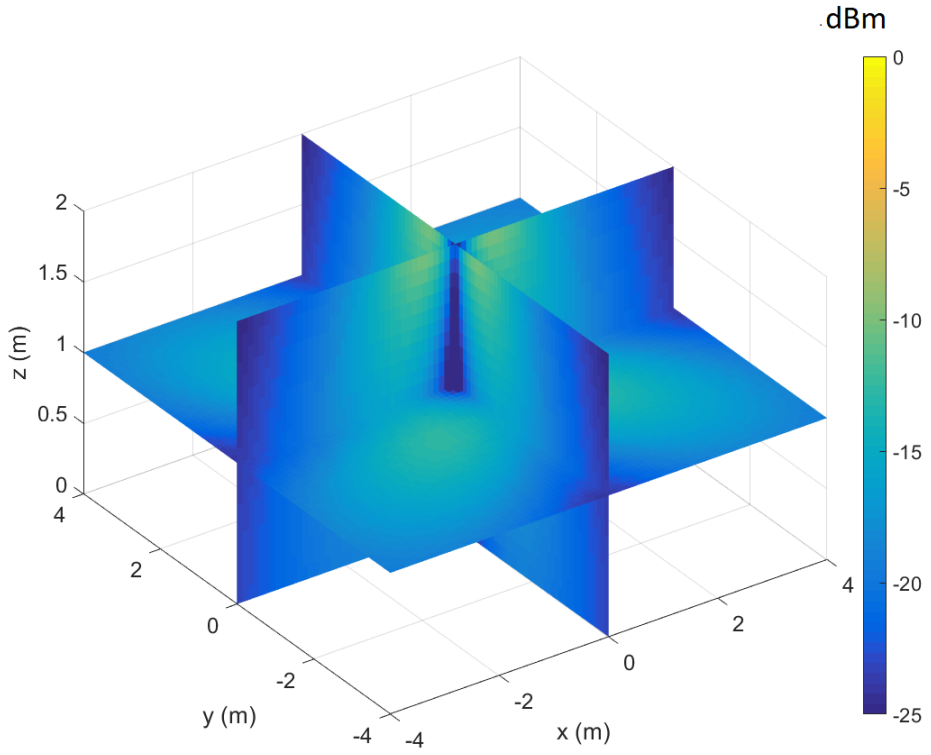

(a) z- oriented tags

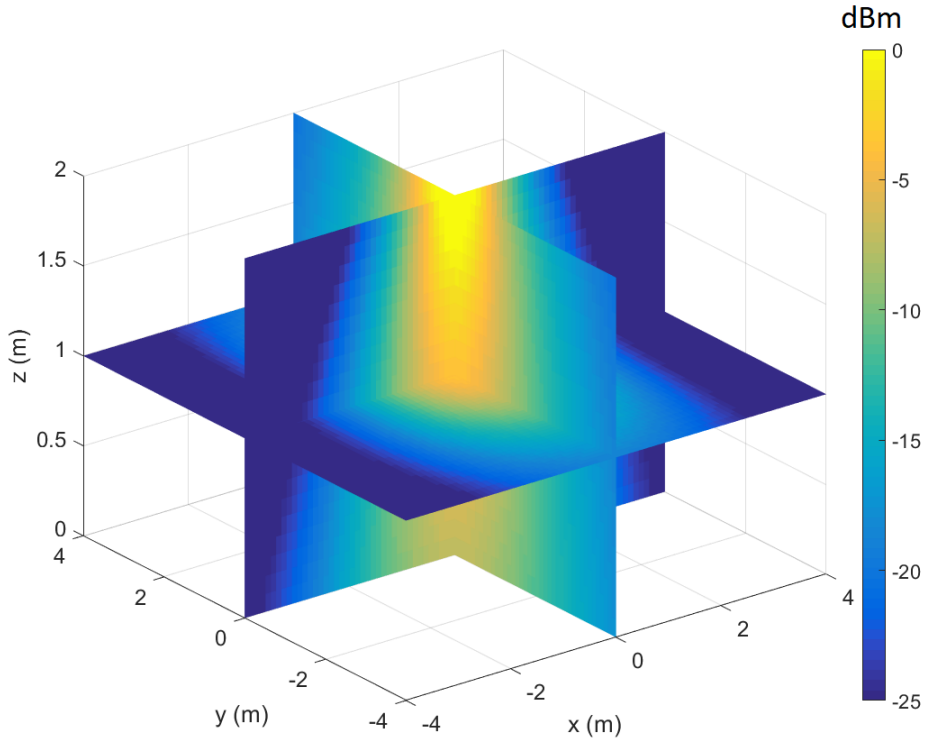

(b) y- oriented tags

Figure 3.4: Model test example for down-pointing antenna at 3m height and 3D grid of tags, showing cuts at the planes $X = 0, Y = 0$ and $Z = 1m$

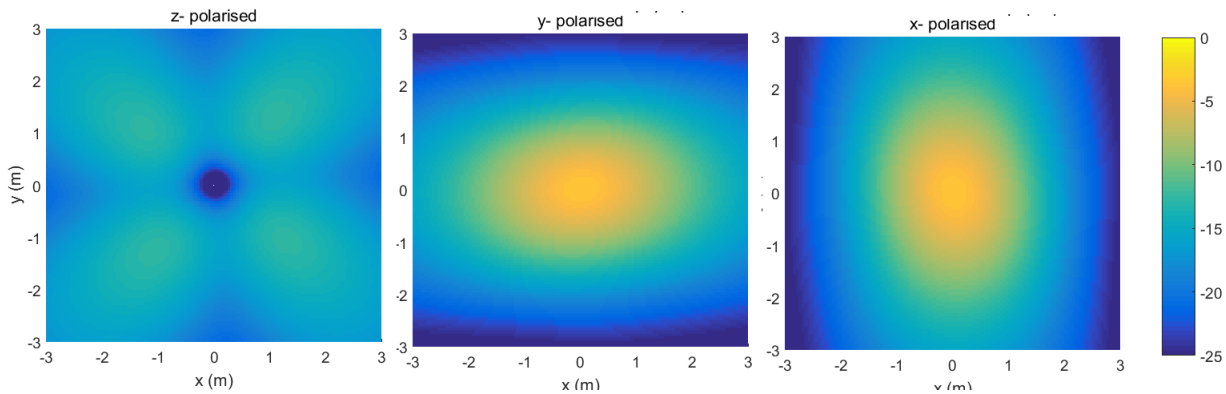

Figure 3.5: Model Test with antenna pointing vertically downwards for tags on the plane $Z = 1m$

It is seen that, for z-oriented tags (whose axes point to the reader antenna, Fig 3.5a), a null point is observed at the centre of the room, where the tags are directly below the antenna. This is due to the null of the dipole antenna pointing to the reader antenna transmission direction, thereby receiving a minimal amount of power. The power then increases gradually as one moves away from the centre, since the reader antenna field is incident on the tag at increasing angles away from the centre. At longer ranges, the received power begins to reduce, as the improvement in the tag antenna gain is negated by both the decrease in the reader antenna gain outside the 3dB beamwidth and increasing free space path loss. For the x- and y-oriented tags (Figs 3.5 b, 3.5 c), maximum receive power is at the centre, and the power decreases away from the centre. It is important to observe that the range in the x-direction is longer than in the y -direction for x-polarised tags. The reason for this is expanded upon in the section following. The same is true for y-polarised tags, with directions reversed.

3.3.5 Multipath

The model has up to this point, included only a single path from antenna to tag. Real environments however experience fading due to multipath. In this section, a first order reflection is included into the model, as illustrated in Fig 3.6. The ground is modelled as a dielectric material of infinite extent in the $-z$ direction, such that the Fresnel reflection coefficients are applicable.

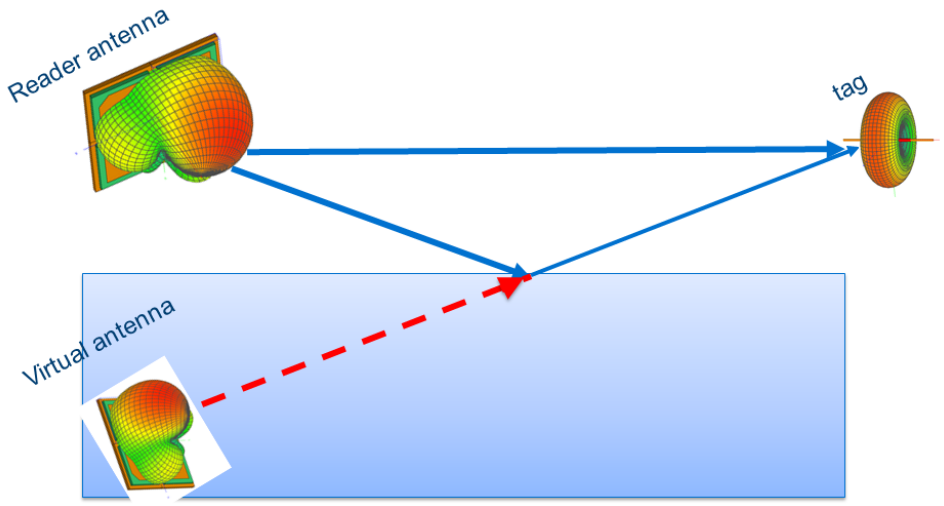

Figure 3.6: RFID model showing ground reflection modelling using virtual antenna images and Fresnel coefficients

Ground Reflections

As illustrated in Fig 3.6, the reflection is modelled using electromagnetic images of the antenna. The equivalent model of a reflection is an additional transmitting antenna, which is a mirror image about the ground surface ($Z = 0$) of the original, and transmitting a modified field given by

$$\mathbf{E_r} = \begin{pmatrix} E_{\parallel,r} \\ E_{\perp,r} \end{pmatrix} = \begin{pmatrix} \tau_{\parallel} E_{\parallel} \\ \tau_{\perp} E_{\perp} \end{pmatrix} \tag{3.32}$$

where τ represent the Fresnel reflection coefficients for TE and TM components, given by

$$\tau_{\parallel} = \frac{n_i \cos\theta_i - n_t \sqrt{1 - \left(\frac{n_i}{n_t}\sin\theta_i\right)^2}}{n_i \cos\theta_i + n_t \sqrt{1 + \left(\frac{n_i}{n_t}\sin\theta_i\right)^2}} \tag{3.33}$$

$$\tau_{\perp} = \frac{n_t \sqrt{1 - \left(\frac{n_i}{n_t}\sin\theta_i\right)^2} - n_t \cos\theta_i}{n_t \sqrt{1 - \left(\frac{n_i}{n_t}\sin\theta_i\right)^2} + n_t \cos\theta_i} \tag{3.34}$$

The indices i and t represent the incident and transmitting media (respectively air and concrete in this experiment). $n_{i,t} = \varepsilon_{i,t}^{\frac{1}{2}}$ is the refractive index, θ is angle of incidence. h is the height of the real transmitter.

Consequently, each tag receives a total field given by the vector sum of the incident

and reflected fields.

$$\mathbf{E} = \mathbf{E_i} + \mathbf{E_r} \tag{3.35}$$

A verification similar to the above is performed, but with a ground plane included, as in Fig 3.3, for which the results are shown in Fig 3.8. The fading effects are observed as the interference patterns. A complex pattern emerges due to reflectance of the floor to fields parallel and perpendicular to its surface, the changing axial ratio of the reader antenna with both azimuth and elevation and the changing gain of the tag antenna in response to the direct and reflected path with position.

It can be observed that the inclusion of a ground brings about multipath fading due to constructive and destructive interference between the direct and reflected components as expected.

The pseudocode for the model is summarised below in Algorithm 1.

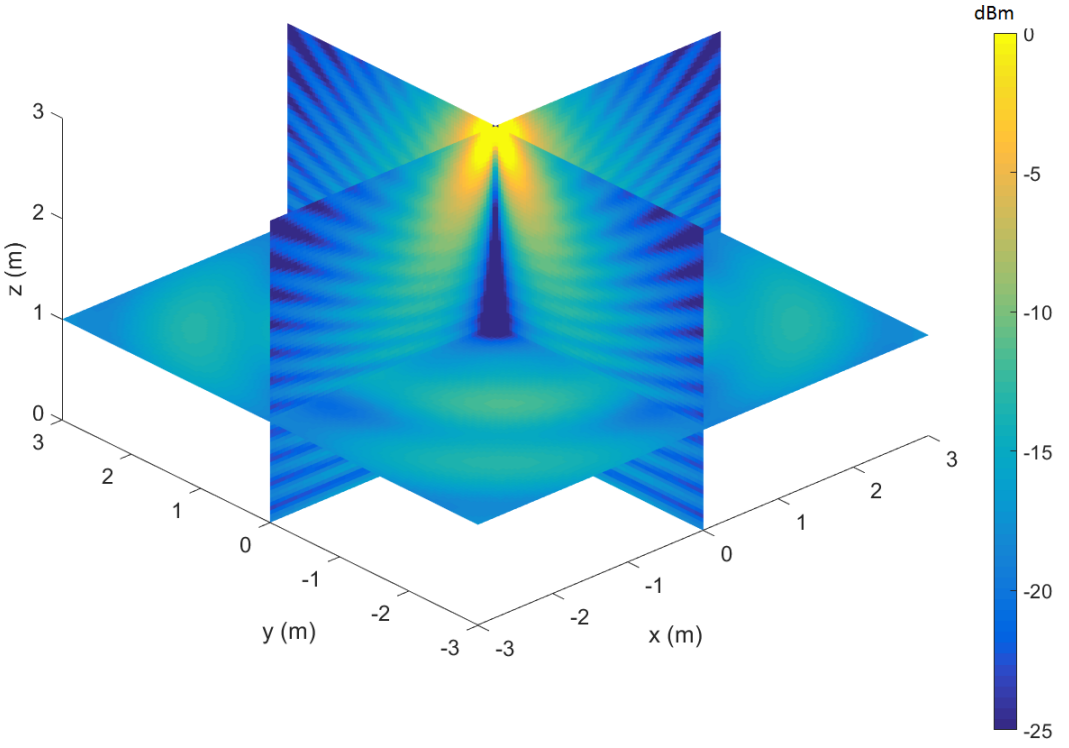

(a) z- oriented tags

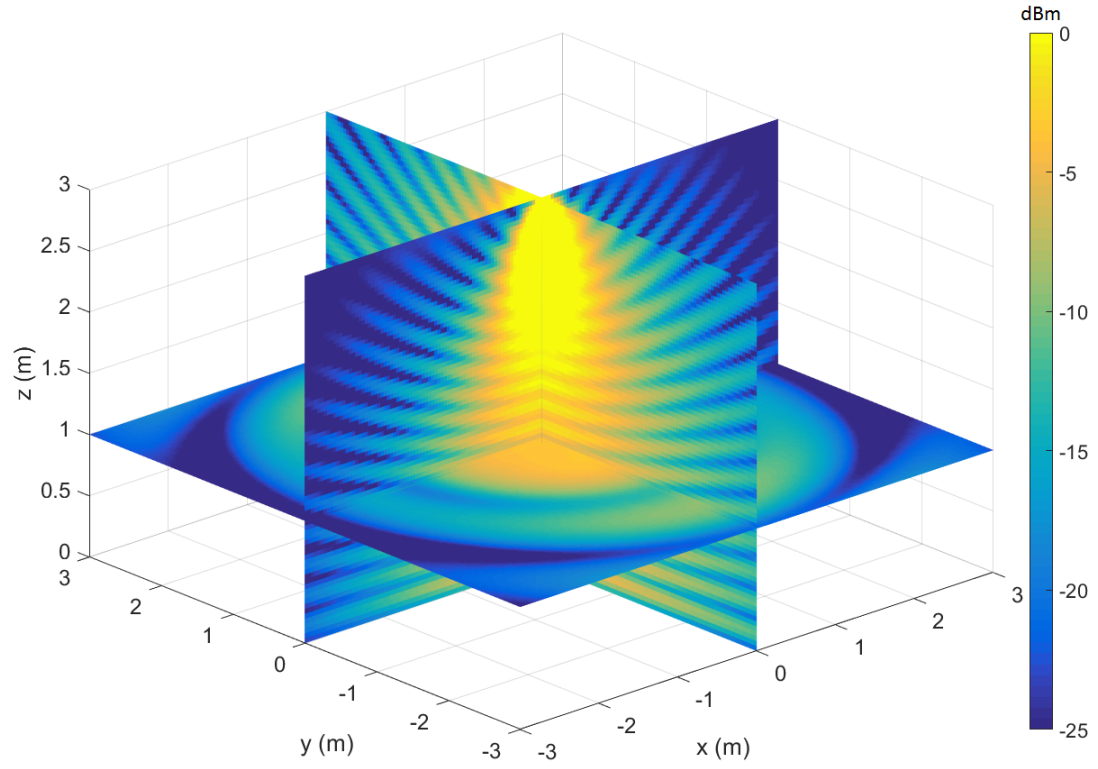

(b) y- oriented tags

Figure 3.7: Model test example for down-pointing antenna at 3m height and 3D grid of tags with dielectric ground, showing cuts at the planes $X = 0, Y = 0$ and $Z = 1m$

Algorithm 1: Pseudocode for RFID model

```
Initialise scene geometry, antenna and tag parameters (number, locations,
orientations, EIRP scaling)
loop
    for each antenna i do
        for each tag j do
            Calculate distance vector from antenna to tag
            Interpolate antenna pattern to get electric field corresponding to direction
            vector (Eqn 3.23)
            Determine electric field incident on tag using Eqn 3.28
            Calculate complex voltage dropped across tag (Eqn 3.29, 3.30 and 3.22)
            Replace antenna with its image and repeat (5) to (8) to account for
            reflections (Eqns 3.32 to 3.34, Fig. 3.6)
            Add results of (8) and (9) to determine voltage across tag due to direct and
            reflected components
        end for
    end for
    Apply beam manipulation (optional, e.g, beam steering)
    Calculate total voltage across each tag due to all antennas to get spatial power
    distribution (by summing for phase dithering or antenna selection for TDM)
    Apply phase hopping to each antenna (optional, for phase dithering)
    Apply frequency hopping (optional, for FDM)
    Calculate spatial power distribution (Eqn 3.31)
end loop
```

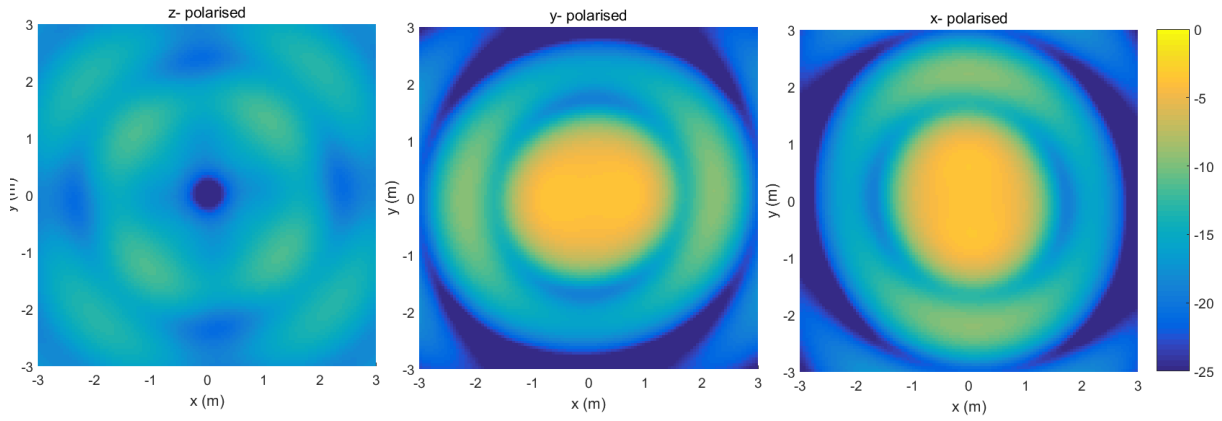

Figure 3.8: Model Test with antenna pointing vertically downwards for tags on the plane $Z = 1m$ with dielectric ground

3.3.6 Model Validation

In this section, the model is validated using FEKO simulations. However, it is important first of all to normalise the fields in order to enable the antennas to transmit with desired power levels. This is important when performing simulations, as arbitrary power levels can be set to suit the application being modelled, as well as adhere to regulated limitations of maximum EIRP.

Field normalisation

Since the antenna fields imported from electromagnetic software may not always be normalised or may depend on the input power used, it is important to normalise the electric field based on Equivalent Isotropic Radiated Power (EIRP). EIRP is defined as the product of the transmit power and the antenna gain. The simulated or measured antenna pattern will have an EIRP given by:

$$P_A = P_{rad} G_{max} \tag{3.36}$$

$$= \iint \left(|E_\theta|^2 + |E_\phi|^2 \right) \mathrm{dS} \times \max_{\theta,\phi} \left(\frac{|E_\theta|^2 + |E_\phi|^2}{\frac{1}{4\pi} P_{rad}} \right) \tag{3.37}$$

To obtain the desired EIRP, say, P_E, the antenna electric fields are scaled by k, ie $|E_\theta| \rightarrow k|E_\theta|$ and $|E_\phi| \rightarrow k|E_\phi|$ where k is given by

$$k^2 = \frac{P_E}{P_A} \tag{3.38}$$

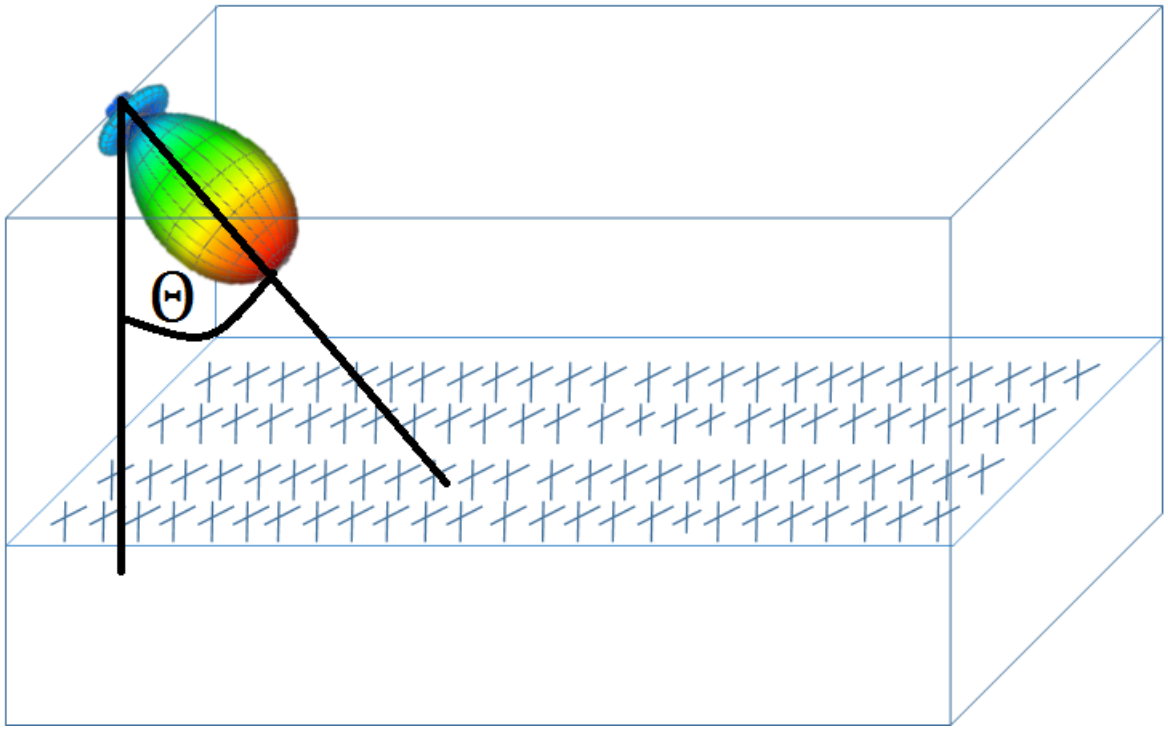

Figure 3.9: Setup for model validation. A single antenna pointing at a defined angle to the vertical, and the power received by each tag, making a 2D grid on a defined height in the xy plane.

The antenna then has an EIRP of P_E, which can be set to satisfy the specific requirements of the application.

Comparison with Full wave Simulations

A validation is done using full wave simulations in FEKO. A series of experiments are performed in FEKO according to Fig 3.9 for different antenna orientations, and compared to the presented model. The Reflection Coefficient Approximation ground plane was set in FEKO. The transmit antenna has a gain of 11 dBiC while the tags are dipoles with gains of 2.0 dB. The transmit power is 30 dBm. The experiment consists of a single antenna 3m above the ground level tilted at an angle. A tag is placed directly below the antenna at a height of 1m, and the received power is recorded. The tag is moved along the x axis and the results collected for power variation with distance. Three angles are investigated in this experiment from Figs 3.10 to 3.12.

It can be seen that close agreement is obtained with the FEKO simulations for each case. An advantage to using such hybrid models, as here presented lies in their ability to

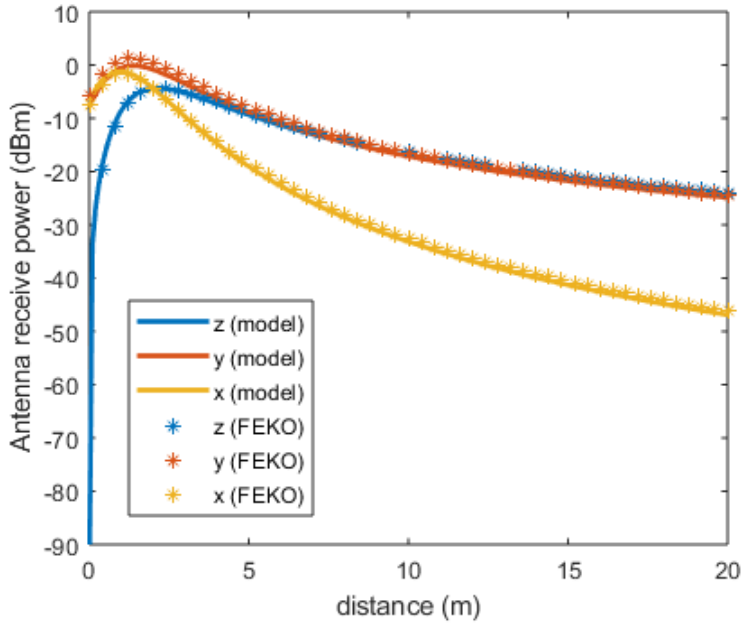

Figure 3.10: Model comparison with FEKO for antenna tilted 45^0 in free space

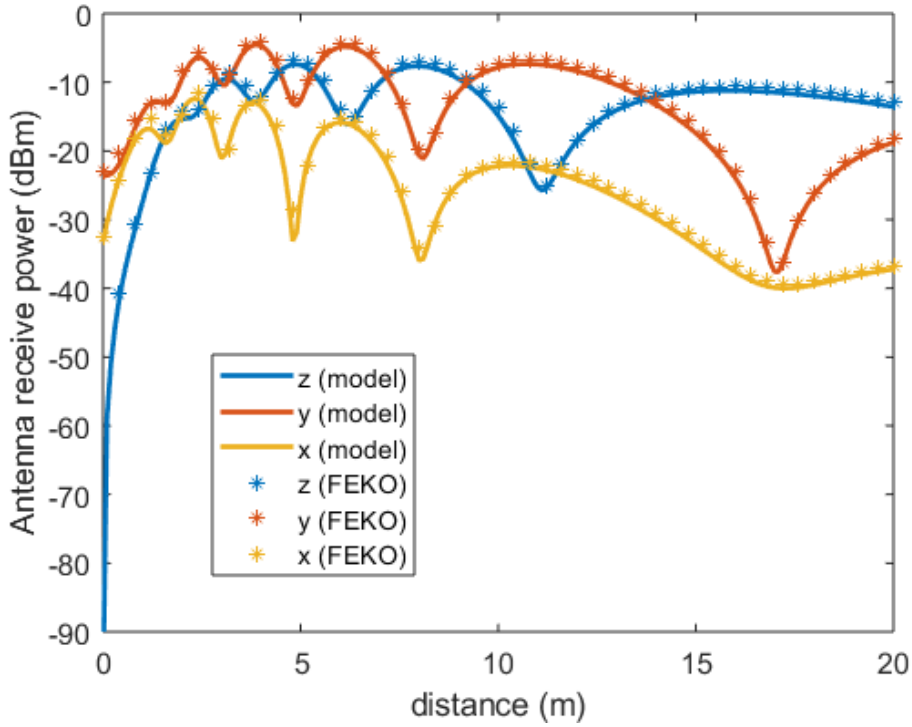

Figure 3.11: Model comparison with FEKO for antenna tilted 90^0 with perfect ground

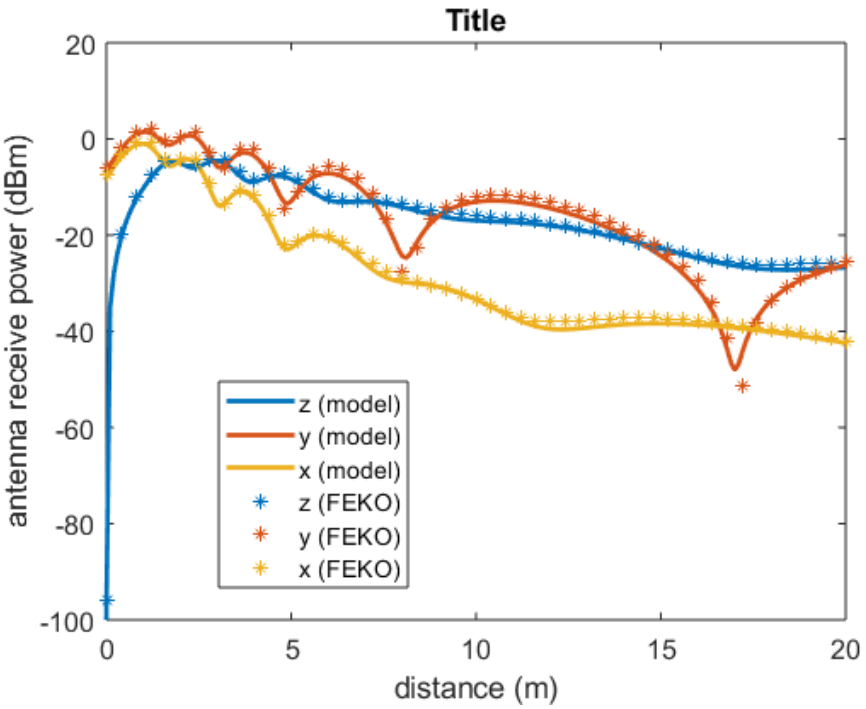

Figure 3.12: Model comparison with FEKO for antenna tilted 45^0 with a concrete ground

perform rapid simulations in comparison to full wave solvers, which are not specifically suited to such applications. For example, to perform the simulation described by Fig 3.9 required 10 hours in FEKO using a grid spacing of 10mm. Extending this to a volumetric grid, with 20 points in the z direction, for example, will require 200 hours, which is excessive. Conversely, the above simulations took about one second (plus $\sim$ 5 minutes for antenna simulations) in the presented model. Furthermore, the model is capable of antenna pattern manipulations (such as beam steering as done in the following chapters), multiple antenna multiplexing schemes (as done in the section below), as well as multi-cell RFID simulations, which will prove challenging for FEKO, or indeed any full wave simulation method.

3.4 Performance Evaluation

This section establishes the performance criterion used to compare different RFID systems based on the power received by the tag. A histogram can be used to plot the probability density function (pdf) of the distribution of power in the interrogation zone. The vertical and horizontal polarisations for Fig 3.8 above are compared to illustrate this. A histogram

representation of their power distributions are shown in Fig 7.6.

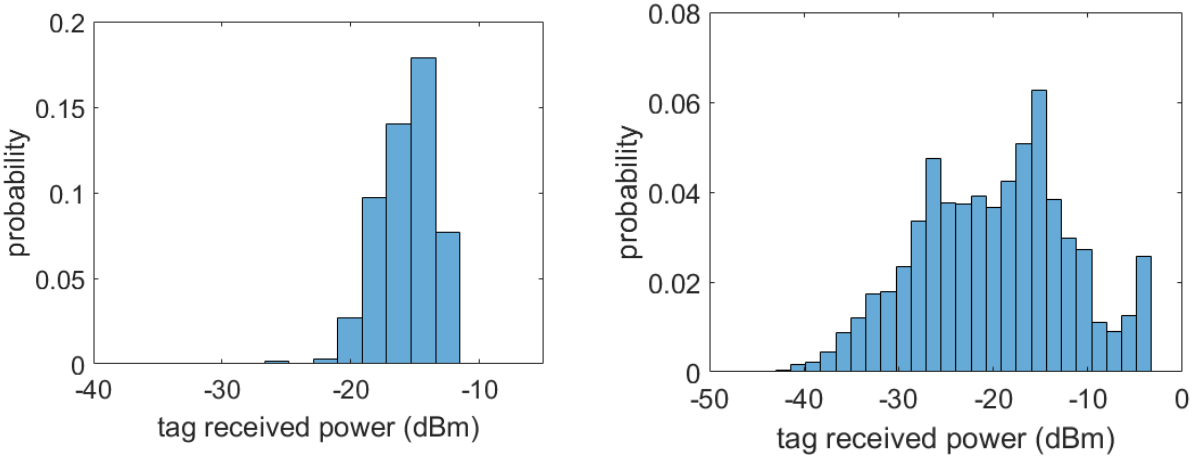

(a) Vertical tags (z)

(b) Horizontal tags (x or y)

Figure 3.13: Tag read histogram for power distributions in Fig 3.7b

A comparison is made between them by observing the cumulative distribution function (cdf) as plotted in Fig 3.14. It is observed tat the vertical tags, which have a narrower histogram spread have a steeper cdf curve. Also, the vertical tags will attain a higher read percentage in a practical system, since the tags with the lowest received power determine the read success rate, even though both polarisations have the same median (cdf=0.5) power. The cdf will be used as a tool to compare the performance of different systems.

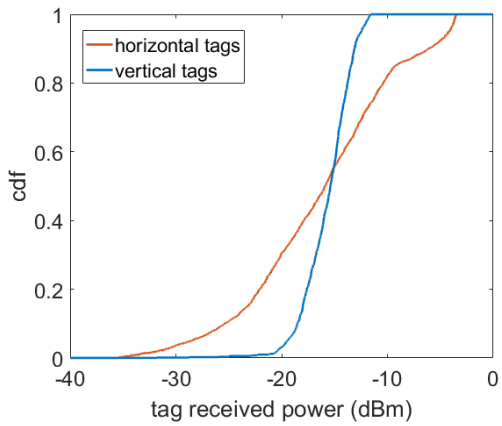

Figure 3.14: Tag read cdf for power distributions in Fig 3.8

3.5 Case Study: Diversity Schemes in a Multi-antenna RFID System

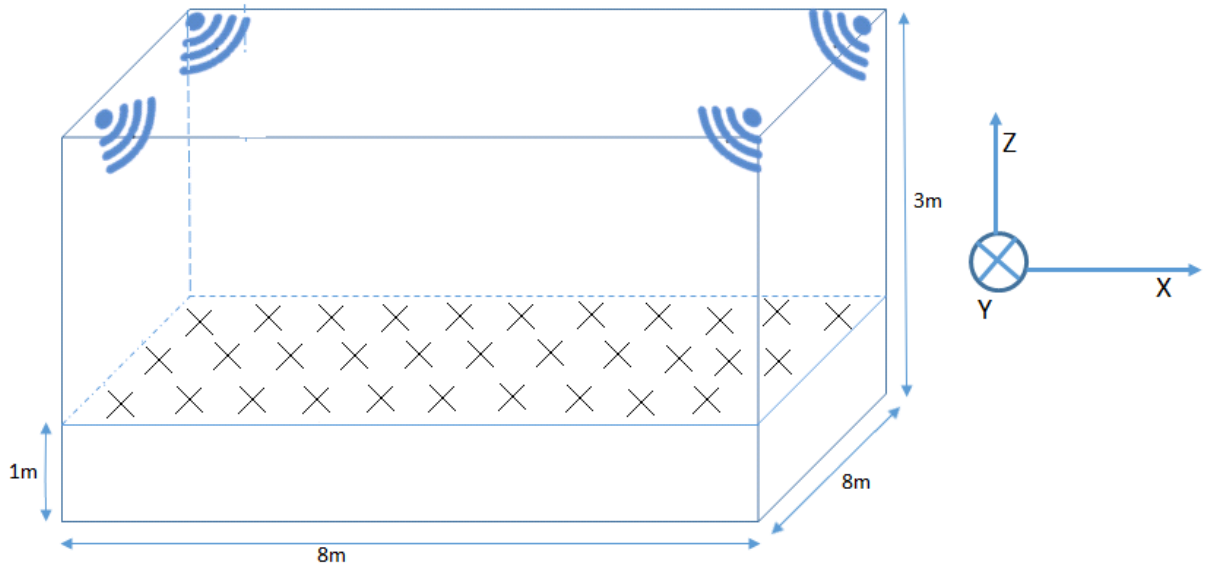

Figure 3.15: Setup for case study investigating multi-antenna multiplexing schemes in a four-antenna RFID cell system

In this section, a case study using the model is presented. A typical rectangular cell with four antennas as illustrated in Fig. 3.15 is considered. The setup simulated is in the context of a multi-cellular system, in which the cell in Fig 3.15 is repeated across the interrogation area. As a result, the effect of walls can be neglected. The specific case studied is of an antenna at a height of $3m$, and tags in a 2D grid at a height of $1m$.
The use of multiple, simultaneously transmitting RFID antennas fails to provide the expected increased receive power at the antenna due to mutual interference among the antennas, leading to a degraded performance, as described in Chapter 1 and 2. This is caused by the blind spots introduced by destructive interference. i.e. points in the interrogation zone where a tag would receive less than its threshold power. As a result, several diversity or multiplexing schemes are used to resolve this problem.

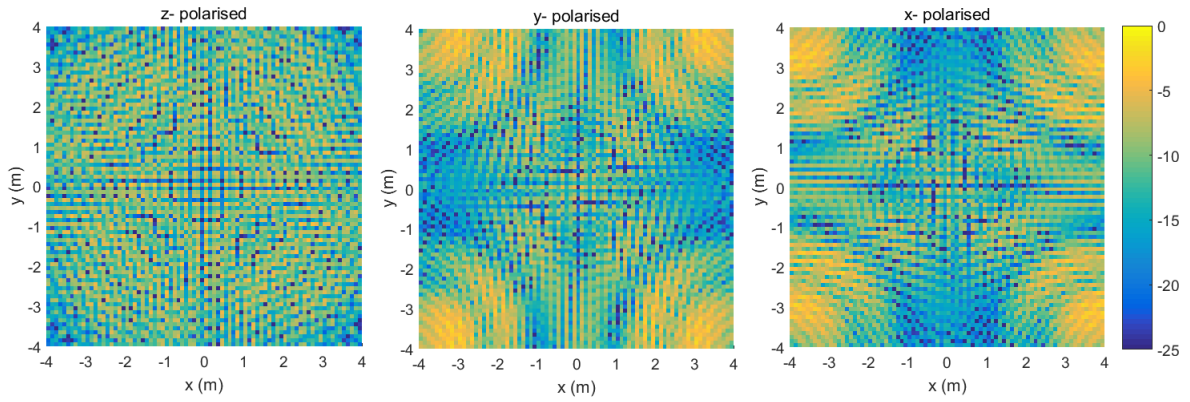

Figure 3.16: Power distribution of a four-antenna system as seen by tags on plane Z=1m, showing intra-cell multi-antenna mutual interference in an $8m \times 8m$ zone, leading to blind spots

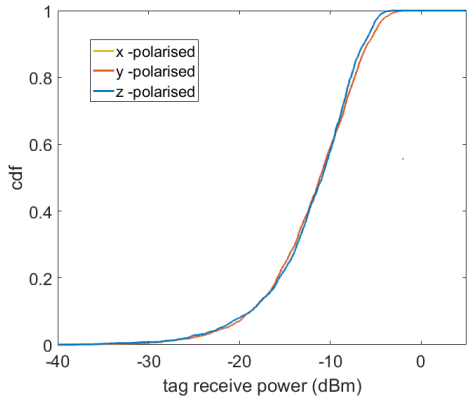

Figure 3.17: Tag cdf of multi-antenna system with mutual interference

As is demonstrated in Fig 3.16, deep nulls exist randomly in the interrogation zone, which means that the read rate probability is severely degraded as demonstrated in Fig 3.16 and Fig 3.17.

Diversity, as used in communication systems, refers to the use of two or more versions of the same signal with different paths to the receiver, and the use of a selection or combination scheme to maximise performance by some criterion e.g. received power, P, which is at least equal in performance to any of the individual paths, i.e. $P_{div} \geq P_i$, $\forall i$, where P_i represents the power due to the ith path. This is especially useful in multipath environments, relying on the fact that separate antennas will experience different paths (channels). Several diversity schemes have been applied to multi-antenna RFID systems, to improve performance. Three principal diversity schemes are explored, and their relative

performances analysed.

3.5.1 Time Division Multiplexing (TDM)

In a TDM system, each antenna is allocated a time slot within which to transmit, so as to avoid the problems of interference described above. In practice, this is usually implemented using a circuit which switches between different antenna ports, thereby ensuring a single antenna to be active at any given moment in time. TDM is implemented in many commercial multi-port RFID readers e.g the Impinj Speedway reader.

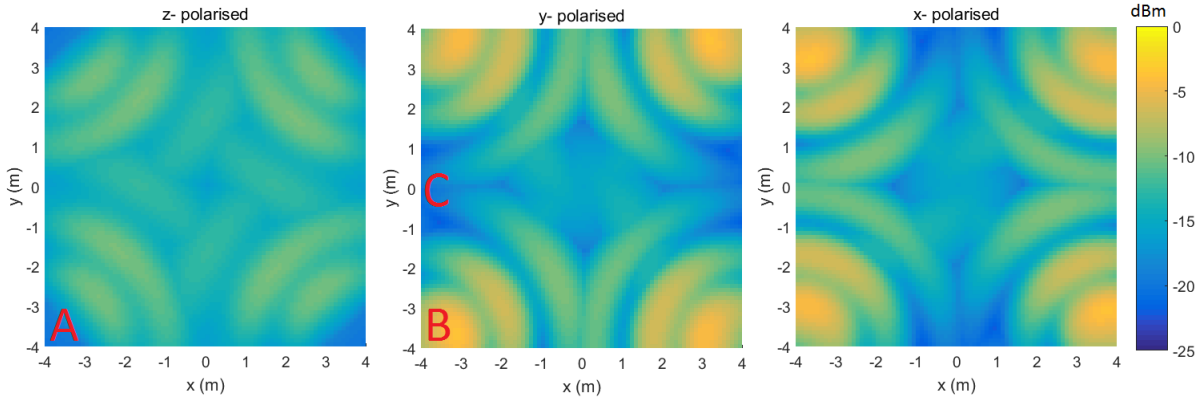

Figure 3.18: Power distribution of a four-antenna system as seen by tags on plane Z=1m for TDM system

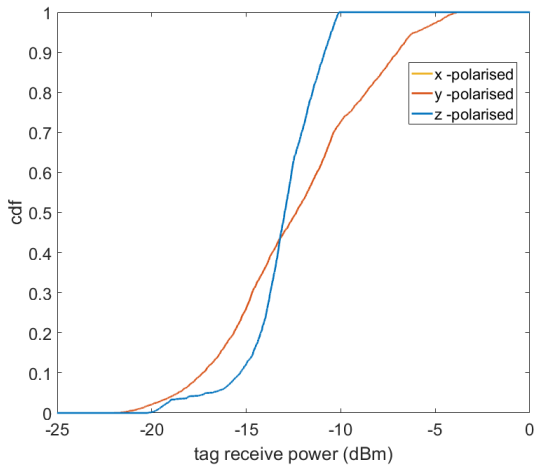

Figure 3.19: Tag cdf for TDM system

The power distributions in space as seen by tags with their axes oriented in x, y and z directions are plotted in Figs. 3.18 and 3.19. It can be seen that the deep nulls in Fig 3.16

due to antenna interference are absent in the TDM case. The nulls present are rather as a result of multipath due to reflections, and are not solved by any multiplexing scheme. This results in 99% of tags in the TDM system receiving at least -22 dBm, compared to -31 dBm for the case with no diversity.

Some Observations on tag placement

It is also possible to infer from the power distributions some important general properties of a four-antenna cell. It is observable for example that the ideal orientation for placing tags under such a scheme is highly dependent on the tag polarisation. A typical commercial RFID tag has a sensitivity of -15 to -20 dBm. In this case the ideal tag orientation is in the z direction. Considering, for example, a sensitivity of -15dBm, an 88% read rate for vertical (z) tags and 74% for horizontal (x or y) tags are observed. i.e a margin of 14%. On the other hand, low tag sensitivities favour horizontal polarisations. For example, tag arrays have been shown to degrade the sensitivities of tags when compared to isolated tags [116]. Considering a tag sensitivity of -10 dBm, caused for example by a non-ideal situation such as closely-spaced items, it is observed that no z-polarised tag can be read, whereas, up to 30 % of the horizontal (x or y) tags could be read.

It is also important to analyse the tag readability in terms of their location in the cell, as this is also orientation-dependent. In the z orientation, the worst position for placing the tags is directly underneath the antennas (for example position A in Fig 3.18). This is because the tag (dipole) is powered mainly by this single antenna, and its (null) axis is parallel to the direction of the incident wave, therefore minimal power is received. On the other hand, the remaining antennas, which have a more favourable relative orientation to the tag, face a high free space loss due to the wide separation. Moving the tag away from A on the x-y plane, the relative orientation between the reader antenna at A and tag becomes favourable, and increased power is observed.

For the x- polarisation, the tags directly underneath the antennas receive the greatest power due to an ideal alignment with respect to the reader antenna (e.g. position B). The remaining three antennas have little effect on this tag in comparison, due to the long range and consequent high free space loss coupled with the less favourable relative orientation. However, the power drops as one moves away from B, and at different rates depending on the tag orientation. Considering Fig 3.18, moving from point B along the x direction,

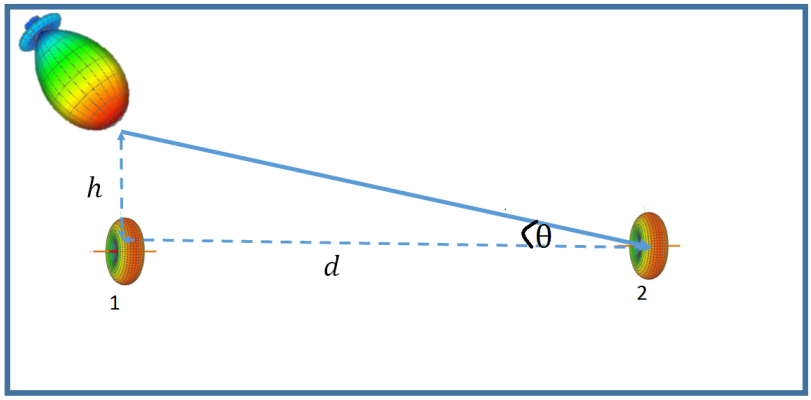

Figure 3.20: Tag power variation at different horizontal separations from antenna

the power drops due to free space loss alone. Along the y-direction, in addition to the free space loss, the tag orientation with respect to the antennas also plays an important role. This could be explained using Fig 3.20. At position 1, the horizontally oriented tag is directly beneath the antenna, and therefore receives a field $E \sim \frac{1}{h}\sin\theta$, which is maximum, since $\theta = 90^0$, where the $\sin\theta$ factor results from the radiation pattern of a dipole antenna, $1/h$ is free space loss factor. At position 2, the received electric field is $E \sim \frac{1}{\sqrt{h^2+d^2}}\sin\theta$. Far away from the antenna, i.e when $d >> h$, $\sin\theta \rightarrow 0$, and therefore the received power vanishes. In other words, the tag's axis is effectively aligned to the direction of the incident wave, and therefore no power is received. This explains the reason for the low received power at point C in Fig 3.18. The same argument for x polarised tags applies to y- polarised tags, but with the orientations reversed.
It should also be noted that these arguments are independent of multiplexing scheme, and apply equally to all.

3.5.2 Frequency hopping

It is well known that frequency diversity is used to resolve fading problems in communication systems [63, 100, 117, 118]. The scheme makes use of different frequency channels carrying the RF signal. Because different frequencies undergo different paths, the least faded path can be selected, thereby improving the performance. In order for this to be effective, a wide bandwidth is required. However the low bandwidth of ETSI RFID systems limits the efficacy of such technique in overcoming this problem [63]. In [65], the entire 860-960 MHz is used to limit the problem, although this is not permissible under the reg-

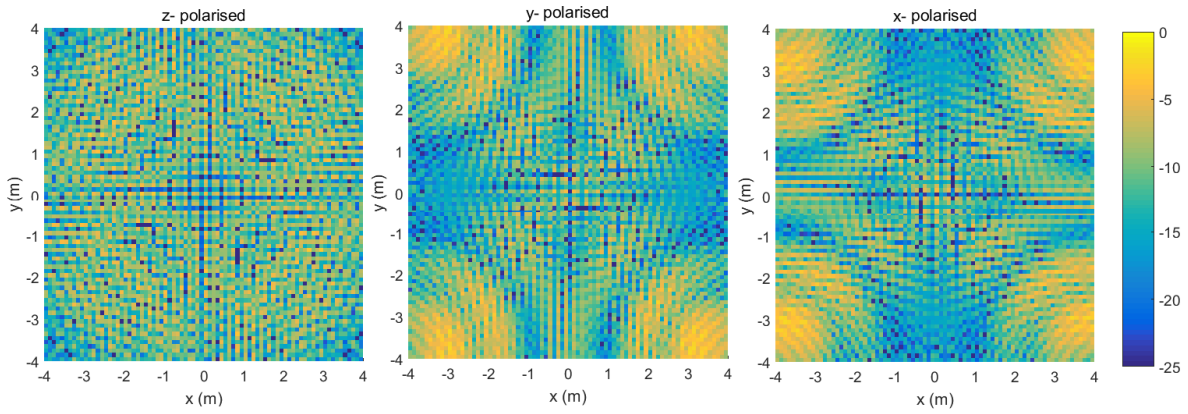

Figure 3.21: A four-antenna system with frequency hopping for 865.6-867.4 MHz (ETSI narrow band) shows little reduction of nulls

ulations [36]. This scheme is run over N iterations, where N is the number of frequency channels available. The maximum power delivered to each location is then recorded and plotted, as this represents the maximum amount of power that can be delivered to a tag at that location. In this section, Fig3.21 shows the power distribution for frequency hopping scheme for the 865-868 MHz using four channels centred at 865.6 MHz, 866.5 MHz, 867.8 MHz and 868.5 MHz. The entire 860-960 MHz band is also simulated in 1MHz steps in Fig 3.22. All four antennas transmit simultaneously, and the frequency in incremented.

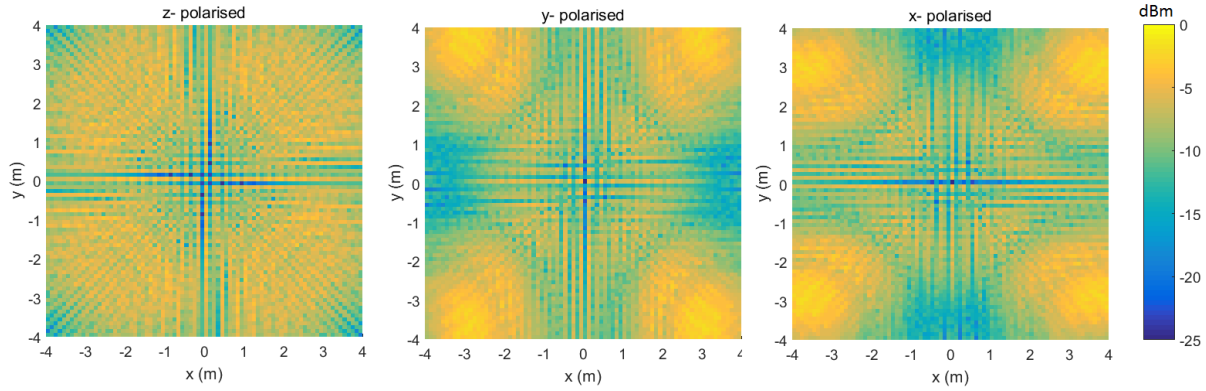

Figure 3.22: A four-antenna system with frequency hopping for 860-960 MHz (RFID global band) shows significant null resolution

It is seen that the frequency hopping using the ETSI band provides a minute improvement to the performance of the system, but not significant, due to the afore-mentioned reasons, while for the 860-960 MHz, a much less faded power distribution is observed.

3.5.3 Phase hopping

The effect of phase hopping as described in the previous chapter is also modelled. Here, each antenna undergoes random phase shifts between 0 and 180^o at each iteration. Over many iterations, the received power at each location is maximised [101]. Figs 3.23 show the results of such a system over 1000 iterations of phase hop states. It is seen that the overall tag received power is greatly increased due to phased field summations.
Multipath is still present nevertheless due to reflections, which are not resolved by phase hopping. However, the applied field summation greatly reduces the depth of the fading.

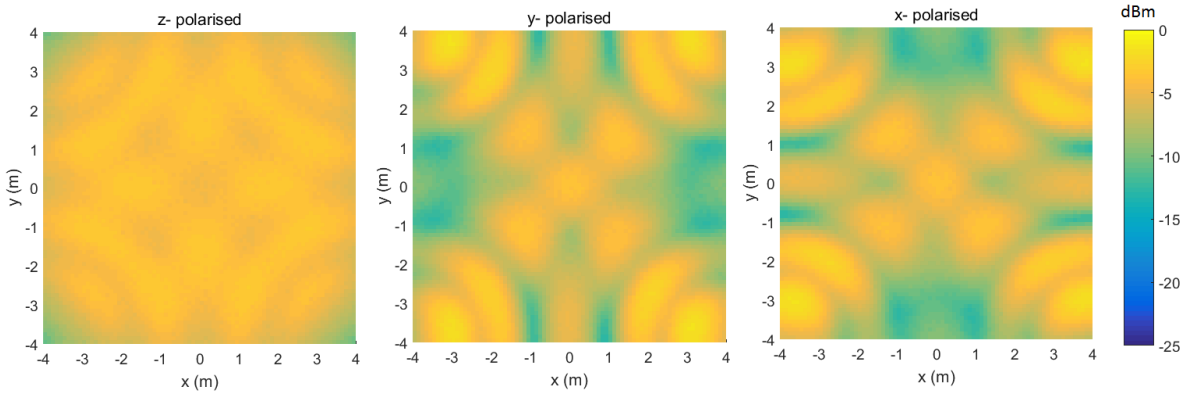

Figure 3.23: Power distribution of a four-antenna system as seen by tags on plane Z=1m for a phase hopping system

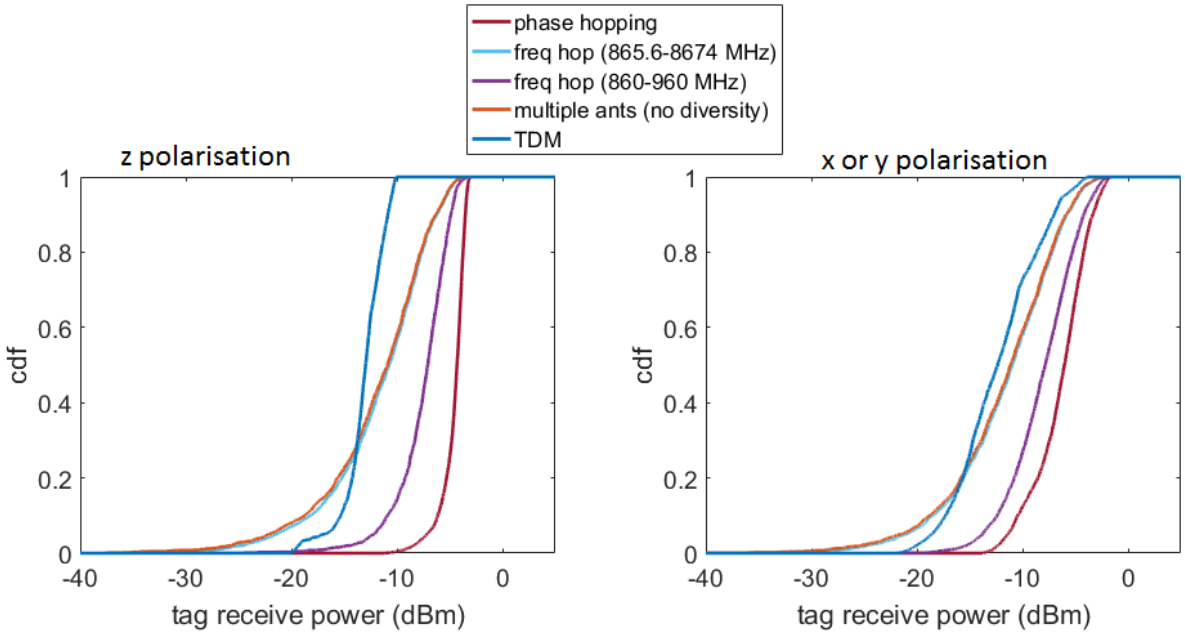

Figure 3.24: Comparing different multiplexing schemes in a four-antenna RFID system

A comparison of all the simulated diversity schemes is plotted in Fig. 3.24. It is seen that the best performance is provided by phase hopping for all tag orientations, and the least by the narrowband frequency diversity.

3.6 Summary

A novel 3D field-based model has been presented, which can provide rapid multi-antenna simulations for RFID systems. Based on electric field interactions between multiple antennas, it is capable of implicitly modelling varied propagation properties of an RF channel which are useful in RFID, including antenna patterns, multipath, polarisation and orientation. This is done at a fraction of the time it would take with a full wave solver , but with closely matched results, and is therefore suitable for rapid RFID field predictions. It has been used to analyse different multiplexing schemes for a four-antenna RFID cell. Insightful observations have been made about the properties of such antenna arrangements with respect to the tags, and the effect of tag orientations has also been analysed.
This model provides a useful tool with which to analyse phased array antennas in wide area RFID systems, owing to the fact that the beam patterns of the antenna can be varied dynamically during the simulation process with little extra computation time. It is used in the rest of the dissertation for modelling beam steering of phased arrays. The next chapter introduces the use of antenna arrays in RFID systems. The design, fabrication and characterisation of an antenna array is presented. Different array multi-casting schemes for use in RFID systems are then investigated.

Chapter 4

An Investigation into Multicasting approaches with Phased Array Antennas in RFID Systems

Distributed Antenna Systems provide spatial diversity to an RFID system by providing multiple independent signal paths from each antenna to the tags. Phased array antennas introduce additional spatial diversity through beam steering, and therefore, antenna multiplexing needs to be studied in that context.

In the previous chapter, a 3D model for simulating multiple RFID reader and tag antenna interactions in a multipath environment was presented. The model was used to analyse a case study involving a rectangular arrangement of four reader antennas in a Distributed Antenna System interrogating a tag population using different antenna multiplexing schemes: TDM, FDM and phase diversity.

This chapter extends the study of antenna multiplexing techniques to phased array antennas. Three different multiplexing schemes are investigated in a beam steering system. The first is beam steering with TDM, in which antennas transmit in disjoint time slots while steering their beams. The second is antenna multicasting with beam steering and no phase diversity, in which antennas transmit simultaneously while steering their beams. The phase relationship is kept constant between individual arrays in this case. The third is multicasting with beam steering and phase diversity. The latter two (multicasting with and without phase diversity) are of particular interest because two antennas simultaneously transmitting with beam steering naturally undergo some phase dithering due to

the multiple signal path combinations provided to the tag as the beams are steered and the change in phase due to steering. It is therefore not obvious whether phase diversity needs to be implemented explicitly in order to eliminate antenna-antenna interference. A two-array system is used to compare the performance of transmitting arrays under the different schemes by simulation and experiment. A four- and six- array system are also simulated to study the impact on power delivered to tags due to antenna scaling.
A set of phased array antennas is necessary for the work, and the first section of this chapter is dedicated to the design of RFID antenna arrays used for the experimental part.

4.1 Antenna Design and Measurement

4.1.1 Antenna Requirements

The reader antenna in an RFID system, as was discussed in the previous chapter, transduces the electrical RFID signal from the reader into an RF wave for transmission in free space. It also receives the backscattered tag response. For many applications, low profile, flat panel reader antennas are desired. This is due to space constraints, low visibility requirements and aesthetics in many applications, so that they can easily be fitted into ceiling tiles in wide area retail applications, for example, without being unsightly. Another desired feature for reader antennas is circular polarisation (CP). RFID tags are usually linear polarised dipoles due to size and complexity constraints, and therefore transmit and receive only one polarisation. The reader antenna therefore needs to be circularly polarised to be able to detect arbitrarily-oriented tags (in the plane normal to the reader transmission direction). The second reason for desiring CP antennas is for multipath mitigation. An ideal CP antenna has total cross polarisation isolation so is unable to detect oppositely handed signals, and as a result suppresses self interference due to reflection. This is because the handedness of a wave is reversed upon reflection [119]. Furthermore, the ETSI regulations allow for an extra 3dB of transmit power if the power is divided into orthogonal polarisations [36], so there is no transmit power penalty in using CP antennas. Considering the above requirements, the design aims of the required antenna can be summarised in Table 1.1. A good candidate that can satisfy the above requirements is the microstrip patch antenna. Before the design is described, an overview of the theory of antenna arrays is presented.

Design Parameter	Requirement
Geometry	Flat, planar array
Frequency Range	865-868 MHz (European lower band)
Polarisation	Circular
Handedness	LHCP or RHCP
Size	$< 60cm \times 60cm \implies 2 \times 2$ array

Table 4.1: RFID antenna design requirements

4.1.2 Background theory on phased array antennas

A phased array antenna or antenna array is a set of two or more antennas working together to boost the radiation pattern of the whole in terms of gain and beam diversity. The radiation pattern of an identical element array can be analysed in terms of its unit antenna element. The results presented here follow the derivations of Orfandis [111]. As described in the Chapter 3, the radiation vector of an antenna with current density source distribution $\mathbf{J(r)}$ is given by

$$\mathbf{F}(\mathbf{k}) = \iiint_V \mathbf{J}(\mathbf{r}) e^{j\mathbf{k}.\mathbf{r}} d^3\mathbf{r} \tag{4.1}$$

where $\mathbf{k}$ is the wave vector. If the antenna is translated by a vector $\mathbf{d}$, then the current density distribution becomes $\mathbf{J}(\mathbf{r}-\mathbf{d})$, and the radiation vector becomes

$$\mathbf{F}(\mathbf{k}) = \iiint_V \mathbf{J}(\mathbf{r}-\mathbf{d}) e^{j\mathbf{k}.\mathbf{r}} d^3\mathbf{r} \tag{4.2}$$

$$= e^{j\mathbf{k}.\mathbf{d}} \iiint_V \mathbf{J}(\mathbf{r}) e^{j\mathbf{k}.\mathbf{r}} d^3\mathbf{r} \tag{4.3}$$

$$= e^{j\mathbf{k}.\mathbf{d}} \mathbf{F}(\mathbf{k}) \tag{4.4}$$

where the Fourier shift property has been used to arrive at the last step (Equation 4.1 is a 3-D spatial Fourier transform).

Now, given an array of N identical antennas of source current density $\mathbf{J}(\mathbf{r})$, each displaced from the origin by $\mathbf{d_n}(x_n, y_n, z_n)$ with relative feed coefficients $a_0, a_1, ..., a_N$, the current density of the nth element will be $\mathbf{J_n} = a_n \mathbf{J}(\mathbf{r}-\mathbf{d_n})$, and the total current density will

be $\mathbf{J_t}(\mathbf{r}) = \sum_n a_n \mathbf{J}(\mathbf{r} - \mathbf{d_n})$. This will result in a radiation vector given by:

$$\mathbf{F}(\mathbf{k}) = \iiint_V \sum_n a_n \mathbf{J}(\mathbf{r} - \mathbf{d_n}) e^{j\mathbf{k}.\mathbf{r}} d^3\mathbf{r} \tag{4.5}$$

$$= \sum_n a_n \iiint_V \mathbf{J}(\mathbf{r} - \mathbf{d_n}) e^{j\mathbf{k}.\mathbf{r}} d^3\mathbf{r} \tag{4.6}$$

$$= \sum_n a_n e^{j\mathbf{k}.\mathbf{d_n}} \iiint_V \mathbf{J}(\mathbf{r}) e^{j\mathbf{k}.\mathbf{r}} d^3\mathbf{r} \tag{4.7}$$

$$= \left(\sum_n a_n e^{j\mathbf{k}.\mathbf{d_n}} \right) \mathbf{F}(\mathbf{k}) \tag{4.8}$$

$$\equiv A(\mathbf{k})\mathbf{F}(\mathbf{k}) \tag{4.9}$$

$A(\mathbf{k}) = \sum_n a_n e^{j\mathbf{k}.\mathbf{d_n}}$ is called the array factor, and is used to modify the radiation pattern of the unit element by multiplication.

$\mathbf{k} = k\hat{\mathbf{r}}$ ($\hat{\mathbf{r}}$ is the radial unit vector in spherical coordinates) is the wave vector given by [111]

$$\mathbf{k} = \frac{2\pi}{\lambda}\hat{\mathbf{r}} = \frac{2\pi}{\lambda}(\sin\theta\cos\phi, \sin\theta\sin\phi, \cos\theta) \tag{4.10}$$

The array factor can therefore be written as a function of the radial bases (θ, ϕ):

$$A(\mathbf{k}) = A(\theta, \phi) = \sum_n a_n e^{k(x_n \sin\theta\cos\phi + y_n \sin\theta\sin\phi + z_n\cos\theta)} \tag{4.11}$$

The design of phased array antennas therefore lies in the appropriate selection of the array complex weights a_n, in order to produce a desired beam pattern. i.e. the amplitude and phase of the signal feeding the individual elements can be modified in order to change the array factor, and the antenna far field pattern as a result. Depending on design requirements, there exist several methodologies for designing the array factor. The simplest method is the uniform feed method, in which the same weighting factor is applied to each element. i.e. $a_n = 1\ \forall n$. Using a uniform element spacing in the z direction of $z_n = nd$ results in an array factor in 1D of

$$A(\theta) = \sum_{n=1}^{N} e^{knd\cos\theta} = \sum_{n=1}^{N} e^{jn\Psi} \tag{4.12}$$

$$= \frac{1 - e^{jN\Psi}}{1 - e^{j\Psi}} \tag{4.13}$$

$$= e^{j\frac{N-1}{2}\Psi} \frac{\sin\frac{N\Psi}{2}}{\sin\frac{\Psi}{2}} \tag{4.14}$$

where $\Psi = knd\cos\theta$.

The maximum gain for the uniform array in Eqn 4.14 can be verified to be of magnitude N

in the direction $\theta = 0°$. To steer the beam to an angle θ_0 away from 0°, the transformation $cos\theta \rightarrow cos\theta - \cos\theta_0$ needs to be performed in order to move the maximum to $\theta = \theta_0$. This implies a required weighting factor of

$$a_n = e^{-jknd\cos\theta_0} \tag{4.15}$$

i.e. a progressive phase tapering is required for beam steering.
Eqn 4.14 is generalisable to planar arrays [109]. An $M \times N$ array with element spacings of d_x in the x direction and d_y in the y direction will have an array factor of:

$$AF(\theta, \phi) = \frac{\sin\frac{N\Psi_x}{2}}{\sin\frac{\Psi_x}{2}} \frac{\sin\frac{M\Psi_y}{2}}{\sin\frac{\Psi_y}{2}} \tag{4.16}$$

where $\Psi_x = k_x n d_x \sin\theta\cos\phi$ and $\Psi_y = k_y n d_y \sin\theta\sin\phi$.
The uniform amplitude feed analysed above will produce beams with the minimum possible beam width for arrays of the same element number.
Another feed method is the binomial feed method, in which the element weights are determined using the binomial coefficients. This method gives a beam pattern without sidelobes, but with the maximum possible beam width for arrays of similar element count. The Dolph-Tchebyshev Method uses the Tchebyshev polynomials to determine the excitation coefficients, and aims to design arrays with a specified main beam to sidelobe ratio. The Schelkunoff Polynomial Method is used to design arrays for interference rejection by producing a null in a particular direction [111].

A major problem with antenna array design is mutual coupling. This occurs when radiation from an antenna element is absorbed by a neighbouring element. This depends on the number, size, shape and spacing of array elements. Mutual coupling leads to reduced radiation efficiency, distorted beam patterns and scan blindness, especially in closely spaced arrays [120]. Spacings of less than half a wavelength can cause substantial mutual coupling, whereas large spacings ($>> 0.5\lambda$) lead to grating lobes due to spatial aliasing amplifying some side-lobes [111]

4.1.3 Design of Antenna Array

The first step in designing the array is to design a unit element from which the array will be built. As mentioned above, microstrip antennas are an ideal candidate to satisfy the requirements for the antenna described. They consist of a metallic resonating

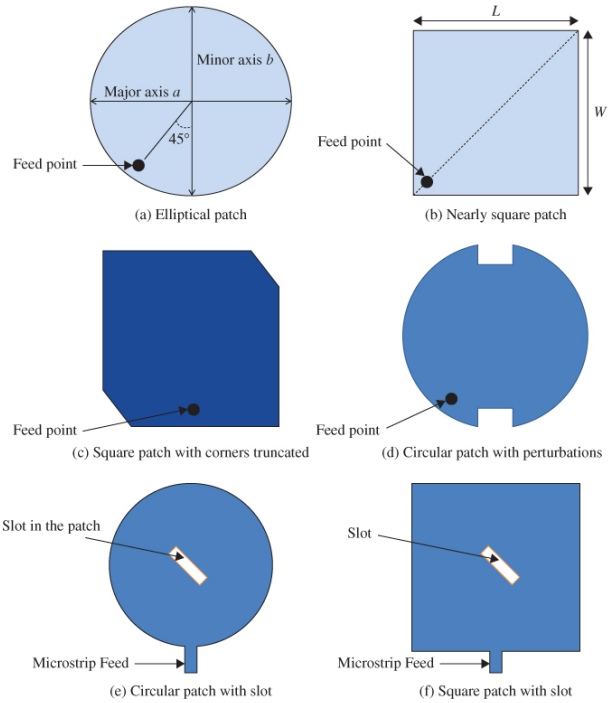

Figure 4.1: Common methods for obtaining circular polarisation in patch antennas [119]

structure on a dielectric material, which itself lies on a metallic ground plane. Microstrip patch antennas have been well-studied, designed and analysed in many different shapes-rectangular, elliptical, annular, triangular, square and circular [51]. They present several desirable features such as flatness (i.e. they are largely two-dimensional), compatible with standard PCB processing, relative low cost, easy to make and can be made with variable impedance, polarisation and resonant frequency by using loads between the antenna and the ground plane [109]. The drawbacks include low polarisation purity, low bandwidth and poor efficiency, especially with thick substrates due to surface waves [109]. They have been applied in many RFID reader antennas [121].

Circular polarisation is produced in microstrip patches by exciting orthogonal modes with signals that are offset in phase by 90°. This is normally realised by using two feeds to the antenna with a 90° phase difference. Due to the additional complexity for such an antenna (i.e. a phase shifter and extra feed line), several methods for introducing circular polarisation with a single feed have been reported [119]. The most common of them are illustrated in Fig 4.1

The procedure described in [109] was used for the design of the antenna used in this work. A square patch design was used. The substrate used was PTFE (Poly tetrafluoroethylene, Teflon, $\varepsilon_r = 2.1$) due to its low loss tangent, and therefore reduced potential

mutual coupling. Truncated corners were applied to obtain circular polarisation with a single feed. Initial design values were obtained using a design frequency of $f = 866.5MHz$. This gives a patch length of $L = \frac{c}{2\sqrt{\varepsilon}f} \approx 119.5mm$. An optimisation was performed in FEKO to obtain the correct matching and polarisation, as well as correct the length for the fringing effect in patch antennas [109]. The radiation pattern of a single designed element is shown in Fig 4.2.

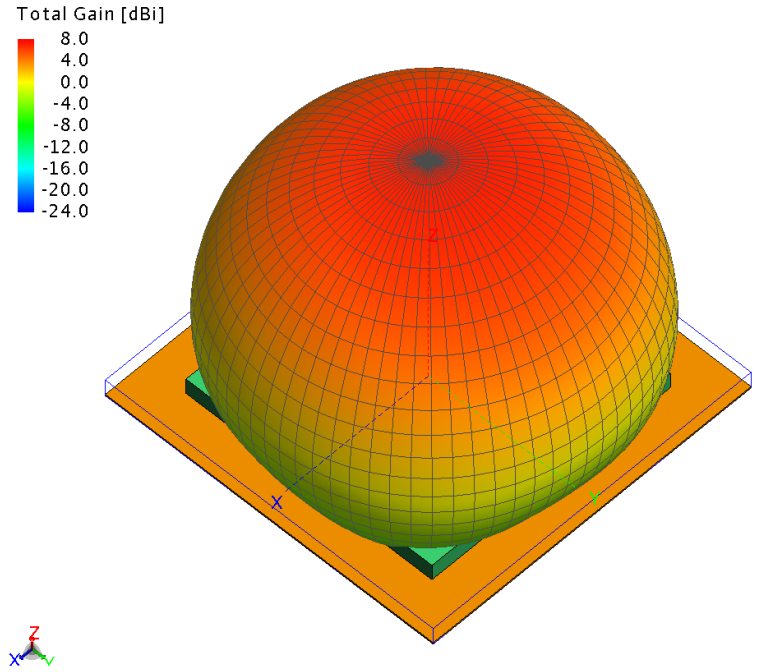

Figure 4.2: Single antenna element beam pattern

The array was formed by assembling the individual patch elements on a 400mm × 400mm ground plane into a 2 × 2 pattern with a spacing of $\lambda/2$ at 866.5MHz≈ 173mm.

Improving Circular Polarisation using sequential rotation

The sequential rotation technique has been used to improve the design of arrays in terms circular polarisation [122]. As illustrated in Fig 4.3, the elements are physically rotated counter-clockwise by 90° sequentially i.e. by $0°, 90°, 180°$ and 270°. When fed with the corresponding phase shifts, they produce CP radiation even if the individual elements are linear polarised. They also maintain better CP during beam steering especially at high scan angles [123]. This is implemented to mitigate the low CP in patch phased array antennas. Considering the Sequentially Rotated Array (SRA) in Fig 4.3, an observer in the far field of the array along the z propagating direction (out of the page) will see an

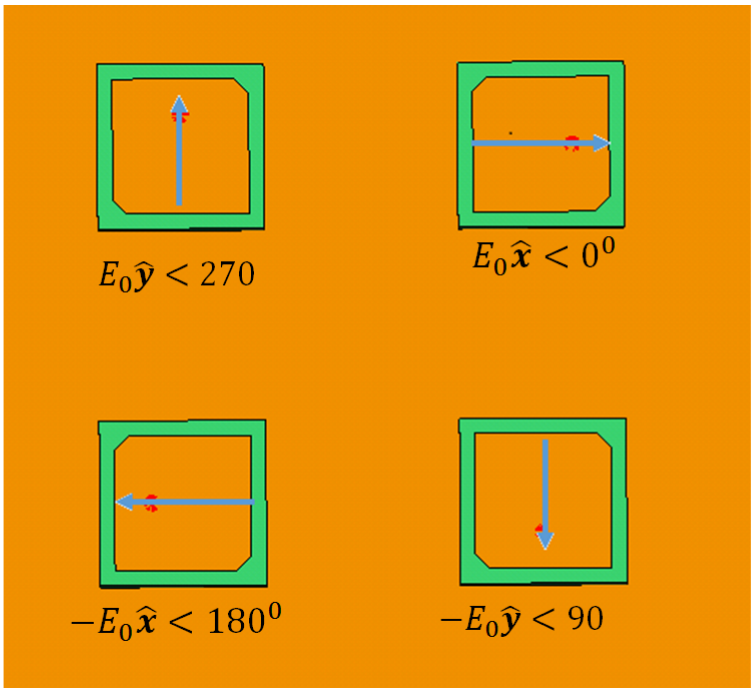

Figure 4.3: Sequential Rotation Technique showing rotated antenna elements, polarisation and phases of the signal feeds. The arrows show the polarisation of the electric field for each antenna element

electric field with polarisation given by

$$\mathbf{E} = E_0 \left(e^{j0}\hat{\boldsymbol{x}} + e^{j\frac{-\pi}{2}}.(-\hat{\boldsymbol{y}}) + e^{-j\pi}.(-\hat{\boldsymbol{x}}) + e^{j\frac{\pi}{2}}.\hat{\boldsymbol{y}} \right) \tag{4.17}$$

$$= 2E_0(\hat{\boldsymbol{x}} + j\hat{\boldsymbol{y}}) \tag{4.18}$$

which is a circular polarised wave, even though the individual elements are linear polarised. This technique was used to enhance circular polarisation. Some examples of simulated radiation patterns formed by the antenna steered to different directions are shown in Fig 4.4

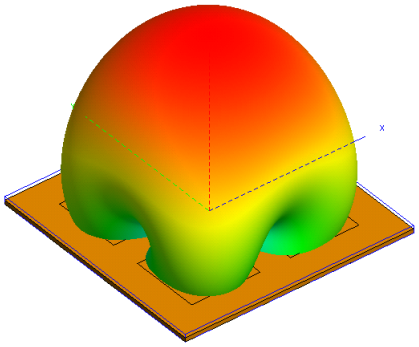

(a) Antenna beam pattern pointing to broadside direction$(0°, 0°)$

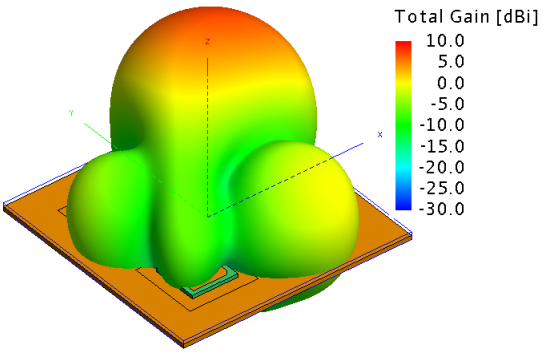

(b) Antenna beam steered to $(45°, 30°)$

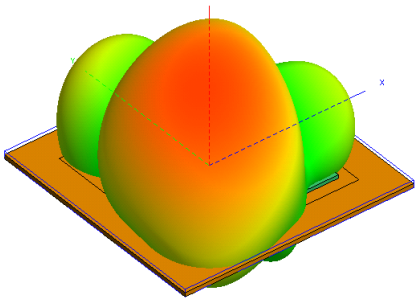

(c) Antenna beam steered to $(-45°, 30°)$

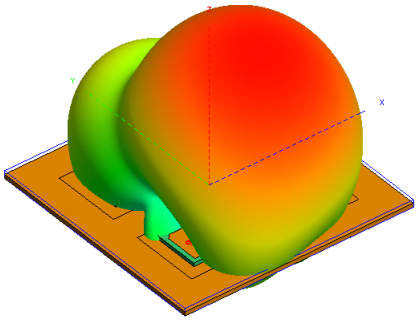

(d) Antenna beam steered to $(-90°, 30°)$

Figure 4.4: Simulated antenna 3D pattern simulations at different (ϕ, θ) scan directions

Because numerous copies must be produced, subsequent arrays used commercial patch elements (APAKN1304-C2G-T from ABRACON) on an aluminium ground plane for ease of manufacture. Some final antenna samples are shown in Fig 4.5.

4.1.4 Pattern measurements

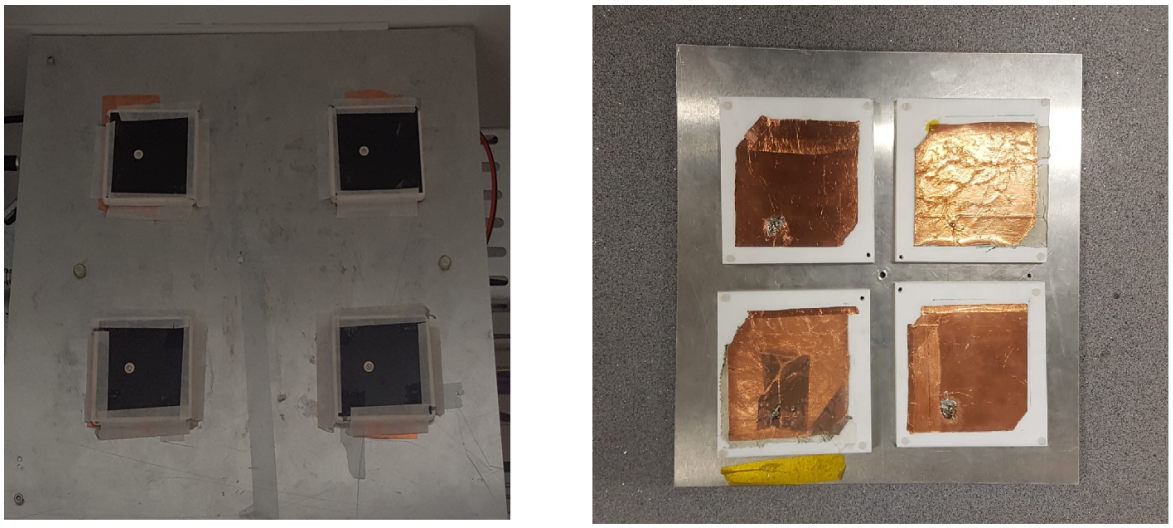

Figure 4.5: Manufactured antenna samples

Measurements were performed using the MVG StarLab system [113]. This is an antenna measurement setup, which uses a set of sensors around the antenna in the elevation plane, while rotating the antenna in azimuth in order to measure the 3D pattern of the antenna in the near field. It then applies a Near-to-Far Field (NFF) transformation to obtain the far field pattern. Some measured patterns for gain and axial ratio are shown in Figs 4.6 and 4.7.

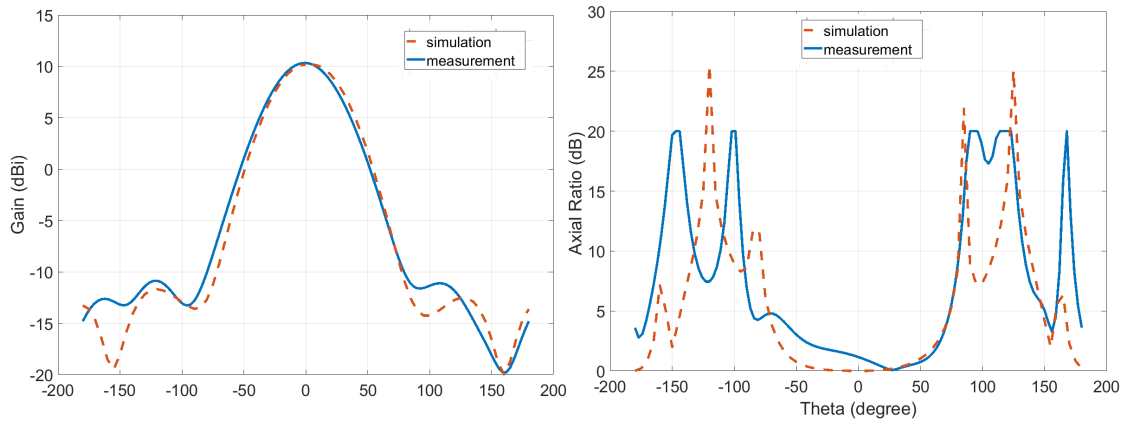

Figure 4.6: Antenna beam pattern pointing to broadside direction showing cut at $\phi = 0°$

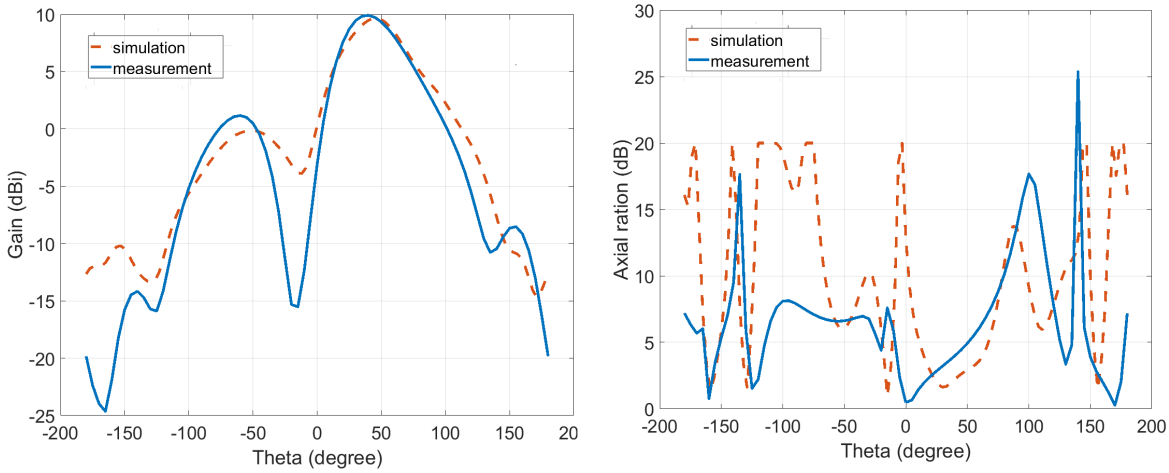

Figure 4.7: Antenna beam pattern steered to $(45°, 45°)$ showing cut at $\phi = 45°$

4.2 Comparison of Multiplexing approaches in an RFID Array System

In this section, the different approaches for the use of phased arrays in an RFID DAS system are investigated. Two 2×2 arrays are used to investigate multi-casting in an RFID inventory session. The aim is to maximise the power delivered to the tag, since this will be the most important metric for tag detection when the tag is close to its threshold power [124]. Beam steering with TDM, beam steering without phase hopping and beam steering with phase hopping are investigated and compared. To this end, an experiment involving two phased array antennas was setup as illustrated in Fig 4.8. An $8m \times 8m$ interrogation zone is used, with a concrete floor (dielectric constant, $\varepsilon_r = 5 + j0.4\Omega$ [125]). The antennas are placed at a height of 3m from ground level with a $4m$ separation, while tags form the plane 1m above the ground.

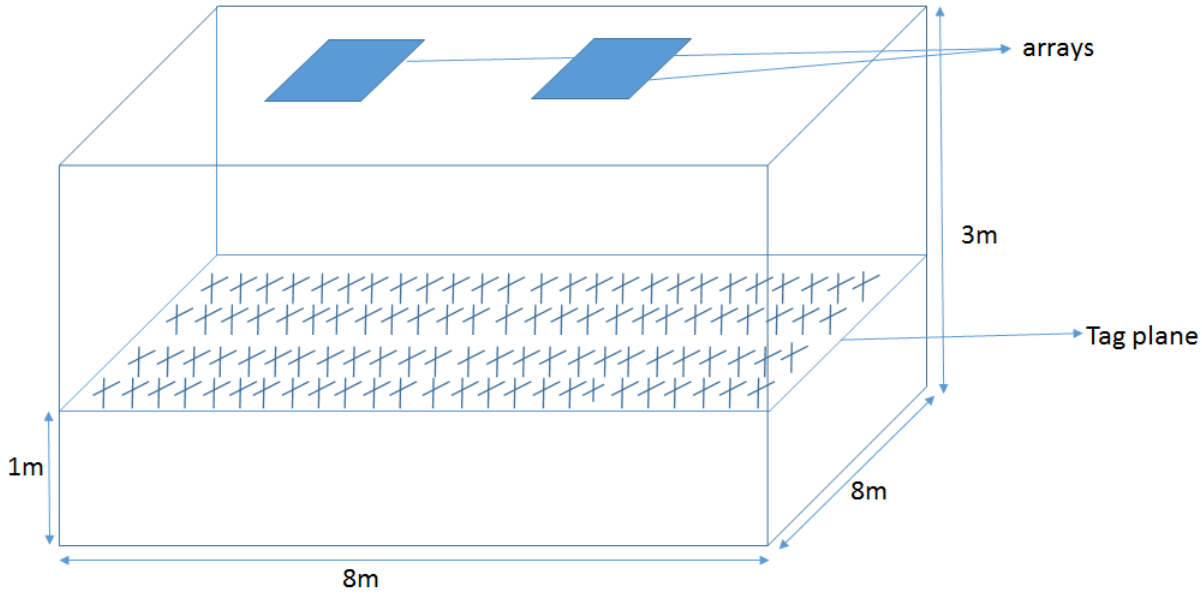

Figure 4.8: Setup for array multicast experiment

4.2.1 Simulation

For simulating beam steering in the experiment, several array beam patterns are generated in FEKO and imported into the model. A total of nine beam states are used, as shown in Fig 4.9. The beam states used can provide a full 360° azimuth coverage up to 45° of elevation. During each iteration of the model, a random beam is selected for each array,

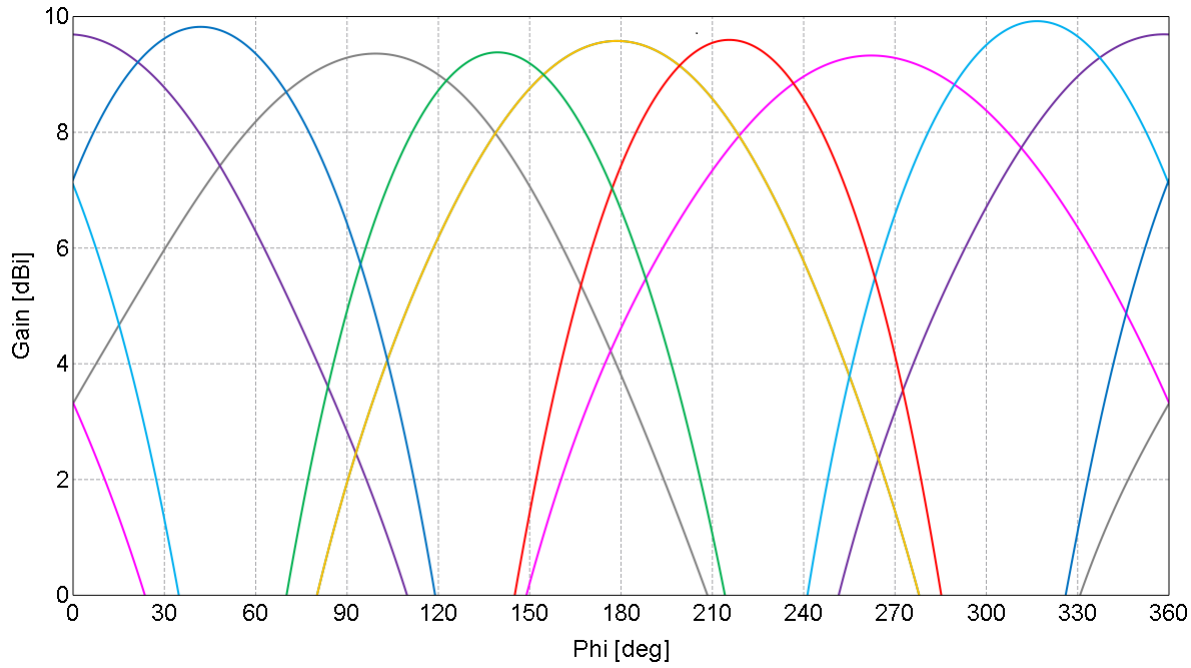

Figure 4.9: Beam states for array multicasting experiment, at an elevation angle of 30°. The broadside (maximum at $\phi = 0°, \theta = 0°$) beam is not shown

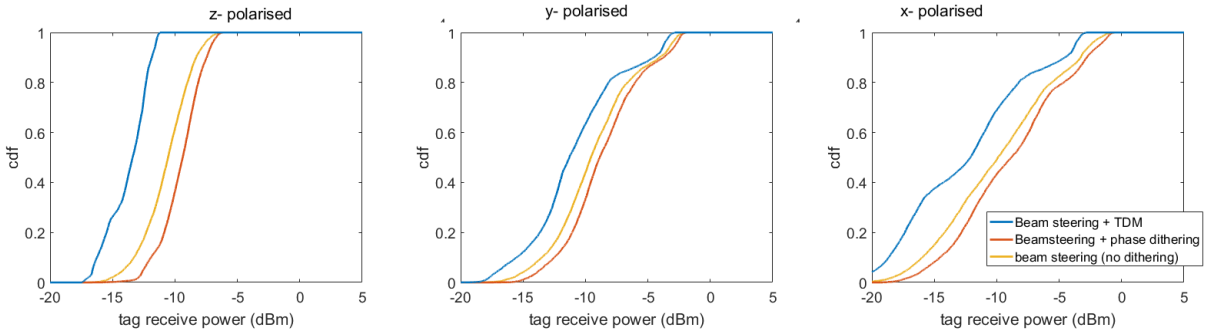

Figure 4.10: Simulation results showing cdf for three different array multicasting schemes

and the power received at the tag is computed for each of three scenarios described above. The maximum power at each location is then recorded for all three cases. Results are shown for the three orthogonal tag orientations z, y and x in Figs 4.10 and 4.11.

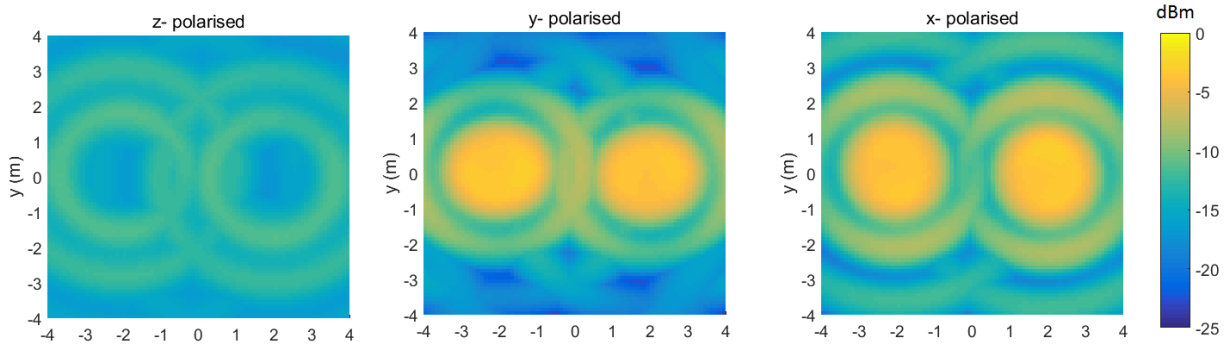

(a) Beam steering + Time Division Multiplexing

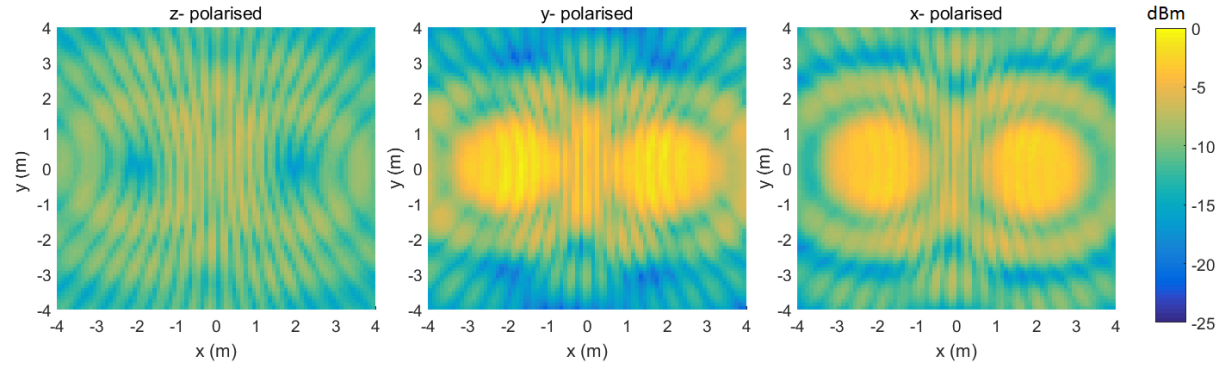

(b) Multicasting with Beam steering (No phase dithering)

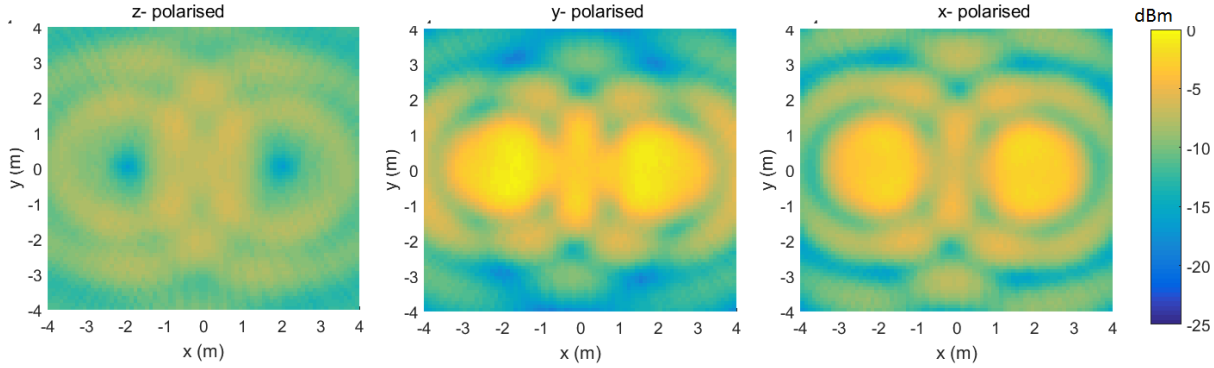

(c) Multicasting with beam steering + phase dithering

Figure 4.11: Simulation results for three different array multi-casting schemes: Beam steering + Time Division Multiplexing, Beam steering (No phase dithering) and Beam steering + beam steering for z, y and x tag polarisations for tags at Z=1m plane.

The power distribution in the interrogation zone as seen by the tags (dipoles) aligned along the three orthogonal directions for all three cases is presented in Fig 4.11. The cumulative distribution plot (cdf) of the tag received power is shown in Fig 4.10. It is seen that the TDM system provides the least power to the tags, as tags are served by only a single antenna, whereas the multicast systems enable the tags to receive the sum of fields

from both antennas. The fringes in the multi-cast system without phase diversity are a result of interference, while their absence in the phase diversity multicast system indicate they have been effectively cancelled over time as the relative phase between the arrays is changed. This shows that phase hopping increases the power delivered to the tags, albeit only marginally. An average improvement of 0.7 dB for z polarised tags and 0.5 dB for x/y polarised tags is observed over the case of multicast without phase diversity. Multicasting with phase hopping achieves an average 2dB of power per tag over the TDM.

4.2.2 Experimental Demonstration

The experimental demonstration is described in this section.

System Architecture

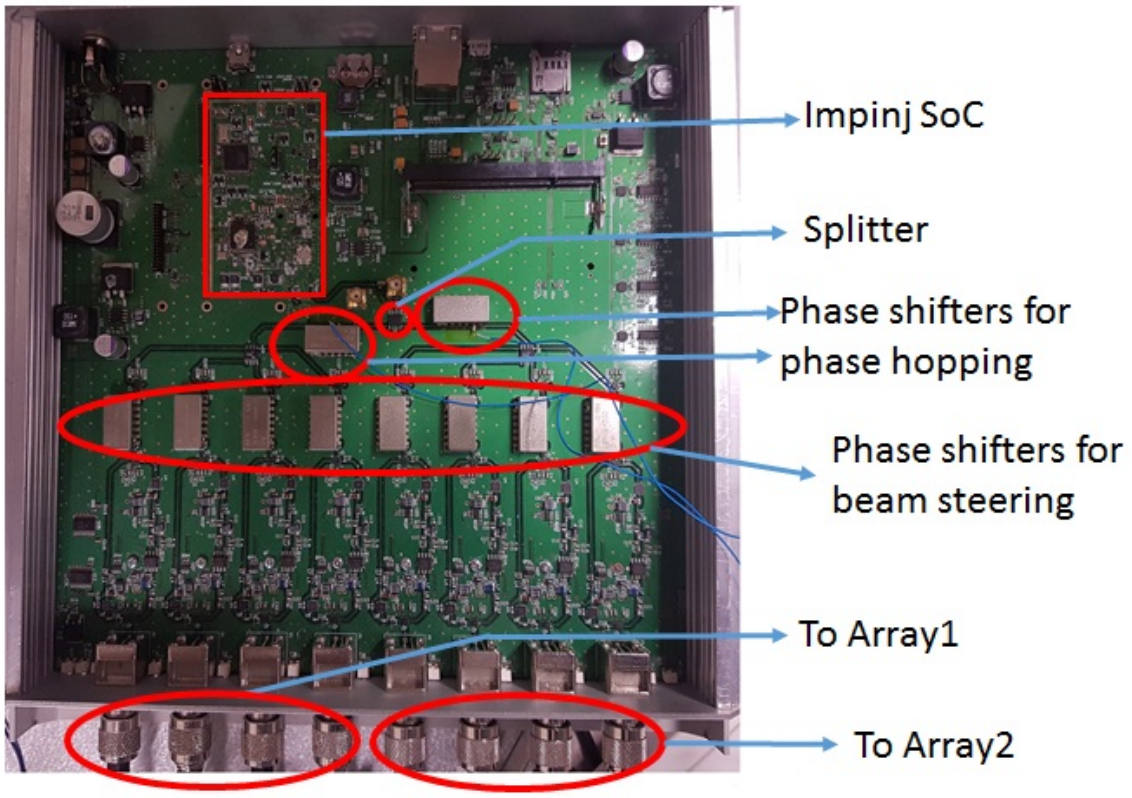

Figure 4.12: Multiport Reader structure

The RFID reader architecture used for the experimental demonstration is shown in Figs. 4.12 and 4.13. The Impinj R2000 is a commercial RFID System on Chip (SoC), which is deployed in the used reader to implement the RFID Class 1 Gen 2 protocol. i.e. generate RFID modulated carrier for transmission to the tag, and process responses from tags. During transmission, the modulated carrier from the Impinj SoC is first split into two RF chains, each of which is phase shifted using a voltage controlled phase shifter. These phase shifters dither the phases of the signal randomly in order to introduce phase diversity between the two chains. Each of the two RF chains is further split into four, giving two pairs of four RF chains. Each pair of four further undergoes phase shifting, designed to form appropriate beams as in Fig. 4.9. Each pair of four is then amplified and fed to the appropriate antenna and port, the first pair to one array, and the other

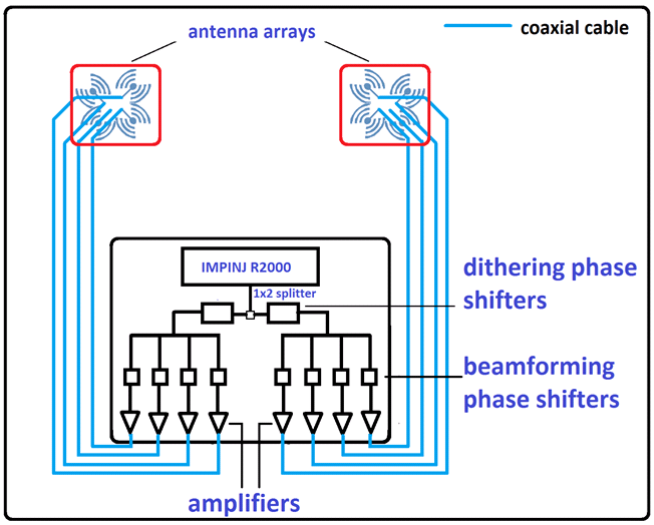

Figure 4.13: Multicast RFID System Architecture

pair to the next array, via coaxial cable. The phase shifters used were the Minicircuits JSPHS-1000+ phase shifters, which are able to produce a continuously variable phase shift of up to 180° at 868 MHz. Two separate fixed antennas were used in the receive link since the purpose of this experiment was solely the downlink improvement in the power received by the tag.

Experiment

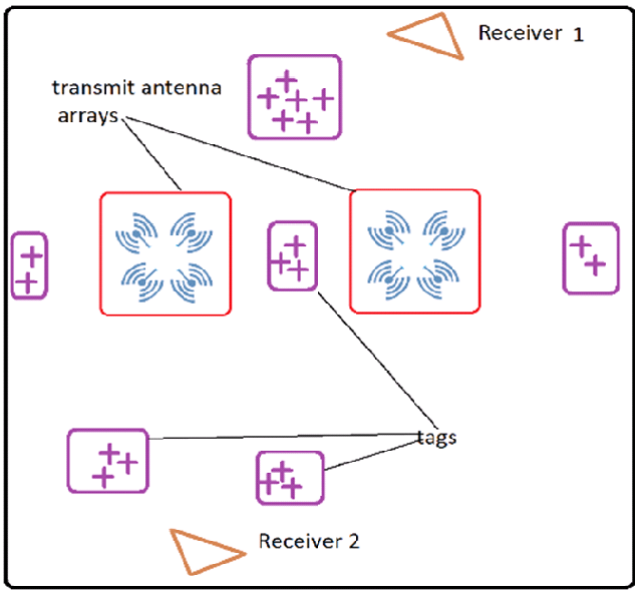

Figure 4.14: Diagrammatic representation of experimental setup showing transmit arrays, receive antennas and RFID tags. The number of crosses indicate the relative concentrations of tags at different locations (total = 100)

The experiment was carried out in a $8m \times 6m$ laboratory for the three multiplexing scenarios. i.e. TDM, multicast with phase diversity and multicast without phase diversity. The nine beam states in Fig 4.9 were pre-programmed into the reader MCU as a look-up table (see Fig 4.12). During an inventory, a random selection from these phase values (representing a specified beam pattern), is applied to each array. The beam pattern for each array is independently selected, therefore they may not be the same for the two arrays at any given time. The beams were then also randomly changed throughout the inventory cycle. For the case of TDM, the arrays were allowed to transmit for one second alternately.

For the case of multicast without phase diversity, the arrays transmitted simultaneously, and the two phase shifters responsible for phase shifting were idle.

For the case of multicast with phase diversity, a varying phase offset was applied using the phase hopping phase shifters shown in Fig 4.12. This applies the same phase shift to each group of four RF chains, thereby the beam pattern is maintained since all the elements undergo the same phase shift. However, a varying phase difference is introduced with respect to the other array as is desired. Two antennas were used as receivers as shown in

Fig. 4.14. Inventories were run for 10 minutes in each case under Class 1 Gen 2 Session 0 (i.e. no persistence). The maximum RSSI for each unique tag was then collected for each experiment. Plots of cumulative RSSI show the maximum power seen by tags for each experiment. The cumulative plots show the cdf. In the first set of experiments a transmit power of +35 dBm EIRP was used for each array.

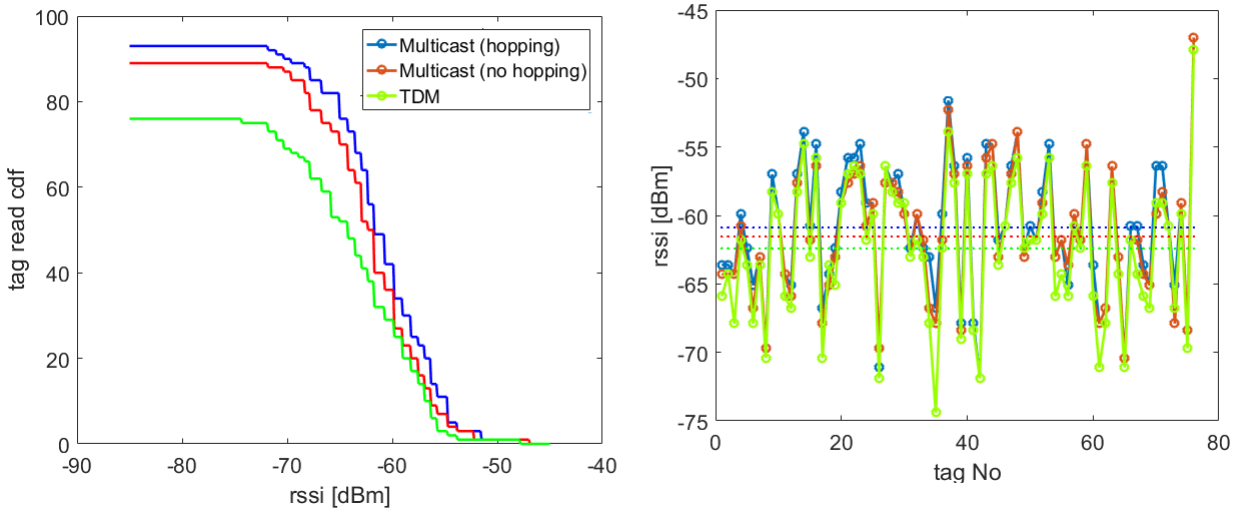

Figure 4.15: Experimental comparison of different multicasting schemes (complemetary) cumulative tag reads and (left) and power differences for commonly detected tags (right)

The results are displayed in Fig. 4.15. By extrapolating the curves to the y axis (cumulative tag reads)It can be seen that the multicast systems (with and without phase diversity) achieve 93% and 89% success rates respectively, while the TDM system achieves 77%. Multicasting with phase diversity provides an average of 1.4dB per tag over the TDM system (compared to 2 dB from the simulations). This represents, according to the Friis equation ($P \propto 1/r^2$), an 18% increase in read range. A 0.6 dB extra power is also observed over the case without phase hopping (compared to 0.7 dB) from simulations), which corresponds to a 6% increase in read range.

This shows a close correlation between simulation and experiments in terms of power differences. It should be noted that the experiments measure the tag backscattered power, which undergoes tag nonlinear effects [1], and is therefore not directly comparable to the tag simulations. However, the trends in power differences will indicate the better performing system and the margin of performance improvement.

To further investigate the potential improvements, the transmit power was decreased to +33 dBm, and the same experiments were performed. In this case, respective read success

rates of 57%, 72% and 80% were recorded as shown in Fig. 4.16. The greater performance improvement is due to a greater proportion of the tags being just below threshold, resulting in any extra power from phase hopping being exploited by the multicast system to bring about more tags being read [124]. Without phase diversity, a number of tags remain in nulls caused by antenna-to-antenna interference, which results in fewer tags activated.

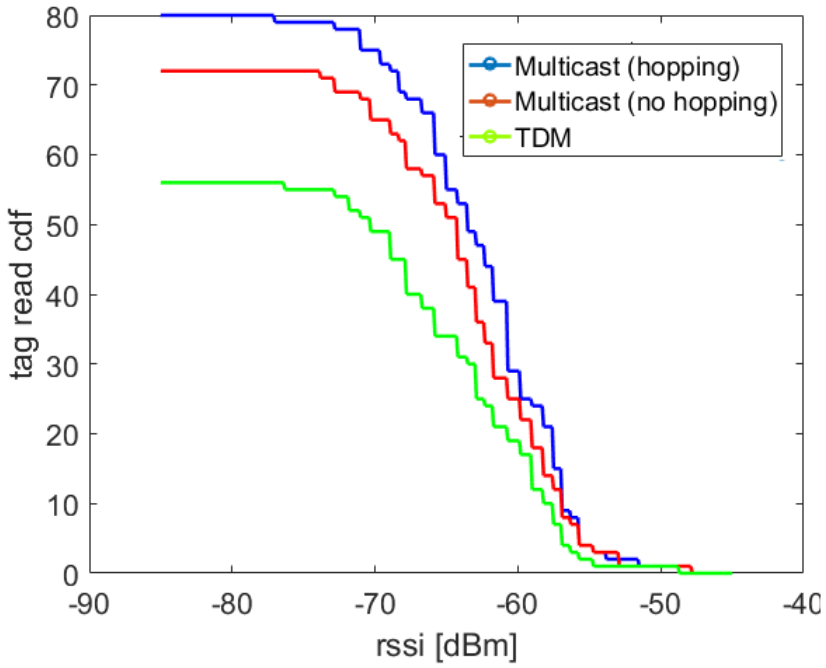

Figure 4.16: Experimental comparison of different multicasting schemes a reduced power

Therefore, the multicast system (with and without phase diversity) outperforms the TDM system, and the advantage is especially evident at a reduced power, where the read success rate is significantly improved over the TDM system. It is also observed, as seen in the simulated power distributions in Fig. 4.11, that beam steering, without any phase hopping provides some phase diversity, but there still exists some shallow nulls (seen as fringes in the plots). The use of phase diversity between the two arrays mitigates the antenna interference.

4.2.3 What about increasing the number of arrays?

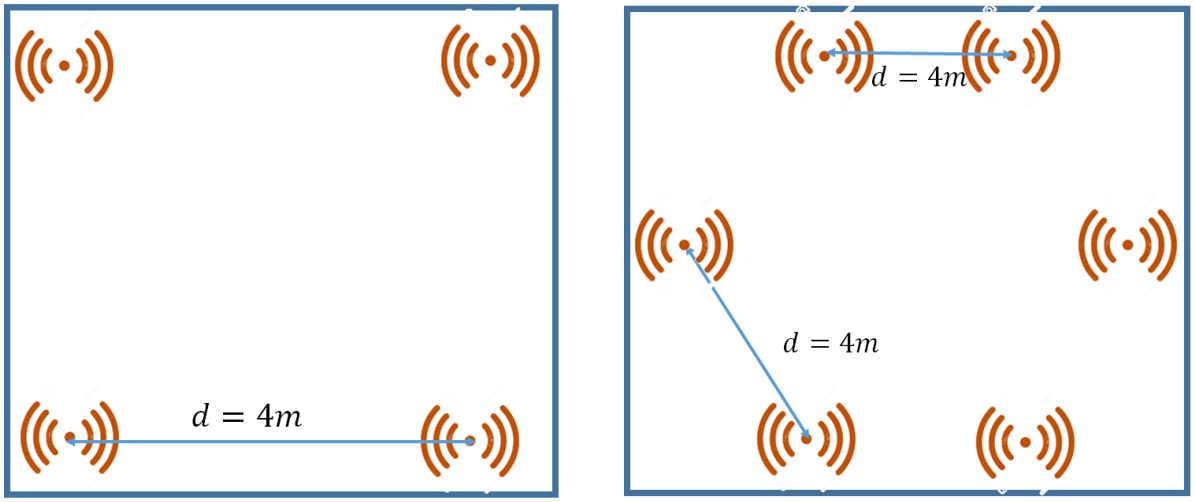

Figure 4.17: Rectangular and Hexagonal antenna arrangement

In this section, the number of multicast antennas is increased to investigate by simulation the effect of antenna count on the improvement in tag received power due to phase hopping. A rectangular and hexagonal arrangement of antennas with four and six antennas respectively are simulated as shown in Fig 4.17. Neighbouring antenna separations are constant at $4m$ in each case. The power distribution for the rectangular arrangement is shown in Fig 4.18 and cdfs for both cases in 4.19.

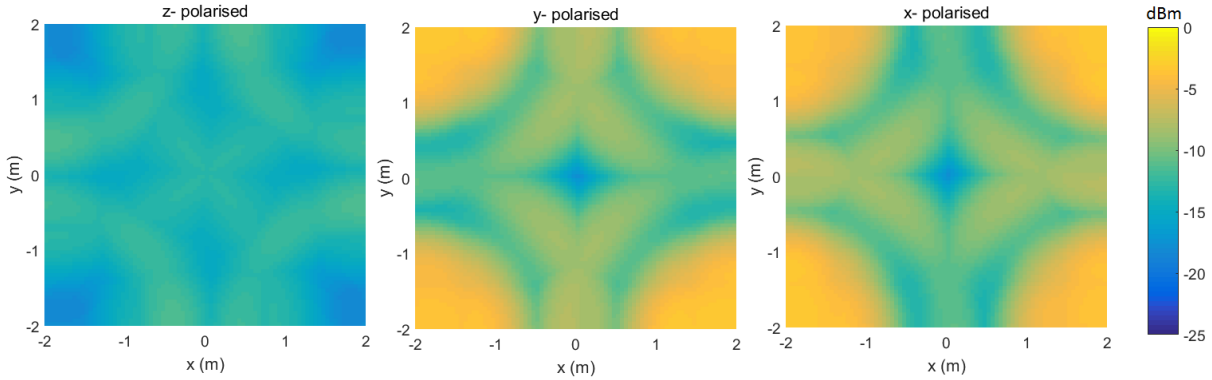

(a) Beam steering + Time Division Multiplexing

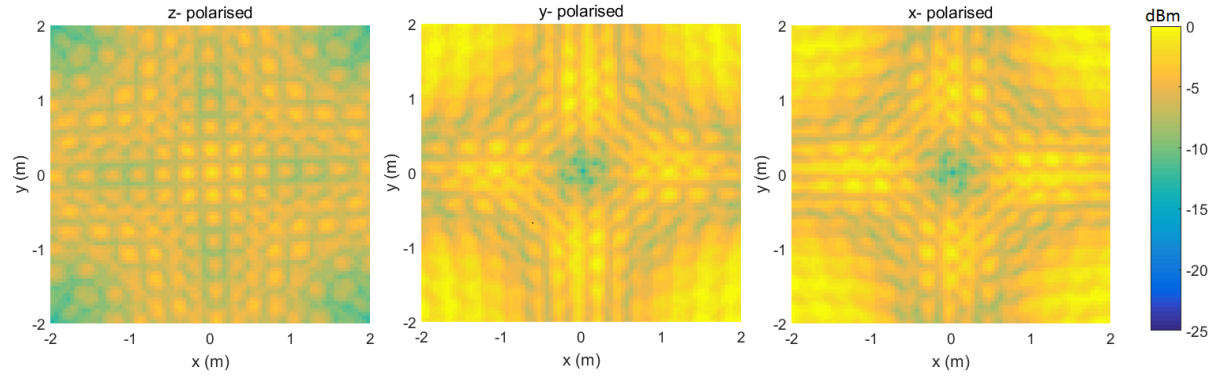

(b) Beam steering (No phase dithering)

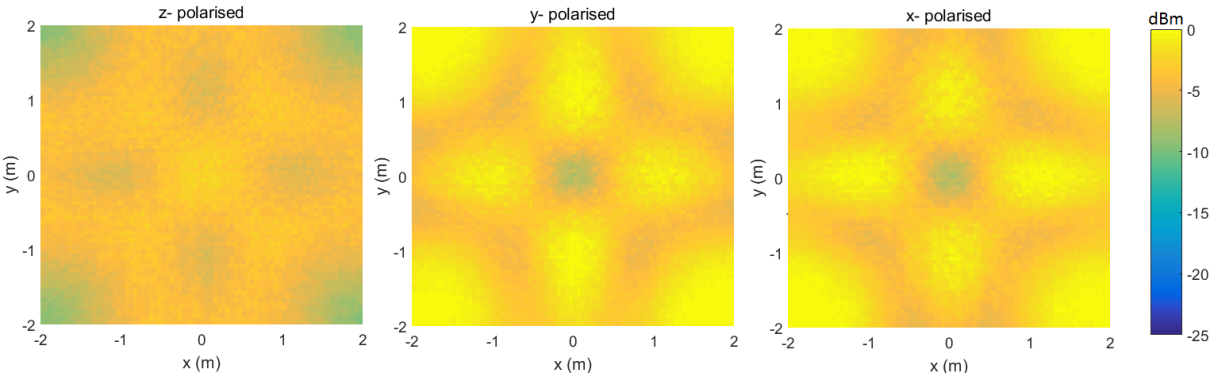

(c) Beam steering + phase dithering

Figure 4.18: Simulation results for three different array multicasting schemes in a four-array system. The rows represent (from left to right) the z, y and x tag orientations respectively. The first column represents the TDM scheme. The second column represents beam steering without phase diversity. The third column is the system with beam steering and phase diversity

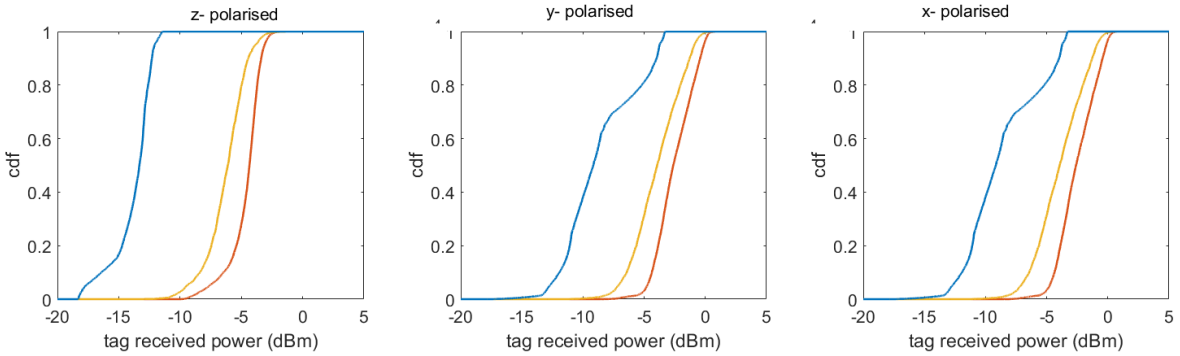

(a) Four array system

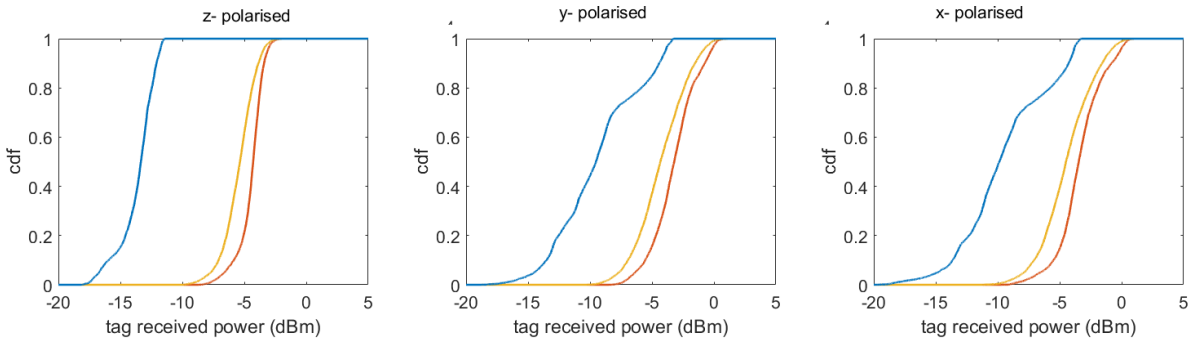

(b) Six array system

Figure 4.19: Simulation results for three different array multicasting schemes in a four-array system for four and six-array system.

It is observed that using a multicast signal with or without beam steering provides a significantly better performance compared to the TDM scheme. As has been explained earlier, this is because each tag is powered by only one antenna in the TDM scheme, whereas in the multicast schemes, tags receive the sum of fields from all transmitting antennas. The power is therefore bound to increase with the number of antennas.
It is also observed that employing phase diversity introduces an average difference of $\sim$ 1.7dB for vertical (z) tags and $\sim$ 1.3 dB for horizontal (x and y) tags in the four-array multicast system. In the six array system, the difference is $\sim 1.1dB$ for all three polarisations. This shows that the power delivered to the tag is marginally improved by the use of phase hopping, but this does not scale with the number of antennas. In a fixed antenna system, each point in space sees a single channel path combination, leading to deep nulls for tags located at points of destructive interference. With phased array antennas, each tag receives a field combination due to multiple channel path combinations, as the beams are steered. This leads to the cancellation of deep nulls as marked by their

absence in Figs. 4.18 and 4.11. The effects of antenna interference are still however seen as shallow interference fringes. Although this gives a helpful insight into the system, it should be noted that RSSI is not an accurate measure of tag received power, as it is biased towards low-powered tags due to tag non-linearity. The assumption used here is that all the setups are equally biased.

4.3 Summary

This chapter has presented the design and characterisation of a 2×2 RFID antenna array. These antenna arrays have then been used to investigate different multi-casting methods that can be used in an RFID system with multiple phased array antennas.

Three different methods have been investigated using two array antennas: TDM, simultaneous transmission without phase dithering and simultaneous transmission with phase dithering. In each case, beam steering is applied to both antennas.

The TDM system has been shown to have the worst performance in terms of power delivered to the tag. The problem of antenna-antenna interference has also been shown to be overcome by beam steering, even without phase dithering, as simultaneous array transmits without phase dithering detected 16% more tags than the TDM system, while the difference is 24% with phase dithering. The average tag power has also been shown to be higher for the simultaneous transmit systems over the TDM system, resulting in potentially higher tag detection rates, as demonstrated. It can therefore be concluded that beam steering introduces phase diversity, and overcomes blind spots. However, an explicit phase dithering is still required to get the maximum power to the tag. It has also been demonstrated by simulation that the advantage of phase dithering does not grow by increasing the number of antennas, although it delivers more power to tags.

The next chapter extends the use of phased arrays to detect tags in the context of a Distributed Antenna System. A Distributed Antenna Array System (DAAS) with phase dithering is introduced and compared with a standard fixed DAS system.

Chapter 5

An RFID Distributed Antenna Array System

The previous chapter investigated different multiplexing schemes for use with phased array antennas in an RFID system. It was shown that the most suitable method is a multicast system with phase diversity. This was demonstrated experimentally using two antenna arrays.

Building on this, the present chapter demonstrates an RFID Distributed Antenna Array System (RFID DAAS) in the context of a multicell RFID system. A network of antenna arrays, making use of phase diversity and beam steering is used to interrogate tags in a wide area. The performance is compared to a fixed RFID DAS system. The DAAS is proposed as a more efficient solution to wide area RFID in that it decreases antenna count and increases cell area.

A typical multi-cell wide area RFID system makes use of a repeating pattern of rectangular cells, with an antenna at each of the vertices of each cell as shown in Fig 5.1. The rectangular cell system shown requires four antennas per cell. Due to the fixed nature of the antenna patterns, antennas cannot be reassigned to different cells, leading to fixed antenna-to-cell allocations. This results in clusters of antennas at the vertices of each cell, four, in the case of rectangular antennas considered here as shown in Fig 5.1, and leads to a large number of required antennas.

Since phased array antennas (specifically planar or circular arrays) are capable of being steered 360^0 in azimuth, a single antenna placed at the vertex of a cell could address all

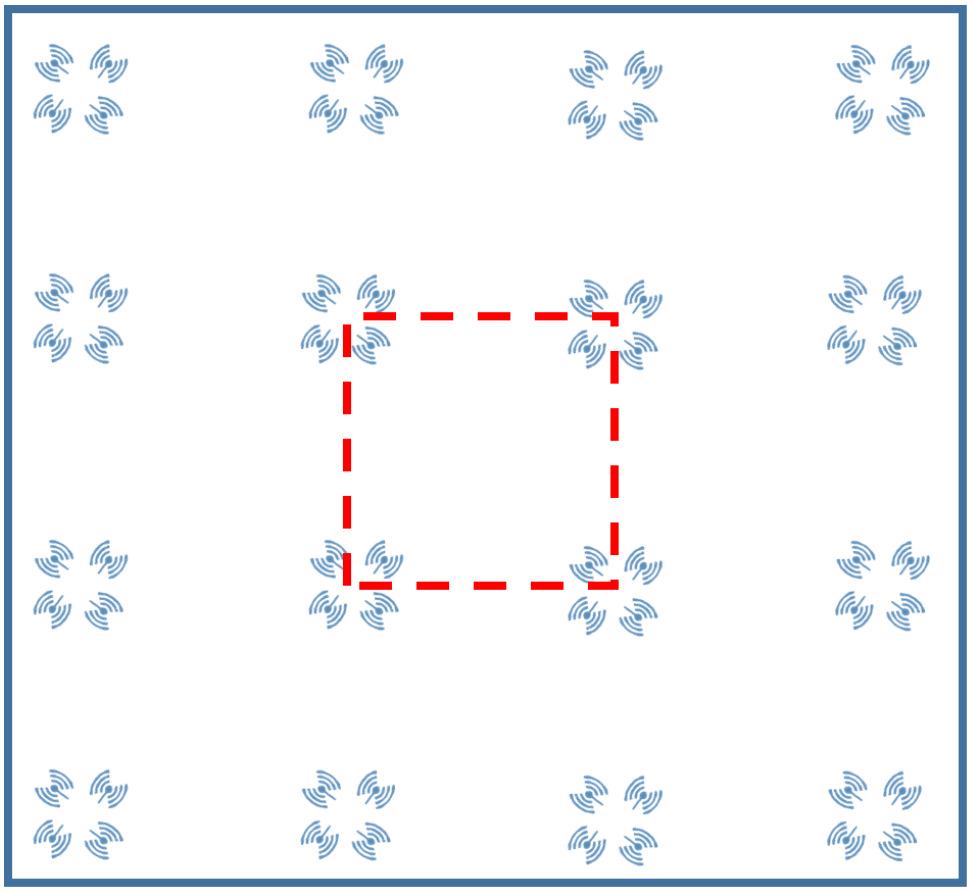

Figure 5.1: A typical four-antenna RFID cell

surrounding cells. Therefore, a dynamic cell allocation scheme could be used in which antennas are reallocated to different cells during the inventory process. This has the potential to decrease the required number of antennas and overall system complexity and cost, since a single antenna is effectively reused where multiple fixed antennas would otherwise be required. For the case of Fig 5.1 here considered, if the system with antenna arrays can be shown to achieve a similar performance to the fixed antenna system in a single cell, then it could be argued that a four-fold reduction in the number of antennas can be achieved for massive areas with many cells (i.e. neglecting antennas at the edges of the interrogation zone). The justification for this is that the array can be expected to replicate the same performance in all adjacent cells. Furthermore, since fixed antenna systems use time division multiplexing (TDM) to avoid inter-cellular interference, there should be no real time penalty in scanning the area with phased array antennas.

In this chapter, a DAAS is designed and demonstrated, using four phased array antennas, whose beam patterns can be controlled from the reader. This enables the simulation of

a single rectangular RFID cell. The system is compared to an equivalent standard DAS system of four fixed-beam antennas. It is demonstrated that the presented Distributed Antenna Array System outperforms a fixed antenna system in a single cell, thereby satisfying the condition above, and a reduction in the number of antennas required to cover a specific area. In addition, it has the potential to enable larger cells (i.e. cells with wider inter-antenna spacing) as demonstrated by higher tag detection rates achieved for the same cell dimensions. This is achieved in part by compensating for the reduction in array gain due to beam steering by increasing the transmit conducted power into the antenna to maintain a constant EIRP as the array is steered.
Finally, a single port reader is used to implement an RFID DAAS system by daisy-chaining several antenna arrays with coaxial cable. The chapter begins by comparing the read performances of a single fixed antenna and a single antenna array.

5.1 A Primer study on a single Phased Array Antenna

Scanning antenna arrays have been shown to provide better coverage and improve the read performance of RFID systems over fixed standard antennas [4, 126, 86] . The scanning ability of antenna arrays, especially of a 2D steerable antenna, enables an effective wider field of view, thereby allowing tags to be read over a wider area, and improve coverage as a result. Second, because this wide area is covered temporally as the beam pattern is steered, the effects of multiple tag-to-reader collisions are minimised compared to a fixed wide beam-width antenna. This enables more tags to be read at a quicker rate. Finally, multipath is reduced, especially for high gain antennas, as a narrower beam sweeps across the interrogation area. As a result, an improved read performance in terms of tag detection in a given area is expected from a single array than from a fixed antenna.

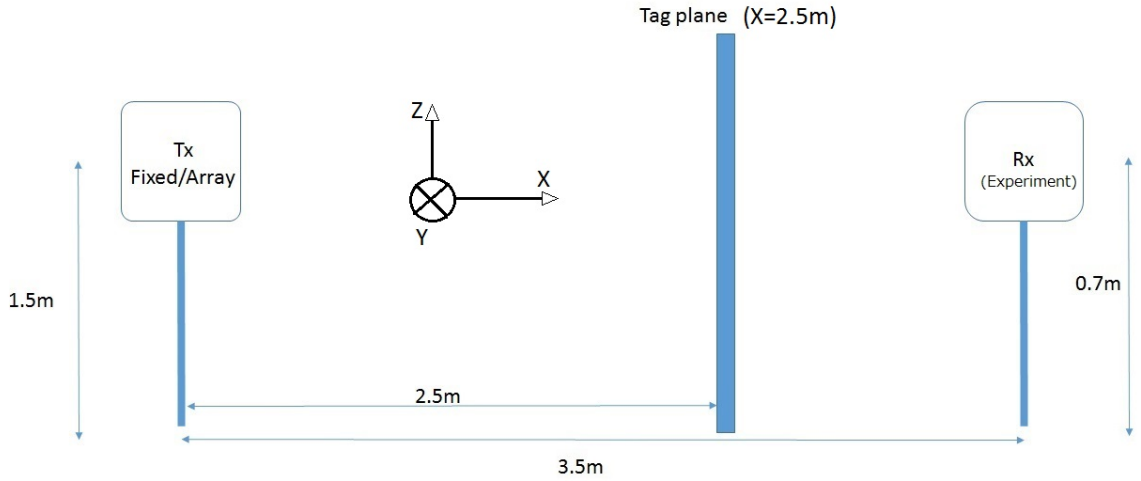

Figure 5.2: Phased array antenna case study

In this section, a preliminary study comparing the performance of a single antenna - one fixed and one steerable - is performed by interrogating a set of tags. The experiment is illustrated in Fig. 5.2. Tags are arranged on the vertical plane 2.5m horizontally from the transmit antenna (X=2.5m plane). The transmit antenna is pointing in the direction normal to the plane of the tags.

To explore the full potential of such a system, instead of using a limited number of pre-stored beam states, a complete array scanning system capable of being steered to arbitrary directions is used.

5.1.1 Beamforming

Simulations and experiments on arrays in the previous chapter made use of pre-programmed beam states, in which FEKO simulations for all required beam states are imported into MATLAB for modelling. During each iteration of the simulation process, a random beam is selected to perform an inventory for each array. For the experiments, a look-up table is used to store ordered sets of phases which generate the particular beams of interest. The problem with this approach is the limited number of beams which are feasible, as one would have to perform thousands of simulations to generate every possible beam state, or store a huge look-up table on the reader's MCU.

In this section, beams are synthesised using the array synthesis equations introduced in the previous chapter, as this enables a much wider range of directions to be covered using

a single beam pattern, and avoiding the need for running full wave simulations for every possible beam state. A single antenna is simulated in FEKO and the steered beam is synthesised using equal amplitude and uniform progressive phase excitation of the elements. For a given desired beam direction (θ_0, ϕ_0) and antenna element pattern, $E(\theta, \phi)$, the steered beam is given by:

$$F(\theta_0, \phi_0) = \sum_{n=0}^{N-1} \sum_{m=0}^{M-1} E(\theta, \phi) a_{mn} e^{jkd(n\psi_x + m\psi_y)} \tag{5.1}$$

where

$$\psi_x = sin\theta cos\psi + \phi_0 \text{ and } \psi_y = sin\theta sin\psi + \theta_0 \tag{5.2}$$

$E(\theta_0, \phi_0)$ is the electric field of a single element antenna obtained from FEKO, $F(\theta, \phi)$ is the resulting steered beam of the array, d is the array separation distance $(\lambda/2)$, $k(= \frac{\pi}{\lambda})$ is the wave number. In this case M=N=2, as we are utilising 2x2 circularly polarised patch antennas. As a result, any direction (θ_0, ϕ_0) can be scanned, all within the limitations of the antenna. This method is limited in that it does not model the effects of mutual coupling on the antenna beam pattern, but the antenna element separation $(\sim \lambda/2)$ is wide enough for such effects to be minimal [127].

5.1.2 Simulation Results

The simulated power distribution and cdf for this setup are shown in Figs 5.3 - 5.5.

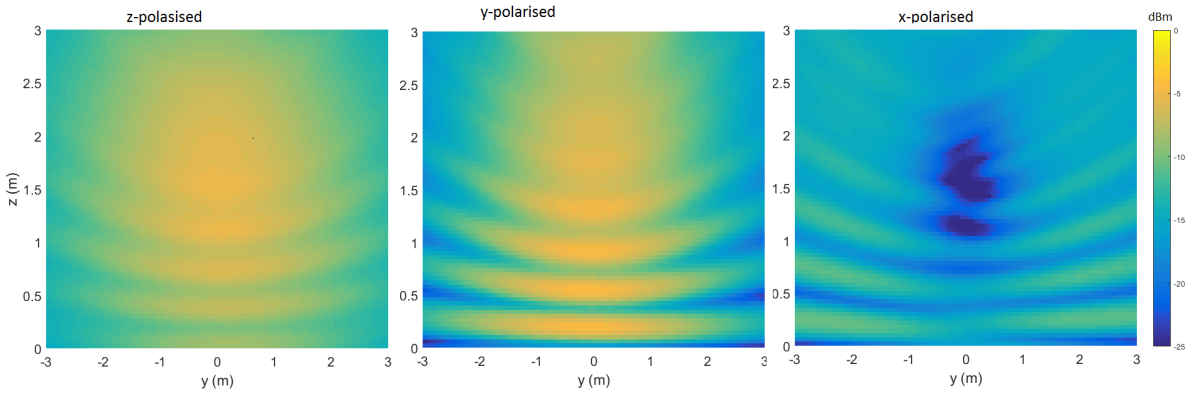

Figure 5.3: Power distribution on plane X=2.5m for a single antenna array

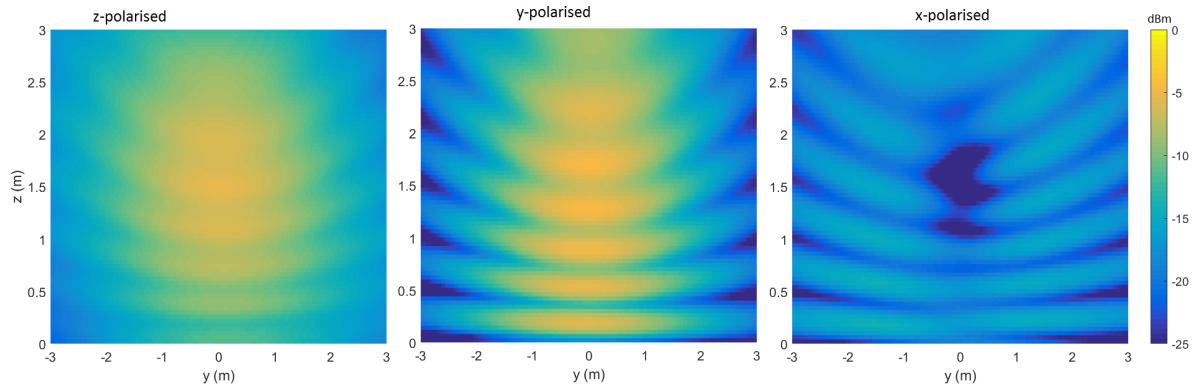

Figure 5.4: Power distribution on plane X=2.5m for a fixed antenna

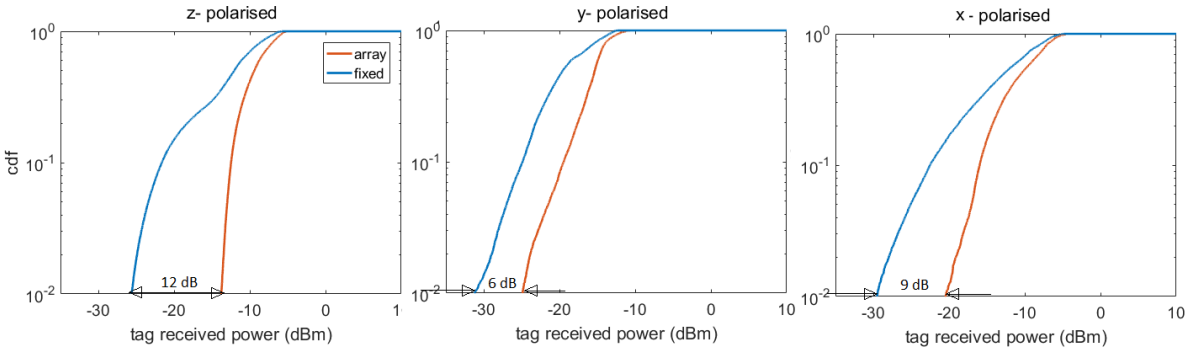

Figure 5.5: cdf for tags on plane X=2.5m for single antenna array

Comparisons are done using the the 1st percentile of tags. i.e the 1% of tags to receive the least power as shown in Fig 5.5, since these are the tags which determine the read success rate in a practical system. Depending on polarisation, a power margin of up to 12dB is observed. This can be explained in terms of the beam scanning, which provides an effective wider beam width to the array, while minimising the multipath effects from such a beam by changing scan direction with time. As a result, much higher read rates are obtained.

5.1.3 Experimental Demonstration

A simple experiment is performed to demonstrate the improvement of an antenna array over a fixed antenna. The experiment is modelled on the above simulations and the setup is shown in Fig 5.9. A receive antenna (absent in the simulation) is included 1m from the plain of the tags, so the rssi could be measured.

Control PCB Design

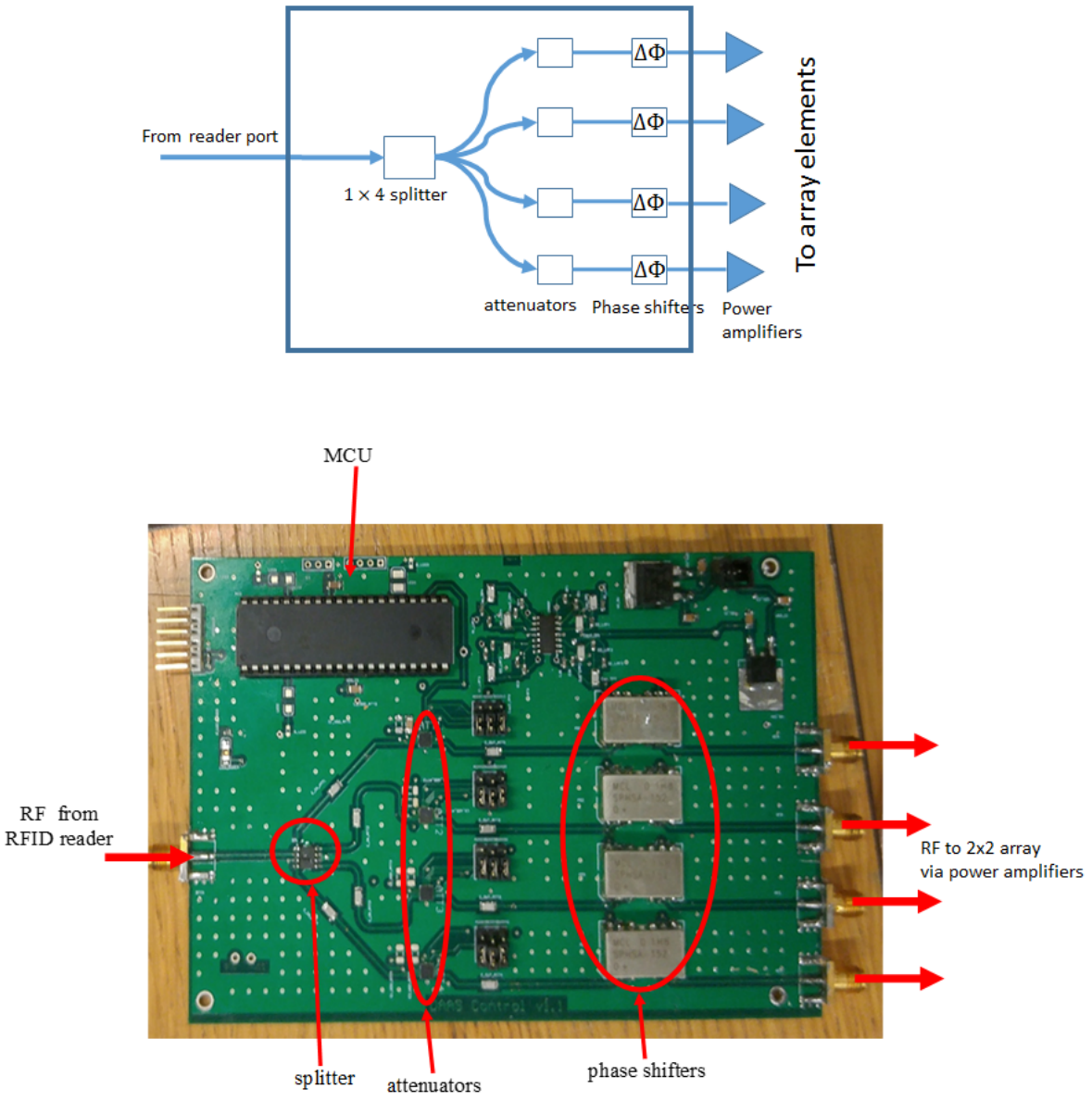

Figure 5.6: Control circuit for array showing system diagram (top) and manufactured PCB (bottom). The circuit takes in a single modulated carrier and performs beam steering. Beam steering is controlled via an onboard MCU.

A control PCB responsible for beam-forming and phase hopping is designed as shown in Fig 5.6. This facilitates the extension of the system to multiple antennas, as the beam-forming and phase diversity functionality are carried away from the reader and distributed to each antenna. It also enables ease of installation, as only a single coaxial cable per antenna from the reader is required. Finally, any phase offset due to multiple coaxial cables

to the ports of a single array is removed, thereby eliminating the need for phase-matched cables.

The designed PCB contains a splitter, attenuators and phase shifters, and is designed for use with any four-element array. The input signal is split into four using a splitter (Minicircuits BP4C+ [128]). Each of four output arms from the splitter is attenuated by a digital step attenuator (DSA, Qorvo RFSA3714 [129]). The attenuator enables each antenna to be able to dynamically control its power, as well as the power from each antenna port. As a result, alternative unbalanced amplitude beamforming schemes could be implemented. Each arm is then passed through a voltage variable phase-shifter (Minicircuits SPHSA-152+ [130]). The phase shifters have a range of 360 degrees, and are therefore able to simultaneously perform beam steering and phase dithering. The combined action of phase shifter and attenuator provide the necessary functionality required for beam forming. All functionality is controlled from the microcontroller unit (MCU, PIC16F1779 [131]). This is a 32 MHz MCU, with SPI links to each attenuator. The MCU is also equipped with four 10-bit onboard Digital-to-Analogue Converters (DACs), which are used to drive the phase shifters. However, due to the high voltage requirement for the phase shifter (12 V) to achieve full phase control, an amplifier circuit is implemented, and a 2-pole Sallen-key filter (cut off frequency at $10kHz$) added in order to filter out any noise from the phase shifter, which has a control bandwidth of $50kHz$. The measured phase shifter response is shown in Fig. 5.7 There is also a digital signal from the reader to the MCU in order to control the beam switching times, and prevent the antenna switching states during an inventory. This could also be used to communicate other information with the reader. The design is based on a 50Ω line to facilitate matching to the antenna at the design frequency of 865-868 MHz

The four outputs of the array control PCB are each connected to power amplifiers (Wavelex WPA0409N [132]) mounted on the back of the antenna (see Fig 5.8). These amplifiers have a 1dB compression point of +27dB and are capable of driving the antennas at high enough power at 50Ω to meet the maximum permitted +35.15 dBm EIRP. The output of each amplifier is then connected to each port of the reader antenna, which is also matched at 50Ω.

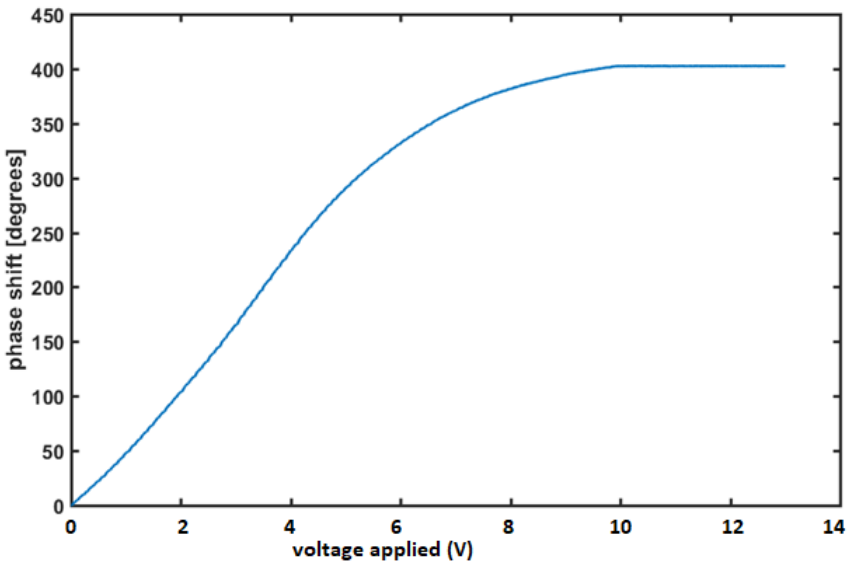

Figure 5.7: Phase shifting characterisation of beam control PCB

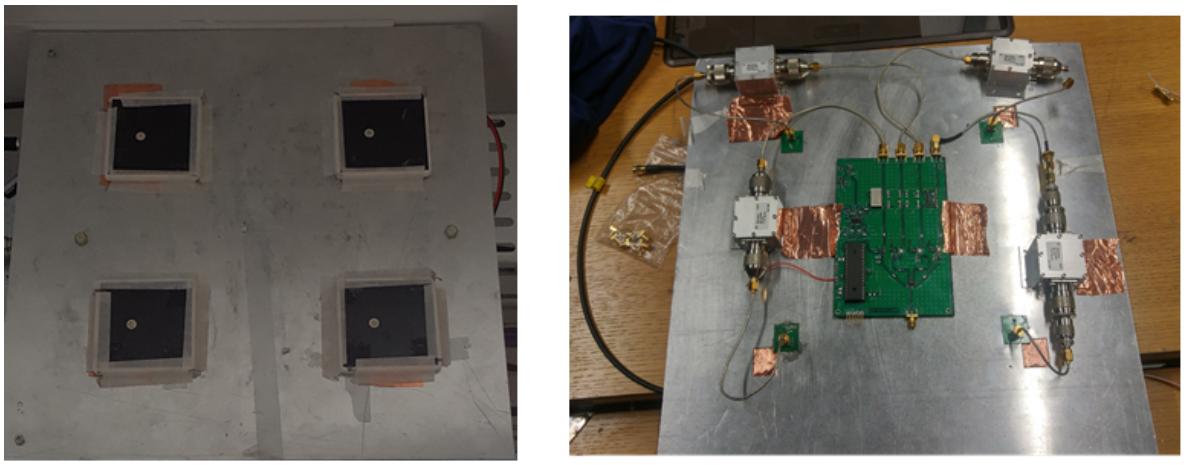

Figure 5.8: Antenna front (left) and back (right) showing PCB mounted on antenna, together with the four power amplifiers

Experiment

The power is set such as to give an EIRP of 32 dBm EIRP for both cases. A total of 250 tags is targeted.

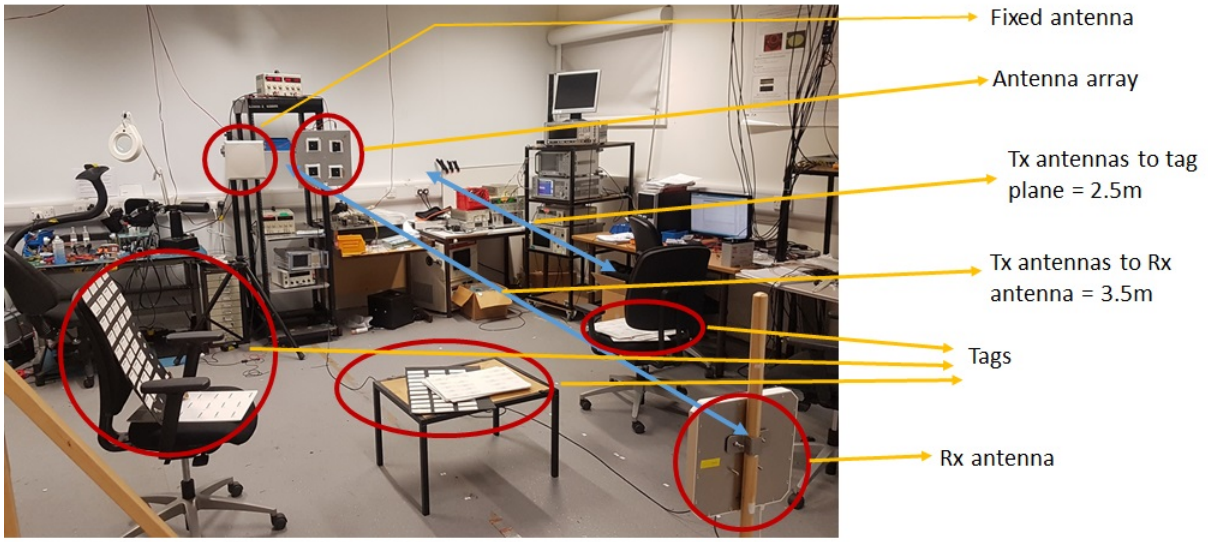

Figure 5.9: Experiment comparing read success rate of tag arrays for scanning antenna array and a fixed antenna

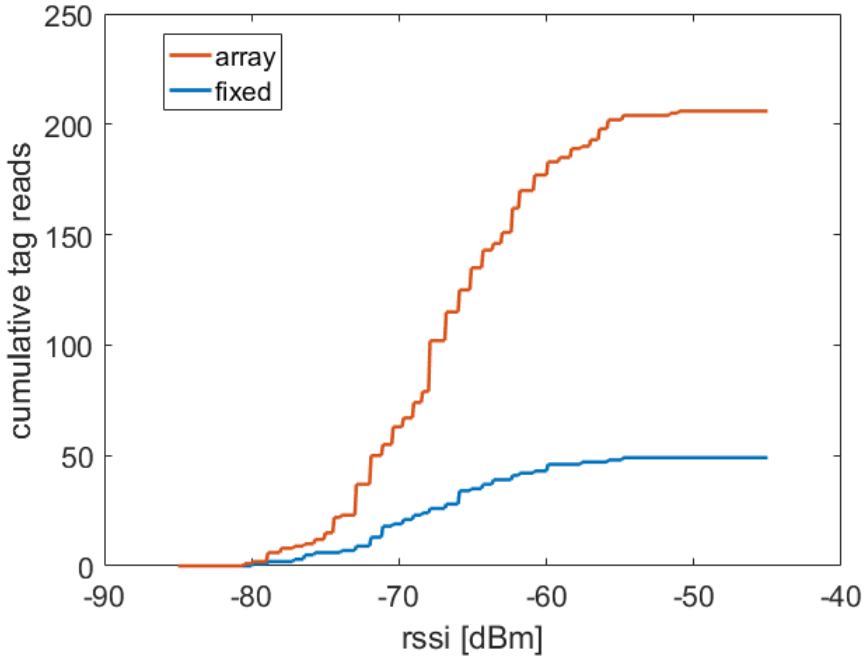

Figure 5.10: Experiment comparing single fixed antenna and single antenna array

It is observed that the antenna array provides a significantly higher number of successfully detected tags of up to four times the fixed antenna.

5.2 Simulations on Distributed Fixed and Antenna Array Systems

As has been discussed in the introduction, wide areas are usually divided into cells, each addressed by a unique reader connected to multiple antennas. e.g. four antennas per cell in a rectangular arrangement as in Fig 5.1. In this section, a single rectangular cell is investigated with both a fixed and array distributed antenna system. The aim is to compare the relative power delivery performance of a fixed and antenna array RFID system.

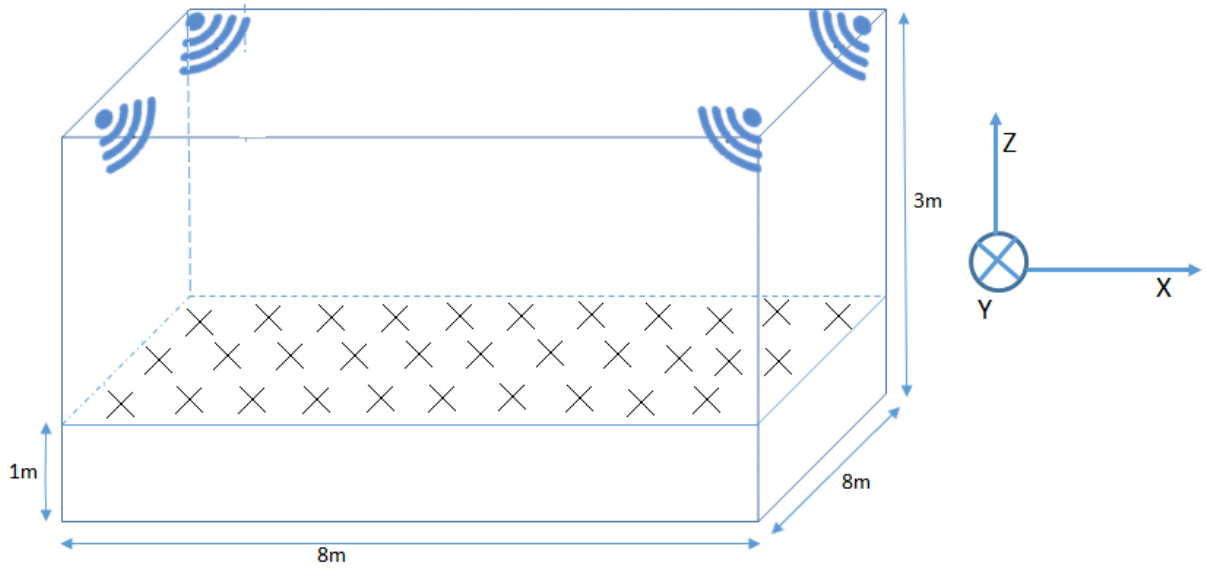

Figure 5.11: Experimental setup for comparison of fixed and array distributed antenna system. This model represents a single cell in a multi-cell wide area RFID system. The antenna are placed at the cell vertices.

Because the array system can interrogate all four adjacent cells, it can be said to reduce the required antenna number by four if a similar performance is obtained to the fixed system. The case is considered of a reader antenna placed at a height of 3m above the ground level, while tags occupy the plane 1 m above ground level in an 8m×8m room.

5.2.1 Distributed Fixed Antenna Systems

For each iteration of the simulation, a random phase is applied to each antenna in order to simulate phase diversity. The fixed DAS system has been simulated in Chapter 3, and

the results are recalled in Fig 5.13. Here, the same simulation is performed for different elevation tilt angles to find the optimum value, which is 70^0. The antennas are also titled 45 ^{0} in azimuth to face the centre of the cell, as shown in Fig 5.12

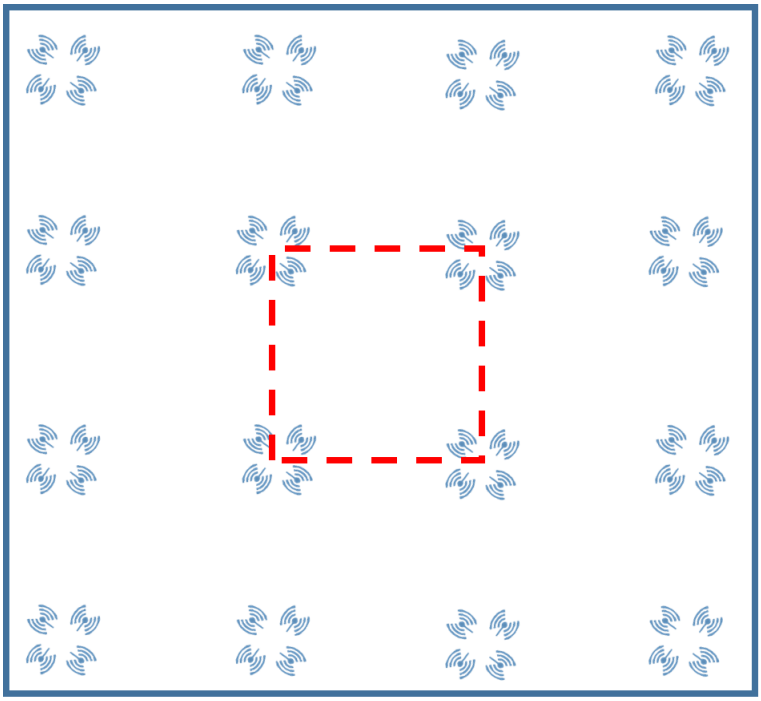

Figure 5.12: Fixed antenna RFID system

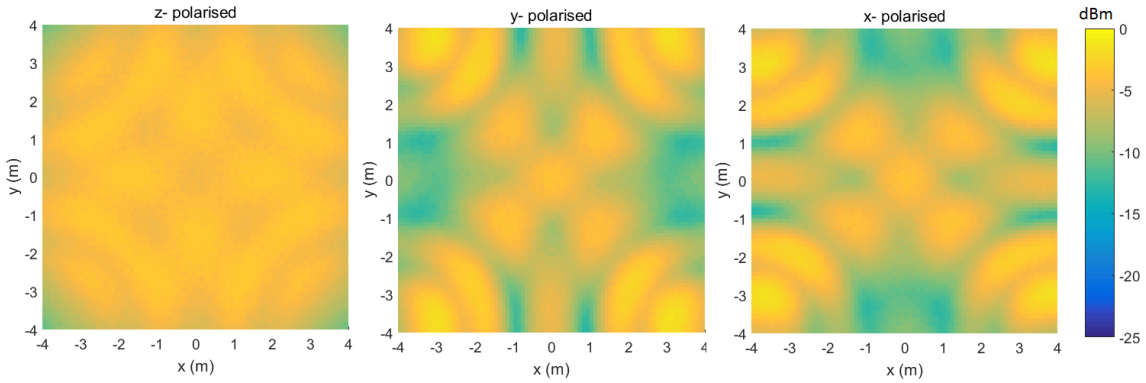

Figure 5.13: Power Distribution for fixed four-antenna Distributed Antenna System for antenna tilt angle of 70 ^{0}

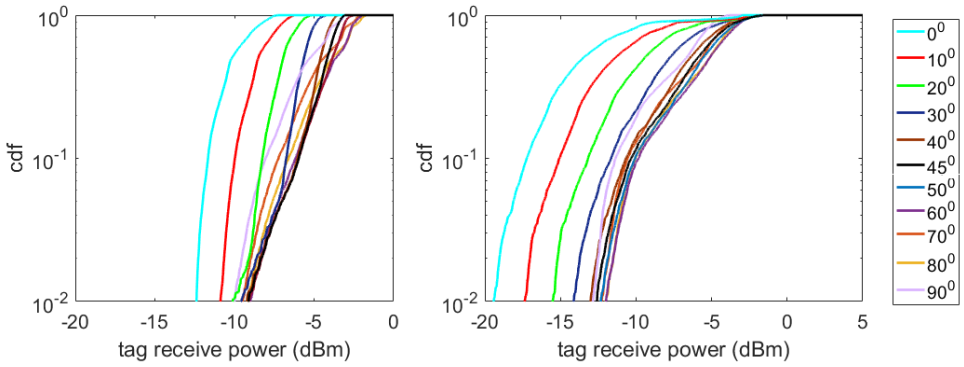

Figure 5.14: cdf plot of fixed antenna system for different antenna tilt angles

5.2.2 Distributed Antenna Array System

A distributed Antenna Array System makes use of an antenna array at the vertex of each cell. Because an array can be steered in the azimuth direction, a single array at the vertex of four cells can be used to interrogate all these cells, as discussed in the introduction. Two methods for generating the beams are simulated, and their relative merits are discussed.

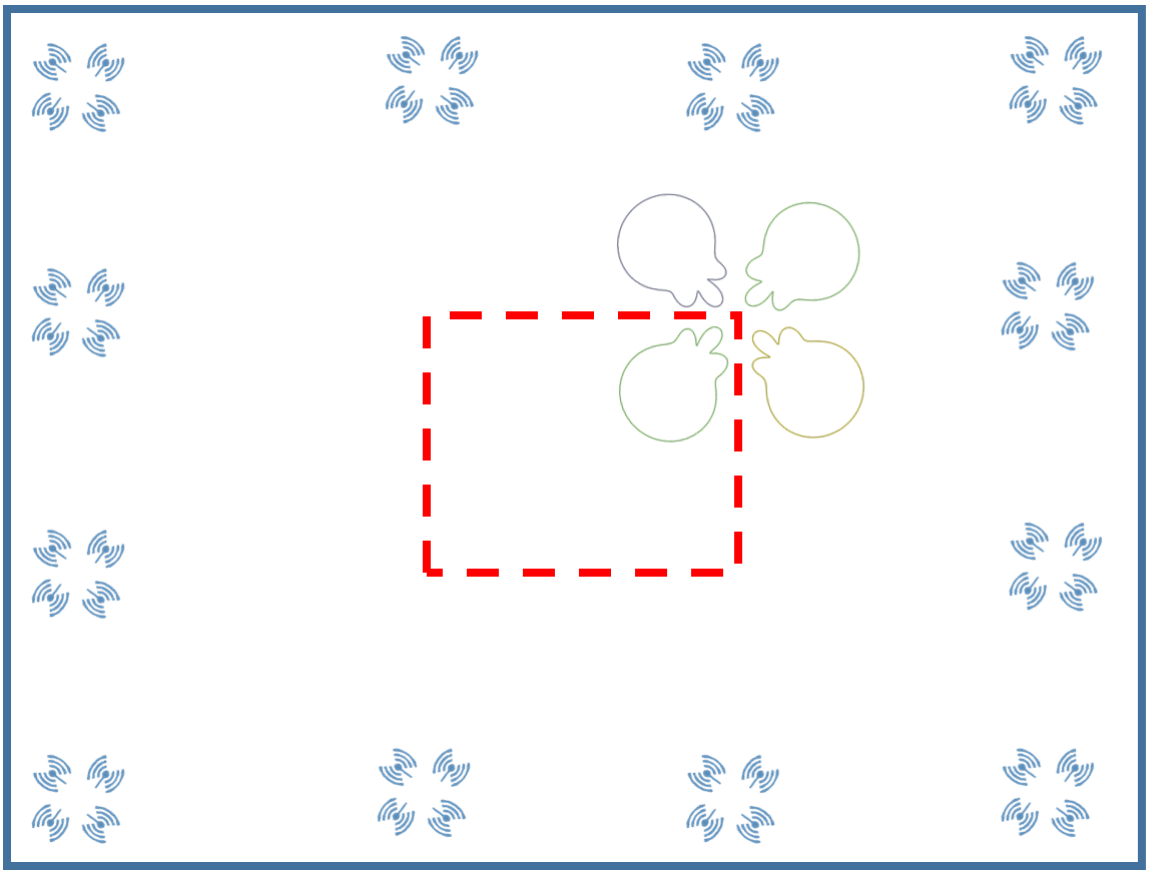

Figure 5.15: Switched antenna array RFID system with a Butler matrix-fed array at each cell vertex. Each array can switch between four different beams and scan each surrounding cell.

Switched Beam Array System

Switched beam antennas use fixed RF circuits such as Butler matrices to provide beam diversity, as discussed in Chapter 2. They have the advantage of being simple and passive. They can be designed entirely using microstrip, as the only required components are hybrid couplers, fixed phase shifters, and RF crossovers. Fig 5.16 shows an example of a Butler matrix which has been used in a 2×2 RFID array antenna. The beams are varied by switching the input signal. The input into each port of this feed circuit is seen phase-shifted at the input of all the antenna elements, resulting in one of four beams shown in Fig 5.16. The antenna is placed at the vertex of the cell, and the appropriate beam is selected in order to direct the beam into the cell of interest. The resulting power distribution is shown in Fig 5.17. Table 2.1 shows the phases and beam directions corresponding to feeding different ports.

Feed port	antenna element phases (degrees) I,II,III,IV	Activated beam
A	0, 90, 180, 90	A
B	90, 180, 90, 0	B
C	90, 0, 180, 90	C
D	180, 90, 0, 90	D

Table 5.1: RFID antenna design requirements

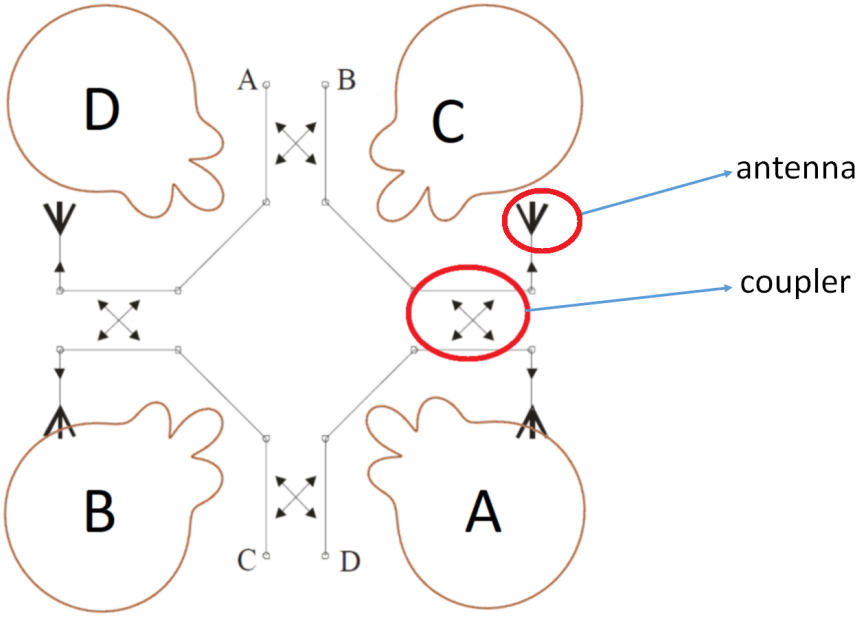

Figure 5.16: A Butler-type matrix for a 2×2 array showing input ports and the corresponding beam. e.g. feeding Port A generates Beam A

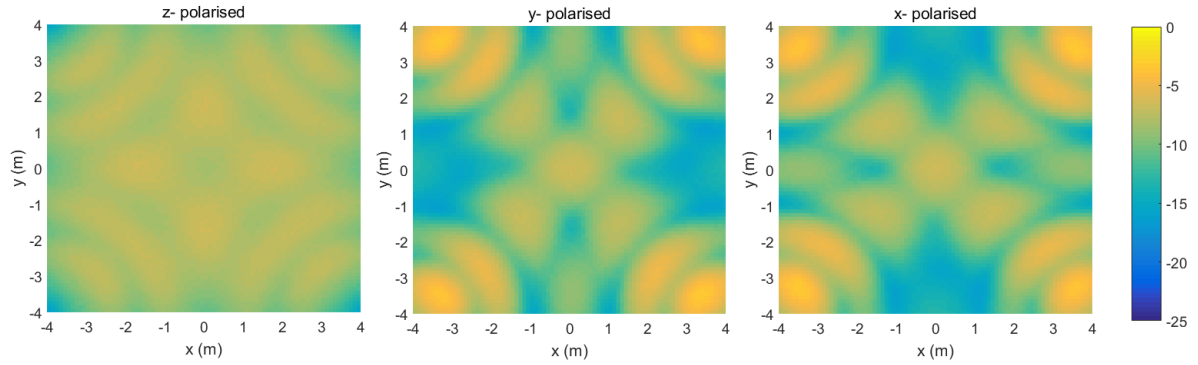

Figure 5.17: Power distribution for switched array antenna system of four arrays located at vertex of cell

The disadvantage of this system is the limited degree of freedom in the beam steering, and therefore limited performance compared to a fully steered antenna. The number of beams in this case is limited to four, i.e. one beam per adjacent cell, and there is no control over the elevation angle, which is determined by the nature of the antenna element (patch antenna in this case). The indicated phases produce beams at an elevation angle of 30^0.

Steerable Array System

In this section, a steerable beam is implemented, similar to that described in section 1 of this chapter, where use is made of the array factor equation (Eqn. 5.3) to steer the beam to an arbitrary direction. As described above, this system is capable of scanning to arbitrary directions at the expense of more complex functionality, including programmable phase shifters, attenuators, and the associated control functions.

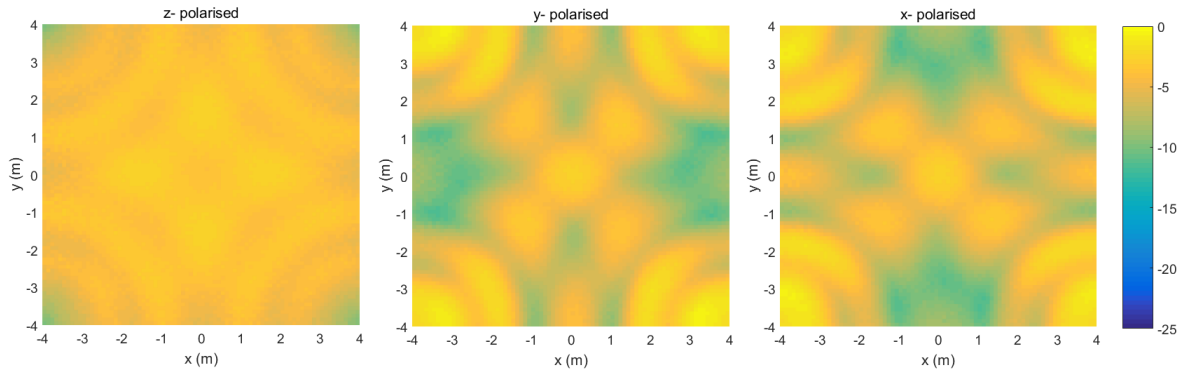

Figure 5.18: Power distribution for steerable array antenna system of four arrays located at vertex of cell

The power distribution for this system is shown in Fig 5.18.

5.2.3 Analysis and Discussion

The tag read cumulative probability for the different systems are plotted in Fig 5.19. i.e. the probability that the received tag power is less than a given value on the x-axis.

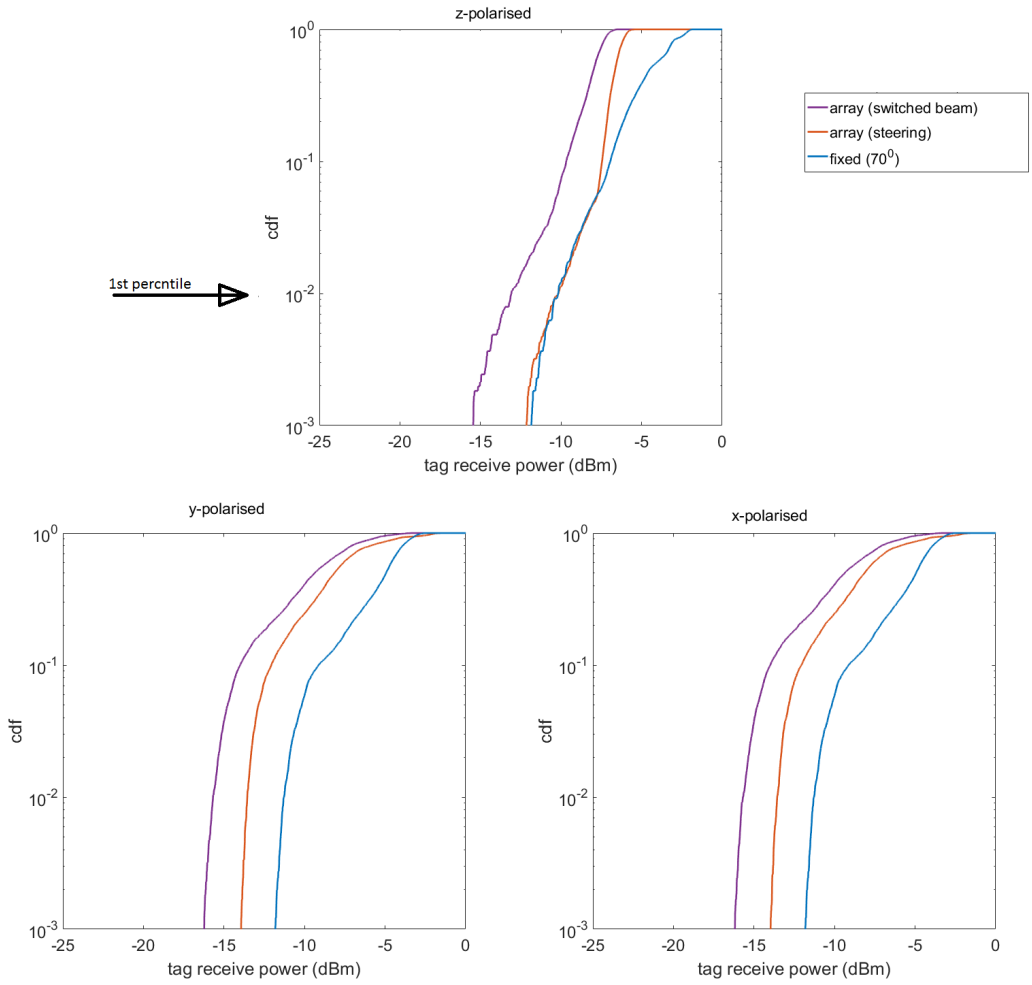

Figure 5.19: Cumulative distribution of tag received power for a distributed system of fixed and array antenna

The performance criteria is taken to be the the 1st percentile. i.e. the power received by the least powered 1% of tags determines the performance of a particular system. This is expected in practical systems since the most vulnerable tags and not the average power determines the read success rate. It can be observed that the switched beam array system performs least well in terms of delivering power to the tag of all orientations. The least

powered 1% of tags in this case receive $\sim -13dB$ for vertical tags, which is $\sim 3dB$ less than the steered array system. For the horizontally-polarised tags, the switched array system lags the steered array system by $\sim 2dB$. As has been mentioned, this is due to the increased diversity with beam steering, as opposed to the single beam produced by a switched beam system using a fixed feed network.

The fixed antenna system performs similarly to the steered array for vertical tags and provides $\sim 2dB$ more power to the horizontal tags than the array system. The reason for this is the reduced gain of the antenna array with steering angle, such that at high elevation steering angles, the power delivered to the tag is severely degraded, leading to less received power than otherwise would be. The fixed antenna, on the other hand, has been optimised to maximise performance in the cell to which it is assigned. 2 dB represents, according to Friis equation, $\sim 20\%$ of read range. As a result, the array system in this case could be used to decrease the antenna count over a fixed system by four, but with a corresponding $\sim 20\%$ decrease in cell size or antenna separation. This is because the results presented are replicated by the same array in all four surrounding cells, whereas the fixed antenna addresses only a single cell. This represents an effective $4 \times 0.8^2 \approx 2.6\times$ reduction in the required number of antennas compared to a fixed system.

The switched array system averages a $\sim 3dB$ power reduction at the one percentile compared to the fixed system for vertical tags and $4dB$ for horizontal tags, which results in a respective 30% and 37% cell size reduction and four-fold antenna count reduction or an effective $4 \times 0.7^2 = 2\times$ and $4 \times 0.63^2 = 1.6\times$ antenna count reduction.

5.3 Experimental Demonstration

5.3.1 Experimental Setup

Experiments are carried out in a lab to demonstrate a full DAAS system. A single cell is demonstrated using four designed 2×2 antenna arrays. A similar standard DAS experiment is carried out along side and comparisons are made.

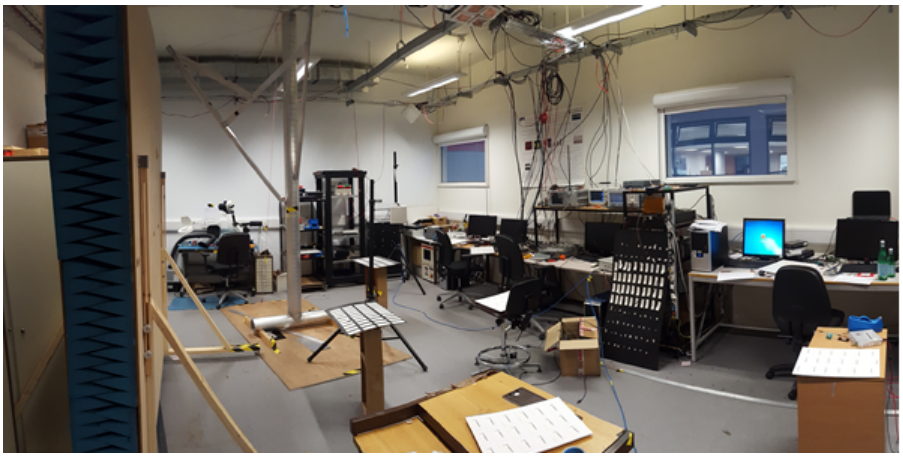

Figure 5.20: Laboratory experiment setup

The experiment is carried out in an 8m×6m laboratory area for four phased array antennas in one experiment, and four fixed antennas in another, each attached to the ceiling at the four corners of the lab. 312 tags of interest are distributed across the room. The lab environment is shown in Fig. 5.20. The tags are placed in clusters of 18-40 tags with a roughly uniform distribution in a highly scattering environment. The clustering of tags is for experimental convenience and to provide a more realistic and difficult target case than widely spaced individual tags. A single coaxial cable from the reader feeds each antenna. The fixed antennas are fed directly, while the arrays are mounted with the control PCBs described in above, and provide the four outputs required at the 2×2 array used. Three separate circularly polarised antennas are used as the receive antennas in both cases, to allow comparison of the downlink only.

The experiment is run in session 2 in order to maximise tag detection, as each tag is rendered idle after detection, and therefore the RSSI recorded is the first value received by the tag above its threshold power. The experimental results are presented in Fig 5.21. It is shown that the array achieves a tag detection read success rate of about 97% (302 tags), while the fixed system achieves 95% (297 tags). It is seen that the experiment slightly favours the array system, giving better detection probability for a single cell.

5.3.2 Discussion

The presence of walls, metallic shelves and lab equipment make the environment highly scattering, which tends to favour a beam-diverse system. Phase diversity cannot overcome multipath fading, which makes a fixed DAS system struggle in a highly scattering

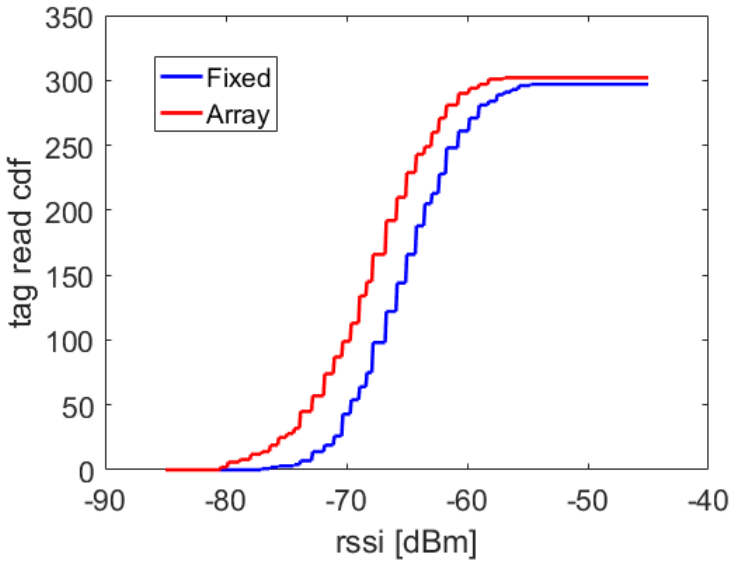

Figure 5.21: Cumulative tags read against RSSI for four-antenna system of fixed antennas (blue) and antenna arrays (red)

environment. The array system can overcome fading due to multiple beams in addition to phase diversity.

A time evolution of the tag detection rate is also shown in Fig 5.22. It can be observed that the read rate of the array system matches that of the fixed system until additional tags are read. This implies that there is no time penalty in tag detection caused by steering the arrays.

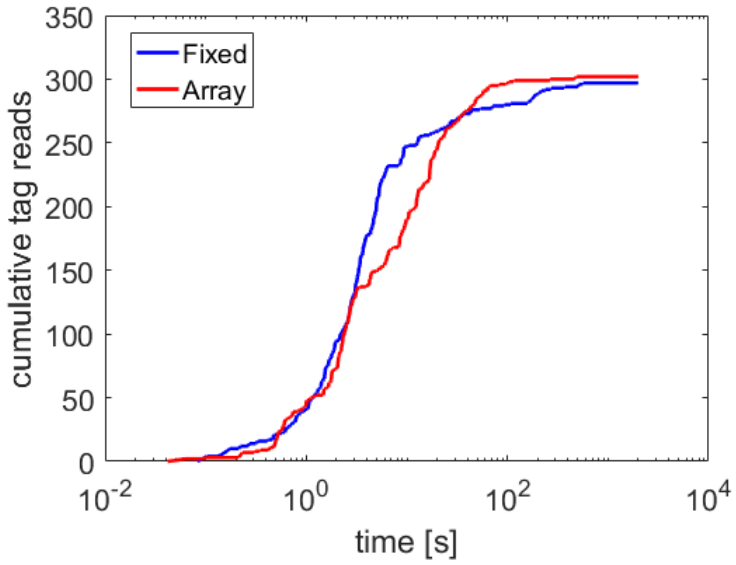

Figure 5.22: Cumulative tags read against time for four-antenna system of fixed antennas (blue) and antenna arrays (red)

5.3.3 Adaptive Steering Transmit Power Control

It is well known that the gain of an antenna array decreases with scan angle [110]. This means that at high scan angles, the gain of the array may be severely degraded, reducing the power available at some tags. This can be resolved by dynamically varying the conducted input power to the array in order to maintain a constant EIRP, and therefore boost the power transmitted by the arrays at high scan angles where the gain is degraded. The method is modelled by scaling the electric field to obtain a specific EIRP for each antenna during each iteration of the simulation.

The equation for the field pattern of a phased array antenna steered to a direction (θ_0, ϕ_0) is recalled:

$$F(\theta,\phi) = \sum_{n=0}^{N-1}\sum_{m=0}^{M-1} E(\theta,\phi) a_{mn} e^{jkd(n\psi_x + m\psi_y)} \tag{5.3}$$

where

$$\psi_x = sin\theta cos\phi + \phi_0 \text{ and } \psi_y = sin\theta sin\phi + \theta_0 \tag{5.4}$$

$E(\theta,\phi)$ is the electric field of a single element antenna obtained from FEKO, $F(\theta,\phi)$ is the resulting steered beam of the array, d is the array separation distance $(\lambda/2)$, $k(=\frac{2\pi}{\lambda})$ is the wave number.

The maximum value for the electric field, F_{max} is obtained at broadside, i.e. when $\phi_0 =$

$\theta_0 = 0$. For $\phi_0 \neq 0$ or $\theta_0 \neq 0$, $F < F_{max}$, and therefore a scaling of the electric field is needed in order to compensate for this, and is given by

$$k(\theta_0, \phi_0) = \frac{F_{max}}{F(\theta_0, \phi_0)} = \frac{F(\theta_0 = 0, \phi_0 = 0)}{F(\theta_0, \phi_0)} \tag{5.5}$$

This means that when the array is transmitting in a direction (θ_0, ϕ_0), its electric field is scaled by a factor of $k(\theta_0, \phi_0) > 1$, to maintain the non-steered EIRP. In this way, higher performance gains could be expected, as the steering loss factor is compensated. The distribution of difference in power received at the tags between this implementation and the case without power scaling for the steered array system is shown in Fig 5.23

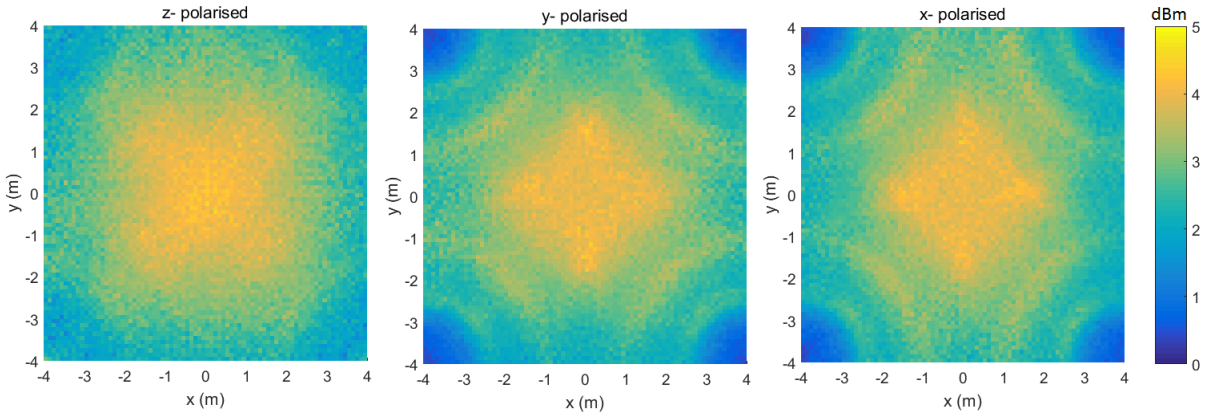

Figure 5.23: Power gain introduced by power scaling compared to no-scaling case. The dB difference in power distributions is plotted.

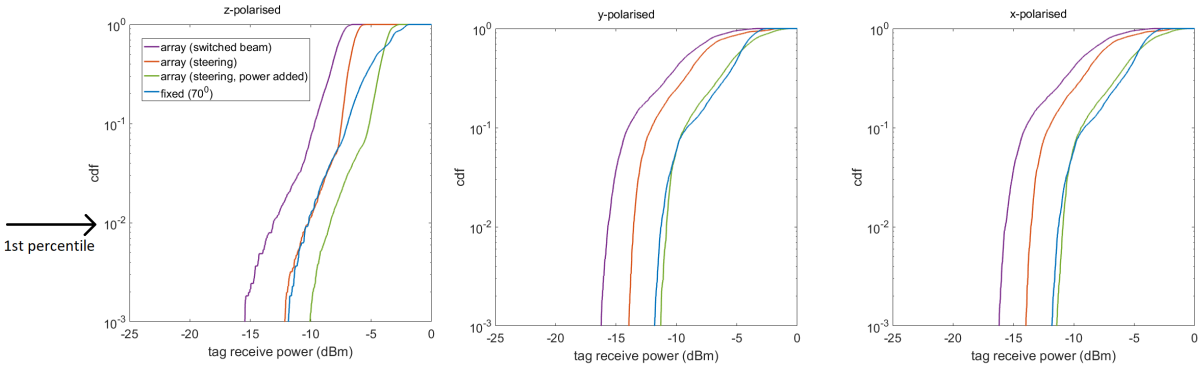

Figure 5.24: cumulative distribution of tag received power for a distributed system of fixed and array antennas

Discussion

It is observed that the power scaling leads to improvements in the power received by the tag in all orientations. As can be seen in Fig 5.23, the tags directly underneath the antenna

receive minimal extra power. This is because these tags receive most of their power solely from the closest antenna, since the distance to the other antennas make the free space path loss relatively high, and therefore the contributed power of little significance to the tags' total received power. Also, the beam is approximately in broadside (non-steered), and therefore there is no field scaling, and consequently, no power gain with this technique. The most power gained using this method is at the centre of the cell, as this represents the area with the most gain degradation for all four antennas, and therefore maximum scaling is applied to the feed. In Fig 5.24, an improvement is seen over the case with no scaling of $\sim 2dB$ for vertical polarised tags and $\sim 2.5dB$ for horizontally polarised tags. It is also observed that the array system now outperforms the fixed system by $\sim 2dB$ for vertical tags and similar performance for horizontal tags. This represents a four-fold decrease in antenna number, with a $\sim 25\%$ cell size increase for vertical tags.

Experiment

Experimentally, it is infeasible to implement the above solution as described due to the the requirement to dynamically measure the gain of the antenna during inventory and compute the power scaling factor. Instead, a lookup table of scan angles and corresponding scale factors is created.

Antenna gain as a function of scan direction, $G(\theta_0, \phi_0)$, can be obtained by characterising the maximum antenna gain for each scan direction, as shown in Fig 5.25. FEKO simulations are performed for several scan angles in steps of 10^0, and the maximum gain for each was recorded. It can be seen that, depending on scan direction, the gain can decrease to as low as 7.5 dB from a maximum of 10 dB, and therefore, a conducted power into the antenna of up to 2.5 dB more is required for the maximum allowed EIRP at some scan angles. It should be noted that, due to the directional nature of patch antenna radiation patterns, and the use of a 2×2 array, the actual main beam direction differs from the intended scan angle as calculated by Eqn 5.3. The plotted progressive phase shifts of $(\theta_0, \phi_0) = \pm 150^0$ corresponds to achieved scan angles of 360^0 in azimuth and $\pm 45^0$ in elevation. Therefore, beam scanning can be obtained for 360^0 in azimuth and up to about 45^0 in elevation. It is therefore possible to dynamically evaluate the additional power that can be conducted into each antenna.

A similar experiment to that described by the simulations above in section 5.3.3 is per-

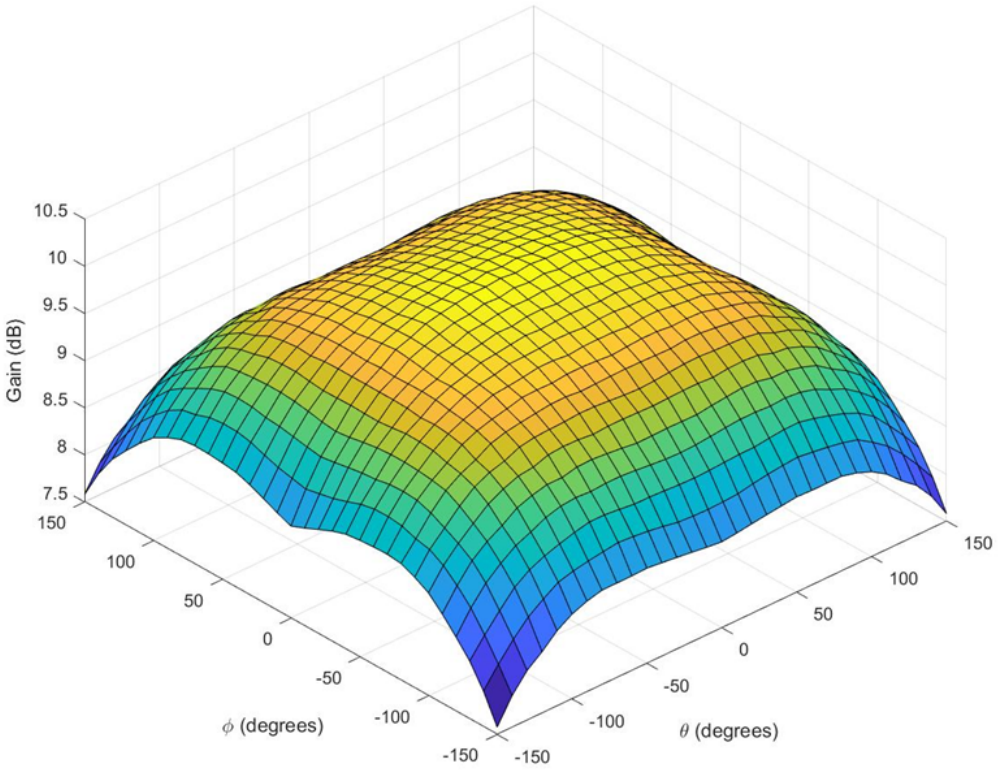

Figure 5.25: Maximum array gain with progressive excitation phases (θ) and ϕ showing gain degradation at the edges. Because of the directional nature of patch antennas, and the limitations of a 2×2 array, the actual scan angle is significantly lower.

formed with the power scaling implemented. The same experimental setup described by Fig 5.20 is used. The array processing PCB circuit presented in section I is equipped with attenuators, which have a resolution of 0.25 dB, and can be used to vary the output power from the antenna. Depending on scan direction, and according to a lookup table of Fig 5.25, the attenuators are set such that the EIRP is constant at maximum irrespective of scan direction. This is done by setting the attenuator initially to 3dB, and then decreasing the attenuation to allow for more transmit power depending on scan direction.

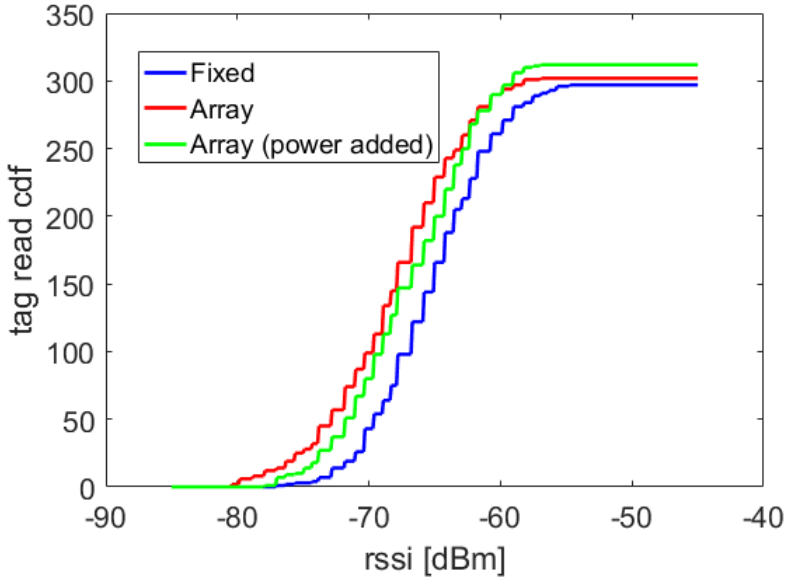

Figure 5.26: Cumulative tag read success rate with RSSI for fixed antenna system achieving 95% (297 tags) after 10 minutes (blue) and antenna array system achieving 97% (302 tags) and antenna array system with added power achieving 100% (312 tags)

The results of this system are presented in Fig 5.26. It is shown in this case that a slight increase in tag read rate is achieved, bringing success rate to 100% (312 tags) in 10 minutes.
Again, the modest improvements in RSSI can be explained by the fact that experiments are run in session 2 and represent the RSSI of the first configuration of antenna patterns and phases which result in a received power at the tag above the tag threshold.

It is also observed that the power delivered by the fixed system is greater than that delivered by the array system (both cases), although the read rate for the fixed system is lower. Furthermore, the median power (cdf=0.5) for the enhanced array system in simulation is greater than that of the fixed system, even though the experimental results show higher tag power by the fixed system. The explanation lies in the fact that the simulations attempt to maximise tag delivered power, while the experiments attempt to maximise tag read rates. As a result, the experiments are run in the s2 session of the RFID protocol standard. This means that a tag, once read, is switched off to reduce tag collisions and maximise read success. This favours the fixed system, as it takes a longer time for the array system to 'find' the beam pattern combinations of the four arrays which maximise power to the tags. By contrast, The fixed system has only one

already-optimised beam combination, and so the tags' power is maximised earlier on in the inventory process. As a result the fixed system delivers a higher median RSSI in the experiment.

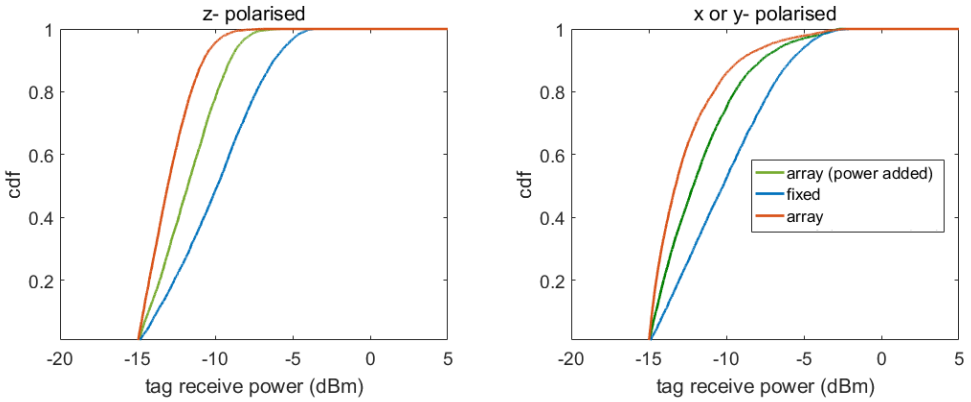

Figure 5.27: Simulation of s2 inventory session. The first value of received power above tag threshold (-15dBm) is used instead of cumulative maximum.

The s2 session is simulated to illustrate this. Instead of recording the maximum cumulative power for each location over all iterations, the first value greater than the tag threshold ($-15dBm$) is recorded, as this represents the RSSI reported in the experimental part. The result is shown in Fig 5.27. It shows that the fixed system records a higher tag received power than the array system (normal and enhanced) under an s2 inventory. However, when considering the cumulative maximum received power, the array can deliver more power to the tags as has been shown in Fig 5.24.

5.4 Use of a Single Port reader

The Distributed Antenna Array System presented requires a coaxial cable for each antenna, as well as a control line (which carries the control signal for beamforming from the reader to each antenna) as shown in Fig 5.28a, which leads to increased complexity. In this case, an N-antenna cell requires N RF cables + N control lines = $2N$ cables in total from the reader. However, since the RFID signal is being multicast to all the antennas, it is possible and convenient to use a single cable to distribute the RF and control signals to all antennas as in Fig 5.28b. This section demonstrates a single port Distributed Antenna Array System, making the system compatible with any standard single port RFID reader.

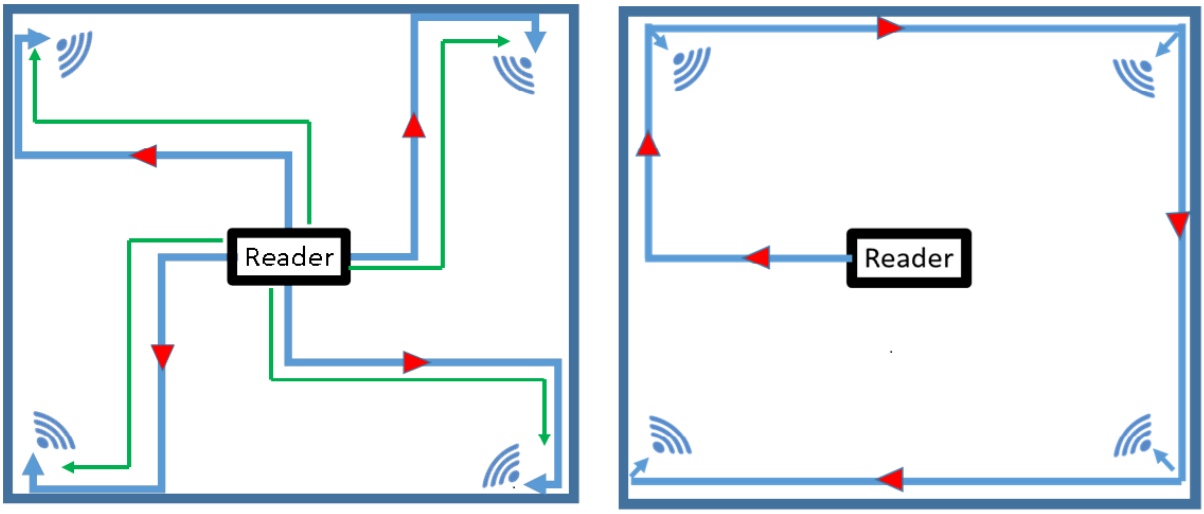

Figure 5.28: RFID Distributed Antenna Array System with multi-port reader using separate RF and control cables to each antenna (a) and single port reader using single coaxial cable in daisy-chain arrangement for both RF and control signals (b)

The proposed circuits for this implementation are shown in Fig 5.29.
At the reader side of the single port DAAS system, a diplexer is used to combine the RF and control signals on a single coaxial cable. Two signals occupying disjoint frequency bands input into a diplexer can be combined into a single output port without interference, and vice-versa. Because of the wide frequency separation of the RF ($\sim 900MHz$) and the control ($\sim 1MHz$) signals, they are easily carried on the same coaxial cable to the antennas without any interference. At each antenna, the RF signal is tapped using a directional coupler. A directional coupler unevenly splits an input signal into two, while

maintaining impedance-matched ports. The larger portion of the signal is called the 'through' signal, while the smaller potion is the coupled signal. The through signal is usually a direct metallic trace from the input, while the coupled signal is obtained by passing another metallic trace close to the 'through' line. As a result, the scattering characteristics of a directional coupler imply that all input frequencies are present at the through output port, whereas only the design frequency is output at the coupled port (see Fig 5.29 b.). The low frequency control signal of the DAAS system is therefore absent at the coupled port of a directional coupler fed with a RF+control signal. The coupled RF signal is amplified and fed directly into the local antenna. Amplification is required, since the tapped signal is degraded in power. A distributed amplification system localised at each antenna is employed. The other possibility is a large amplifier at the reader, but this will require handling of enormous power levels to account for losses from the reader along the line to the last antenna.

The through line of the coupler contains both the control and RF signal. A Bias-T circuit is used to tap some of the control signal, which is then fed to the local antenna control PCB as shown. The through line of the coupler, which contains the RF+control signal continues through coaxial cable to the next antenna. The last antenna in the network uses a diplexing circuit to separate RF and control signal into the antenna and PCB ports as required.

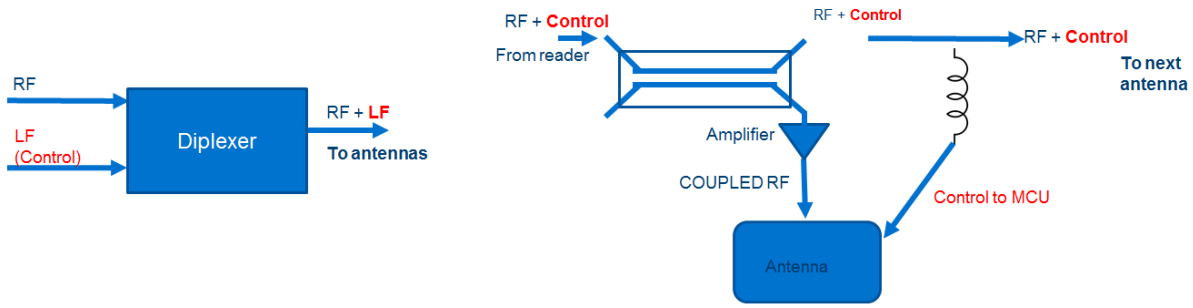

Figure 5.29: Single port DAAS system implementation using a diplexer for the reader end (left) and a directional coupler, amplifier and bias-T for the antenna end (right)

5.4.1 Experimental Demonstration

A simple experiment is performed to demonstrate this concept. A PCB is designed to implement the described functionality as shown in Fig 5.30. Both the reader side (diplexing

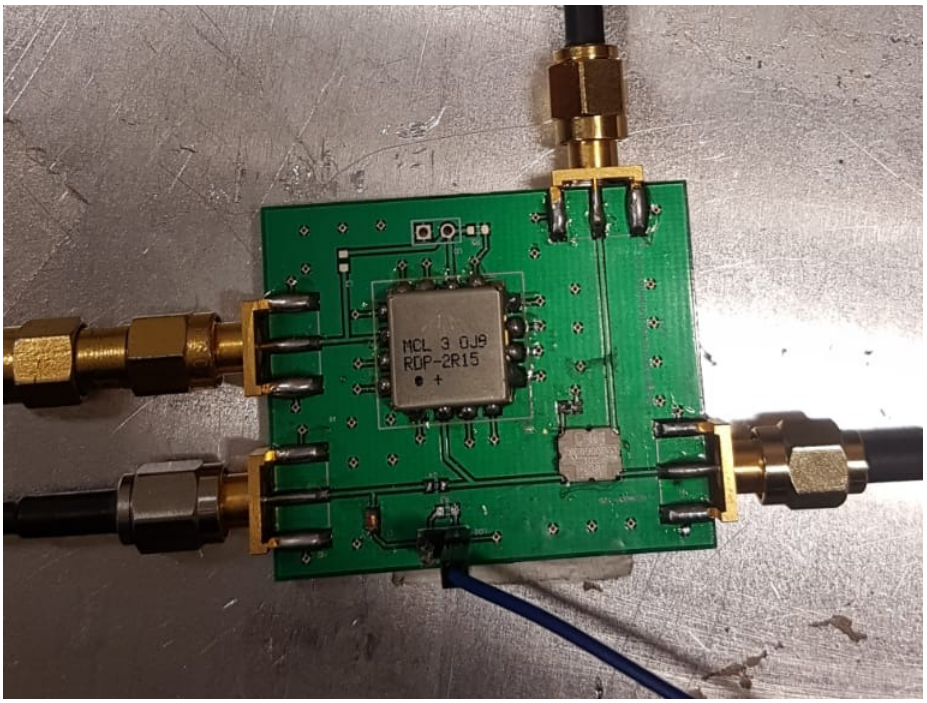

Figure 5.30: PCB implementing diplexing and RF tapping functionality for single reader port RFID Distributed Antenna Array System

circuit) and the antenna side (directional coupler + Bias-T are implemented). A Minicircuits RDP-2R15+ diplexer [133] was used, which has a low band of $DC - 20MHz$ and a high band of $850 - 2150MHz$. A 10 dB coupler is used for RF tapping. A ZX60-V63+ amplifier [134] from Minicircuits is used for signal amplification after RF tapping, but before feeding into the antenna. The signal at each amplifier is attenuated at the appropriate level to maintain equal power output at each antenna array. The maximum output power used in the experiment was limited to +19 dBm, imposed by the 1dB compression point of the amplifier used.

A simple inventory is performed on the tags, and the results are displayed in Fig 5.31 side by side with results for a similar configuration using four separate reader ports, with a dedicated RF coax and control signal cable to each antenna.

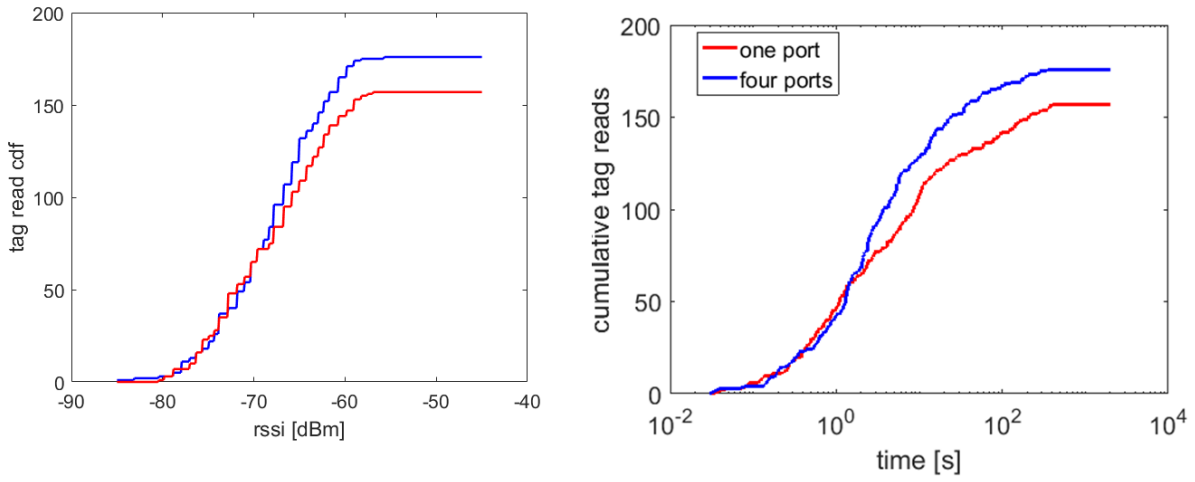

Figure 5.31: Single port RFID DAAS experiment compared with a four-port system

It is seen that the single port reader DAAS is able to detect tags, albeit 19 tags (10%) less than were detected by the four-port system.
Given that the mean power received by the detected tags for both systems is similar (-68.5dBm for single port and -68.1 dBm for four-port), a possible explanation for the difference is in terms of the added noise due to the use of off-the-shelf unoptimised components. A complete PCB-packaged combined coupler-diplexer-amplifier design will be expected to produce similar results with a four-port system. The noise figure added by the extra amplifiers is not expected to sufficiently increase the the noise figure (0.5dB NF), so as to affect system performance.

5.5 Summary

This chapter has demonstrated experimentally the design of a system of distributed phased array antennas interrogating passive RFID tags in a wide area. Four phased arrays were designed, along with beam control circuits, and made to interrogate tags cooperatively in order to maximise tag detection. The system was compared to an equivalent DAS system of fixed antennas, and was shown to provide better performance over the fixed system. Unlike the fixed system, which requires tilted antennas to maximise its coverage, the phased array antenna has the advantage of being flat, and therefore is preferable in terms of form factor.

First of all, a comparison was made between a single antenna array and a single fixed

antenna, in which the array is shown to provide up to four times better coverage. Further to this, the RFID Distributed Antenna Array System (DAAS) using four antenna arrays was designed. This simulates a single cell in a multicell wide area system of arrays. This was compared to the RFID DAS system which makes use of fixed antennas. The DAAS system was shown to outperform the fixed DAS system by making use of gain reduction compensation of antenna arrays during beam steering. It was argued that these results imply a possible four-fold reduction in antenna count over the DAS system with up to a $\sim 25\%$ increase in antenna separation.

Finally, a single port DAAS system using a power distribution network with local RF power tapping was designed and demonstrated. This is possible because each array is capable of phase dithering and beam steering by itself, eliminating the need for special purpose readers to perform this. use has been made of the fact that each array is capable of beam steering and phase diversity to obtain a single port DAAS system by using RF power tapping and amplification, thereby further reducing the complexity of such systems. This enables a standard single-port RFID reader to implement a DAAS system.

The antennas used so far in this work have been 2×2 antenna arrays, with a maximum elevation scan angle of $\sim 45^0$, which will limit the cell size. The next chapter investigates the performance gains that can be obtained by making use of perfectly steerable antenna arrays (i.e. antennas which are steerable to 360^0 in azimuth and $\pm 90^0$ in elevation). These antennas are used to introduce the concept of a cell-less RFID system.

Chapter 6

Perfectly Steerable DAAS and towards a Non-Cellular DAAS

The previous chapter introduced an RFID Distributed Antenna Array System (RFID DAAS), which makes use of multiple distributed phased array antennas to interrogate an RFID tag population. The system was shown to outperform a similarly configured fixed DAS system, owing to the ability of the arrays to steer their beam patterns to multiple surrounding cells. This chapter aims to investigate the upper performance bounds of such distributed array systems by considering the theoretical limits on the beam steering capability of phased array antennas with the objective of examining the trends which could guide future system design.

The first aim is to investigate the maximum comparative advantage of a DAAS RFID system using perfectly steerable antennas. i.e, an antenna which can be steered to any direction in 3D space. In this way, the upper limit on the power delivery advantage which can be gained by using antenna arrays can be investigated. Each antenna in a cell is steered towards a particular location of tags, with phase dithering applied to maximise the power at that location. A raster scan procedure is then used to scan the entire interrogation zone and obtain what is logically the optimal power distribution. i.e., the maximum possible power over time to each tag for the particular antenna arrangement considered.

Practical antennas, especially flat ones, are however limited in their scan ability. As a result, the limitations of limiting the array's maximum scan angle are studied. Conditions are derived under which an array limited to a given maximum scan angle will approximate

a perfectly steerable array.

The second part of the chapter explores a cell-less or non-cellular wide area RFID system. The proposed system seeks to eliminate the fixed allocation of antennas to particular cells as in fixed DAS systems or of phased arrays to multiple surrounding cells in the DAAS system. Instead, the global antenna population is used to interrogate any area of interest, since the antennas are perfectly steerable and can be steered to any direction. Therefore, the RFID system is changed from a cell-based to a location-of-interest-based interrogation system, thereby eliminating the need for the cellular partitioning of the interrogation area. This is expected to boost tag received power, as many more antennas are involved in powering up any given tag. In addition, reader collision problems which result from cell partitioning are implicitly eliminated, since cells have been discarded.

The last part of the chapter studies the resilience of the cellular and non-cellular systems to antenna failure. The non-cellular system is shown to be more resilient due to the many more antennas used for any interrogation. This will also be useful in assigning receive antennas.

6.1 Perfectly Steerable DAAS

This section investigates the use of perfectly steerable antennas to investigate the maximum advantage that can be obtained from the use of a DAAS system. Because the antennas can be steered to an arbitrary direction, each location in the room can receive the maximum possible power available by directing all the antennas in the cell to that location. As a result, the optimum power distribution is obtained. Use is made of a raster scan method to obtain a scan of the entire interrogation zone, as demonstrated in Fig 6.1.

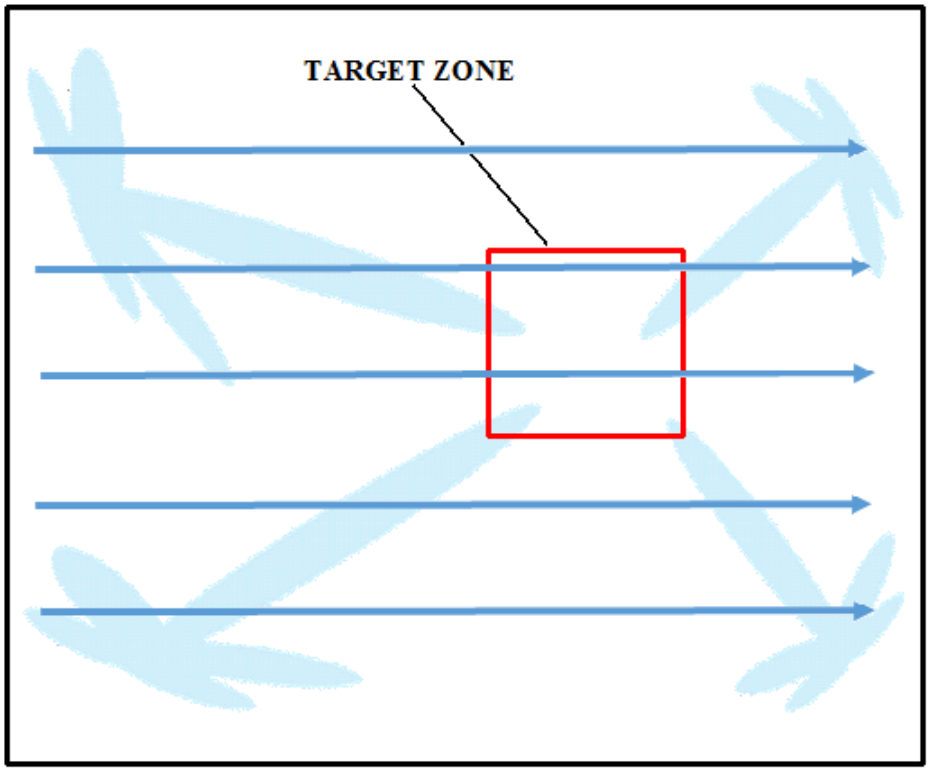

Figure 6.1: Raster scan system with perfectly steerable antennas. All antennas are steered to a particular location, and phase dithering is applied to maximise power there. The raster scanning procedure is followed to cover the entire cell.

A perfectly steerable antenna can be steered up to 360^0 in azimuth and $\pm 90^0$ in elevation. This is modelled by applying a geometrical rotation to a standard directional antenna radiation pattern in order to point its maximum gain to the desired location. All antennas in the cell are directed to the same location, and phase dithering is applied. A raster scan is then followed to cover the entire interrogation zone as shown in Fig 6.1.

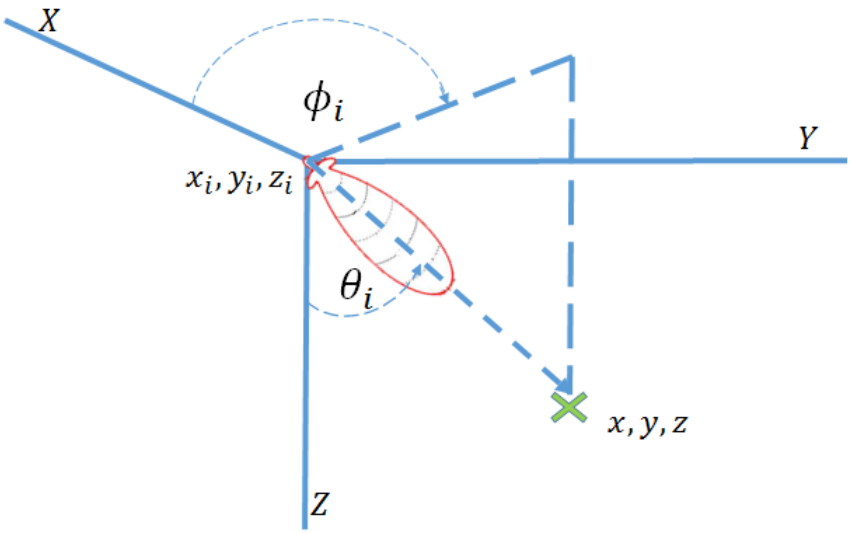

Figure 6.2: Geometrical rotation of a standard antenna as a model for a perfectly steerable antenna. Rotating the d antenna by upto $\theta_{max} = \pm 90^0$ in elevation and $\phi_{max} = 360^0$ in azimuth is used to represent perfect 2D beam steering.

Consider the problem of trying to interrogate a particular tag located at the position (x, y, z), by N antennas, with the ith antenna located at (x_i, y_i, z_i), as shown in Fig 6.2. Assuming all antennas are initially pointing vertically downwards, this could be done by rotating the ith antenna by angles (ϕ_i, θ_i) in azimuth and elevation respectively given by:

$$\tan \phi_i = \frac{y_i - y}{x_i - x} \tag{6.1}$$

$$\tan \theta_i = \frac{r_i^{xy}}{z_i - z} \tag{6.2}$$

where $r_i^{xy} = \sqrt{x_i^2 + y_i^2}$ is the horizontal distance distance (i.e. $L2$ norm) from the ith antenna to the tag location.

The procedure is repeated using all cell antennas, and the fields coherently summed at the target location with phase dithering applied. Since the target location receives the coherent sum of each antenna's maximum EIRP and with phase dithering applied, this will be the maximum achievable power at the target location with the given antenna arrangement. Fig 6.3 shows examples of four antennas, located at the vertices of the shown cell area, pointing to different locations in a $12m \times 12m$ cell.
The example uses a simulated high gain (15 dB) antenna to show that a target location can be addressed by all four antennas, while delivering little power to other locations.

Evidently, higher gain antennas will provide more pin-point power delivery, whereas the contrast in power distribution will be lower if low gain antennas are used.

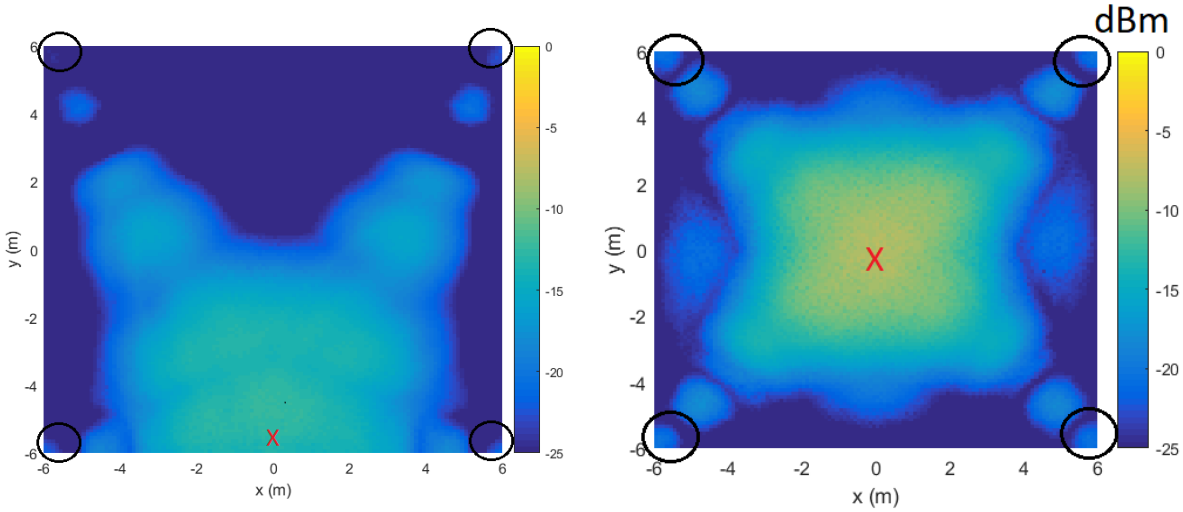

(a) Antennas pointing to (0,-6,1)m

(b) Antennas pointing to (0,0,1)m

(c) Antennas pointing to (-6,0,1)m

(d) Antennas pointing to (3,3,1)m

Figure 6.3: System of four antennas at vertices of a $12m \times 12m$ cell pointing to different target locations (X). Antennas are on the $Z = 3m$ plane and indicated by circles. Only Y-polarised tags are used on the $Z = 1m$ plane.

It follows therefore that repeating this procedure in a raster pattern will produce the best possible power distribution for a DAAS system.

6.1.1 Raster scan study on different cell areas

Repeating the above procedure in a raster scan fashion will produce the optimal power distribution for the given antenna setup. In this section, a raster scan method is applied to cells of different sizes, and compared to a fixed DAS system. The power distribution for the fixed antenna system is recalled from Chapter 5 in Fig 6.4 using the obtained ideal tilt angle of 70^0.

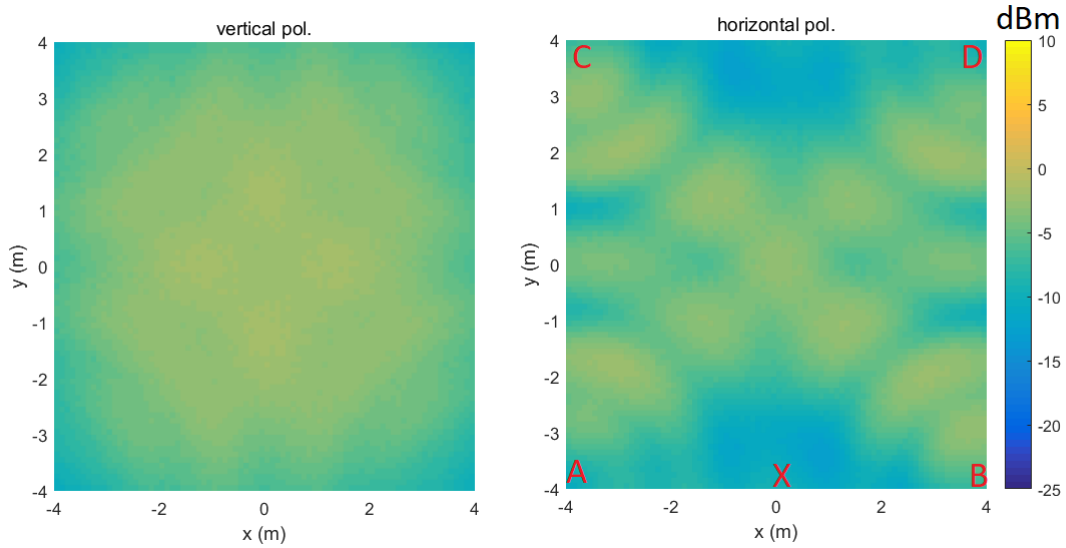

Figure 6.4: Simulation of power distribution produced by a fixed antenna system, with all four antennas pointing to the centre of a $8m \times 8m$ room

Cells of different sizes are simulated: $8m \times 8m$, $12m \times 12m$, $16m \times 16m$ and $20m \times 20m$. The power distributions are shown in Fig 6.5. Due to the symmetries about the $x = 0$ and $y = 0$ axes in Fig 6.4 for example, scanning only a quarter of the area would give the same cdf plots, and reduce computation time. Only one quadrant is scanned and plotted i.e., $x = -L/2$ to $x = 0$ and $y = -L/2$ to $y = 0$, where the cell dimensions are $L \times L$. The simulations are performed with the antenna designed in Chapter 4 (gain=10 dBiC). The results are shown in Figs 6.5 and 6.6

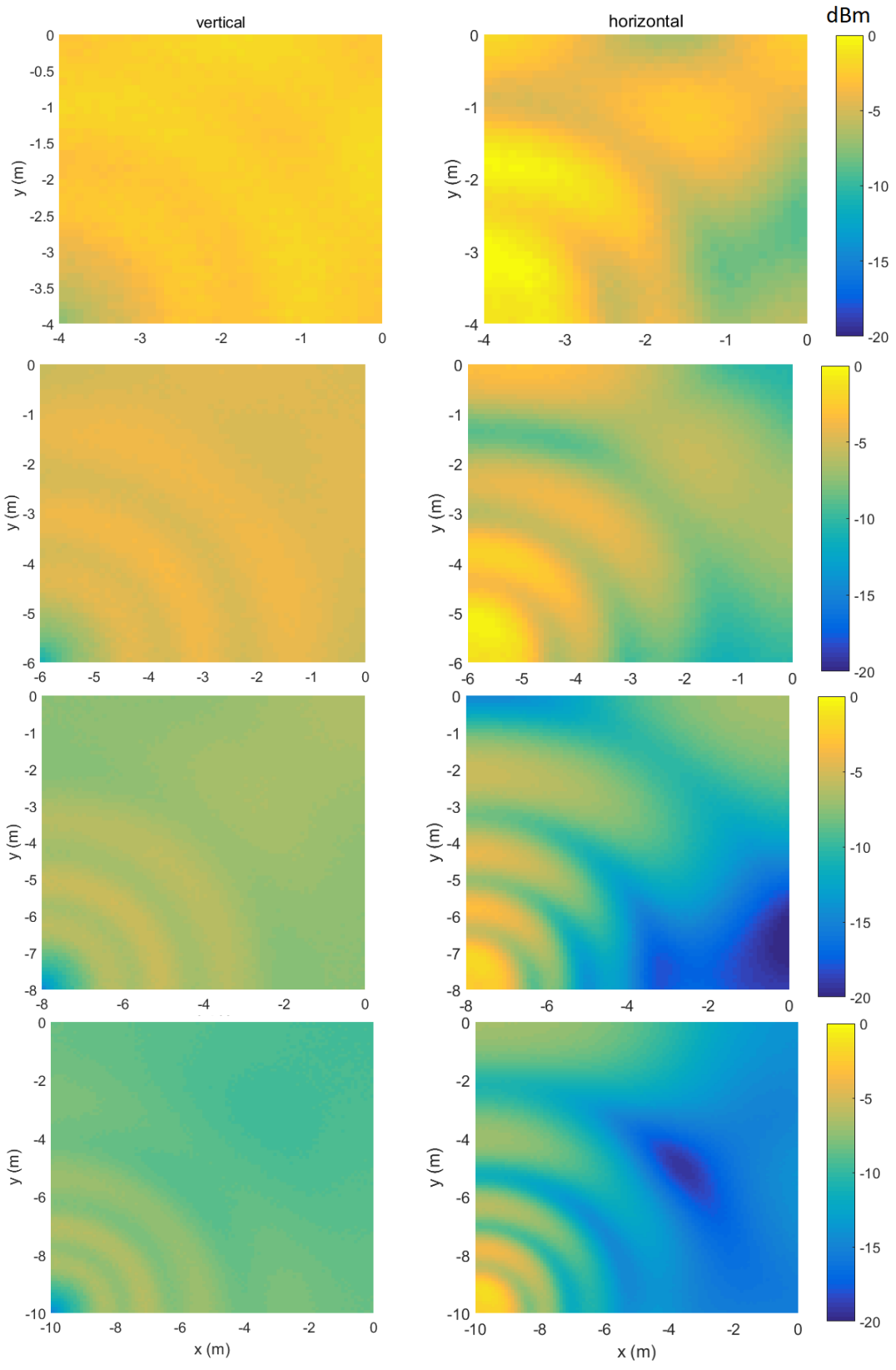

Figure 6.5: Power distributions for system of four perfectly steerable antennas using raster scanning in cells of different cell sizes: $8m \times 8m, 12m \times 12m, 14m \times 14m, 16m \times 16m$ and $20m \times 20m$.

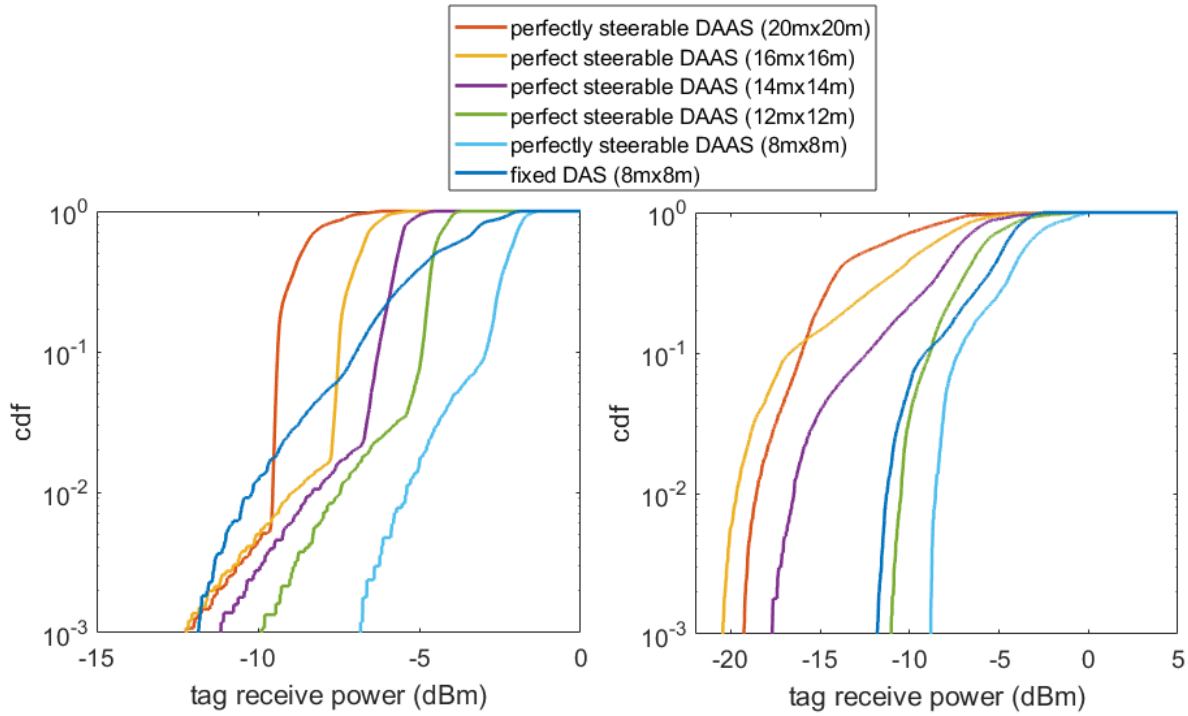

Figure 6.6: cdf for perfectly steerable DAAS system for different cell sizes $8m \times 8m$, $12m \times 12m$, $14m \times 14m$, $16m \times 16m$ and $20m \times 20m$. Comparison is made with a standard fixed DAS in a $8m \times 8m$ cell.

For a similarly sized $8m \times 8m$ area, improvements over the fixed DAS system for the least-powered tags (1st percentile) are about $\sim 4.5dB$ for vertically polarised and $\sim 2dB$ for horizontally polarised tags, as in Fig 6.6. Increasing the cell separation of the antennas to $12m \times 12m$, reveals that the raster scan system still outperforms the fixed system for both polarisations. At $20m \times 20m$ separation, the horizontally oriented tags undergo a huge reduction in received power ($\sim -19dB$ for 1st percentile), while vertically oriented tags achieve a similar performance to the fixed system. The explanation for this is the severe multipath for horizontal polarisation, as well as the effective field seen by the horizontal tags close to the edge of of the cell, as explained in chapter 3. Multipath also explains the anomaly between the $16 \times 16m$ area and $20m \times 20m$ area for horizontally polarised tags. This is because the $16m \times 16m$ cell experiences severe fading at the locations of minimum tag received power. It is therefore possible to obtain at least 50 % increase in cell size for horizontally polarised antennas and up to 250% for vertically polarised tags. Where large areas are covered in a repeating pattern, a single steerable array replaces four fixed antennas at each cell vertex as describd in Chapter 5. This can

be translated to a respective reduction of $4 \times 1.5^2 \approx 10\times$ and $4 \times 2.5^2 \approx 25\times$ reduction in the required number of antennas in the limit of an infinitely large area.

6.1.2 Removing Multipath

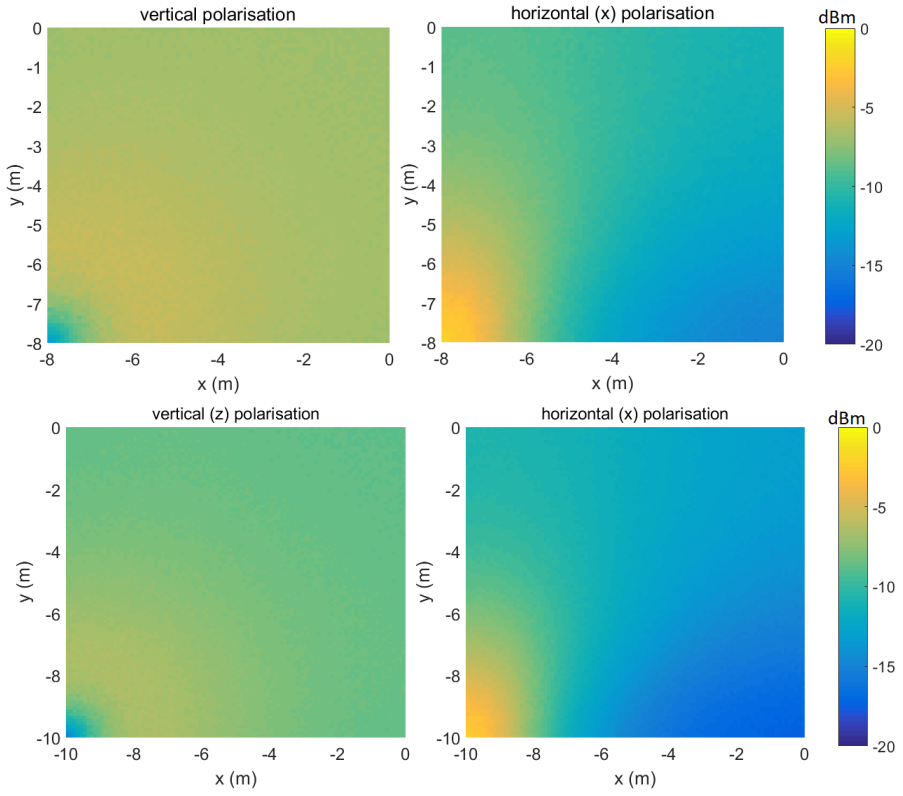

Figure 6.7: Power distributions of distributed system of four 10dB-perfectly steerable antenna for a cell of antenna separations 16m and 20m. Only a single quadrant is shown.

This section studies the effect of removing multipath from the system, as well as investigating the effect of a high gain antenna for eliminating the multipath effects. Adverse effects from multipath may suggest that high gain antennas are required to maximise power delivery. The ground reflection components have been removed, and only the direct path to tags has been considered in Figs 6.7. A high gain antenna (20 dB) is also simulated in Fig 6.8.

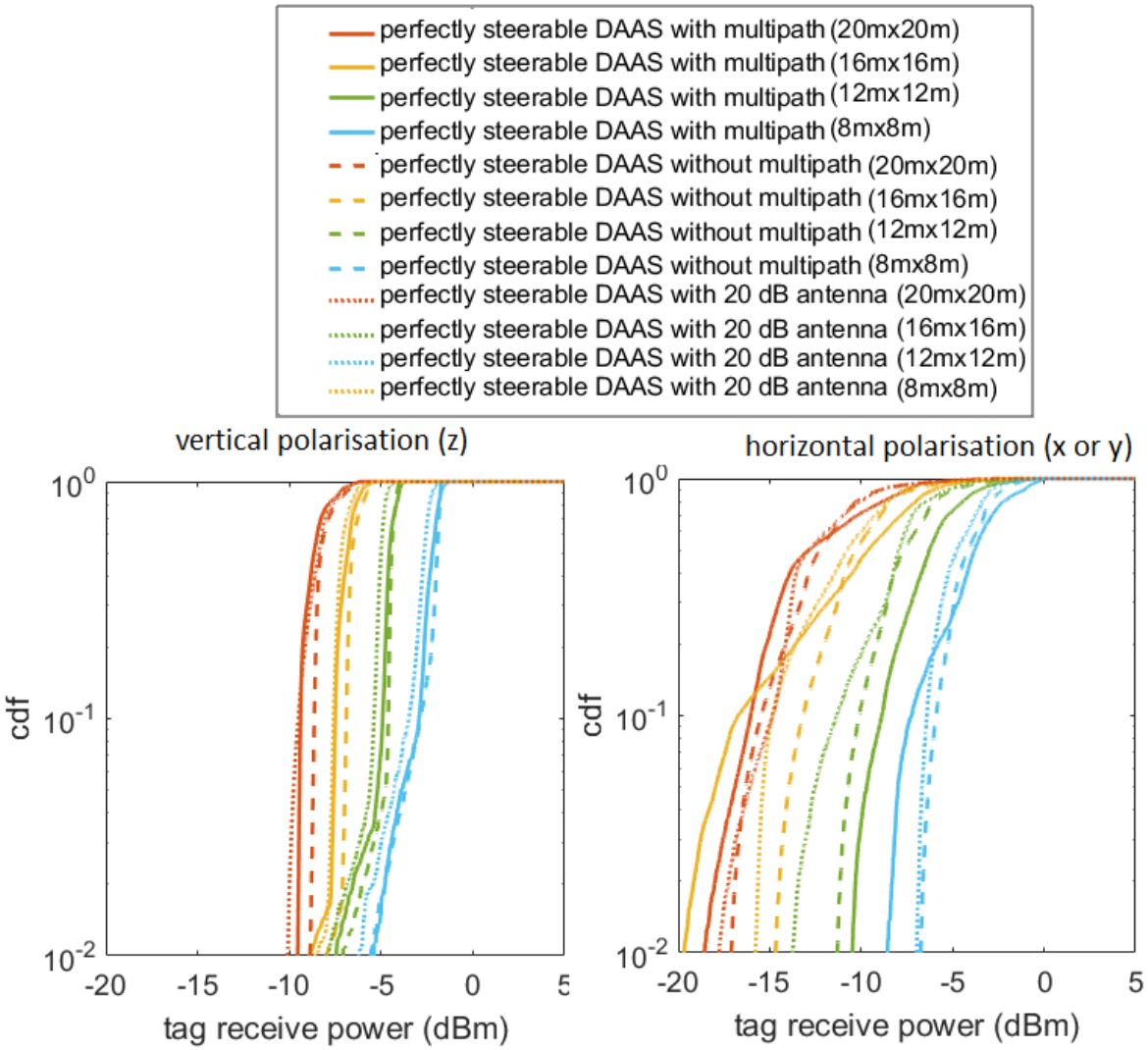

Figure 6.8: cdf for different room sizes with multipath, without multipath, and with a 20 dB antenna

It is seen that removing reflections affects the horizontal polarisation alot more, since this polarisation experiences much more fading, compared to the vertically polarised (z) tags. The deep fade in the $16m \times 16m$ cell is seen to be removed, and the power of its least-powered 1% of tags is increased by $\sim 5dB$ compared to the case with multipath. On the other hand, some other cell sizes are negatively impacted, since multipath resulted in constructive interference at their locations of minimum tag received power. e.g the $12m \times 12m$ cell by $\sim 1dB$. The effect of using a 20 dB antenna is also plotted, and is seen to provide a close approximation to the no-multipath case. It can be concluded that a higher antenna gain reduces the influence of floor reflections, but the size and cost

constraints to high gain antennas at UHF frequencies will render them challenging to apply in real systems.

6.1.3 Limited Elevation scan angle

The simulations presented so far have assumed a perfect scan ability from the antennas. This could in practice be achieved mechanically. However, it is difficult with a planar antenna to obtain a circularly polarised antenna capable of 90 degree elevation angle scans. It is therefore important to investigate the effect of limited scan angles on the performance of these systems. In this section, the elevation angle, θ, is limited to some threshold value and the same simulations are performed. This will enable the study of the limits imposed on the system by the limitations of the antenna. Fig. 6.9 shows the case of an antenna in a $12m \times 12m$ room with an antenna limited in scan ability to different angles in the elevation plane: 45°, 60°, 75° and 90°.

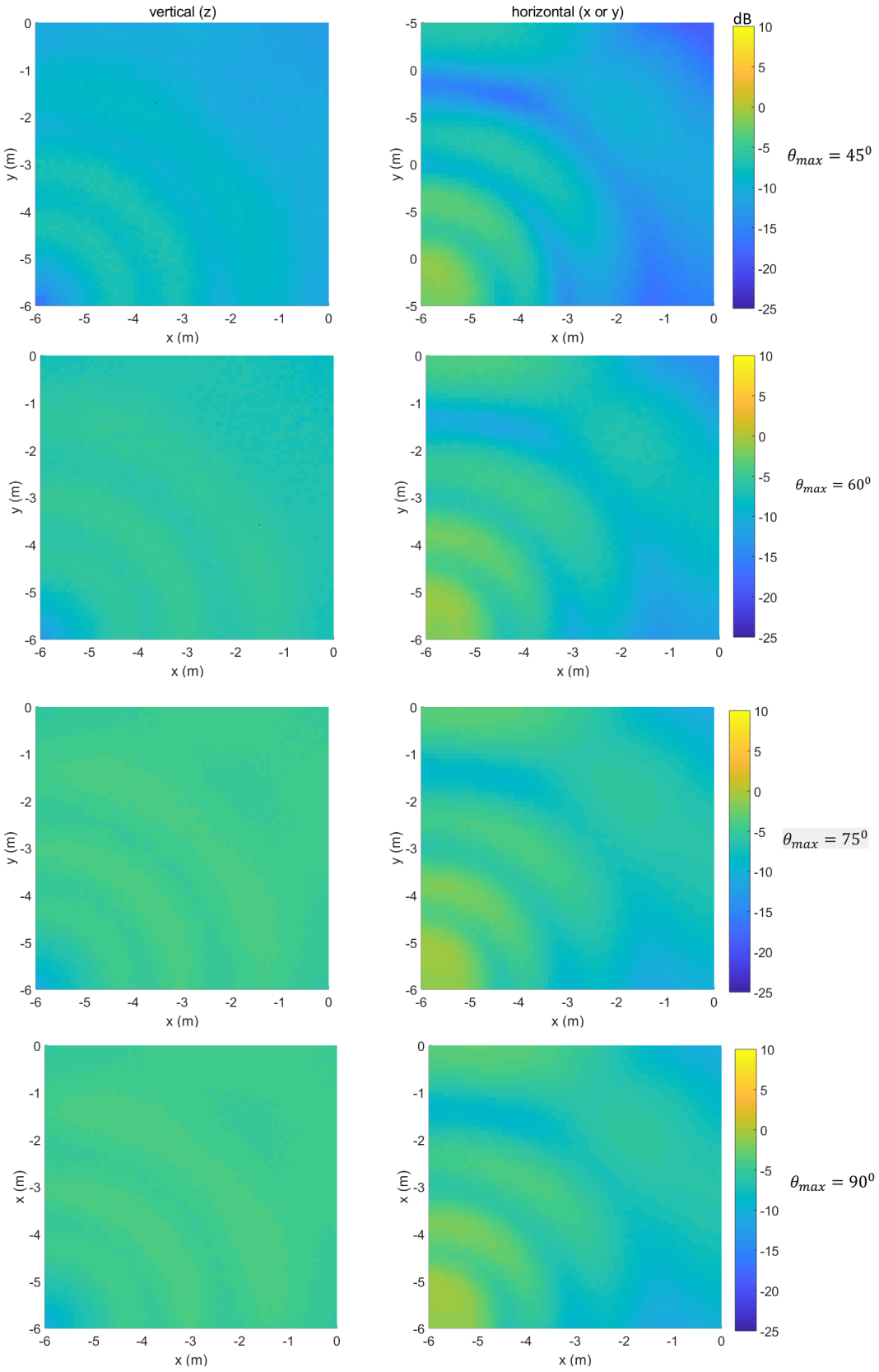

Figure 6.9: Power distribution for $12m \times 12m$ room for antenna limited to maximum elevation steering angles $45^0, 60^0, 75^0$ and 90^0. The power distribution is seen to improve with increased maximum scan angle as expected.

It is seen that as the maximum attainable scan angle in the vertical plane is increased, the power distribution becomes better. There is however little change when increasing from $\theta_{max} = 75^0$ to $\theta_{max} = 90^0$, and therefore a 75^0 capable antenna could replace a perfectly steerable one. This arises because the maximum required angle depends on the ratio of horizontal distance to height of the antenna above the tags according to Eqn 6.2.

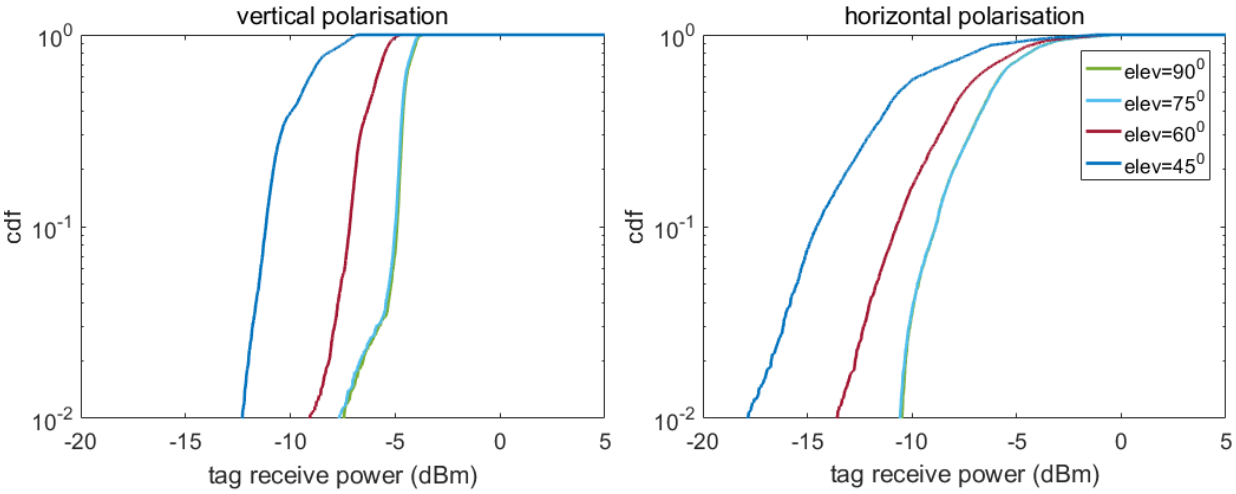

Figure 6.10: cdf plot for antennas with different maximum elevation angles in a 12m × 12m room

In the general case of a rectangular antenna arrangement of separation L, and vertical distance to tag plane of h, according to Eqn. 6.2, the antenna is required to be capable of attaining a vertical steering angle of θ_{max}, where

$$\tan\theta_{max} = \frac{L\sqrt{2}}{h} \tag{6.3}$$

in order to replace a perfectly steering antenna. This maximum is attained when the antenna is directed to the diagonal end of the cell. In the above simulated case of antenna height above the tag plane of 3m and antenna-antenna separation of 12m, the maximum steering angle requirement is $\theta_{max} = 84°$.

The requirement for maximum steering angle becomes less strict as the L/h ratio decreases. Relaxing this condition will enable antennas without extreme wide steering capability to be used. A reasonable first step will be to require the antenna to point to the position of least received power, with the condition that no other point in the interrogation area receives less power than this. The position in a rectangular cell with the least received power was shown in Chapter 3 to be midway along the edges of the cell (point

X in Fig 6.4, page 129). This will require two antennas (A and B) to have a maximum steering angle given by $\tan\theta_{max} = \frac{L}{h}$, while antennas C and D will require $\tan\theta_{max} = \frac{L\sqrt{3}}{2h}$. A compromise condition can be considered by limiting the maximum required steering angle to when the antenna is pointing to the centre of the cell, such that all antennas require a maximum steering angle of:

$$\tan\theta_{max} = \frac{L\sqrt{2}}{2h} \tag{6.4}$$

and then imposing some conditions on the antenna. A reasonable condition will be to require that $\geq 50\%$ of the antenna's gain is available at the diagonal end of the room (see Fig. 6.11). In this case, a lower bound on the antenna beamwidth is imposed, derived from Fig 6.11:

$$\tan\left(\frac{\phi_{min}^{BW}}{2}\right) = \tan\left(\theta_2 - \theta_{max}\right) \tag{6.5}$$

$$= \frac{\tan\theta_2 - \tan\theta_{max}}{1 + \tan\theta_{max}\tan\theta_2} \tag{6.6}$$

$$= \frac{L\sqrt{2}/h - L\sqrt{2}/2h}{1 + L\sqrt{2}/h \cdot L\sqrt{2}/2h} \tag{6.7}$$

$$= \frac{hL\sqrt{2}}{2(h^2 + L^2)} \tag{6.8}$$

If this condition is satisfied on the antenna beamwidth, then the performance obtained using the relaxed maximum steering angle in Eqn 6.4 approximates that of a perfectly steerable antenna. E.g , for $L = 12m$, and $h = 2m$, we get $\phi_{min}^{BW} = 2\tan^{-1}\frac{2\times12\sqrt{2}}{2(2^2+12^2)} = 13^0$ which is easily satisfied in the 10dB antenna being used ($BW \approx 50^0$). Also, $\theta_{max} = \tan^{-1}\left(\frac{12\sqrt{2}}{2\times2}\right) = 76^0$.

For the same antenna separation and $h = 5m$, we get $\phi_{min}^{BW} = 28^0$ and $\theta_{max} = 59^0$. These are confirmed in Figs 6.10 and 6.12.

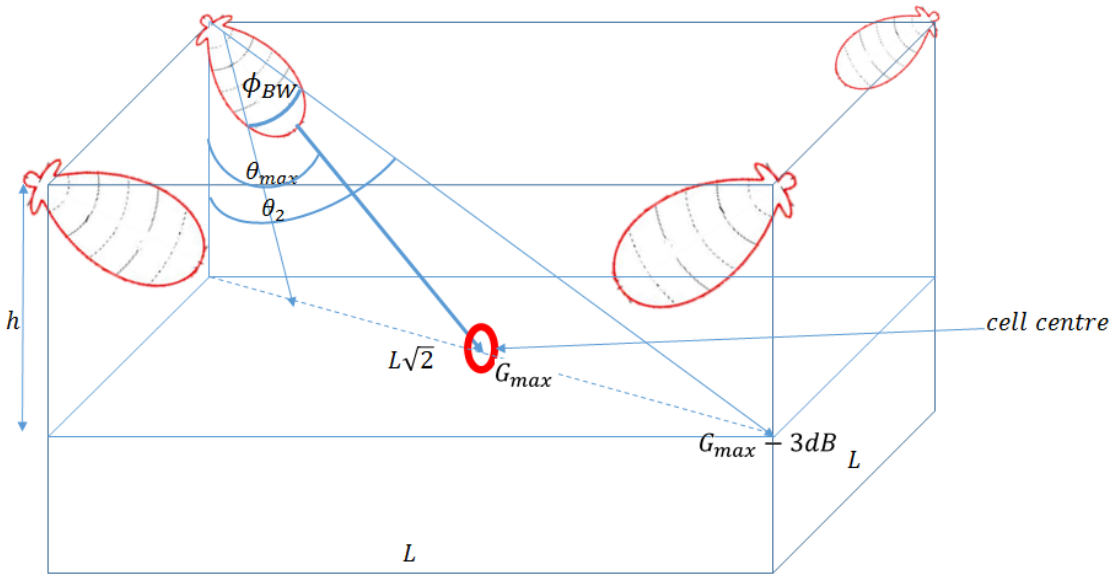

Figure 6.11: cdf plot for antennas with different maximum elevation angles in a 12mx12m room

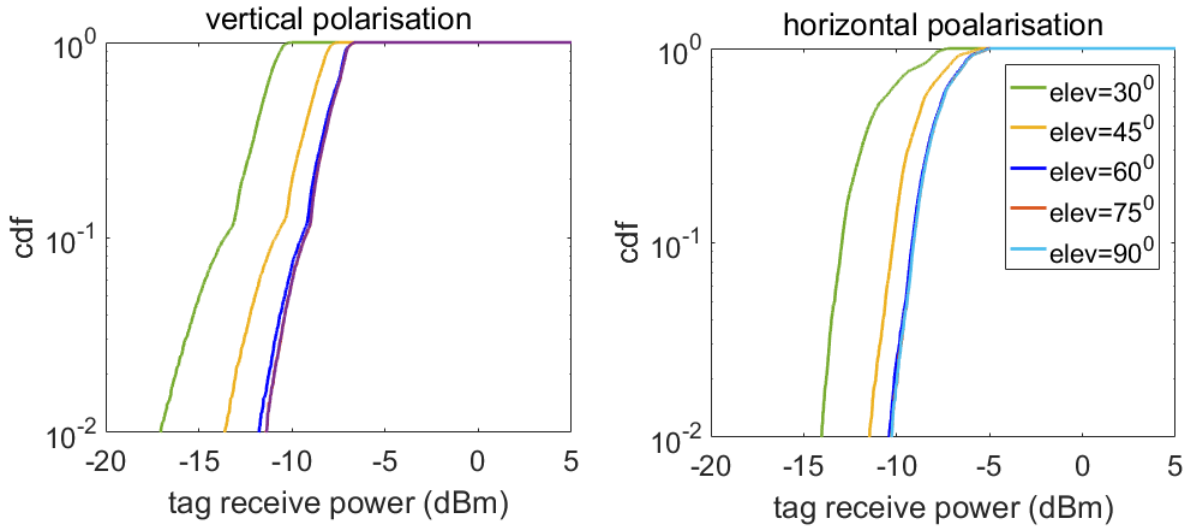

Figure 6.12: cdf plot for antennas with different maximum elevation angles in a 12mx12m room and antenna-tag plane separation of 5m, showing that an antenna capable of 60 degrees can perform similarly to a perfectly steerable antenna.

6.2 Non-cellular Perfectly Steerable DAAS

All work so far reported in this dissertation has made use of the cellular division of wide area RFID interrogation zones, in which groups of antennas are assigned to particular readers or cells each covering a small area, so as to provide coverage to the whole region [135, 136, 137]. With this cellular division comes the problems of inter-cell interference, which is resolved by several multiple access and power control schemes, as described in Chapter 2. The standard DAS system uses a fixed cell allocation policy of four antennas per cell, repeated across the entire interrogation zone.

The DAAS system introduced in chapter 5 uses a dynamic antenna allocation policy, in which an antenna array is assigned to any one of four surrounding cells by controlling its beam pattern appropriately in order to direct it towards the desired cell. This eliminates the need for multiple antennas to address adjacent cells as in the fixed DAS system, thereby significantly reducing the required number of antennas. The same applies to the perfectly steerable DAAS system introduced in section 6.1 above. However, all but the few cell-allocated antennas are still idle with respect to any given cell during an interrogation session as shown in Fig 6.13a.

In this section, the wide area RFID coverage problem is approached from the perspective of a non-cellular or cell-less interrogation zone using perfectly steerable distributed antenna arrays. A system of distributed antenna array nodes is proposed to provide coverage as in Fig 6.13b. These array nodes are connected to a central server with global knowledge of the interrogation zone, and are therefore able to perform tag location-based interrogations. i.e. the antenna radiation patterns are controlled such that the cooperative scan of the interrogation area could maximise tag detection in a given section of the room. This is possible because all antennas are perfectly steerable, and can be directed to any direction. The resulting system is shown to provide significant improvements in tag received power, since the number of antennas interrogating a particular cell increases from the usual cell-allocated number to the total number of available antennas. The increase in available number of antennas is shown to exactly compensate for the large distances involved.

The requirement for the example demonstrated in Fig 6.13 is to detect the objects located in the shown target zone. For this problem, the DAAS and perfectly steerable DAAS systems treat the region as a cell and activate the appropriate antennas and beam patterns

as shown in Fig 6.13a. All other antennas and readers remain idle. A non-cellular system, on the other hand, is proposed to steer all available antennas towards the location of interest, and perform the raster scan scheme described in section 6.1 above. This leads to potentially much higher power delivered to the tags, and fewer required antennas overall, as the resulting antenna spacings could be increased.

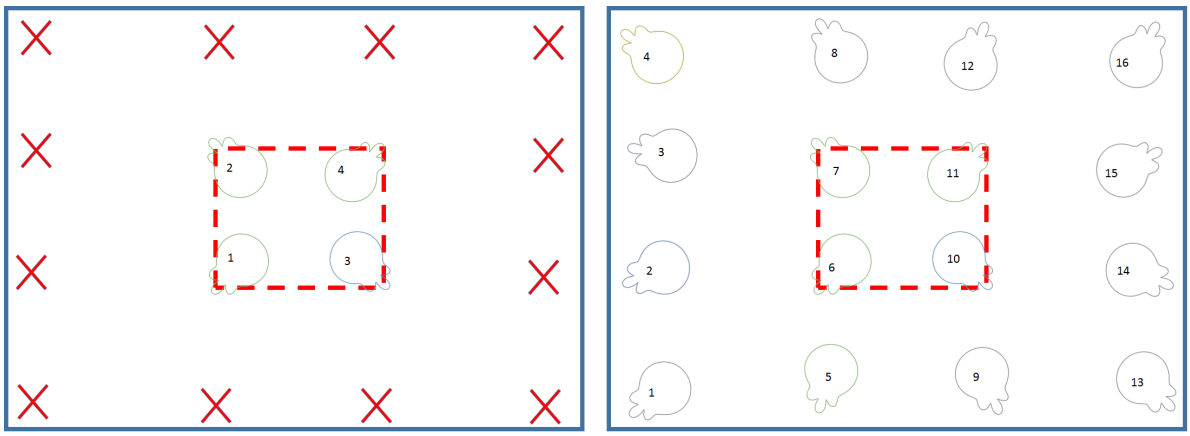

Figure 6.13: Cellular raster scan system (left, a) and non-cellular system (right, b). The red crosses (X) in the cellular system indicate idle antennas, which are absent in the non-cellular system, thereby better performance is expected.

The case illustrated in Fig 6.13 is simulated with varying antenna separations, and the system is compared with the fixed antenna system already presented above. Only the central cell is considered as the intention is to simulate the power that can be provided to a cell surrounded all-round. This allows contributions from 12 extra antennas for each cell when compared to the cellular perfectly steerable system, albeit at much further distances.

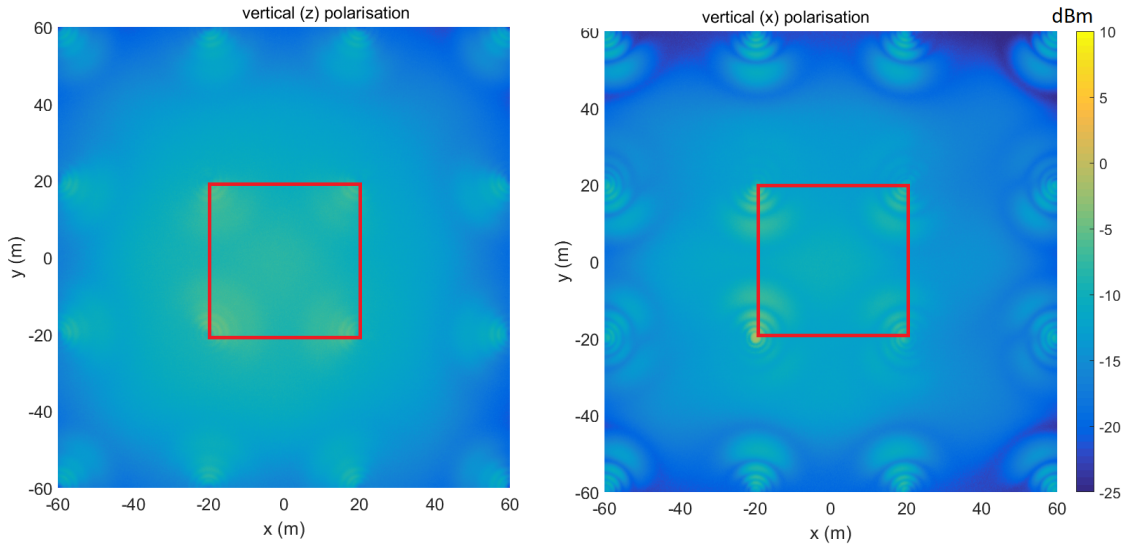

Figure 6.14: Power distribution produced by a multi-cell system of perfectly steerable antennas. Only the central cell has been scanned. Furthermore, only the bottom left quadrant of this cell has been scanned to exploit the symmetry of the system. Antenna separation is 20m

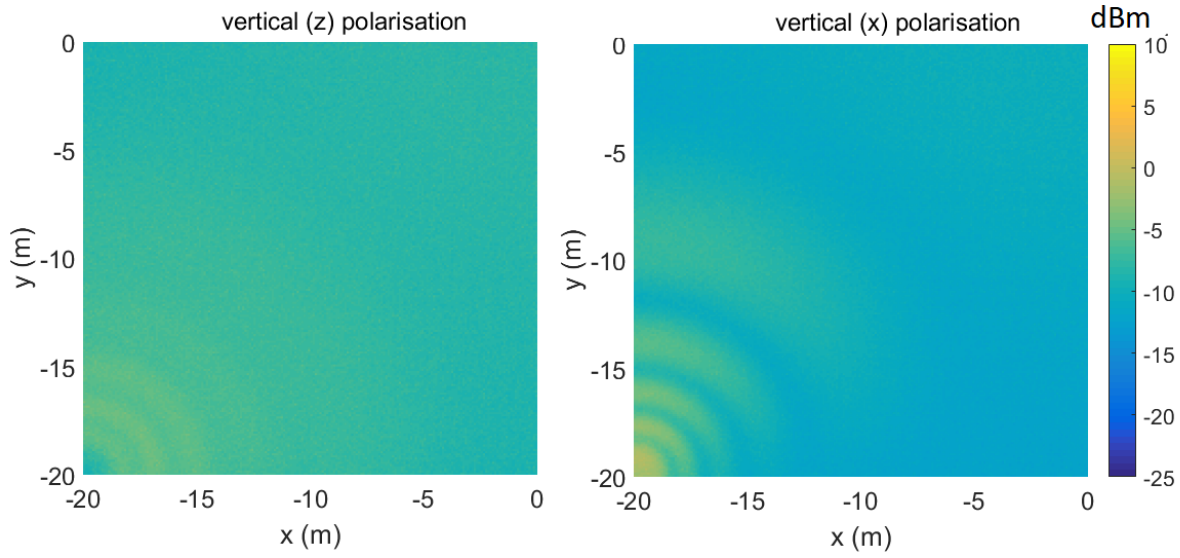

Figure 6.15: Power distribution produced by a multi-cell system of perfectly steerable antennas showing scanned quadrant of central cell.

The power distribution for an antenna separation of 40m is shown in Fig 6.14. It should be noted that only the lower quadrant of the central cell is scanned, as the cdf is the same as the whole due to symmetry. The cdfs for a similar configuration at different antenna separations of 8m, 20m, 30m and 40m are shown in Fig 6.16. It is seen that an-

tenna separation increases over a fixed system of up to $\frac{40}{8} = 5$ times for vertical polarised tags and $\frac{36}{8} = 4.5$ for horizontally polarised tags can be achieved when considering the most critical 0.1% of tags (cdf=10^{-3}). This is done by comparing the cell sizes for the non-cellular system (perfect non-cellular) and the fixed system at cdf=10^{-3}. This is in addition to a 4× reduction in antenna number since each array replaces four fixed antennas when used in a large multi-cell system, as described in chapter 5. Using the same argument as in Chapter 5, this can be translated to an overall reduction in the required number of antennas of at least $4 \times 5^2 = 100\times$ for vertical tags and $4 \times 4.5^2 = 81\times$ for horizontal tags in the limit of an infinitely large interrogation area.

The advantage over a cellular system is also significant. A $40m \times 40m$ non-cellular arrangement performs marginally better ($\sim 2dB$) than a cellular $20m \times 20m$ arrangement for vertically polarised tags, giving an effective cell size increase of at least $\frac{40^2}{20^2} = 4$. The advantage for horizontally polarised tags is even more significant a margin of $\sim 6dB$. This is because the many extra antennas (12 in this case) in the non-cellular system help to resolve multipath effects, which cause performance degradation in the cellular system.

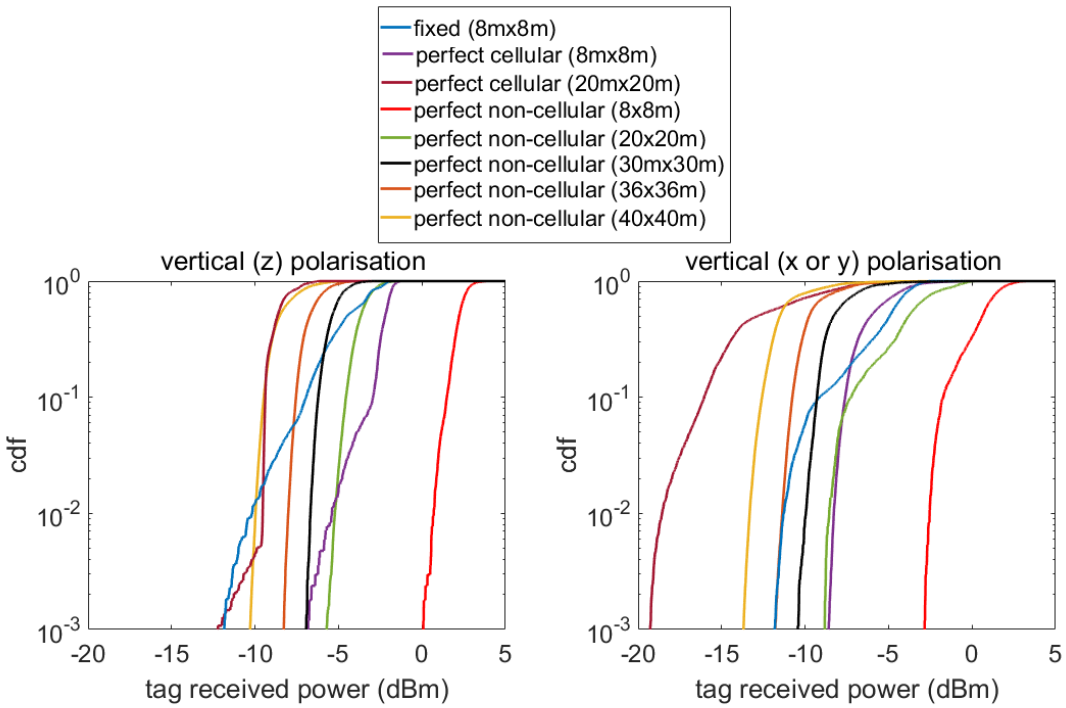

Figure 6.16: cdf for cellular and non-cellular DAAS for various antenna separations. Comparison is made with a fixed DAS system (blue)

6.2.1 An Infinitely Large Non-Cellular DAAS System

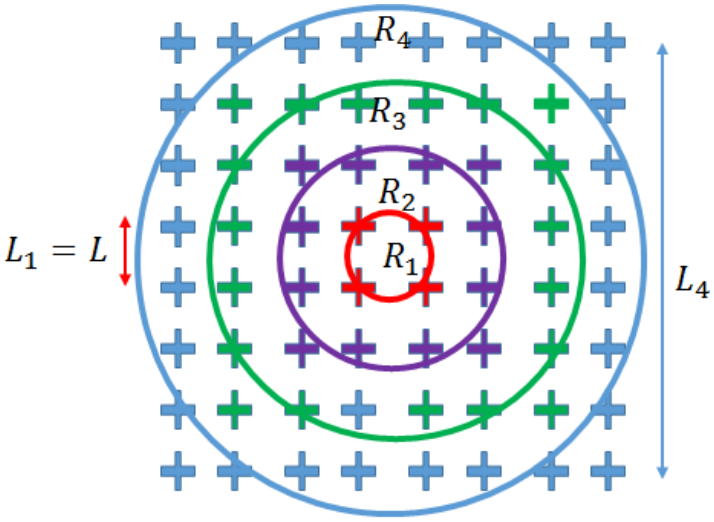

Figure 6.17: Interpreting a regular grid of equally separated antennas as concentric rings of antennas. The rectangular rings are approximated as equi-areal circular rings of an equal number of antennas to estimate the contribution of each ring to the received power in the central cell. Crosses of different colours represent antennas on different concentric rings.

In general, for an infinitely large multicell area with a regular grid of equally separated antennas, the target cell could be considered to be surrounded by rectangular, concentric rings of antennas as shown in Fig 6.17. The innermost ring (red) has $N_1 = 4$ antennas, the second ring (purple) has $N_2 = 12$ antennas, and the ith ring can be verified to have $N_i = 4(2i-1)$ antennas. The ith square ring can also be verified to have a side length of $L_i = (2i-1)L$, where L is the separation between neighbouring antennas. We aim to estimate the contribution of each ring to the interrogation of the central cell. This is done by considering the power received at the central point, and approximating each ring with an equi-areal circular equivalent with an equal number of antennas. The radius of a circle of equal area to a square of length l can be shown to be $r = l/\sqrt{\pi}$. The circular equi-areal equivalent ring for the ith square ring above will have a radius of

$$R_i = L_i/\sqrt{\pi} \tag{6.9}$$

$$= \frac{(2i-1)L}{\sqrt{\pi}} \tag{6.10}$$

Since all antennas now lie on a circle, the distance to the centre point is equal for all

antennas, and given by the annular radius of R_i. Due to the circular symmetry involved in the above arrangements, the effects of multipath can be assumed to be similar for each ring, and therefore is neglected in this analysis for simplicity. If each antenna transmits a voltage of V, then the electric field contribution of the jth antenna of the ith ring to the received power at the central point can then be derived as:

$$E_{i,j} = \frac{V_{i,j}}{R_{i,j}} e^{jkR_{i,j}} \tag{6.11}$$

The contribution by all antennas on the ith ring is:

$$E_i = \sum_{j=1}^{N_i} E_{i,j} = \sum_{j=1}^{N_i} \frac{V_{i,j}}{R_{i,j}} e^{jkR_{i,j}} \tag{6.12}$$

$$= \frac{N_i V}{R_i} e^{jkR_i} \tag{6.13}$$

$$= \frac{4(2i-1)V}{(2i-1)L/\sqrt{\pi}} e^{jkR_i} \tag{6.14}$$

$$= \frac{4V\sqrt{\pi}}{L} e^{jkR_i} \tag{6.15}$$

This gives an electric field magnitude of

$$|E_i| = \frac{4V\sqrt{\pi}}{L} \tag{6.16}$$

which is independent of the ring. This implies that any concentric ring contributes equally to the total received power at the central cell, irrespective of the distance from the cell if separation between neighbouring antennas is constant. The statement is exactly true for circular rings, and approximate for rectangular rings, as per the discussion above. This is because the increase in the number of antennas compensates for free space loss, as we move outwards. This is demonstrated in Figs 6.18 and 6.19

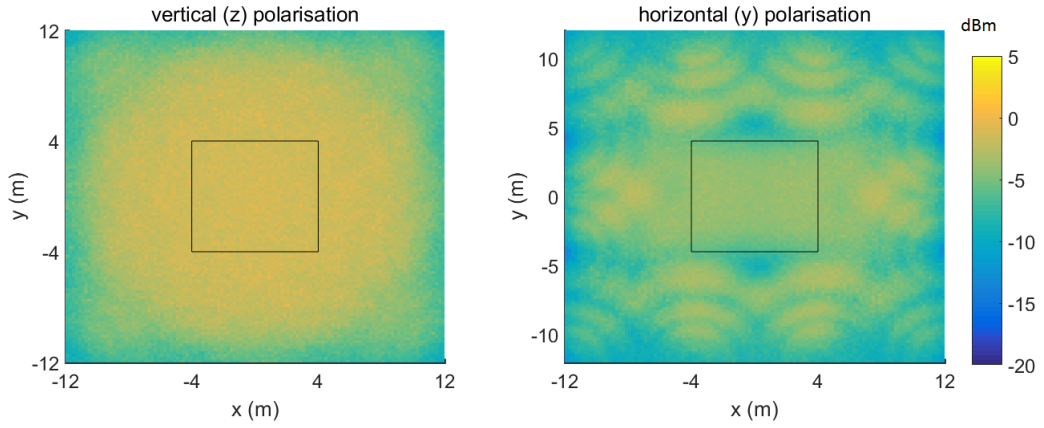

(a) Ring 2 only

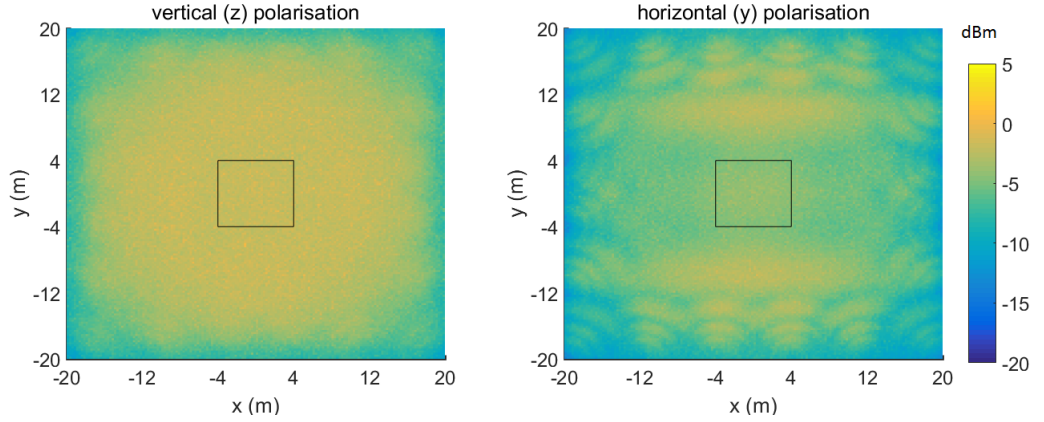

(b) Ring 3 only

Figure 6.18: Power distributions due to antenna on Ring 2 and on Ring 3 in a system of $8m \times 8m$ antenna separation. Only the central area (within border) has been scanned

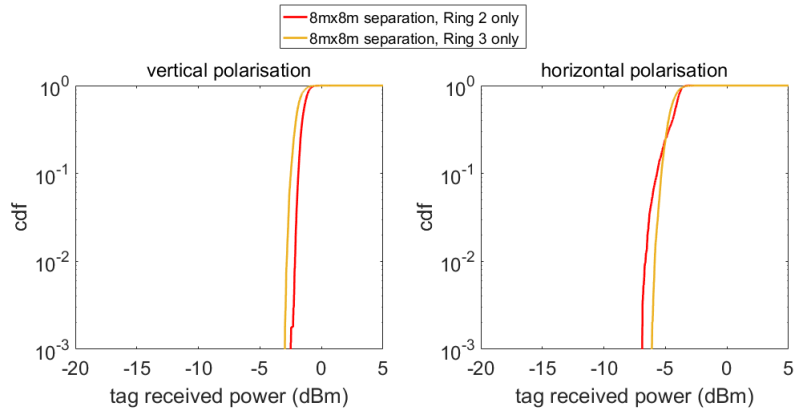

Figure 6.19: cdf for Ring 2 and Ring 3 in a system of $8m \times 8m$ antenna separation, showing close agreement in their delivered power. This verifies the assertion of equal power delivery by each ring.

It is seen that the two rings provide similar power levels to the tags located in the central cell, as predicted. The little difference ($<$ 1dB for all polarisations) can be explained by the fact that the rectangular ring used is an approximation of the derived circular ring system. Also, the considered area is the entire innermost cell, whereas the analysis done above considered a single point at the centre.

The above analysis has considered outer rings (2 or 3) scanning the inner cell in a system of infinite concentric antennas. Practical systems impose physical limits on the interrogation area and available antenna rings. Simulations on a single ring are performed for the whole cell to investigate the contribution of the inner ring (1) to the total cdf.

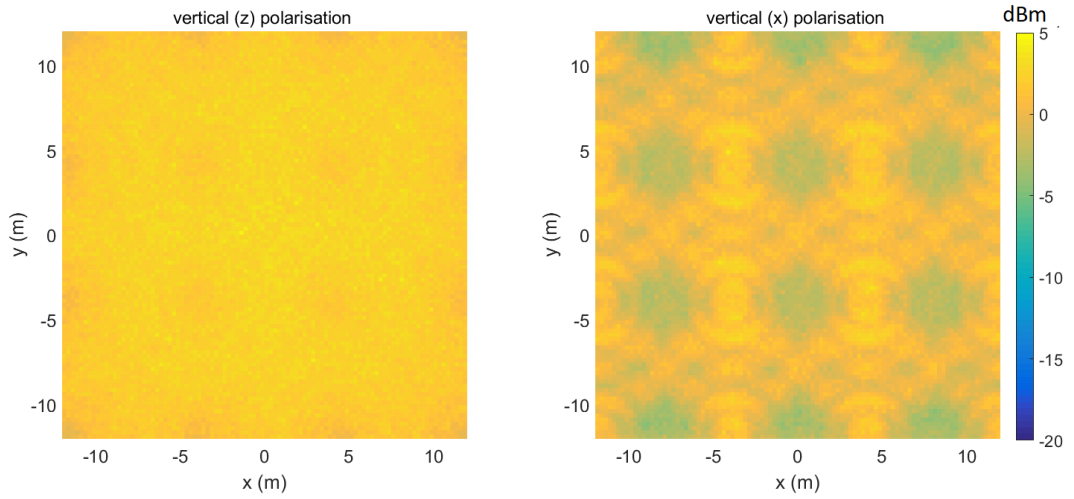

(a) Ring 1 + Ring 2

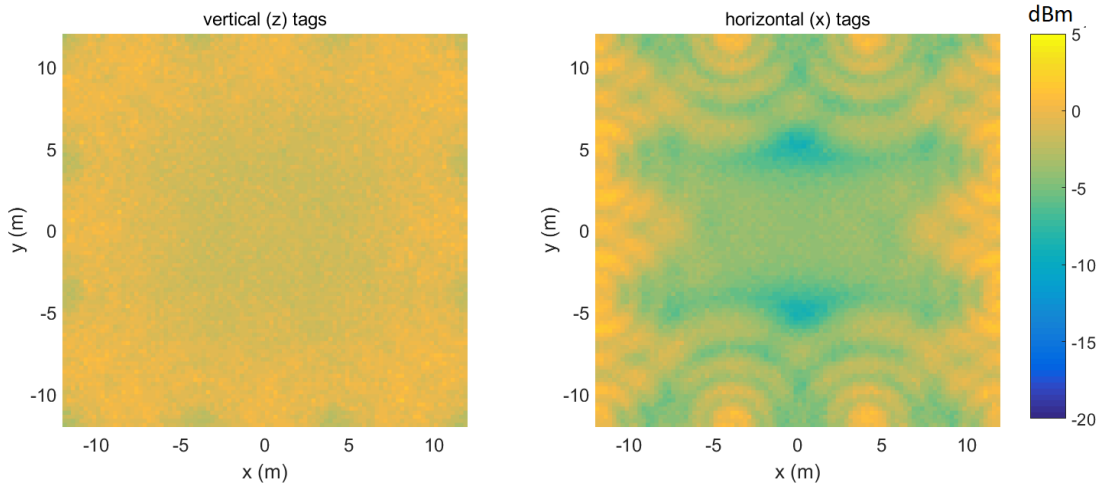

(b)

(c) Ring 2 only

Figure 6.20: Power distribution of rings 1 and 2 vs Ring 2 only for scanning a $24m \times 24m$ area.

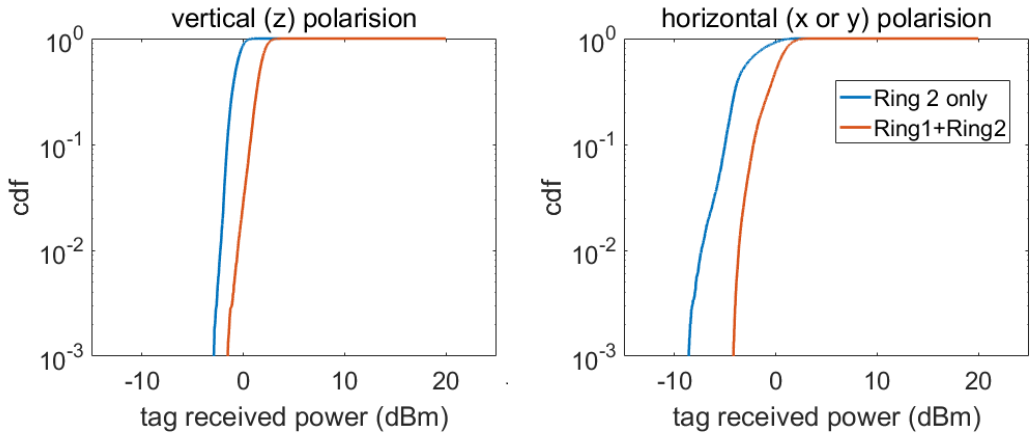

Figure 6.21: cdf of rings 1 and 2 vs Ring 2 only for scanning a $24m \times 24m$ area. It is seen that without the central ring, minimum tag power degrades by 1.5dB and 4.5 dB for vertical and horizontal tags respectively.

It is seen that without the innermost antenna ring, the vertical and horizontal tags receive $\sim$ 1.5 dB and 4.5 dB less than they would otherwise (Fig 6.21). The performance is still far superior to that of a fixed DAS system, and can enable much wider antenna spacings in a practical implementation.

In addition to vastly improved antenna separation and coverage areas, the described system can eliminate the reader collision problems usually encountered in multi-reader RFID deployments. Traditional cellular systems use separate readers for interrogating separate cells, and therefore need to avoid reader collisions, as was discussed in Chapter 2. This normally involves several multiple access schemes. In the presented system, only a single reader is required as the 'cell' to be interrogated can be changed by redirecting the antenna to a different tag location. In multi-reader systems, simultaneous interrogations cause interference and hinder tag detection. In this system, simultaneous antenna transmissions boost tag detection due to phase diversity. As a result, no interference avoidance mechanisms are required in addition to the spatial multiple access which arises due to the directing of the antennas to a particular location at a time.

6.3 System Resilience to antenna Failure

This section studies the resilience of the different systems with respect to antenna failures. The antenna numberings used are labelled in Fig 6.13.

6.3.1 Cellular System

The cellular system uses only four antenna arrays per cell, and therefore is expected to have little resilience to antenna failure. The power distribution for a perfectly steerable DAAS system, with one or two cell antennas failed is shown in Fig 6.22. The corresponding cdf is shown in Fig 6.23. The three tag polarisations are considered here because symmetry does not apply.

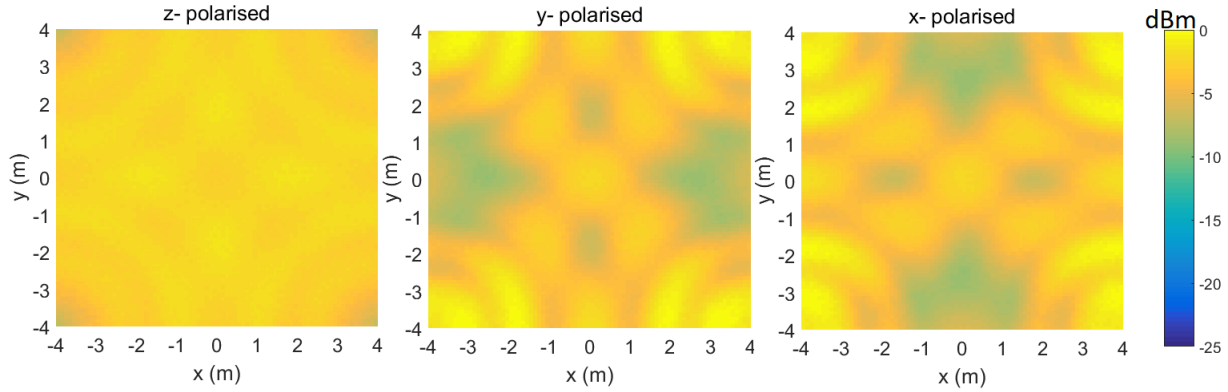

(a) No antenna failed

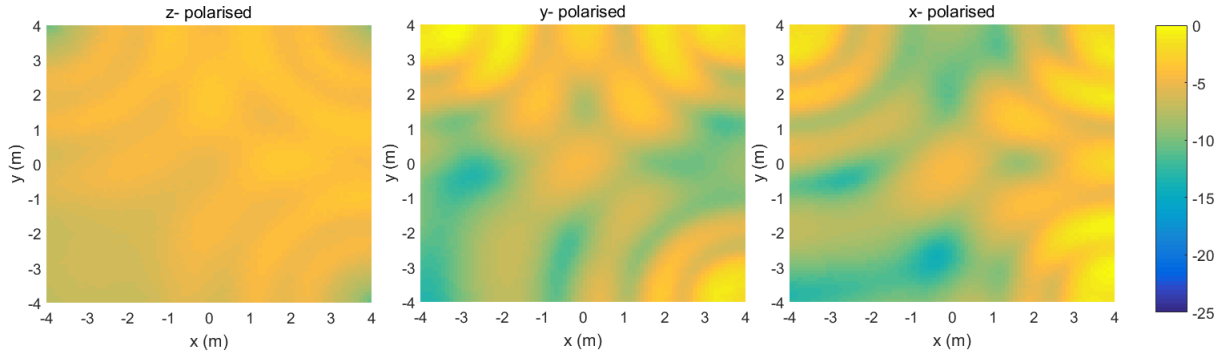

(b) Antenna 1 failed

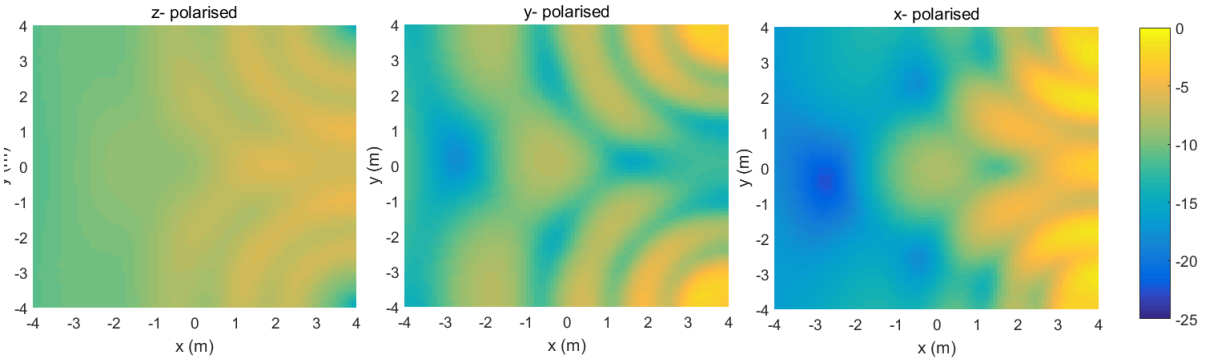

(c) Antennas 1 and 2 failed

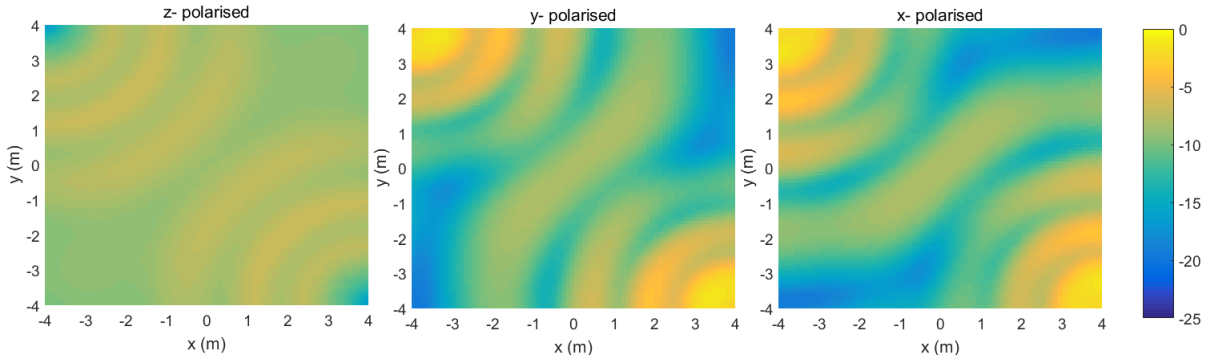

(d) Antennas 1 and 3 failed

Figure 6.22: Effect of antenna failure on perfectly steerable cellular system power distribution in $8m \times 8m$ cell

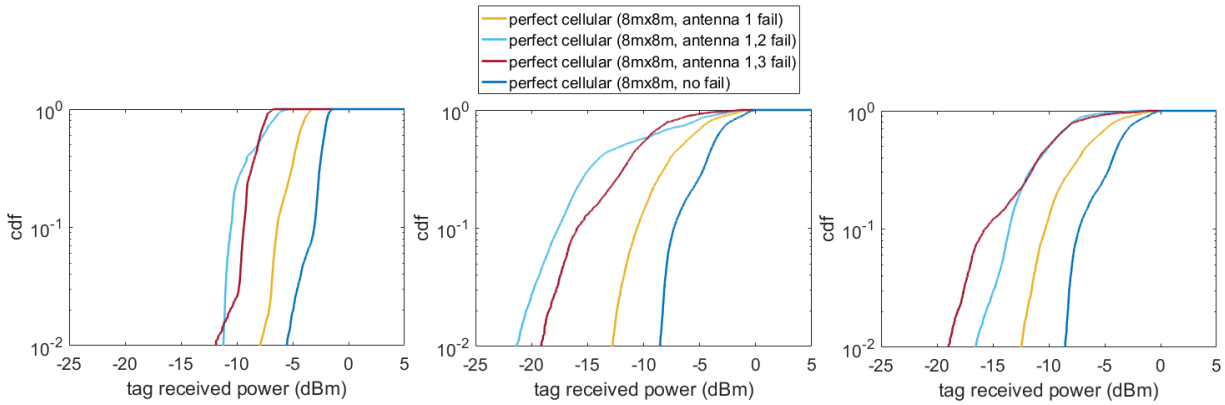

Figure 6.23: cdf for different scenarios of antenna failure in cellular perfectly steerable array system with $8m \times 8m$ antenna separation

It is seen that the tag received power for the most vulnerable tags degrades when a single antenna failure occurs by $\sim 2dB$ for vertical tags, $2dB$ for y -polarised tags and $\sim 2dB$ for x-polarised tags. Two antennas failing can produce a degradation of up to 6 dB for vertical tags and 12 dB for horizontal tags. This represents a drastic drop in the performance.

6.3.2 Non-cellular system

Because multiple many antennas are used to interrogate a cell, it is expected that failure of a single antenna should have little impact on the overall signal, leading to a more resilient network. Cases of several different antennas in the network failing are considered for a $8m \times 8m$ cell, and the results are shown in Fig 6.25.

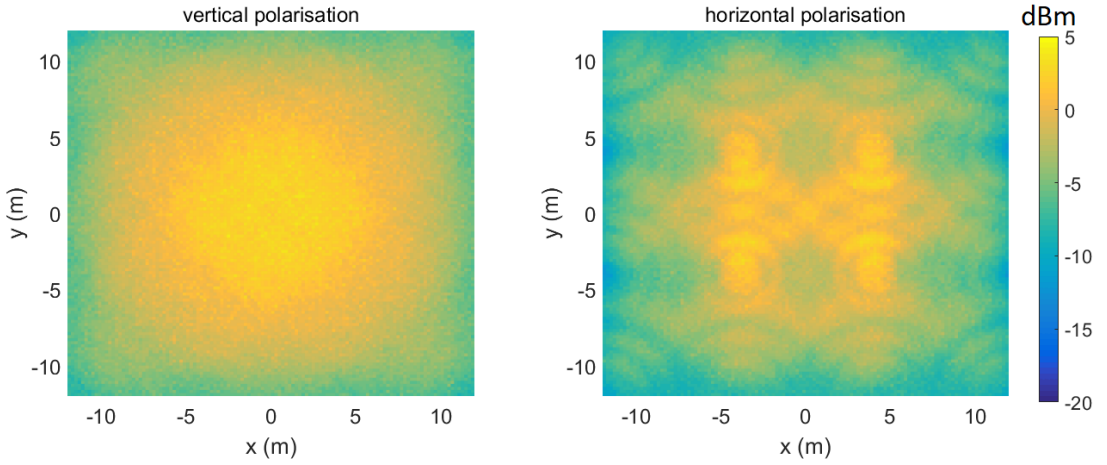

(a) No antenna failed

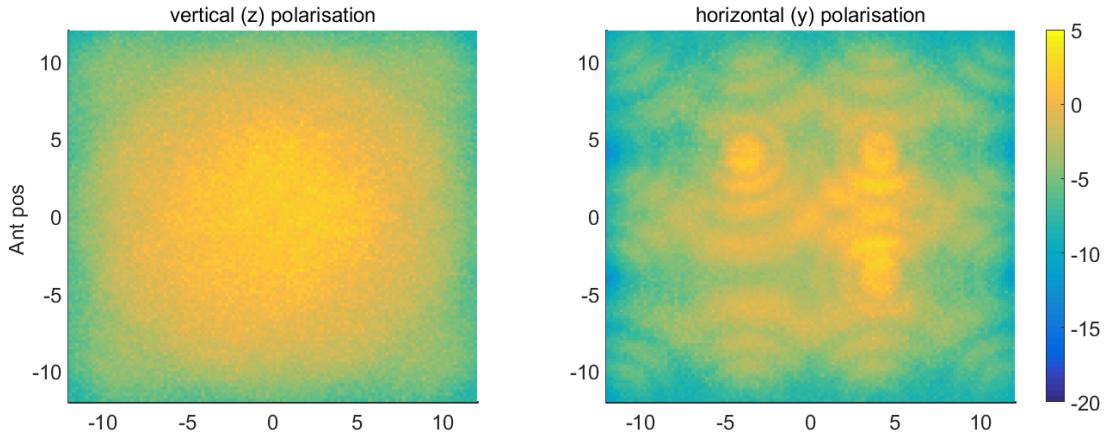

(b) Antenna 6 failed

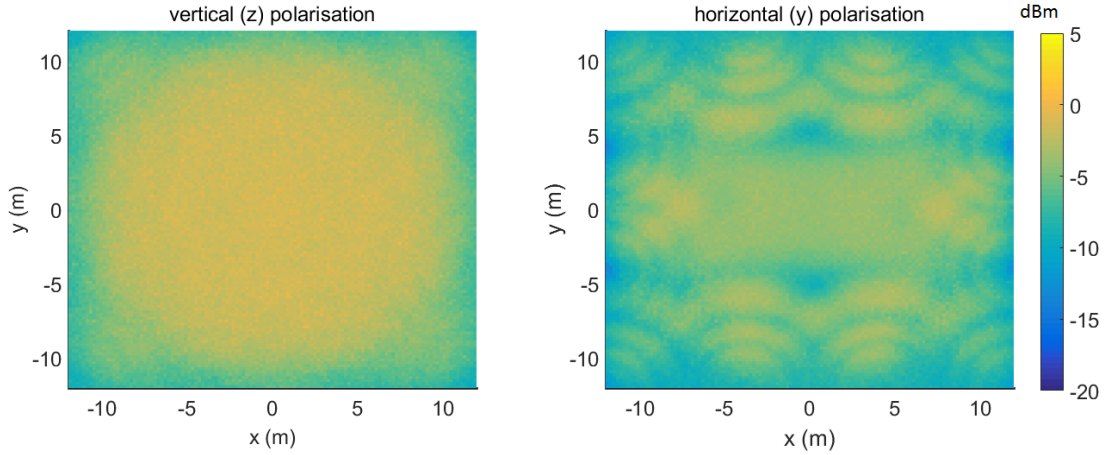

(c) Antennas 6, 7, 10 and 11 (all cell antennas) failed

Figure 6.24: Effect of antenna failure on fixed antenna system power distribution in $8m \times 8m$ cell

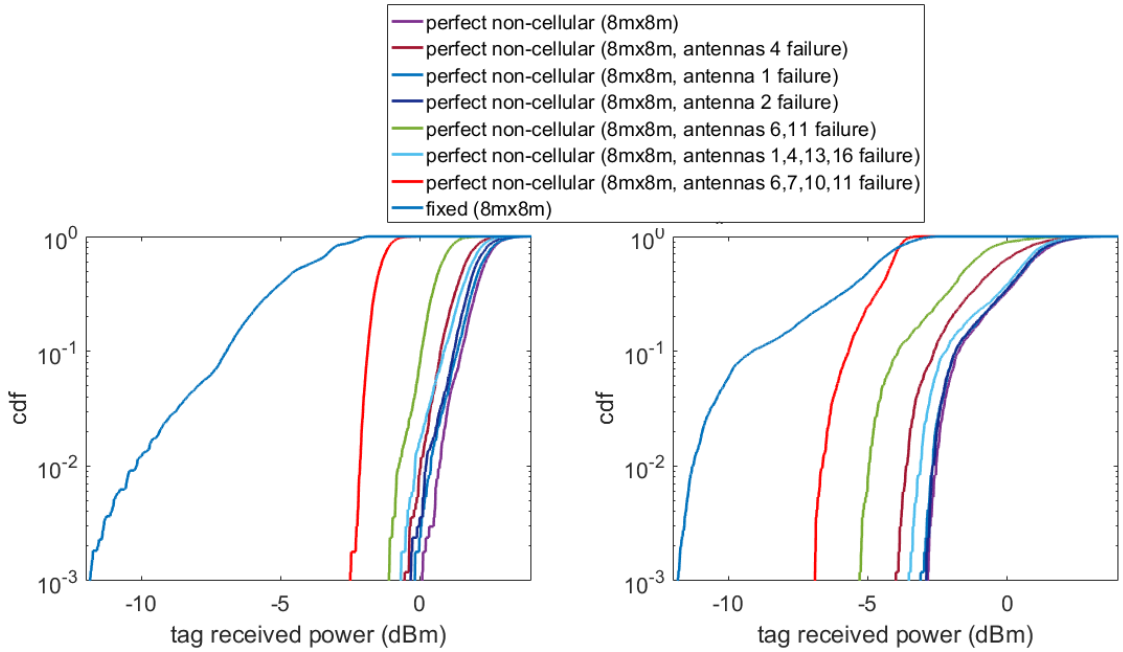

Figure 6.25: cdf for different scenarios of antenna failure in non-cellular perfectly steerable array system with $8m \times 8m$ antenna separation

It is seen that the system is highly resilient in terms of antenna failure compared to a cellular system, in which a single failed antenna node leads a much more drastic decrease in the tag received power. A single antenna failure at any location leads to $< 1dB$ decrease in the tag power of the least 1% of tags for all tag polarisations. Failure of four outer ring antennas (antennas 1, 4, 13 and 16) equally decrease the tag power by < 1 dB. Failure of two antennas on the inner ring (antennas 6 and 11) decrease the tag performance by ~ 1.5 dB for vertically polarised tags and ~ 2.5 dB for horizontally polarised tags. Failure of all four inner ring antennas decrease tag performance by ~ 3.0 dB for vertical tags and ~ 4.0 dB for horizontal tags. The performance improvement over a single cell antenna is still enormous in this case; ~ 8.0 dB for vertical tags and ~ 4.5 dB for horizontal tags. This shows that the non-cellular system provides enormous improvements in tag-delivered power, and provides a substantial amount of resilience in the event of antenna failure. It also suggests that more complex multipath effects such as blocking and shadowing of antennas at some locations may be tolerable.

6.4 Summary

This chapter has used the model developed in Chapter 3 to study the limits of a DAAS system in wide area RFID. A raster scan method was used by perfectly steerable antennas to obtain the best possible performance of a four-cell system. It was shown that such a system could obtain up to 10× reduction in the number of antennas for horizontally polarised and 25× for vertically polarised tags. The system was also studied in the context of limited elevation angles of flat antennas, and conditions were derived and investigated under which a perfectly steerable antenna could be approximated by a limited scan antenna.

In the second section, a wide area system based on global cooperation of perfectly steerable antennas in a non-cellular setup has been presented. This is shown to provide massive improvements in the power delivered to tags, and up 100× reduction in antenna count is possible. The system has been further shown to be highly resilient to several antenna failures, and a maximum drop of $\sim 1.1dB$ is recorded for single or double antenna failures at any location for vertically polarised tags, while for horizontally polarised tags, the corresponding value is $\sim 2.5dB$, including at the cell being interrogated. It is also seen that even with failure of all antennas in the interrogation cell, a drop of $\sim 4dB$ is recorded, and the system still performs better than a corresponding fixed DAS system.

These results show that the performance of the DAAS is limited by the ability of the array antennas to be steered to wide angles, and hence more research into wide-angle scan antennas is required. The next chapter presents the development of an antenna which can achieve high scan angles in a relatively small footprint.

Chapter 7

Conclusion and Future work

7.1 Conclusion

This dissertation has investigated the use of phased array antennas in wide area RFID systems. It has been shown throughout that due to beam steering, better performance can be achieved using phased arrays, compared with fixed antennas. This leads to much reduced number of antennas required to scan a particular area, potentially reducing equipment and installation costs.
The following contributions have been made in this dissertation:

- A new 3D RFID propagation model to provide quick simulations using realistic RFID parameters for wide area RFID environments.
- Demonstration of a distributed antenna array system with phase diversity for RFID tag detection in wide areas, including design of programmable beam control circuitry.
- Demonstration of an RFID DAAS system with a single reader port in a daisy chain link.
- Proposal of perfectly steerable antenna array concept for taking maximum advantage of antennas to maximise tag power delivery. Proposal of a cell-less RFID DAAS system for huge improvements in tag power delivery compared to fixed DAS systems.

7.1.1 Wide Area RFID Antenna Modelling

Accurate modelling is required to plan effectively for system deployment and predict performance. To this end, a novel 3D modelling tool was introduced which has been used throughout this work for simulating different RFID environments and antenna interactions. This was used in chapter 3 to demonstrate different multi-antenna RFID systems using different multiplexing schemes. The model was also used to tell what locations and orientations are best suited for placing tags. It has also been used in the rest of the work for simulation of experimental setups. The use of a hybrid model, making use of realistic antenna patterns (simulated or measured) and RF field propagation allows a rapid determination of field distributions in a particular area, with speeds more than 100 *times* faster than a full wave solver such as FEKO, while obtaining the same results for an equivalent setup in FEKO. In addition, the ability to model complex setups such as dynamic beam steering and geometric antenna transformations, makes this a useful RF propagation modeller for RFID planning.

7.1.2 The Distributed Antenna Array System

The traditional fixed RFID DAS system utilises multiple fixed antennas to overcome multipath fading in wide area systems. Several antenna multiplexing schemes to overcome inter-antenna interference have been modelled including TDM, FDM and phase hopping. Phase hopping was shown to best overcome the problem, with improvements of up to 8 dB over the traditional TDM solution in a four-antenna system. Phased array antennas were further investigated for different multicasting schemes. It was demonstrated that beam steering with phase dithering provided the best performance. It was further shown that beam steering introduces phase diversity due to relative phase changes as the antennas are steered, and an explicit implementation of phase dithering improves average tag received power by a maximum of $2dB$, irrespective of the number of antennas. 2 dB corresponds to a 25% increase in range according to Friis equation, and so this represents a potentially wider antenna separation. This was demonstrated with two, four and six antennas. The advantages provided by phase hopping are therefore only minimal when using phased array antennas.

Further to this, a comparison of fixed and array antennas was performed, and it was demonstrated that an array antenna could provide up to four times successful tag reads as the fixed antenna in a multipath environment. This is significantly higher than has been reported (e.g Weisgerber et al [81] reported 50% increase in tag reads), as dynamic beamforming was used to generate beams in arbitrary directions, rather than fixed beam formers as is more common (e.g. Butler matrix). This improves the power delivered to the tag especially in highly fading environments, and as a result, more tags are detected. In addition, a Distributed Antenna Array System (DAAS) was designed and setup using four phased array antennas. The system was shown to provide a similar performance to a fixed DAS system in a single cell. However, since adjacent cells can be addressed by a single array, only 25% of the antennas are required in the array system. This has the effect of simplifying the system and reducing the cost. The same system was demonstrated with a single port RFID reader, since all functionality for phase dithering and beam steering is moved to the antennas, and a power distribution network and multiplexing scheme is used to feed the antenna using a single coaxial cable. The significance of this is the elimination of special purpose readers, as standard single port readers could be used to implement a DAAS system, thereby further reducing the cost.

7.1.3 Perfectly Steerable DAAS and Cell-less RFID

The theoretical limits of the DAAS system were investigated using perfectly steerable antennas, and these were shown to provide significant improvements to the tag received power, and reduction in required antennas. Up to 25 $\times$ reduction in required antennas while providing similar or better performance compared with a fixed DAS system was demonstrated. It was further shown that under certain conditions, limited scan antennas can approximate the performance of perfectly steerable antennas.

A cell-less DAAS system, making use of the entire reader antenna population for each inventory was then demonstrated, and shown to provide even more gain in the tag received power due to the increased number of interrogating antennas. It was shown that up to 80 $\times$ reduction in antenna count is possible compared with the fixed DAS system when using just two rings of antennas around the interrogation cell. It has also been shown that each surrounding ring contributes equally to the power received by tags at the central cell, as the increasing distance from the cell to the antennas is exactly cancelled out by the

increasing number of antennas.

A significant consequence of the proposed non-cellular DAAS system is the elimination of cell allocation, and consequently, the requirement for reader collision avoidance policies. This is because a single central reader controls all interrogating antennas, and reader collisions are altogether avoided. Also, specific locations of tags are targeted, and therefore few tag collisions are likely to occur, as few tags are simultaneously activated.

7.2 Future Work

7.2.1 Practical Implementation of Non Cellular DAAS

The cell-less DAAS RFID system described in Chapter 6 has the potential to significantly decrease required number of antennas for massive RFID interrogation areas due to the cooperative distributed raster scan method described. A practical implementation of the system will be a natural extension to the work described in this dissertation. However, the described antenna distribution may be unsuitable for many applications, since a repeated pattern of distributed antennas is required throughout the interrogation area. A ring system of antennas could prove to be more practical, as the antennas could surround the interrogation area.

An important result from the chapter was that the periodic antenna system distribution could be analysed as an annular system, with different radii from the centre, and each ring contributes equally to the power received at the centre. This idea could be used to design a ring system of antennas with equivalent performance to the described rectangular periodic arrangement.

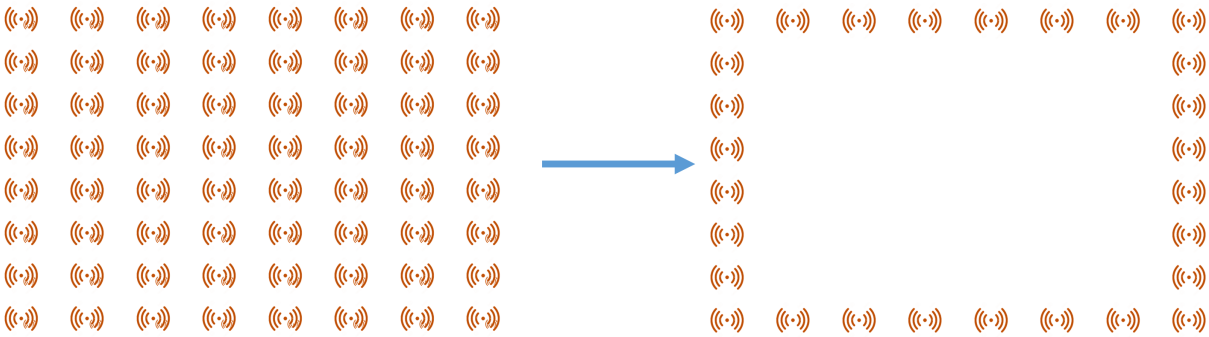

Figure 7.1: From periodic DAAS to Ring DAAS system

Another obstacle for the implementation of the system will be the requirement for wide-angle steerable antennas. The wide-scan metasurface antenna presented in Chapter 7, could be researched more in order to obtain a more cost-effective antenna. A compromise design with poorer polarisation or gain properties could be obtained with a different substrate (with lower dielectric constant and thickness) leading to a reduced, more practical cost.

An alternative solution will be to use a hybrid mechanical/electrical steerable system, where a partially steerable array is mounted on a mechanical rotation platform in order

to achieve full steerability.

7.2.2 Massive MIMO for RFID

The potential for significant increase in the range of an RFID system by using phased array RFID readers has been established. However, the tags have been assumed to be single antenna dipoles. Improvement of the tags could boost performance even more, by realising a full MIMO RFID system with both distributed phased arrays at the readers and antenna arrays at each tag. Mangal et al. demonstrated a retro-directive RFID system, in which a tag scatters its response in the direction of reception via phase conjugation [138]. A 3×3 array was shown to provide a $3\times$ range improvement. The tag works by estimating the angle of arrival of the incident signal, and scatters its response in that direction. However, the DAAS system powers up a tag from multiple directions and several antennas, and therefore this concept is not applicable. For application of tag arrays in an DAAS RFID MIMO system, pattern switching could be used, in which the tag beam pattern is switched sequentially over a set of preselected beams. This will harvest more power, as the instantaneous power is maximised by the higher gain of the tags in multiple directions. Fig 7.2 shows four beams generated from a 1×4 dipole array

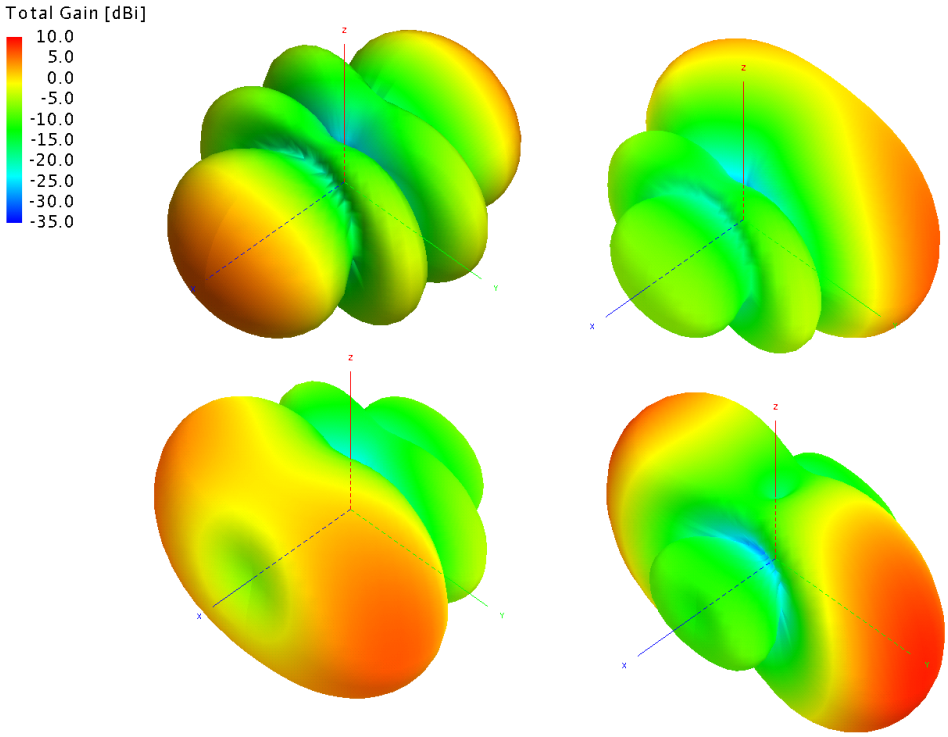

Figure 7.2: RFID MIMO tag pattern switching for a 1×4 tag array showing different beams

It is expected to achieve higher ranges due to to the higher gain of the tags, as well as the already discussed advantages of antenna arrays, such as further reduction of multipath. The difficulty in realising this system will be the size constraints of tag antennas at sub 1 GHz frequencies, and as a result, is more applicable at higher frequencies of 2.4 GHz and 5.8 GHz, where arrays could be fabricated in small footprints. However, the losses at these frequencies are also high, and need to be taken into account.

7.2.3 RFID DAAS over Ethernet cable

Zhe et al. presented an RFID system over Ethernet cable, enabling the extension of RFID signal transmission over long distances [139]. The block diagram for the system is shown in Fig 7.3. The system is based on transmitting the RFID signal in baseband form, and performing frequency upscaling to RF at the antenna. This will enable long distance signal distribution from the reader to the antennas due to the low loss of the base band signal over cat5 compared to huge RF losses on coaxial cables. Additionally, the low cost and flexibility of cat5 cables will enable easy installation, as cat5 cables are cheaper and

easier to install and maintain than the much bulkier coaxial cables.

The central controller extracts the baseband signal from the RFID reader and transmits over an Ethernet cable, while at the antenna end, the antenna modulates the baseband signal unto an RF wave generated by an onboard local oscillator (LO). The signal is then amplified and fed into the antenna. A similar process of LNA and demodulation is followed in the uplink link.

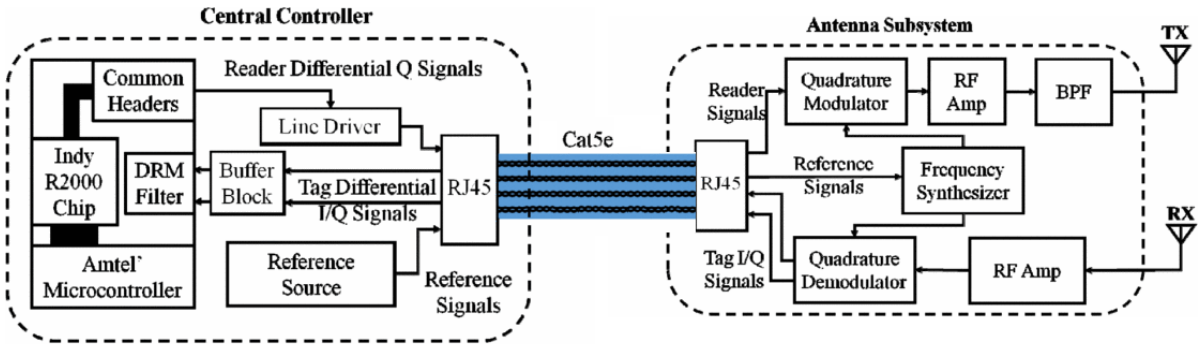

Figure 7.3: RFID over ethernet block diagram [139]

This could be extended to phased array antennas in the daisy chain manner in chapter 5, as shown in Fig 7.4. This will enable a RFID DAAS system with seamless signal distribution over long distances using a single Ethernet line with power tapping into the arrays.

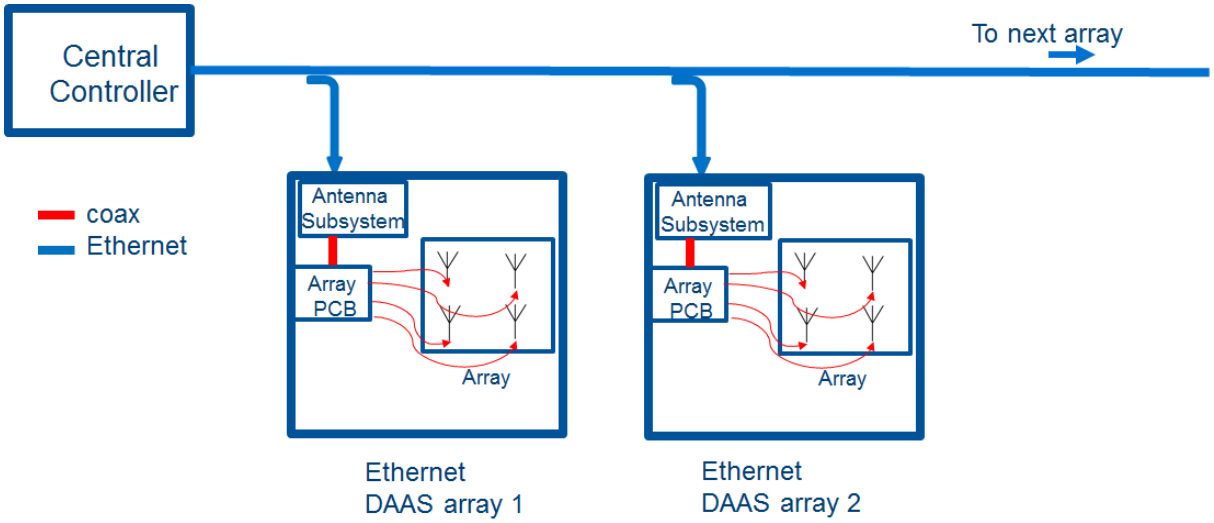

Figure 7.4: Proposed daisy chain RFID DAAS

7.2.4 A wide-angle scan metasurface antenna

It was shown in Chapter 6 that an antenna with a limited ability to scan can approach the performance of a perfectly steerable antenna under certain conditions. However, planar phased arrays can only scan to a maximum elevation angle of $\sim \pm 60^0$ [140] due to element beam width limitations and strong mutual coupling at high scan angles [127]. The requirement for circular polarisation in order to detect arbitrary tag orientations make such designs even more difficult. Several methods have been applied to obtain wide-angle scan antennas. The first is the use of wide beam-width elements which produce widely steerable arrays. Examples include the use of cross dipoles [141], a three-magnetic-current antenna [142], comb-slot-loaded patch elements [143], a crossed L-bar microstrip antenna [144] and a zero order resonance patch antenna [145]. Another method for designing wide angle scan phased array antennas is by employing reconfigurable antennas as the antenna unit element [146, 147, 148, 149, 150, 151].. Because pattern reconfigurable antennas can assume one of several patterns, e.g. a broadside and quasi-endfire pattern in a planar form factor, pattern-reconfigurable antennas make good candidates for the unit element in a wide scan phased array antenna. This is because the switching between beam states can be synchronised with the array steering in order to provide maximum radiation at the desired scan angle. This technique has been demonstrated mainly for the realisation of linear antenna arrays [152, 153, 154]. The disadvantage with pattern-reconfigurable arrays is in their complexity and size, especially for 2D arrays, making them impractical for large arrays [140].

In recent years, the emergence of metamaterials and metasurfaces, and their applications in antenna design and miniaturisation, has opened the way to many-element miniaturised antenna arrays.

They have been applied in the design of beam shaping surfaces, as well as miniaturised antennas and phased array antennas, negative index materials, frequency selective surfaces and planar lenses [155, 156, 157]. Badawe et al. presented an 8×8 metasurface antenna array in a $1.2\lambda \times 1.2\lambda$ footprint at a frequency of 3.0 GHz using cross resonator unit cells [158]. Based on the design, a 6×6 RFID antenna has been simulated. A truncated mushroom unit cell has been used in order to produce circularly polarised beams. Sequentuial rotation has also been used to enhance circular polarisation.

The antenna design is illustrated in Fig 7.5.

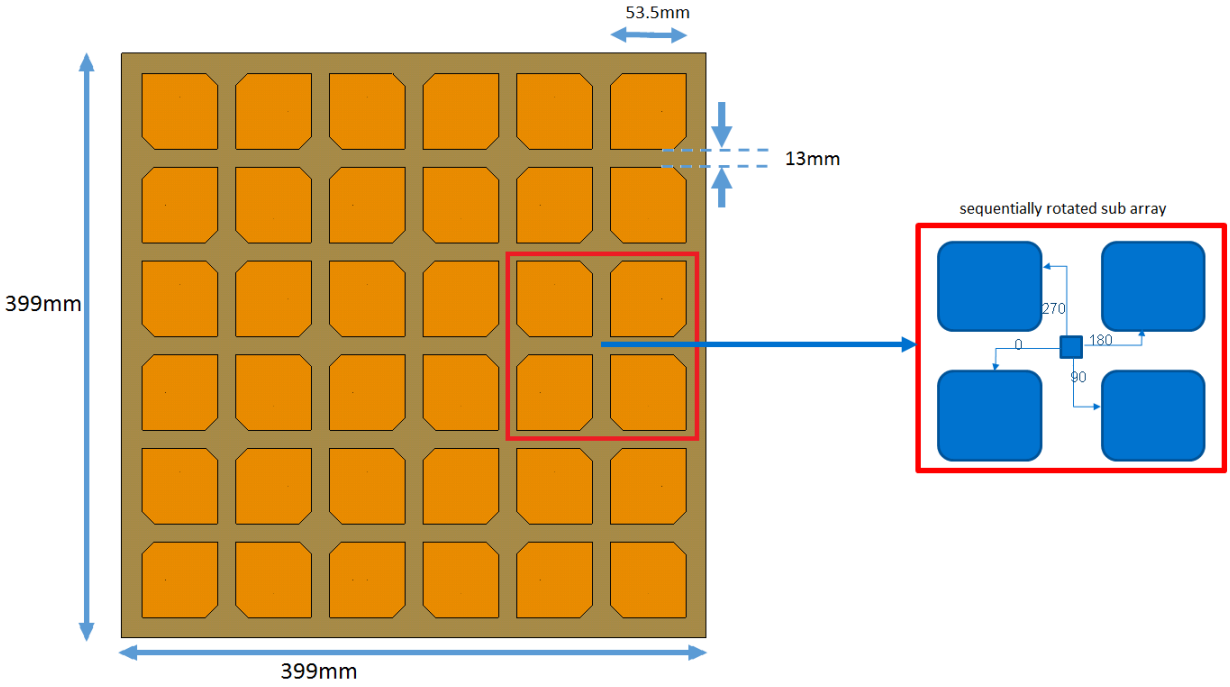

Figure 7.5: Design simulated as a 3x3 array antenna, where each element is a 2x2 sequentially rotated sub-array. A quadrifilar splitter provides sequential phase shifts of 0, 90, 180 and 270 degrees at each of four output ports for sequentially rotated sub-arrays.

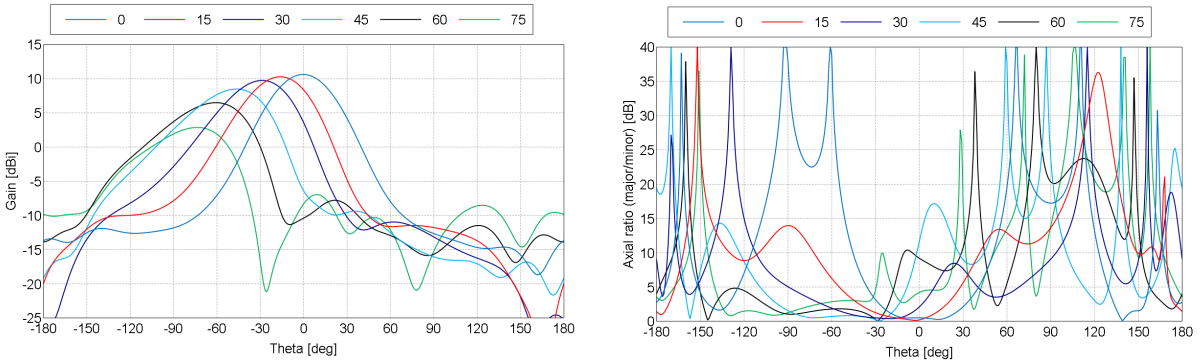

(a) Gain (b) Axial ratio

Figure 7.6: Simulated 6x6 metasurface antenna showing gain patterns and axial ratio for different steering angles in elevation plane at azimuth angle of 45^0. . Plot is cut at $\phi = 45^0$

It is seen that a scan angle in the elevation plane of up to 75^0 is achieved, with an axial ratio of $< 3dB$ in the direction of maximum gain for all steering angles. It is however observed that the gain degrades with steering angle from a maximum of $\sim 10.5dB$ at

broadside to $\sim 4.0dB$ at a scan angle of 75^0, which will limit the performance. The gain reduction compensation technique introduced in chapter 5, can be used in a practical deployment to achieve an effective flat gain at the maximum level irrespective of scan angle. Future research into economical realisation of such an antenna will be critical for realising wide area RFID DAAS.

Publications

1. A. M. Ndifon, M. J. Crisp, R. V. Penty and I. H. White, "Performance improvements of multicast rfid systems using phased array antennas and phase diversity," in *2017 IEEE International Conference on RFID Technology Application (RFID-TA),* pp. 5-56, Sep. 2017.

2. A. M. Ndifon, M. J. Crisp, R. V. Penty and I. H. White, "Enhanced rfid tag detection accuracy using distributed antenna arrays," in *2018 IEEE International Conference on RFID (RFID)*, pp. 1-6, April 2018.

3. R. Chen, S. Yang, A. M. Ndifon, I. H. White, R. V. Penty and M. Crisp, "Beam scanning uhf rfid reader antenna with high gain and wide axial ratio beamwidth," in *2019 IEEE International Conference on RFID Technology and Applications (RFID-TA)*, pp. 374-379, Sep. 2019.

4. R. Chen, S. Yang, A. M. Ndifon, I. H. White, R. V. Penty and M. Crisp, "A uhf rfid reader antenna with tunable axial ratio and

   fixed beamwidth," in *14th European Conference on Antennas and Propagation,* (Accepted).

5. M. Crisp, R. Chen, A. Ndifon and R. Penty, "Antennas for wide area distributed rfid systems," in *International Workshop on Antenna Technology (iWAT),* (Accepted).

Bibliography

[1] D. M. Dobkin, *The RF in RFID*. Newnes, 2008.

[2] M. Yamamoto and T. Yamazoe, "A null-zone control method for rfid systems," pp. 106–109, 2011 2011.

[3] S. Sabesan, M. J. Crisp, R. V. Penty, and I. H. White, "Wide area passive uhf rfid system using antenna diversity combined with phase and frequency hopping," *IEEE Transactions on Antennas and Propagation*, vol. 62, pp. 878–888, Feb 2014.

[4] M. Abbak and I. Tekin, "Rfid coverage extension using microstrip-patch antenna array [wireless corner]," *IEEE Antennas and Propagation Magazine*, vol. 51, pp. 185–191, Feb 2009.

[5] W. S. Lee, S. T. Khang, W. S. Lee, H. S. Tae, and J. W. Yu, "Wide-coverage array antenna using a dual-beam switching for uhf rfid applications," in *2013 IEEE International Conference on RFID (RFID)*, pp. 36–41, April 2013.

[6] W. S. Lee, S. T. Khang, W. S. Lee, and J. W. Yu, "Hemispheric coverage multi-beam switched antenna array using a 4-port feeding network for uhf rfid dead zone avoidance," in *2013 Asia-Pacific Microwave Conference Proceedings (APMC)*, pp. 254–257, Nov 2013.

[7] Impinj, *Mojix Starflex RFID Antenna Array*, Accessed: 2019-05-08.

[8] S. Zou, M. Crisp, S. Sabesan, A. Bekkali, A. Kadri, R. V. Penty, and I. H. White, "Tag read enhancement using unsynchronized signal from adjacent readers in multi-cell rfid system," in *RFID Technology and Applications Conference (RFID-TA), 2014 IEEE*, pp. 62–67, Sept 2014.

[9] R. L. Haupt and Y. Rahmat-Samii, "Antenna array developments: A perspective on the past, present and future," *IEEE Antennas and Propagation Magazine*, vol. 57, pp. 86–96, Feb 2015.

[10] H. Rohling, "Milestones in radar and the success story of automotive radar systems," in *11-th INTERNATIONAL RADAR SYMPOSIUM*, pp. 1–6, June 2010.

[11] J. Landt, "The history of rfid," *IEEE Potentials*, vol. 24, pp. 8–11, Oct 2005.

[12] M. Guarnieri, "The early history of radar [historical]," *IEEE Industrial Electronics Magazine*, vol. 4, pp. 36–42, Sep. 2010.

[13] R. F. Harrington, "Theory of loaded scatterers," *Proceedings of the Institution of Electrical Engineers*, vol. 111, pp. 617–623(6), April 1964.

[14] M. H. Gerst, R. Bunduchi, and I. Graham, "Current issues in rfid standardisation," in *Proceedings of the Workshop Interoperability Standards Implementation, Dynamics and Impact (Interop-ESA 2005), Geneva*, 2005.

[15] R. R. Alliance, "Over 15 billion rain rfid tag chips sold in 2018." `https://www.prnewswire.com/news-releases/over-15-billion-rain-rfid-tag-chips-sold-in-2018-300803213.html`. Accessed: 3rd May 2019.

[16] R. Want, "An introduction to rfid technology," *IEEE Pervasive Computing*, vol. 5, pp. 25–33, Jan 2006.

[17] X. Jia, Q. Feng, T. Fan, and Q. Lei, "Rfid technology and its applications in internet of things (iot)," in *Consumer Electronics, Communications and Networks (CECNet), 2012 2nd International Conference on*, pp. 1282–1285, April 2012.

[18] D. M. Dobkin, "Rfid protocols." `http://www.enigmatic-consulting.com/Communications_articles/RFID/RFID_protocols.html`. Accessed: 2019-05-30.

[19] PhaseIV, *About Ultra Long-Range UHF RFID Sensors - Phase IV Engineering Inc*, 2009 (accessed August 3, 2016).

[20] A. Martnez-Olmos, J. Fernndez-Salmern, N. Lopez-Ruiz, A. R. Torres, L. F. Capitan-Vallvey, and A. J. Palma, "Screen printed flexible radiofrequency identification tag for oxygen monitoring," *Analytical Chemistry*, vol. 85, no. 22, pp. 11098–11105, 2013. PMID: 24116378.

[21] D. P. Rose, M. E. Ratterman, D. K. Griffi, L. Hou, N. Kelley-Loughnane, R. R. Naik, J. A. Hagen, I. Papautsky, and J. C. Heikenfeld, "Adhesive rfid sensor patch for monitoring of sweat electrolytes," in *IEEE TRANSACTIONS ON BIOMEDICAL ENGINEERING*, vol. 62, pp. 1457–1466, June 2015.

[22] R. A. Potyrailo, N. Nagraj, Z. Tang, F. J. Mondello, C. Surman, and W. Morris, "Battery-free radio frequency identification (rfid) sensors for food quality and safety," vol. 60, pp. 8535–8543, 2012. PMID: 22881825.

[23] X. Chen, L. Ukkonen, and T. Bjorninen, "Passive e-textile uhf rfid based wireless strain sensors with integrated references," *IEEE Sensors Journal*, vol. PP, no. 99, pp. 1–1, 2016.

[24] P. Escobedo-Araque, A. Martnez-Olmos, M. . Carvajal, A. J. Palma, and J. Fernndez-Salmern, "Passive uhf rfid tag for spectral fingerprint measurement," in *Microwave Symposium (MMS), 2015 IEEE 15th Mediterranean*, pp. 1–4, Nov 2015.

[25] Y. Zhang, L. T. Yang, and J. Chen, *RFID and sensor networks : architectures, protocols, security, and integrations*. Boca Raton, Fla. ; London : CRC, 2010.

[26] Y. Zhao, A. LaMarca, and J. R. Smith, "A battery-free object localization and motion sensing platform," in *Proceedings of the 2014 ACM International Joint Conference on Pervasive and Ubiquitous Computing*, UbiComp '14, (New York, NY, USA), pp. 255–259, ACM, 2014.

[27] S. Naderiparizi, Y. Zhao, J. Youngquist, A. P. Sample, and J. R. Smith, "Self-localizing battery-free cameras," in *Proceedings of the 2015 ACM International Joint Conference on Pervasive and Ubiquitous Computing*, UbiComp '15, (New York, NY, USA), pp. 445–449, ACM, 2015.

[28] C. Pendl, M. Pelnar, and M. Hutter, *Elliptic Curve Cryptography on the WISP UHF RFID Tag*, pp. 32–47. Berlin, Heidelberg: Springer Berlin Heidelberg, 2012.

[29] D. J. Yeager, S. Member, P. S. Powledge, R. Prasad, S. Member, D. Wetherall, and J. R. Smith, "1 wirelessly-charged uhf tags for sensor data collection," 2010.

[30] Y. Zhao and J. R. Smith, "A battery-free rfid-based indoor acoustic localization platform," in *RFID (RFID), 2013 IEEE International Conference on*, pp. 110–117, April 2013.

[31] S. Tedjini, F. Costa, S. Genovesi, and G. Manara, "Chipless rfid, from principles to applications," in *2017 International Conference on Electromagnetics in Advanced Applications (ICEAA)*, pp. 1906–1908, Sep. 2017.

[32] L. Zhang, S. V. Rodríguez, H. Tenhunen, and L. Zheng, "An innovative fully printable rfid technology based on high speed time-domain reflections," *Conference on High Density Microsystem Design and Packaging and Component Failure Analysis, 2006. HDP'06.*, pp. 166–170, 2006.

[33] J. Havlicek, C. Herrojo, F. Paredes, J. Mata-Contreras, and F. Martn, "Enhancing the per-unit-length data density in near-field chipless-rfid systems with sequential bit reading," *IEEE Antennas and Wireless Propagation Letters*, vol. 18, pp. 89–92, Jan 2019.

[34] A. Habib, M. A. Afzal, H. Sadia, Y. Amin, and H. Tenhunen, "Chipless rfid tag for iot applications," in *2016 IEEE 59th International Midwest Symposium on Circuits and Systems (MWSCAS)*, pp. 1–4, Oct 2016.

[35] C. Herrojo, F. L. J. Muela, J. Mata-Contreras, F. Paredes, and F. Martín, "High-density microwave encoders for motion control and near-field chipless-rfid," *IEEE Sensors Journal*, vol. 19, pp. 3673–3682, 2019.

[36] GS1, "Epc/rfid standards." `https://www.gs1.org/standards/epc-rfid`. Accessed: 3rd May, 2019.

[37] B. Carbunar, M. K. Ramanathan, M. Koyutrk, S. Jagannathan, and A. Grama, "Efficient tag detection in rfid systems," *Journal of Parallel and Distributed Computing*, vol. 69, no. 2, pp. 180 – 196, 2009.

[38] B. Carbunar, M. K. Ramanathan, M. Koyuturk, C. Hoffmann, and A. Grama, "Redundant reader elimination in rfid systems," in *2005 Second Annual IEEE Communications Society Conference on Sensor and Ad Hoc Communications and Networks, 2005. IEEE SECON 2005.*, pp. 176–184, Sep. 2005.

[39] C. Hsu, Y. Chen, and C. Yang, "A layered optimization approach for redundant reader elimination in wireless rfid networks," in *The 2nd IEEE Asia-Pacific Service Computing Conference (APSCC 2007)*, pp. 138–145, Dec 2007.

[40] K. Yu, C. W. Yu, and Z. Lin, "A density-based algorithm for redundant reader elimination in a rfid network," in *2008 Second International Conference on Future Generation Communication and Networking*, vol. 1, pp. 89–92, Dec 2008.

[41] M. Ma, P. Wang, and C. Chu, "Redundant reader elimination in large-scale distributed rfid networks," *IEEE Internet of Things Journal*, vol. 5, pp. 884–894, April 2018.

[42] C. Hsu, C. Yu, C. Chung, C. Yang, and C. Chou, "An overlap aware technique for redundant reader elimination," in *2012 9th International Conference on Ubiquitous Intelligence and Computing and 9th International Conference on Autonomic and Trusted Computing*, pp. 357–360, Sep. 2012.

[43] J. Waldrop, D. W. Engels, and S. E. Sarma, "Colorwave: an anticollision algorithm for the reader collision problem," in *IEEE International Conference on Communications, 2003. ICC '03.*, vol. 2, pp. 1206–1210 vol.2, May 2003.

[44] J. Ho, D. W. Engels, and S. E. Sarma, "Hiq: a hierarchical q-learning algorithm to solve the reader collision problem," in *International Symposium on Applications and the Internet Workshops (SAINTW'06)*, pp. 4 pp.–91, Jan 2006.

[45] H. Liu and Jhen-Peng Ciou, "Performance analysis of multi-carrier rfid systems," in *2009 International Symposium on Performance Evaluation of Computer Telecommunication Systems*, vol. 41, pp. 112–116, July 2009.

[46] D. W. Engels and S. E. Sarma, "The reader collision problem," in *IEEE International Conference on Systems, Man and Cybernetics*, vol. 3, pp. 6 pp. vol.3–, Oct 2002.

[47] H. Seo and C. Lee, "A new ga-based resource allocation scheme for a reader-to-reader interference problem in rfid systems," in *2010 IEEE International Conference on Communications*, pp. 1–5, May 2010.

[48] Kainan Cha, A. Ramachandran, and S. Jagannathan, "Adaptive and probabilistic power control algorithms for dense rfid reader network," in *2006 IEEE International Conference on Networking, Sensing and Control*, pp. 474–479, April 2006.

[49] E. D. Giampaolo, F. Forn, and G. Marrocco, "Rfid-network planning by particle swarm optimization," (Barcelona), 2010.

[50] S. Zhou, Y. Liu, and J. Luo, "A cube based model for rfid coverage problem in three-dimensional space," in *2013 IEEE 9th International Conference on Mobile Ad-hoc and Sensor Networks*, pp. 115–120, Dec 2013.

[51] Y. Gao, X. Hu, H. Liu, and Y. Feng, "Multiobjective estimation of distribution algorithm combined with pso for rfid network optimization," in *2010 International Conference on Measuring Technology and Mechatronics Automation*, vol. 2, pp. 736–739, March 2010.

[52] E. Di Giampaolo, F. Forn, and G. Marrocco, "Rfid-network planning by particle swarm optimization," in *Proceedings of the Fourth European Conference on Antennas and Propagation*, pp. 1–5, April 2010.

[53] H. Yihua and L. Shilei, "Rfid network planning based on k-coverage using plant growth simulation algorithm," in *2012 8th International Conference on Computing Technology and Information Management (NCM and ICNIT)*, vol. 1, pp. 196–201, April 2012.

[54] S. Zou, M. Crisp, S. Sabesan, A. Kadri, R. V. Penty, and I. H. White, "An optimization model for antenna selection and deployment in single and multi-cell rfid systems," in *RFID Technology and Applications (RFID-TA), 2015 IEEE International Conference on*, pp. 87–92, Sept 2015.

[55] J. Zhai and G.-N. Wang, "An anti-collision algorithm using two-functioned estimation for rfid tags," in *Computational Science and Its Applications – ICCSA 2005* (O. Gervasi, M. L. Gavrilova, V. Kumar, A. Laganá, H. P. Lee, Y. Mun, D. Taniar,

and C. J. K. Tan, eds.), (Berlin, Heidelberg), pp. 702–711, Springer Berlin Heidelberg, 2005.

[56] S. E. Sarma, S. A. Weis, and D. W. Engels, "Rfid systems and security and privacy implications," in *Cryptographic Hardware and Embedded Systems - CHES 2002* (B. S. Kaliski, ç. K. Koç, and C. Paar, eds.), (Berlin, Heidelberg), pp. 454–469, Springer Berlin Heidelberg, 2003.

[57] Jihoon Myung, Wonjun Lee, and J. Srivastava, "Adaptive binary splitting for efficient rfid tag anti-collision," *IEEE Communications Letters*, vol. 10, pp. 144–146, March 2006.

[58] W. Shi, Y. Guo, S. Yan, Y. Yu, P. Luo, and J. Li, "Optimizing directional reader antennas deployment in uhf rfid localization system by using a mpcso algorithm," *IEEE Sensors Journal*, vol. 18, pp. 5035–5048, June 2018.

[59] J. Liu and L. Chen, "Placement of multiple rfid reader antennas to alleviate the negative effect of tag orientation," in *2012 IEEE 18th International Conference on Parallel and Distributed Systems*, pp. 432–439, Dec 2012.

[60] W. Su, K. M. Beilke, and T. T. Ha, "A reliability study of rfid technology in a fading channel," in *2007 Conference Record of the Forty-First Asilomar Conference on Signals, Systems and Computers*, pp. 2124–2127, Nov 2007.

[61] J. D. Griffin and G. D. Durgin, "Reduced fading for rfid tags with multiple antennas," in *2007 IEEE Antennas and Propagation Society International Symposium*, pp. 1201–1204, June 2007.

[62] H. Zhu, X. Li, Q. Li, and W. Feng, "A rfid switch beam scanning antenna array for application in complex environment," *Electromagnetics*, vol. 39, no. 1, pp. 51–62, 2019.

[63] J. J. Zhang and A. Papandreou-Suppappola, "Mimo radar with frequency diversity," in *2009 International Waveform Diversity and Design Conference*, pp. 208–212, Feb 2009.

[64] F. A. Cardoso, J. P. Ferreira, L. S. Silva, and J. B. Gerald, "Frequency hopping spread spectrum communication system over the power lines," in *Proceedings of*

ICICS, 1997 International Conference on Information, Communications and Signal Processing. Theme: Trends in Information Systems Engineering and Wireless Multimedia Communications (Cat., vol. 1, pp. 94–98 vol.1, Sep. 1997.

[65] C. H. Loo, A. Z. Elsherbeni, F. Yang, and D. Kajfez, "Experimental and simulation investigation of rfid blind spots," *Journal of Electromagnetic Waves and Applications*, vol. 23, pp. 747–760, 2009.

[66] K. Benson, "Phased array beamforming ICs simplify antenna design." `https://www.analog.com/en/analog-dialogue/articles/phased-array-beamforming-ics-simplify-antenna-design.html`.

[67] G. Marconi, "On methods whereby the radiation of electric waves may be mainly confined to certain directions, and whereby the receptivity of a receiver may be restricted to electric waves emanating from certain directions," *Proceedings of the Royal Society of London. Series A, Containing Papers of a Mathematical and Physical Character*, vol. 77, no. 518, pp. 413–421, 1906.

[68] F. Braun, "Electrical oscillations and wireless telegraphy," *Nobel Lectures*, June 1909.

[69] A. Hewish, S. J. Bell, J. D. H. Pilkington, P. F. Scott, and R. A. Collins, "Observation of a rapidly pulsating radio source," *Nature*, vol. 217, pp. 86–96, Feb 1968.

[70] J. Howell, "Microstrip antennas," in *1972 Antennas and Propagation Society International Symposium*, vol. 10, pp. 177–180, Dec 1972.

[71] M. S. Gatti, "A phased array antenna for deep space communications," in *2008 IEEE Aerospace Conference*, pp. 1–8, March 2008.

[72] R. Hansen, *Phased Array Antennas*. Wiley-Interscience, 2009.

[73] D. Chang, B. Zeng, and J. C. Liu, "Mechanical adjustable phase shifters for WiMAX BTS antenna," in *2008 Asia-Pacific Microwave Conference*, pp. 1–4, Dec 2008.

[74] A. Chakraborty and B. Gupta, "Paradigm phase shift: Rf mems phase shifters: An overview," *IEEE Microwave Magazine*, vol. 18, pp. 22–41, 01 2017.

[75] D. M. Pozar, *Microwave Engineering*. Wiley-Interscience, 2005.

[76] T.-Y. Chin, S.-F. Chang, C.-C. Chang, and J.-C. Wu, "A 24-GHz CMOS Butler Matrix MMIC for multi-beam smart antenna systems," *2008 IEEE Radio Frequency Integrated Circuits Symposium*, pp. 633–636, 2008.

[77] J. Butler, "Beam-forming matrix simplifies design of electronically scanned antennas," 1961.

[78] J. Blass, "Multidirectional antenna - a new approach to stacked beams," in *1958 IRE International Convention Record*, vol. 8, pp. 48–50, March 1960.

[79] F. E. Fakoukakis, T. N. Kaifas, E. E. Vafiadis, and G. A. Kyriacou, "Design and implementation of Butler matrix-based beam-forming networks for low sidelobe level electronically scanned arrays," *International Journal of Microwave and Wireless Technologies*, vol. 7, no. 1, p. 6979, 2015.

[80] T. Ma, C. Wang, R. Hua, and C. Yang, "Phased array antenna for uhf rfid applications using artificial transmission lines," in *2008 International Workshop on Antenna Technology: Small Antennas and Novel Metamaterials*, pp. 454–457, March 2008.

[81] L. Weisgerber and A. E. Popugaev, "Multibeam antenna array for rfid applications," in *2013 European Microwave Conference*, pp. 84–87, Oct 2013.

[82] F. E. Fakoukakis, K. A. Gotsis, G. A. Kyriacou, and J. N. Sahalos, "Beam steering for rfid readers with inherent antenna diversity," in *The 8th European Conference on Antennas and Propagation (EuCAP 2014)*, pp. 2210–2214, April 2014.

[83] X. Li, H. Zhu, D. Zhang, Z. Sun, Y. Yuan, and D. Yu, "Two-dimensional scanning antenna array for uhf radio frequency identification system application," *IET Microwaves, Antennas Propagation*, vol. 8, no. 14, pp. 1250–1258, 2014.

[84] A. Hasan, C. Zhou, and J. D. Griffin, "Experimental demonstration of transmit diversity for passive backscatter rfid systems," *2011 IEEE International Conference on RFID-Technologies and Applications*, pp. 544–548, 2011.

[85] N. C. Karmakar, S. M. Roy, and M. S. Ikram, "Development of smart antenna for rfid reader," in *2008 IEEE International Conference on RFID*, pp. 65–73, April 2008.

[86] N. C. Karmakar, "Fpgacontrolled phased array antenna development for uhf rfid reader," *Handbook of Smart Antennas for RFID Systems*, 2010.

[87] Impinj, *Impinj xArray*, Accessed: 2019-05-08.

[88] A. A. S. A. Shah, N. H. A. Rahman, M. T. Ali, N. F. Fauzi, and A. A. A. Aziz, "Beam scanning of phased array antenna using phase modification method for satellite application," in *2016 IEEE Asia-Pacific Conference on Applied Electromagnetics (APACE)*, pp. 291–295, Dec 2016.

[89] P. Salonen and L. Sydanheimo, "A 2.45 GHz digital beam-forming antenna for rfid reader," in *Vehicular Technology Conference. IEEE 55th Vehicular Technology Conference. VTC Spring 2002 (Cat. No.02CH37367)*, vol. 4, pp. 1766–1770 vol.4, May 2002.

[90] M. H. Hayes, *Statistical Digital Signal Processing and Modeling*. New York, NY, USA: John Wiley & Sons, Inc., 1st ed., 1996.

[91] R. Roy and T. Kailath, "Esprit-estimation of signal parameters via rotational invariance techniques," *IEEE Transactions on Acoustics, Speech, and Signal Processing*, vol. 37, pp. 984–995, July 1989.

[92] S. Azzouzi, M. Cremer, U. Dettmar, R. Kronberger, and T. Knie, "New measurement results for the localization of uhf rfid transponders using an angle of arrival (aoa) approach," in *2011 IEEE International Conference on RFID*, pp. 91–97, April 2011.

[93] C. Angerer, R. Langwieser, and M. Rupp, "Direction of arrival estimation by phased arrays in rfid," 2010.

[94] S. Azzouzi, M. Cremer, U. Dettmar, T. Knie, and R. Kronberger, "Improved aoa based localization of uhf rfid tags using spatial diversity," in *2011 IEEE International Conference on RFID-Technologies and Applications*, pp. 174–180, Sep. 2011.

[95] S. Balon, J. A. Buyco, and J. J. Marciano, "Sectorization of uhf rfid tags using a steerable phased antenna array," in *2010 IEEE Student Conference on Research and Development (SCOReD)*, pp. 16–20, Dec 2010.

[96] L. Qiu, X. Liang, and Z. Huang, "Patl: A rfid tag localization based on phased array antenna," in *Scientific reports*, 2017.

[97] A. F. Mindikoglu and A. van der Veen, "Separation of overlapping rfid signals by antenna arrays," in *2008 IEEE International Conference on Acoustics, Speech and Signal Processing*, pp. 2737–2740, March 2008.

[98] K. V. S. Rao, P. V. Nikitin, and S. F. Lam, "Antenna design for uhf rfid tags: A review and a practical application," *IEEE TRANSACTIONS ON ANTENNAS AND PROPAGATION*, vol. 53, pp. 3870–3877, 2005.

[99] D. Wei, W. Hung, and K. L. Wu, "A real time rfid locationing system using phased array antennas for warehouse management," (Fajardo), pp. 1153–1154, 2016.

[100] S. R. Banerjee, R. Jesme, and R. A. Sainati, "Investigation of spatial and frequency diversity for long range uhf rfid," in *2008 IEEE Antennas and Propagation Society International Symposium*, pp. 1–4, July 2008.

[101] S. Sabesan, M. J. Crisp, R. V. Penty, and I. H. White, "Wide area passive uhf rfid system using antenna diversity combined with phase and frequency hopping," *IEEE Transactions on Antennas and Propagation*, vol. 62, pp. 878–888, 2014 2014.

[102] D. Kim, B. Jang, H. Yoon, J. Park, and J. Yook, "Effects of reader interference on the rfid interrogation range," *Proceedings of the 37th European Microwave Conference*, vol. 37, pp. 728–732, 2007.

[103] M. Cremer, A. Pervez, U. Dettmar, T. Knie, and R. Kronberger, "An improved channel model for passive uhf rfid systems," in *2013 IEEE International Conference on RFID-Technologies and Applications (RFID-TA)*, pp. 1–7, Sept 2013.

[104] A. G. Dimitriou, A. Bletsas, A. C. Polycarpou, and J. Sahalos, "On efficient uhf rfid coverage inside a room," *Proceedings of the Fourth European Conference on Antennas and Propagation*, pp. 1–5, 2010.

[105] A. G. Dimitriou, A. Bletsas, and J. N. Sahalos, "Room-coverage improvements in uhf rfid with commodity hardware [wireless corner]," *IEEE Antennas and Propagation Magazine*, vol. 53, pp. 175–194, Feb 2011.

[106] A. Lazaro, D. Girbau, and R. Villarino, "Effects of interferences in uhf rfid systems," *Progress In Electromagnetics Research*, vol. 98, pp. 425–443, Feb 2009.

[107] A. Bekkali, S. Zou, A. Kadri, M. Crisp, and R. Penty, "Performance analysis of passive uhf rfid systems under cascaded fading channels and interference effects," *IEEE TRANSACTIONS ON WIRELESS COMMUNICATIONS*, vol. 14, pp. 1421–1434, 2015.

[108] A. G. Dimitriou, S. Siachalou, A. Bletsas, and J. Sahalos, "A site-specific stochastic propagation model for passive uhf rfid," *IEEE ANTENNAS AND WIRELESS PROPAGATION LETTERS*, vol. 13, pp. 623–627, 2014.

[109] C. A. Balanis., *Antenna Theory: Analysis and Design.* Wiley-Interscience, 2012.

[110] C. A. Balanis, *Antenna Theory: Analysis and Design.* Wiley-Interscience, 2005.

[111] S. J. Orfanidis, *Electromagnetic Waves and Antennas.* Rutgers University, 2016.

[112] E. Software and S. S. P. Ltd, "Feko user manual." `https://www.altairuniversity.com/wp-content/uploads/2015/03/UserManual.pdf`. Accessed: 3rd May 2019.

[113] MVG, "About ultra long-range uhf rfid sensors - phase iv engineering inc." `"https://www.mvg-world.com/en/products/field_product_family/antenna-measurement-2/starlab"`. Accessed: 3rd May 2019.

[114] W. H. Press, S. A. Teukolsky, W. T. Vetterling, and B. P. Flannery, *Numerical Recipes 3rd Edition: The Art of Scientific Computing.* Cambridge University Press, 2007.

[115] G. Sinclair, "The transmission and reception of elliptically polarized waves," *Proceedings of the IRE*, vol. 38, pp. 148–151, 1950 1950.

[116] Q. Zhang, M. J. Crisp, I. H. White, and R. V. Penty, "Power margin reduction in linear passive uhf rfid tag arrays," *2014 IEEE RFID Technology and Applications Conference (RFID-TA)*, pp. 306–311, 2014.

[117] J. W. Allnatt, E. D. J. Jones, and H. B. Law, "Frequency diversity in the reception of selectively fading binary frequency-modulated signals," *Proceedings of the IEE - Part B: Radio and Electronic Engineering*, vol. 104, pp. 98–, March 1957.

[118] S. J. Lee, "Trade-off between frequency diversity gain and frequency-selective scheduling gain in ofdma systems with spatial diversity," *IEEE Communications Letters*, vol. 11, pp. 507–509, June 2007.

[119] S. Gao, Q. Luo, and F. Zhu, *Circularly Polarized Antennas*. Wiley-IEEE Press, 1st ed., 2014.

[120] R.-L. Xia, S.-W. Qu, P.-F. Li, Q. Jiang, and Z.-P. Nie, "An efficient decoupling feeding network for microstrip antenna array," in *IEEE ANTENNAS AND WIRELESS PROPAGATION LETTERS*, vol. 14, pp. 871–875, April 2015.

[121] D. M. Dobkin, "Chapter 6 - reader antennas," in *The {RF} in {RFID}* (D. M. Dobkin, ed.), pp. 241 – 303, Burlington: Newnes, 2008.

[122] J. Huang, "A technique for an array to generate circular polarization with linearly polarized elements," *IEEE Transactions on Antennas and Propagation*, vol. 34, pp. 1113–1124, Sep. 1986.

[123] L. Baggen, S. Holzwarth, W. Simon, and O. Litschke, "Phased array using the sequential rotation principle: analysis of coupling effects," in *IEEE International Symposium on Phased Array Systems and Technology, 2003.*, pp. 571–576, Oct 2003.

[124] T. Bauernfeind, K. Preis, G. Koczka, S. Maier, and O. Biro, "Influence of the nonlinear uhf-rfid ic impedance on the backscatter abilities of a t-match tag antenna design," *IEEE Transactions on Magnetics*, vol. 48, pp. 755–758, Feb 2012.

[125] A. Robert, "Dielectric permittivity of concrete between 50 MHz and 1 GHz and GPR measurements for building materials evaluation," *Journal of Applied Geophysics*, vol. 40, no. 1, pp. 89 – 94, 1998.

[126] W.-J. Liao, S.-H. Chang, Y.-C. Chu, and W.-S. Jhong, "A beam scanning phased array for uhf rfid readers with circularly polarized patches," *Journal of Electromagnetic Waves and Applications*, vol. 24, no. 17-18, pp. 2383–2395, 2010.

[127] C. A. Balanis, *Advanced Engineering Electromagnetics, 2nd Edition.* Wiley-Interscience, 2012.

[128] Minicicuits, "Bp4c+ surface mount power splitter/combiner." https://ww2.minicircuits.com/pdfs/BP4C+.pdf. Accessed: 3rd May 2019.

[129] Qorvo, "Rfsa3714 50 - 6000 MHz serial/parallel controlled digital step attenuator, 7-bit, 0.25 db steps." https://www.qorvo.com/products/d/da001133. Accessed: 3rd May 2019.

[130] Minicicuits, "Sphsa-152+ surface mount phase shifter." https://ww2.minicircuits.com/pdfs/SPHSA-152+.pdf. Accessed: 3rd May 2019.

[131] Microchip, "Pic16(l)f1777/8/9 28/40/44-pin, 8-bit flash microcontroller." http://ww1.microchip.com/downloads/en/DeviceDoc/40001819B.pdf. Accessed: 3rd May 2019.

[132] Wavelex, "WPA0409N 470 960 MHz, 0.8 Watt power amplifier." http://www.wavelex.com/pdf/WPA0409N_REV_C.pdf. Accessed: 3rd May 2019.

[133] Minicircuits, "Rdp-2r15+ surface mount diplexer." https://ww2.minicircuits.com/pdfs/RDP-2R15+.pdf. Accessed: 3rd May 2019.

[134] Minicircuits, "Zx60-v63+ low noise amplifier." https://ww2.minicircuits.com/pdfs/ZX60-V63+.pdf. Accessed: 3rd May 2019.

[135] S. Ting, S. Kwok, A. H. Tsang, and G. T. Ho, "The study on using passive rfid tags for indoor positioning," *International Journal of Engineering Business Management*, vol. 3, p. 8, 2011.

[136] S. Zou, M. Crisp, S. Sabesan, A. Kadri, R. V. Penty, and I. H. White, "An optimization model for antenna selection and deployment in single and multi-cell rfid systems," in *2015 IEEE International Conference on RFID Technology and Applications (RFID-TA)*, pp. 87–92, Sep. 2015.

[137] S. Zou, M. Crisp, S. Sabesan, A. Bekkali, A. Kadri, R. V. Penty, and I. H. White, "Tag read enhancement using unsynchronized signal from adjacent readers in multi-cell rfid system," in *2014 IEEE RFID Technology and Applications Conference (RFID-TA)*, pp. 62–67, Sep. 2014.

[138] V. Mangal, G. Atzeni, and P. R. Kinget, "Multi-antenna directional backscatter tags," in *2018 48th European Microwave Conference (EuMC)*, pp. 174–177, Sep. 2018.

[139] Z. Fu, M. J. Crisp, S. Yang, R. V. Penty, and I. H. White, "Long distance passive uhf rfid system over ethernet cable," in *2017 IEEE International Conference on RFID Technology Application (RFID-TA)*, pp. 294–298, Sep. 2017.

[140] R. Wang, B. Wang, X. Ding, and X. Yang, "Planar phased array with wide-angle scanning performance based on image theory," *IEEE Transactions on Antennas and Propagation*, vol. 63, pp. 3908–3917, Sep. 2015.

[141] H. Da-cheng, W. Jian, and G. Jin-rui, "Design a wide-scan angle phased-array antenna with circular polarization using a new cross-dipole," in *The 2012 International Workshop on Microwave and Millimeter Wave Circuits and System Technology*, pp. 1–4, April 2012.

[142] R. Wang, B.-Z. Wang, C. Hu, and X. Ding, "Wide-angle scanning planar array with quasi-hemispherical-pattern elements," *Nature Scientific Reports*, vol. 64, pp. 1525–1530, June 2017.

[143] S. E. Valavan, D. Tran, A. G. Yarovoy, and A. G. Roederer, "Planar dual-band wide-scan phased array in x-band," *IEEE Transactions on Antennas and Propagation*, vol. 62, pp. 5370–5375, Oct 2014.

[144] S. E. Valavan, D. D. Tran, A. G. Yarovoy, and A. G. Roederer, "Dual-band wide-angle scanning planar phased array in x/ku-bands," *IEEE Transactions on Antennas and Propagation*, vol. 62, pp. 2514–2521, 2014.

[145] Y. Wen, S. Gao, B. Wang, and Q. Luo, "Dual-polarized and wide-angle scanning microstrip phased array," *IEEE Transactions on Antennas and Propagation*, vol. 66, pp. 3775–3780, July 2018.

[146] Z. Jiajie, W. Anguo, and W. Peng, "A survey on reconfigurable antennas," in *2008 International Conference on Microwave and Millimeter Wave Technology*, vol. 3, pp. 1156–1159, April 2008.

[147] S. Xiao, Z. Shao, M. Fujise, and B. Wang, "Pattern reconfigurable leaky-wave antenna design by fdtd method and Floquet's theorem," *IEEE Transactions on Antennas and Propagation*, vol. 53, pp. 1845–1848, May 2005.

[148] X. Yang, B. Wang, W. Wu, and S. Xiao, "Yagi patch antenna with dual-band and pattern reconfigurable characteristics," *IEEE Antennas and Wireless Propagation Letters*, vol. 6, pp. 168–171, 2007.

[149] W. Kang and K. Kim, "A beam pattern-reconfigurable antenna using pin diodes," in *2010 IEEE Antennas and Propagation Society International Symposium*, pp. 1–4, July 2010.

[150] M. Jusoh, T. Aboufoul, T. Sabapathy, A. Alomainy, and M. R. Kamarudin, "Pattern-reconfigurable microstrip patch antenna with multidirectional beam for wimax application," *IEEE Antennas and Wireless Propagation Letters*, vol. 13, pp. 860–863, 2014.

[151] P. K. Li, Z. H. Shao, Q. Wang, and Y. J. Cheng, "Frequency- and pattern-reconfigurable antenna for multistandard wireless applications," *IEEE Antennas and Wireless Propagation Letters*, vol. 14, pp. 333–336, 2015.

[152] Y. Bai, S. Xiao, C. Liu, X. Shuai, and B. Wang, "Design of pattern reconfigurable antennas based on a twoelement dipole array model," *IEEE Transactions on Antennas and Propagation*, vol. 61, pp. 4867–4871, Sep. 2013.

[153] J. Row and C. Tsai, "Pattern reconfigurable antenna array with circular polarization," *IEEE Transactions on Antennas and Propagation*, vol. 64, pp. 1525–1530, April 2016.

[154] A. Martin, V. Le Neillon, and M. Himdi, "Pattern reconfigurable slot antenna array," in *2016 International Symposium on Antennas and Propagation (ISAP)*, pp. 102–103, Oct 2016.

[155] H.-T. Chen, A. J. Taylor, and B. N. Yu, "A review of metasurfaces: physics and applications," *Reports on Progress in Physics*, vol. 79, pp. 3775–3780, June 2016.

[156] M. Li, S. Xiao, and B. Wang, "Investigation of using high impedance surfaces for wide-angle scanning arrays," *IEEE Transactions on Antennas and Propagation*, vol. 63, pp. 2895–2901, July 2015.

[157] Q.-C. L. Tian La and, Y.-S. Dou, and X.-Y. Jiang, "A study of a wide-angle scanning phased array based on a high-impedance surface ground plane," *International Journal of Antennas and Propagation*, vol. 2019, pp. 2895–2901, January 2019.

[158] M. E. Badawe, T. S. Almoneef, and O. M. Ramahi, "A true metasurface antenna," *Nature Scientific Reports*, vol. 6, p. 8, 2016.